

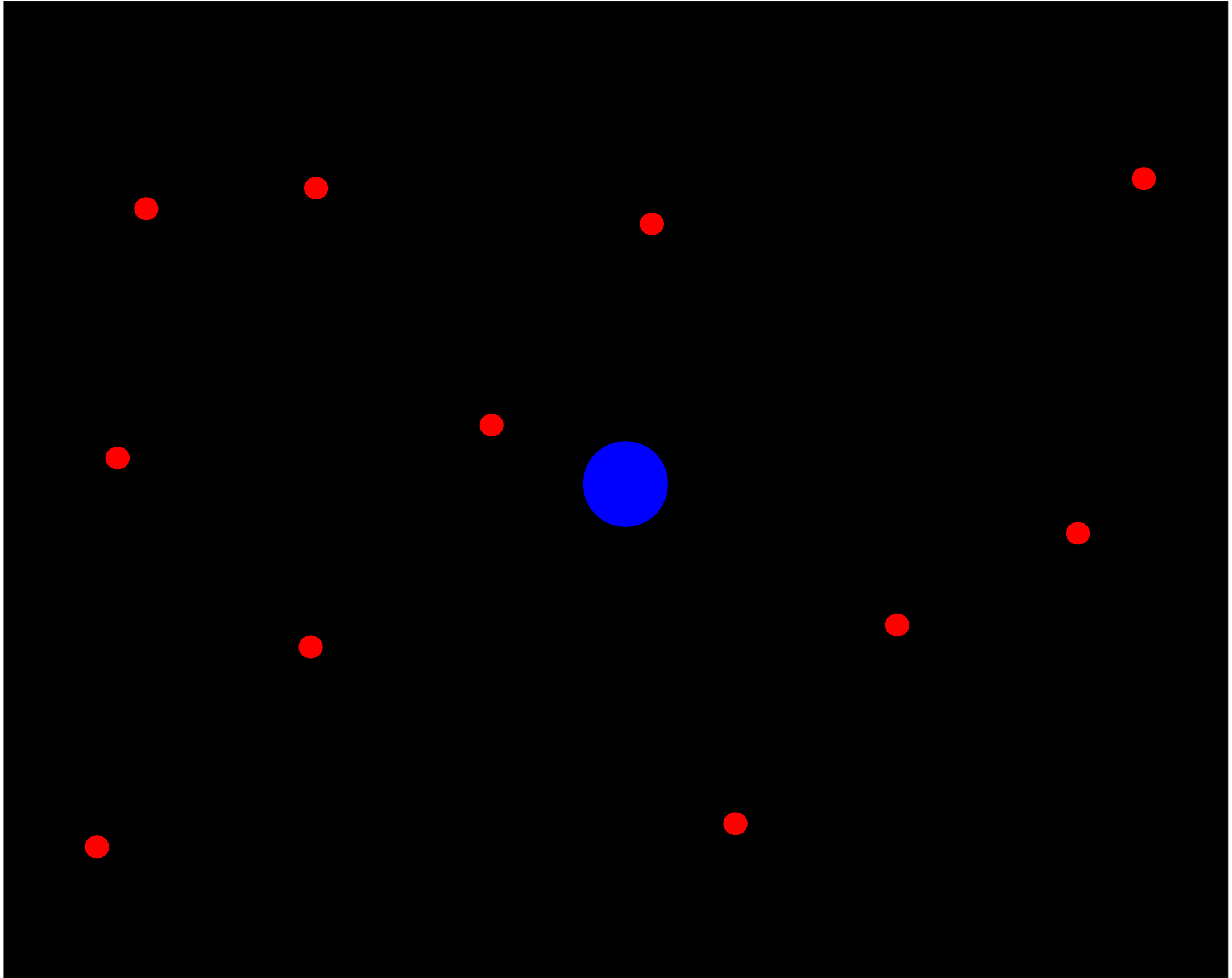
Combined astrometric imaging, coronagraphy and deep wide field imaging

Olivier Guyon (U of Arizona + Subaru Telescope)

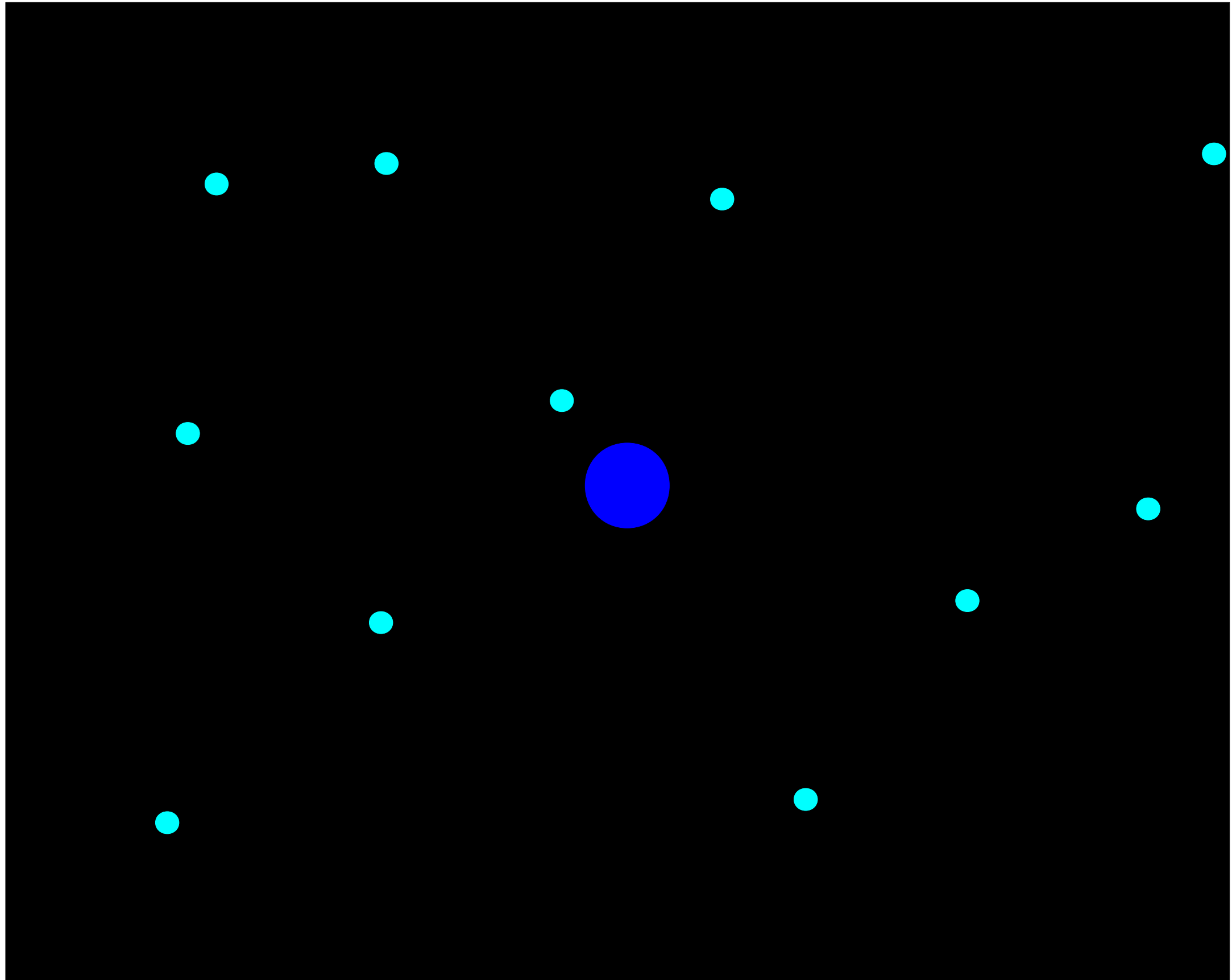
Michael Shao (NASA JPL)	Improvements to original concept, error budget, exoplanet science
Stuart Shaklan (NASA JPL)	Error budget, mission architecture
Robert Woodruff (LMC)	Optical design for wide field telescope compatible with coronagraphy
Bijan Nemati (NASA JPL)	Numerical simulations, modeling approach
Mark Ammons (UofA)	Lab demo design & operation
Eduardo Bendek (UofA)	Lab demo optical design & operation
Marie Levine (NASA JPL)	System engineering, mission architecture
Joe Pitman (Expl. Sci.)	System engineering

Tom Milster (UofA)	Mask manufacturing, scaling of mask manufacturing to full scale PM
Jim Burge (UofA)	Mask manufacturing, scaling of mask manufacturing to full scale PM
Neville Woolf (UofA)	Exoplanet science, concept definition
Roger Angel (UofA)	Exoplanet science, concept definition
Josh Eisner (UofA)	Exoplanet and star formation/evolution science
Ruslan Belikov (NASA Ames)	Compatibility with coronagraphy
Daniel Eisenstein (UofA)	Extragalactic science enabled with wide field camera
Ann Zabludoff (UofA)	Extragalactic science with wide field camera
Dennis Zaritsky (UofA)	Extragalactic & galactic science with wide field camera
Jay Daniel (L3/Tinsley)	Optics manufacturing

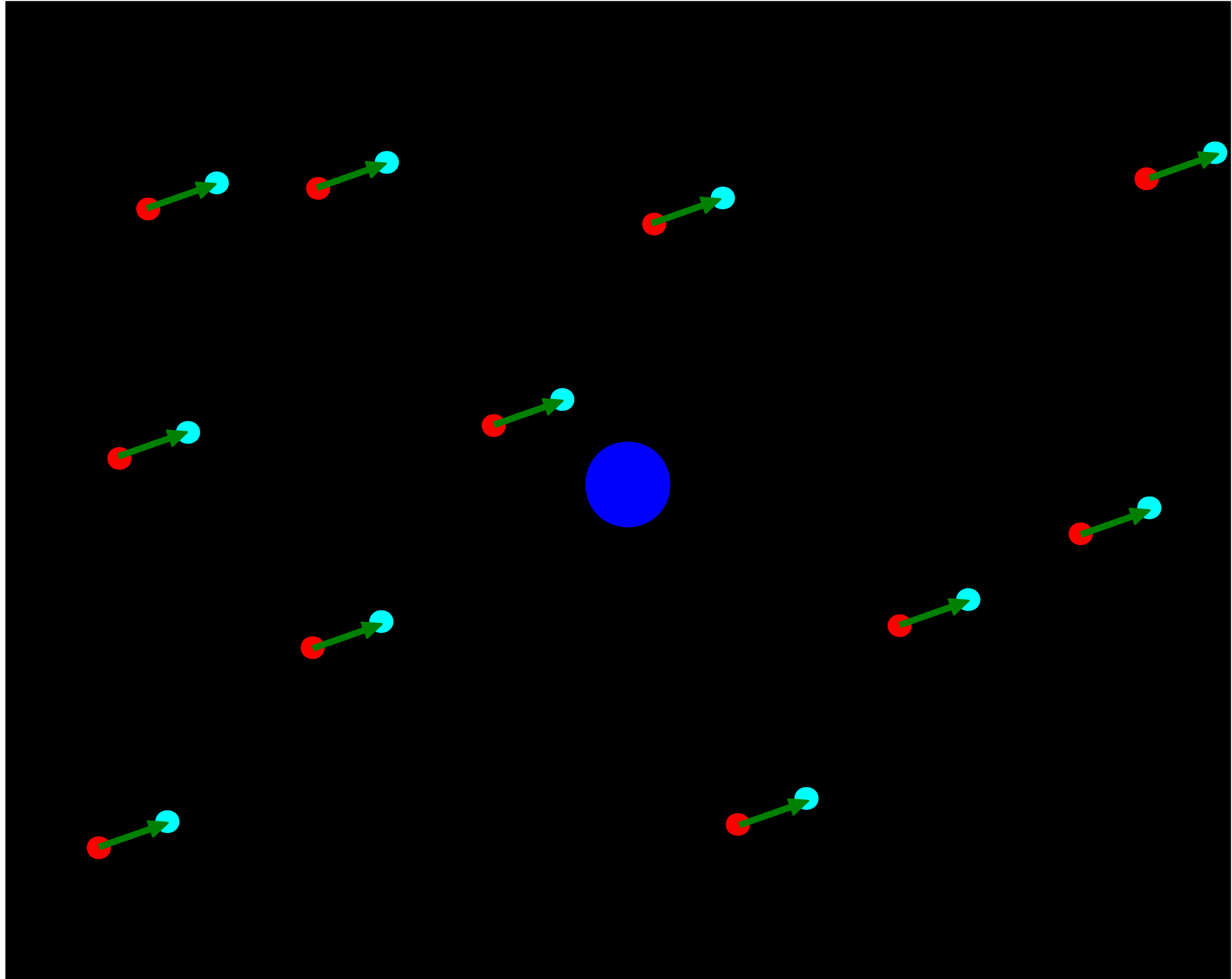
epoch #1 (first observation)



epoch #2 (first observation)



**Blue points show the position of background stars at epoch #2 (second observation)
The telescope is pointed on the central star, so the spikes have not moved between
the 2 observations, but the position of the background stars has moved due to the
astrometric motion of the central star (green vectors).**

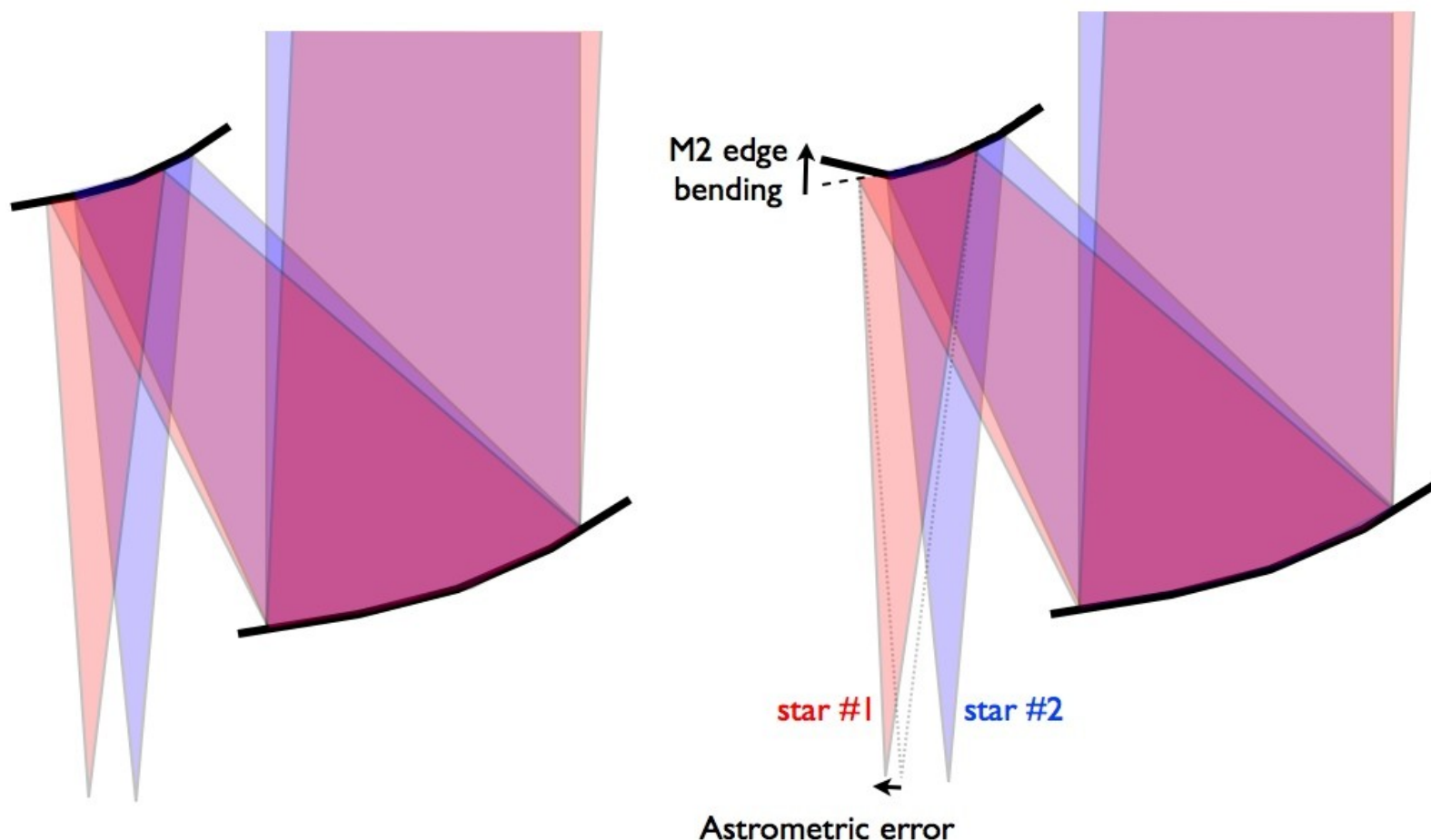


Principle: use background stars around coronagraph target as an astrometric reference

With a 1.4-m telescope in the visible, 0.25 sq deg offers sufficient photons from stars at the galactic pole to provide an astrometric reference at the <50 nano-arcsec after taking into account realistic efficiency, zodi light and pixel sampling.

Why is imaging astrometry difficult ?

On-axis and off-axis stars illuminate different (but overlapping) parts of M2.
Edge bending on M2 is seen by star #1, but not star #2.



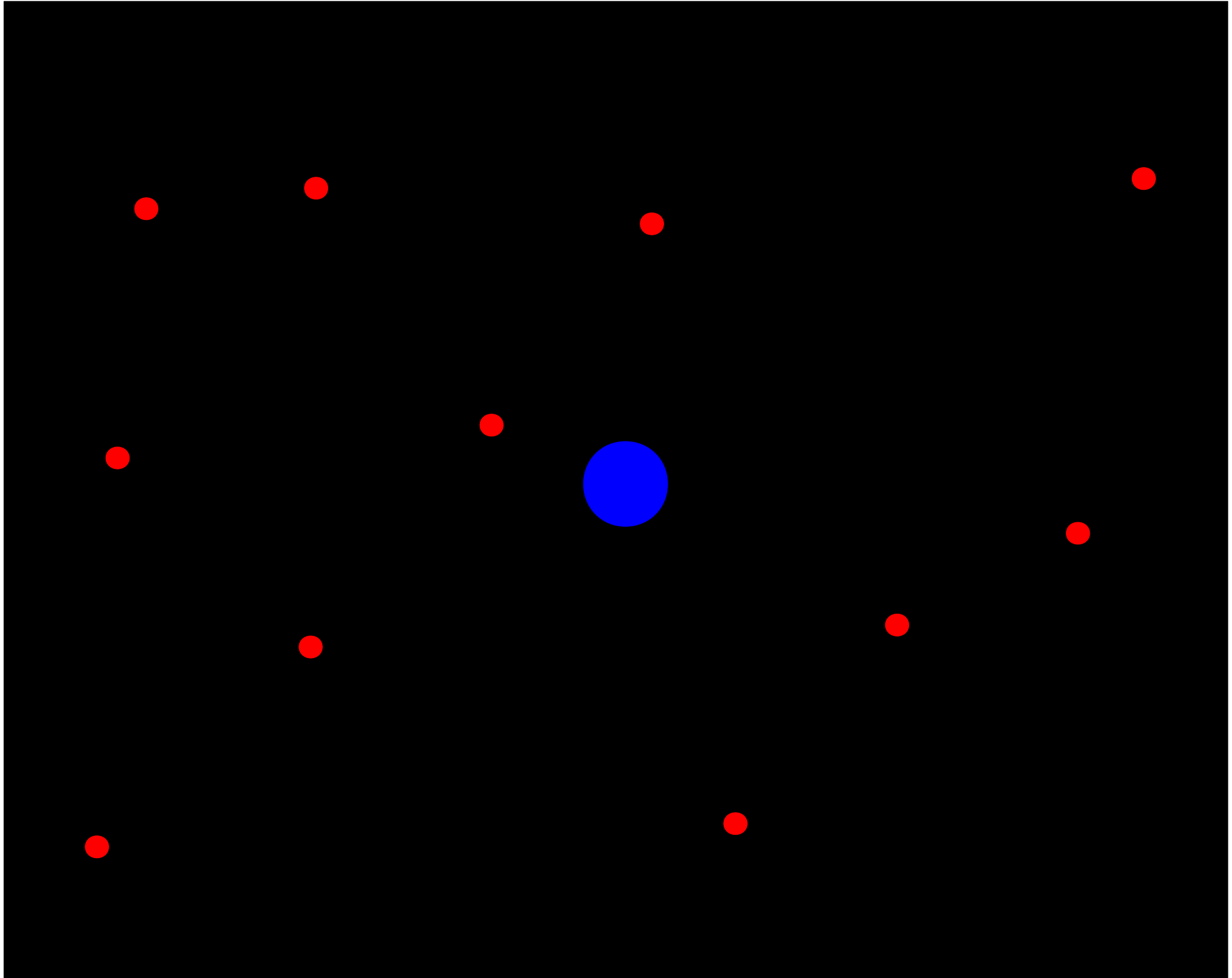
(1) Light from different stars on the sky travels different paths \rightarrow small bending of optics produces field distortions

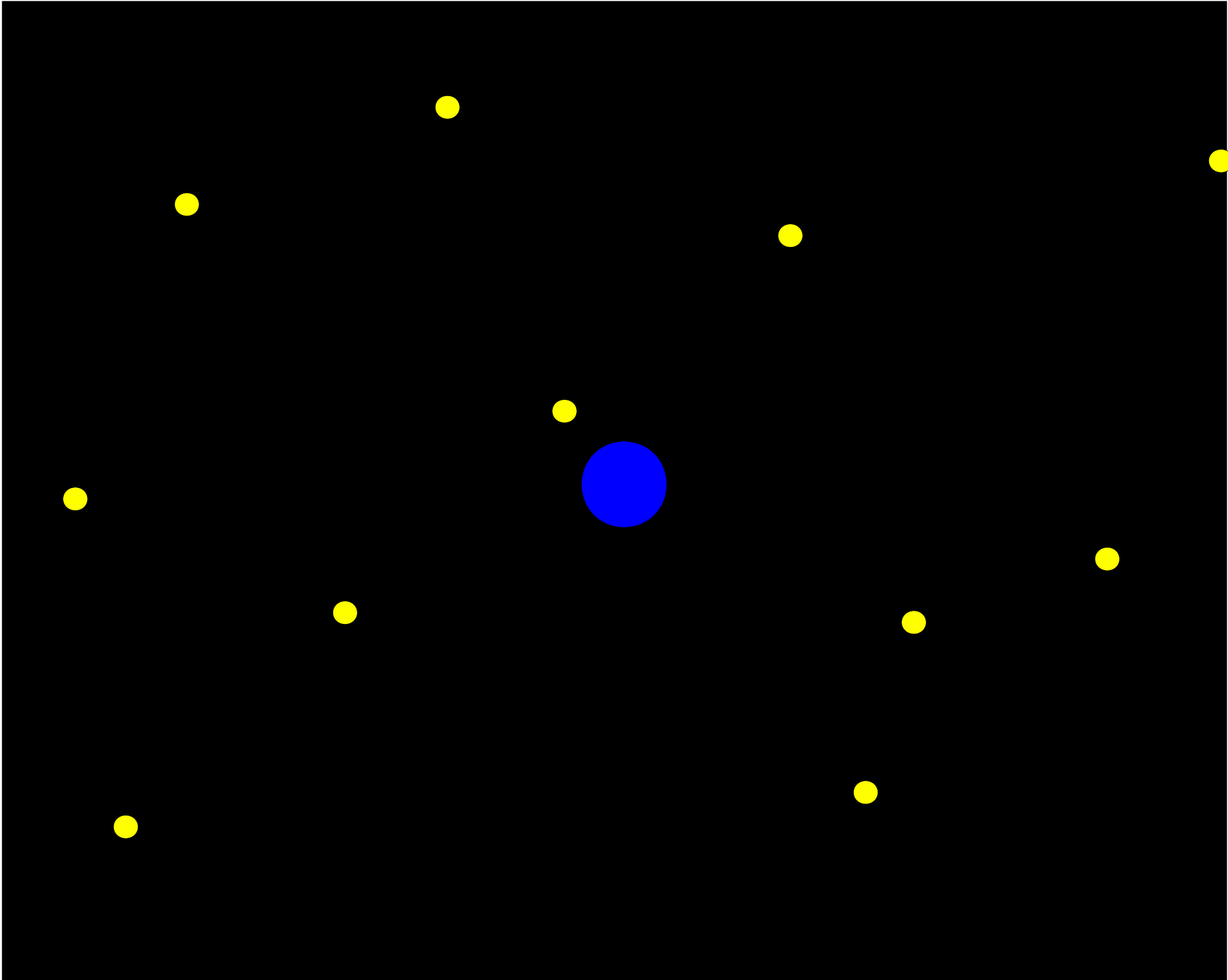
(2) The detector can move between observations (especially when using large mosaics)

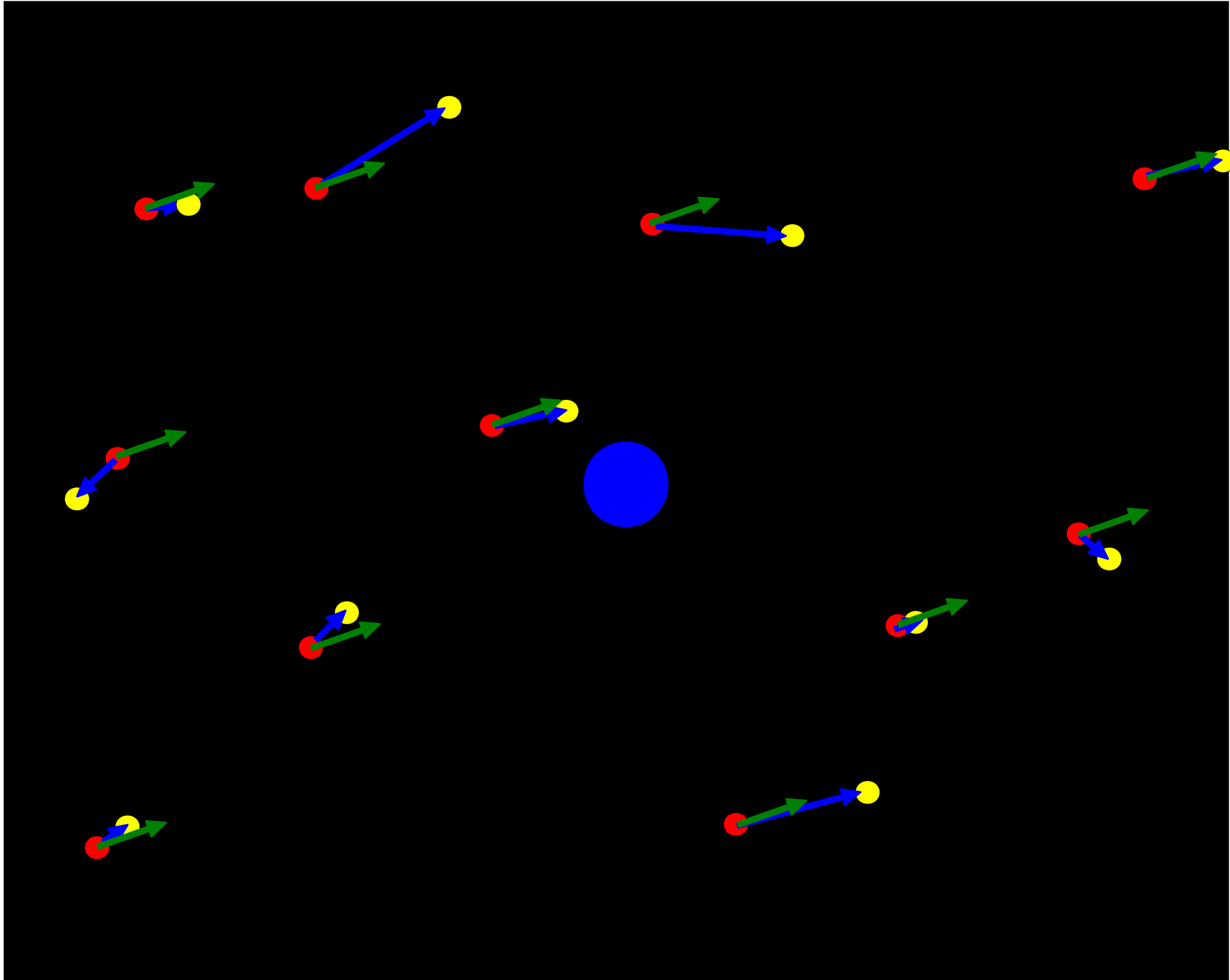
(3) Pixels are not perfect and their response changes with time

+ (4) Central star is much brighter than background stars

epoch #1 (first observation)



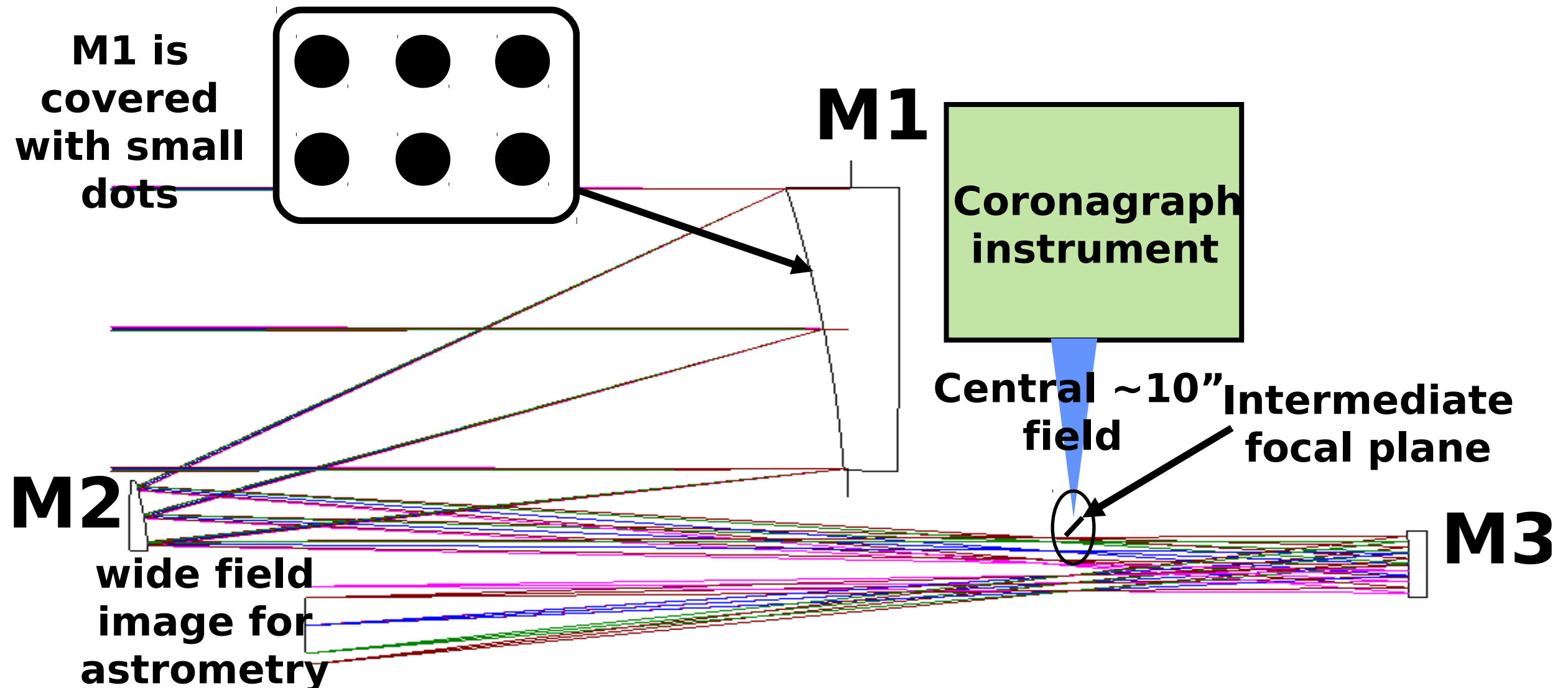




Optical Layout for simultaneous coronagraphy and astrometry

The telescope is a conventional TMA, providing a high quality diffraction-limited PSF over a 0.5×0.5 deg field with no refractive corrector. The design shown here was made for a 1.4m telescope (PECO).

Light is simultaneously collected by the coronagraph instrument (direct imaging and spectroscopy of exoplanet) and the wide field astrometric camera (detection and mass measurement of exoplanets)



Approach & Assumptions

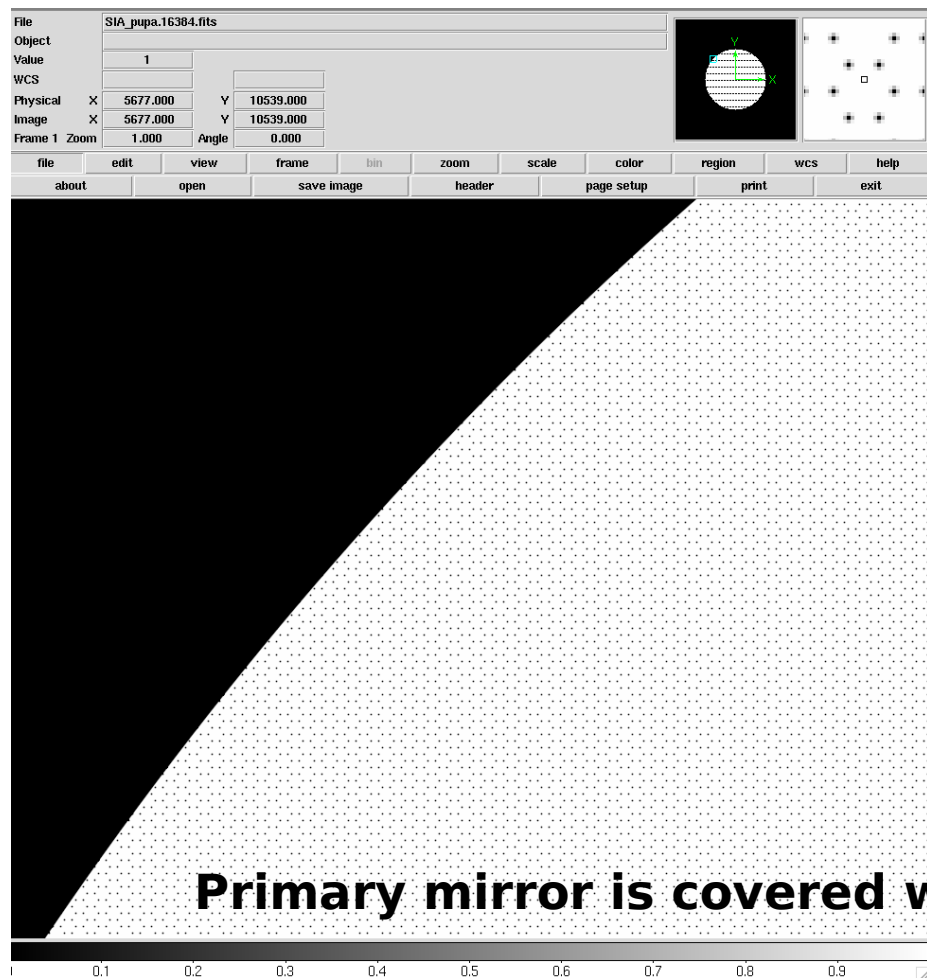
Baseline: 1.4-m telescope, with 0.29 sq deg FOV (0.31 deg radius)

The FOV is **chosen to reach performance goal (0.2 μ as/ measurement)** in a sufficiently stable system (Photon noise limited performance for this FOV is 0.044 μ as single measurement at galactic pole, but actual performance is significantly lower due to distortions and detector limits)

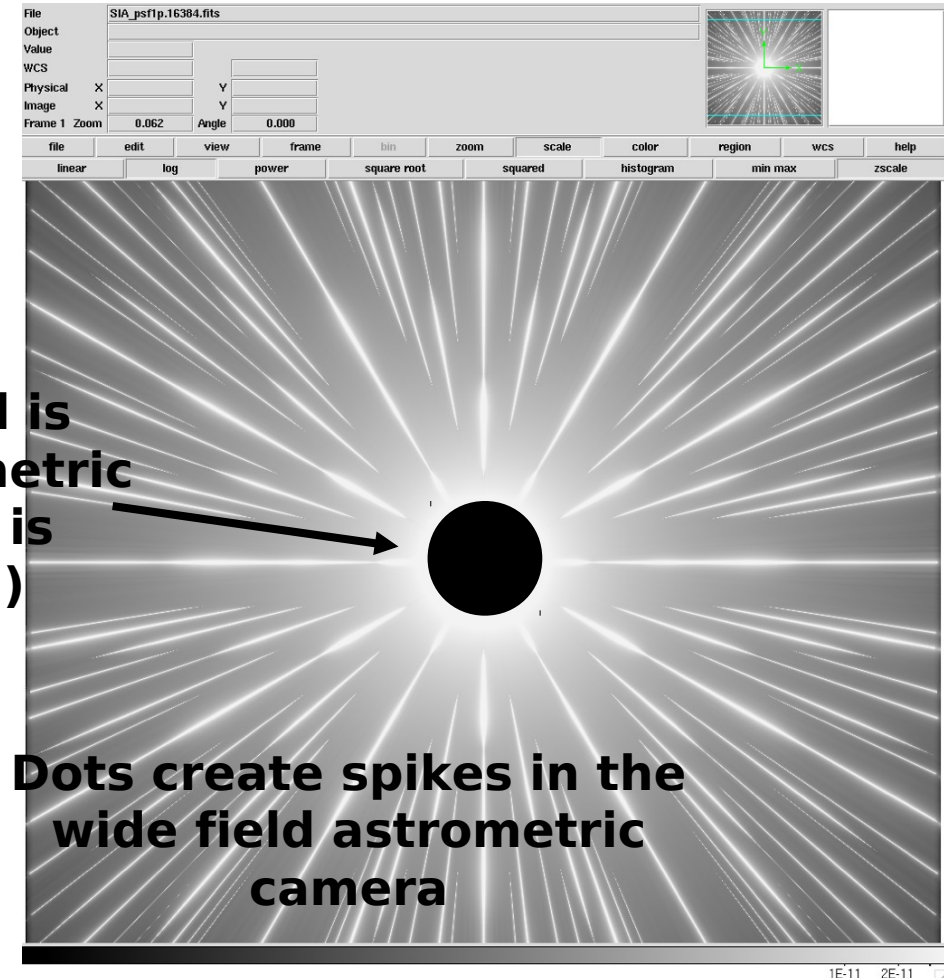
Baseline assumes no special requirements on detector or optics, other than a design to support wide field imaging and dots on M1: ASTROMETRY DOES NOT DRIVE TELESCOPE OR INSTRUMENT DESIGN

- no special detector requirements (standard errors on flat field, geometry), assumes no calibration beyond what is “standard”
- no component requirement exceeds what has already been demonstrated and manufactured
- assumes no data calibration is done between observations of different stars (pessimistic)
- fraction of primary mirror covered by dots kept small (1%) to avoid loss in sensitivity for general astrophysics and coronagraphy

Dots on primary mirror create a series of diffraction spikes used to calibrate astrometric distortions



The center of the field is missing from the astrometric camera (central light is sent to coronagraph)

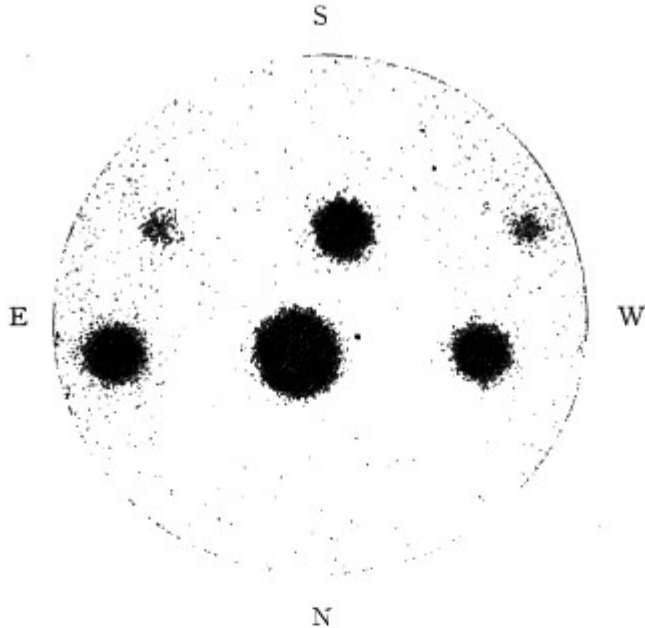


Primary mirror is covered with small dots

Dots create spikes in the wide field astrometric camera

All astrometric distortions (due to change in optics shapes of M2, M3, and deformations of the focal plane array) **are common to the spikes and the background stars**. By referencing the background star positions to the spikes, the astrometric measurement is largely immune to large scale astrometric distortions.

Instead of requiring ~pm level stability on the optics over yrs, the stability requirement on M2, M3 is now at the nm-level over approximately a day on the optics surfaces, which is within expected stability of a coronagraphic space telescope. (Note: the concept does not require stability of the primary mirror).



A 5-seconds exposure of Castor, enlarged 75 times. The separation of the components is 3".74 or 0.198 mm on the plate. The first order spectra are one magnitude fainter than the central image. Taken December 1, 1939, by K. Aa. Strand, with the Sproul 24-inch refractor, aperture reduced to 13 inches, Eastman IV G emulsion, Wratten No. 12 (minus-blue) filter.

age of the fainter component, a compensation for possible magnitude error is provided by using the mean of the measured positions of the two spectral images instead of the central image. As long as the difference in intensity between the images does not exceed half a magnitude, the magnitude error is usually negligible; it is therefore sufficient to have a limited number of gratings, producing first-order spectra which are a whole number of magnitudes fainter than the central image. For example, in his work with the Sproul refractor, Strand^a used four gratings, made of duraluminum, giving differences of one, two, three, and four magnitudes, respectively, between the central image and the first-order spectra. The bars are mounted on 10 cm-wide annular frames, cut from sheets of duraluminum, 3 mm thick. The constants of the four gratings are given below.

CONSTANTS OF SPROUL OBJECTIVE GRATINGS

Grating	—width of— bar	opening	extinction for central image	first order minus central image mag. difference	distance
1	11.25 mm	11.21 mm	1.51 mag	.98 mag	.270 mm = 5".10
2	7.12 mm	15.06 mm	.84 mag	2.05 mag	.273 mm = 5.15
3	3.98 mm	14.80 mm	.52 mag	3.01 mag	.322 mm = 6.08
4	3.20 mm	19.06 mm	.34 mag	3.95 mag	.272 mm = 5.13

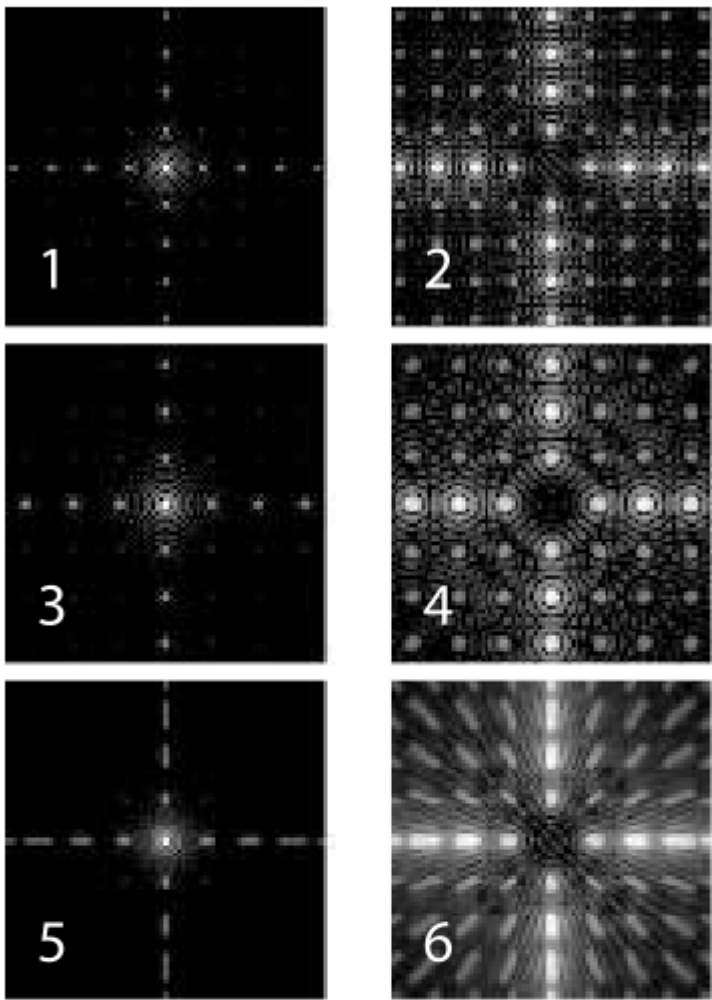
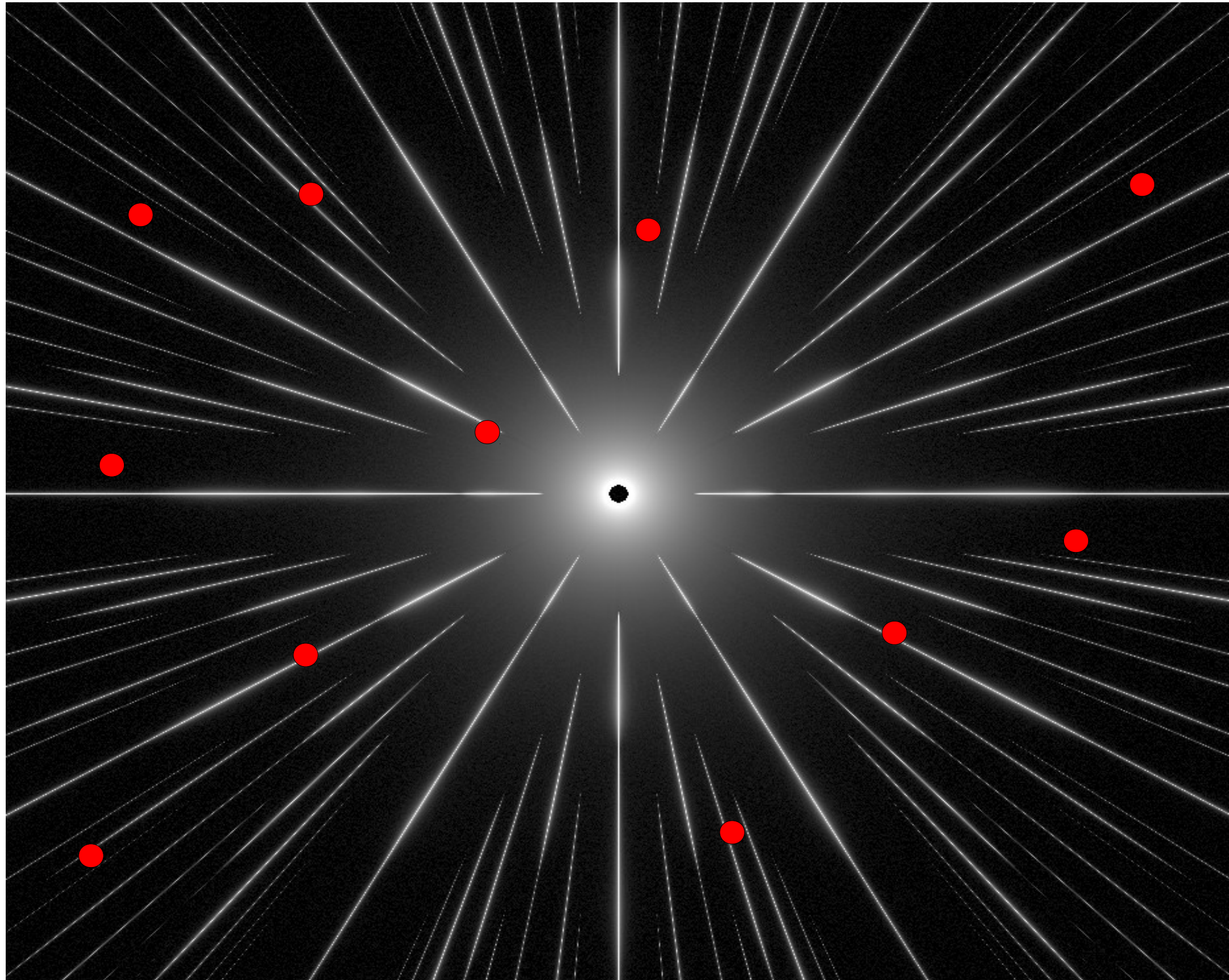


FIG. 1.—Monochromatic and broadband direct and coronagraphic PSFs with a square-geometry reticulate pupil mask. All images are on a logarithmic gray scale stretching 10 mag fainter than their peaks. The pupil is 128 pixels across, and the grid has a wire spacing of 16 pixels, with 2-pixel-wide wires. (1): Direct PSF for the shortest wavelength of a 20% bandwidth filter with uniform transmission within the bandpass, in the absence of phase errors. The satellite PSFs off the origin but along the horizontal and vertical axes are fainter than the central core of the PSF by a factor $\epsilon^2 = (g/d)^2$, where g is the wire thickness and d is the wire spacing. The satellite spots off the axes are ϵ^4 fainter than the corresponding central peak. (2): Coronagraphic PSF at the shortest wavelength of the filter. The off-axis sea of satellite spots are more visible in the coronagraphic image because the core has been suppressed. (3) and (4): Direct and coronagraphic PSFs for the longest wavelength of the filter. (5) and (6): Direct and coronagraphic PSF for the full bandpass. The length of any particular radial streak in this last pair of images (in resolution elements at the central wavelength of the bandpass) is approximately the fractional filter bandwidth multiplied by the radial distance of the spot at band center. The streaks all point toward the origin, so the smearing has no effect on astrometric precision according to Fraunhofer regime image formation theory. We suggest using the four satellite peaks closest to the core as fiducials for the position of the central occulted star in coronagraphic images.

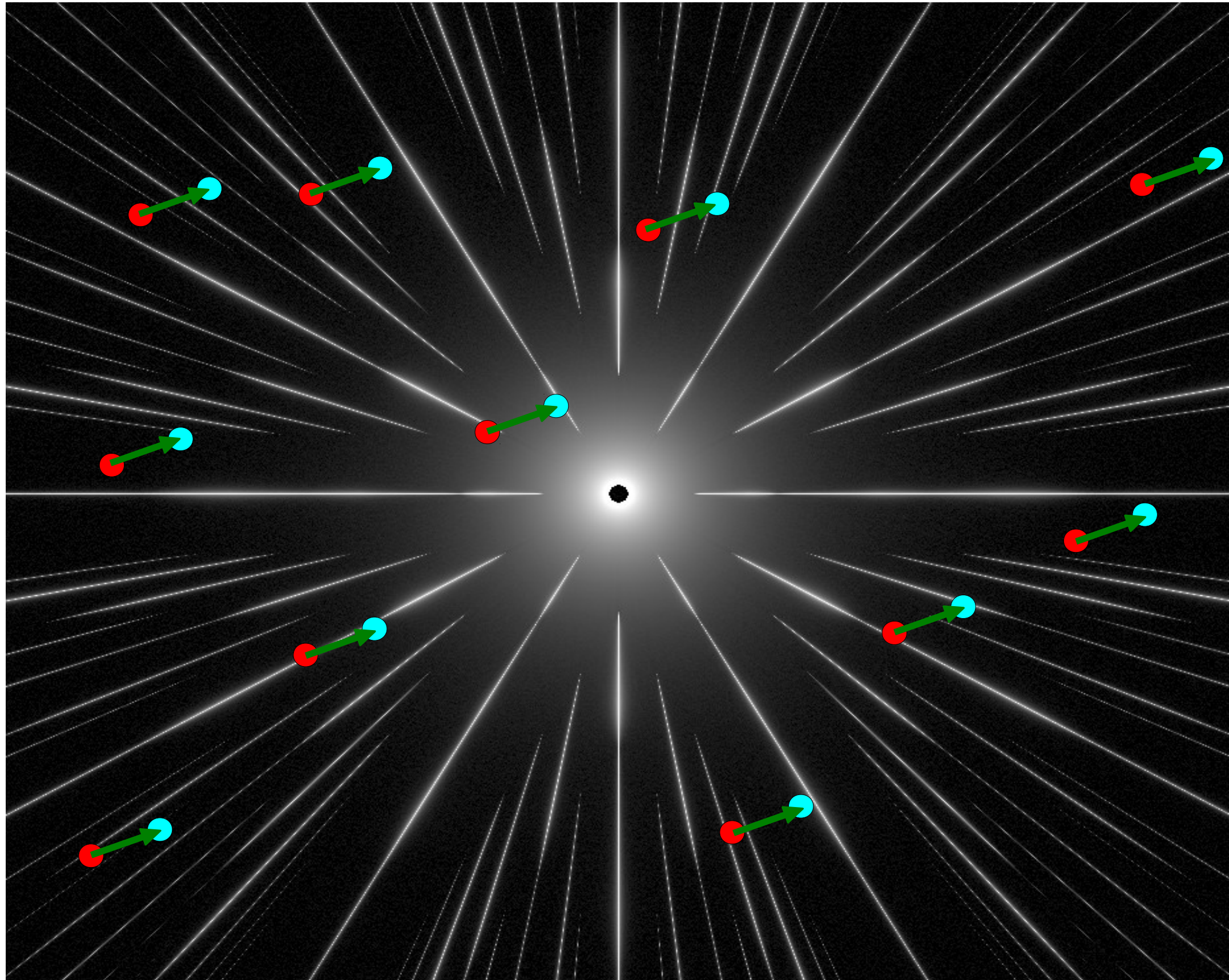
“Long-focus photographic astrometry”, van de Kamp, 1951

“Astrometry and Photometry with Coronagraphs”, Sivaramakrishnan, Anand; Oppenheimer, Ben R., 2006

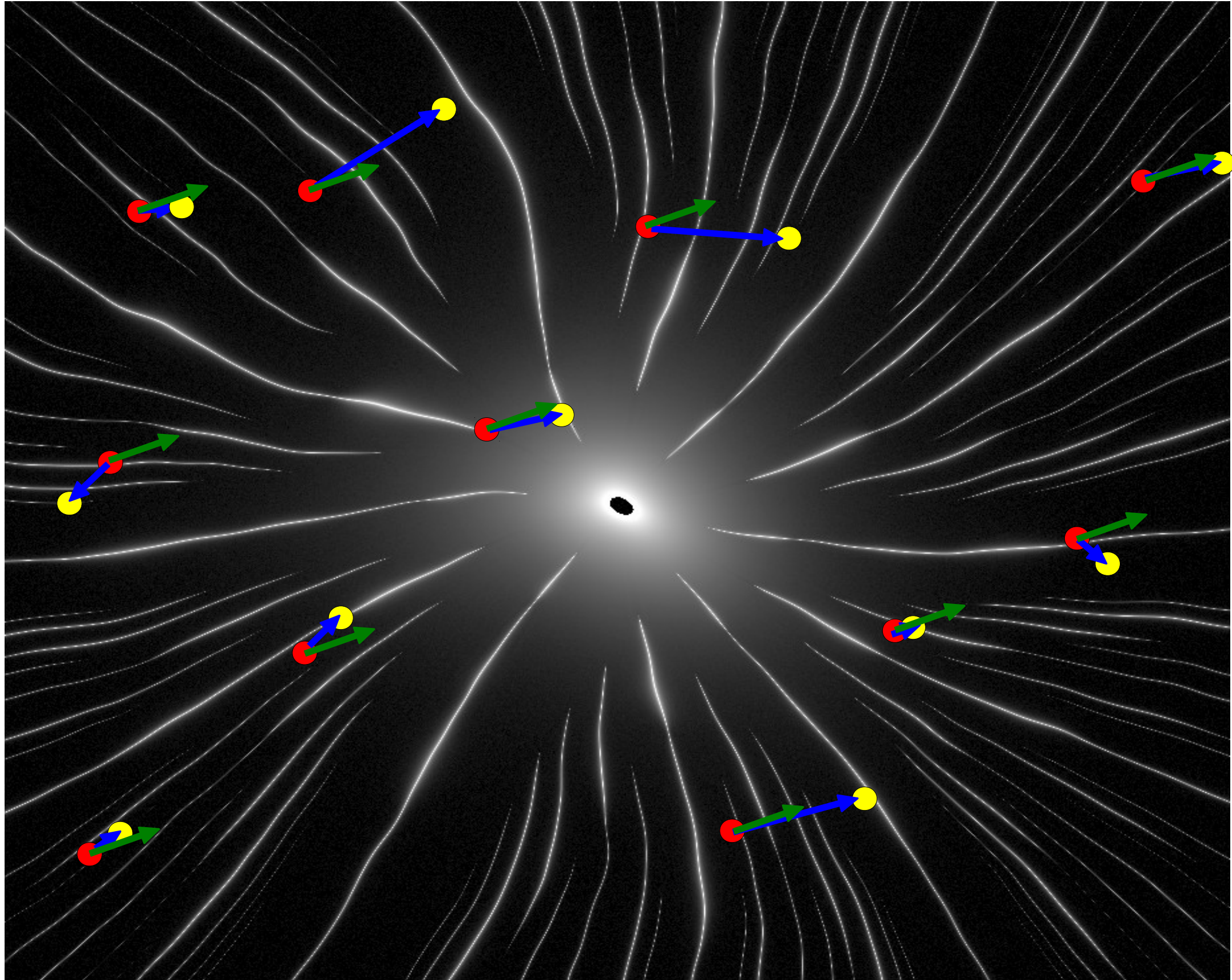
Red points show the position of background stars at epoch #1 (first observation)



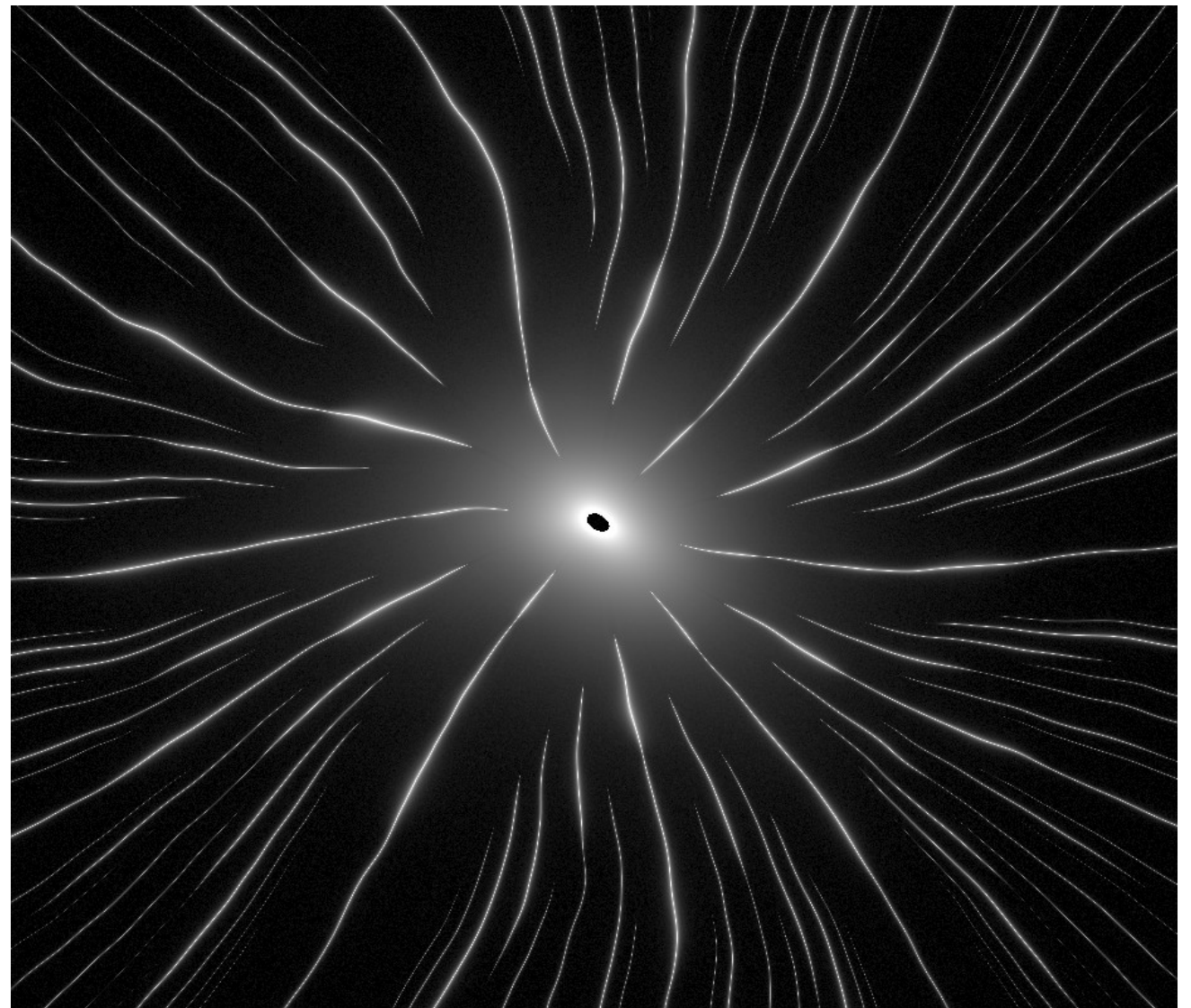
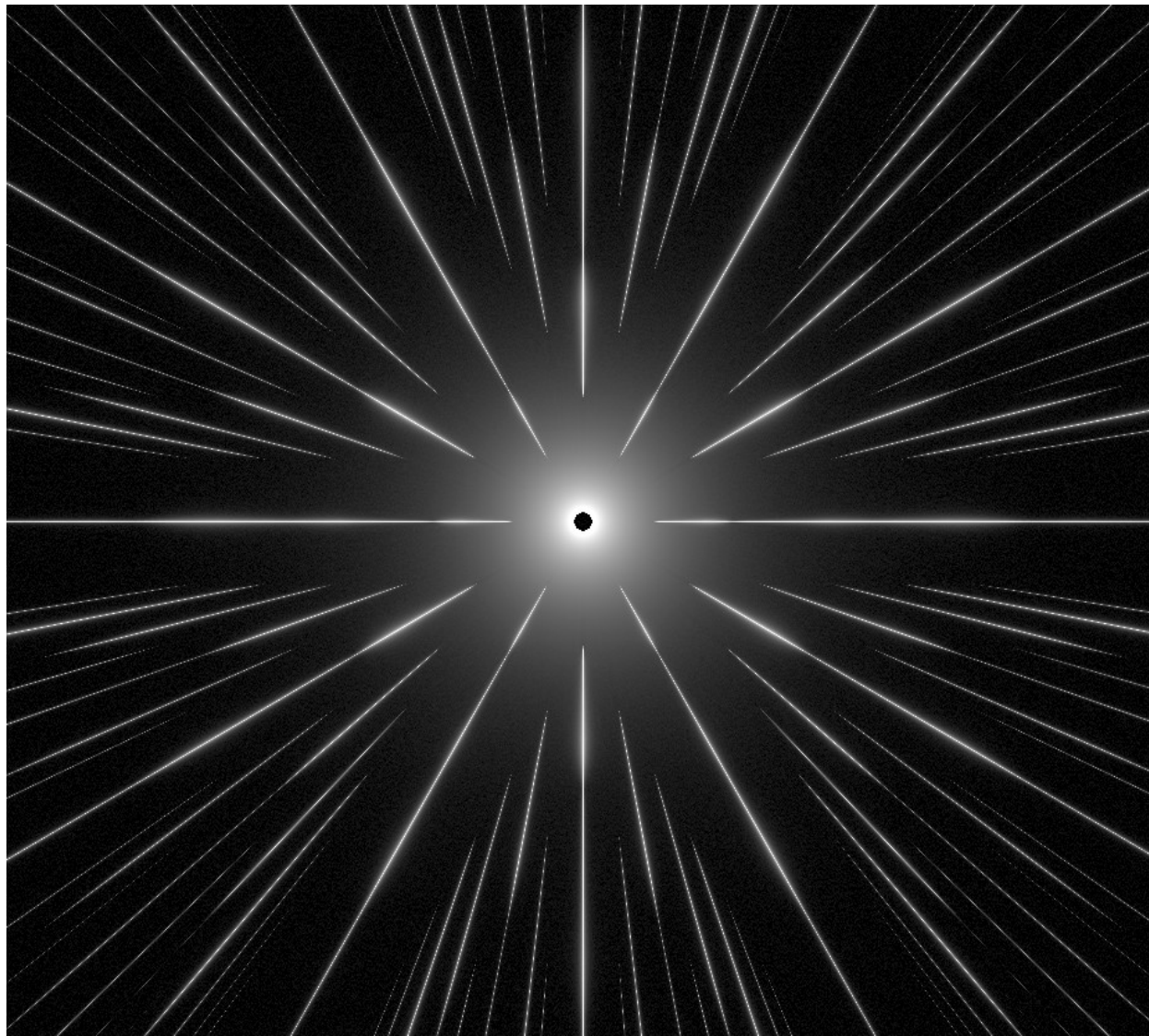
**Blue points show the position of background stars at epoch #2 (second observation)
The telescope is pointed on the central star, so the spikes have not moved between
the 2 observations, but the position of the background stars has moved due to the
astrometric motion of the central star (green vectors).**



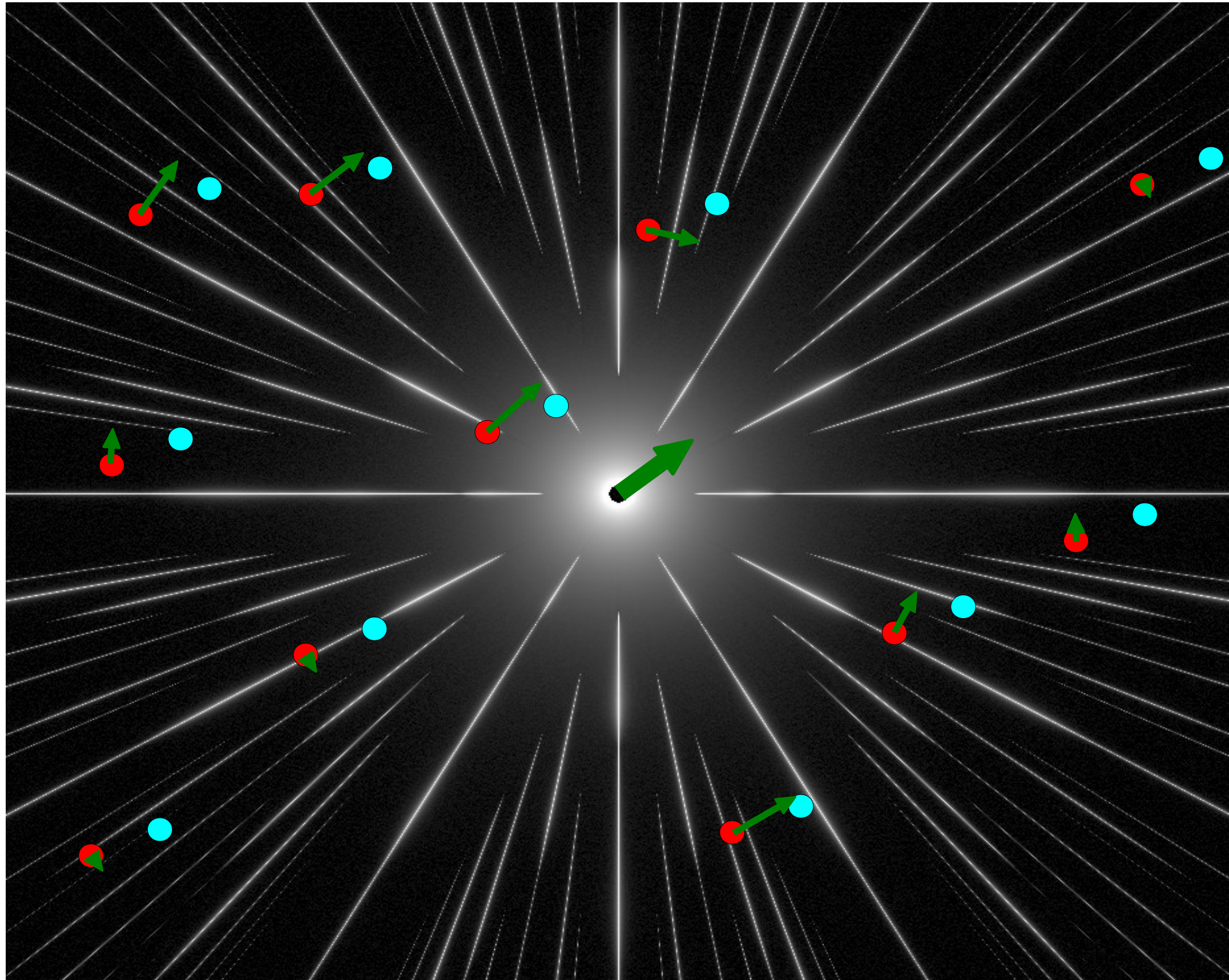
Due to astrometric distortions between the 2 observations, the actual positions measured (yellow) are different from the blue point. The error is larger than the signal induced by a planet, which makes the astrometric measurement impossible without distortion calibration.



The measured astrometric motion (blue vectors in previous slide) is the sum of the true astrometric signal (green vectors) and the astrometric distortion induced by change in optics and detector between the 2 observations. Direct comparison of the spike images between the 2 epochs is used to measure this distortion, which is then subtracted from the measurement to produce a calibrated astrometric measurement.



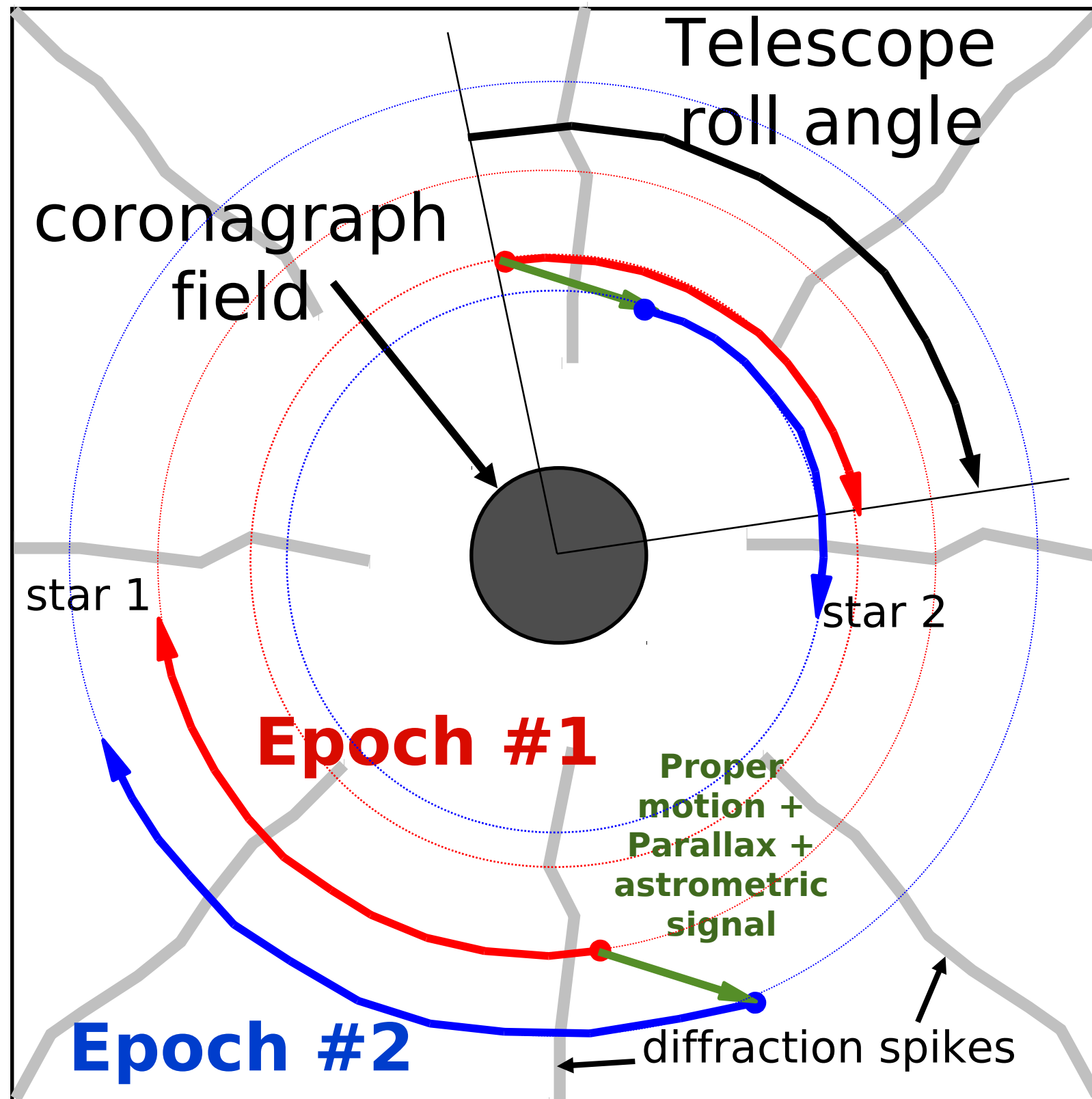
The calibration of astrometric distortions with the spikes is only accurate in the direction perpendicular to the spikes length. For a single background star, the measurement is made along this axis (1-D measurement), as shown by the green vectors. The 2-D measurement is obtained by combining all 1-D measurements (large green vector).



Observation scheme

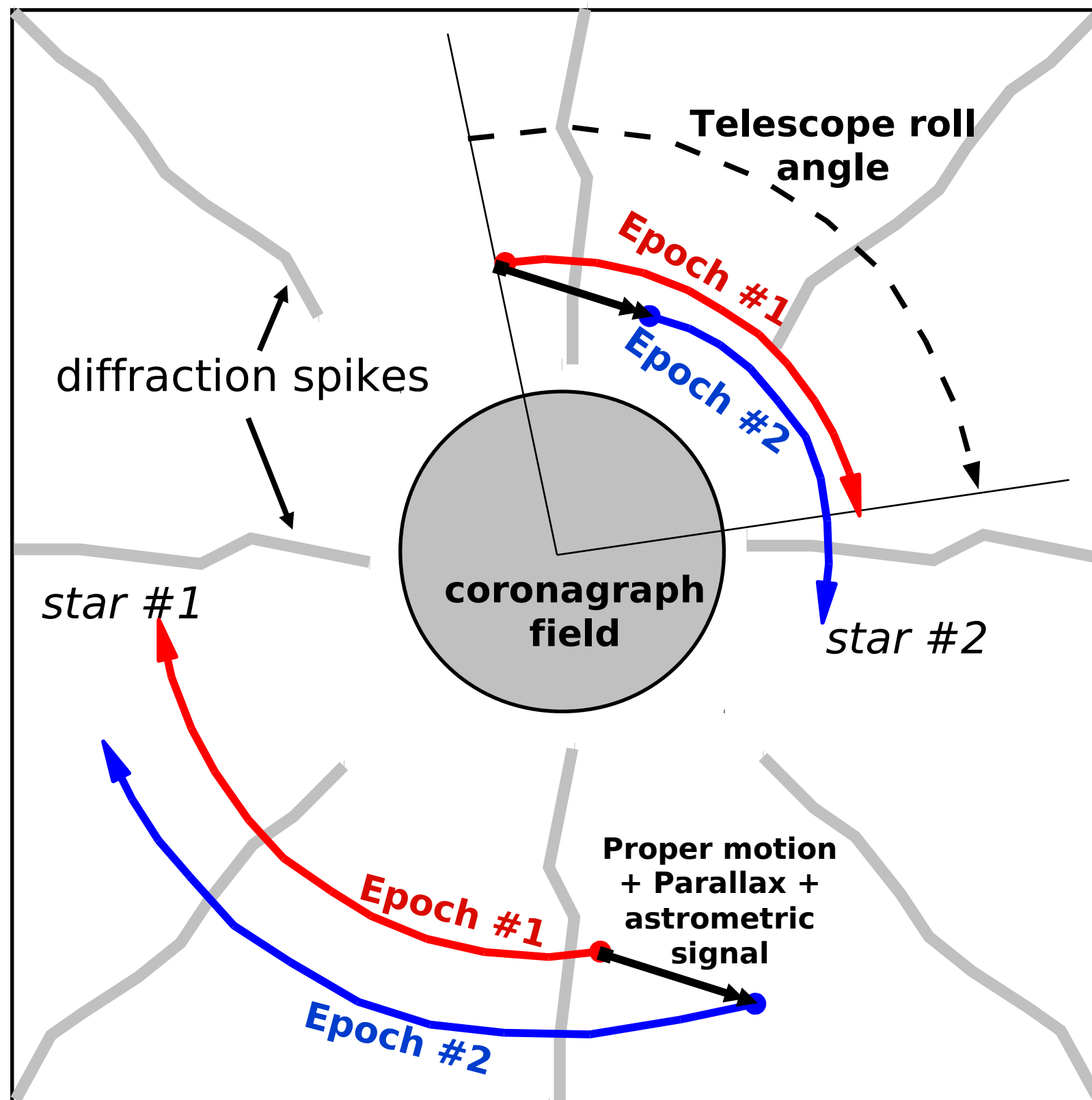
A slow telescope roll is used to average out small scale distortions, which are due to non-uniformity in the pixel size, (spectral) response, and geometry

The green vector is what should be measured



Observation scheme

A slow telescope roll is used to average out small scale distortions, which are due to non-uniformity in the pixel size, (spectral) response, and geometry



Science goals and
required astrometric
accuracy

Science goals

Primary science goal:

Measure planet mass with 10% accuracy ($1-\sigma$) for an Sun/Earth analog at 6pc.

This allows mass measurement of all potentially habitable planets (Earth-like & SuperEarths) imaged by PECO.

SNR>5 detection at $R=5$ in less than 6 hrs along 20% of the planet orbit, assuming 45% system efficiency, and 1 zodi (no WF errors)

Table 4-2: Stars with Earth-like planets in habitable zones (1 AU equiv) easily detectable with PECO

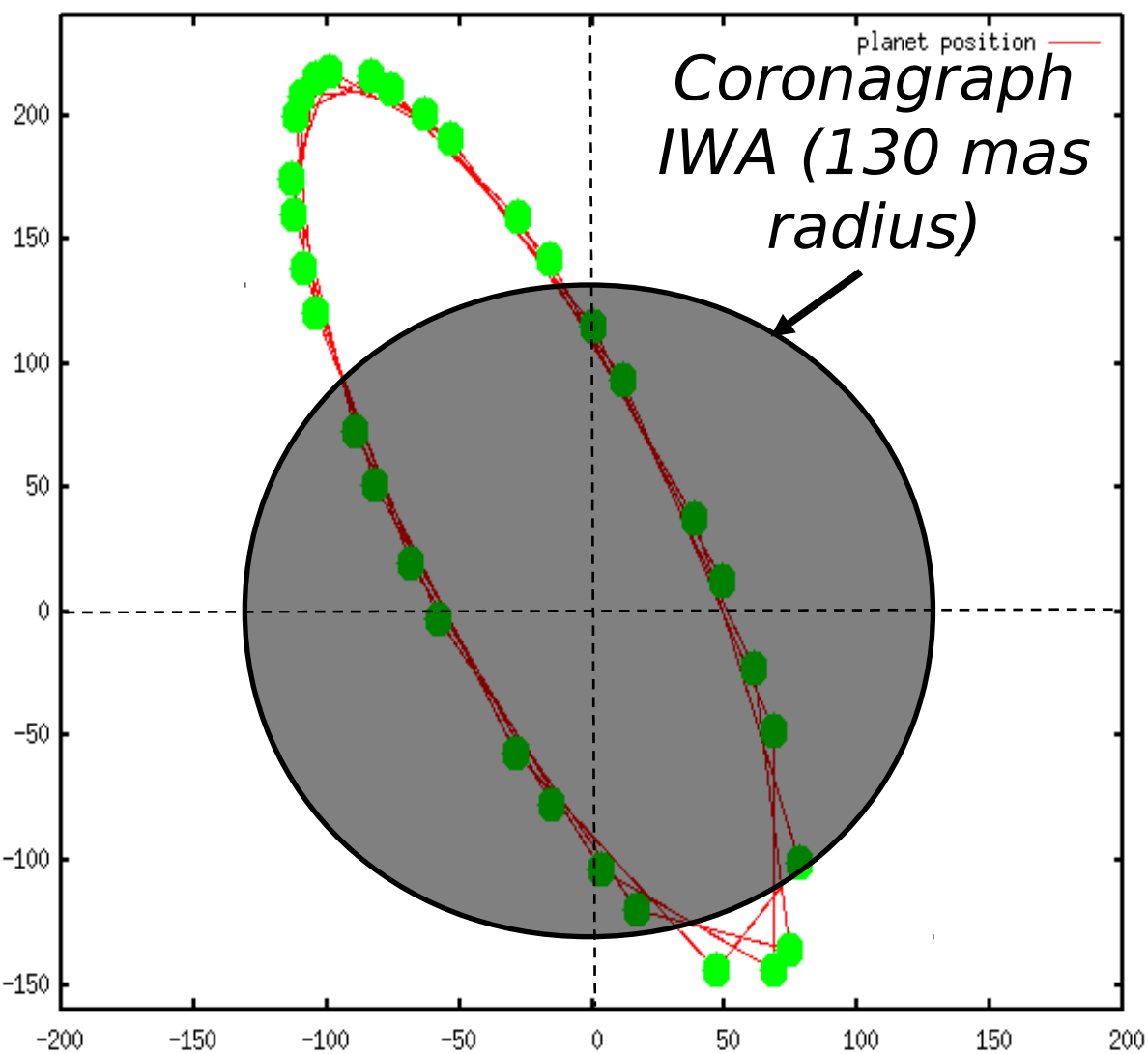
HIP#	dist (pc)	max el (λ/D)	*rad (λ/D)	SNR (1s, tp)	t20% (s, tp)	Comment
71683	1.3	11.5	0.06	0.49	35	Alf Cen A G2 V, V=0
71681	1.3	6.6	0.04	0.45	44	Alf Cen B K2 IV, V=1.3
8102	3.6	2.3	0.01	0.08	2750	Tau Cet G8.5 V, V=3.5 **
16537	3.2	2.2	0.01	0.09	2968	Eps Eri K2 V, V=3.7 **
3821	6.0	2.3	0.01	0.04	14329	Eta Cas G0 V V=3.5 ***
2021	7.5	3.1	0.01	0.03	14878	Bet Hyi G0 V, V=2.8
99240	6.1	2.2	0.01	0.03	19636	Del Pav G8 IV, V=3.6

Table extracted from PECO SRD (http://caao.as.arizona.edu/PECO/PECO_SRD.pdf)

Simulated observations

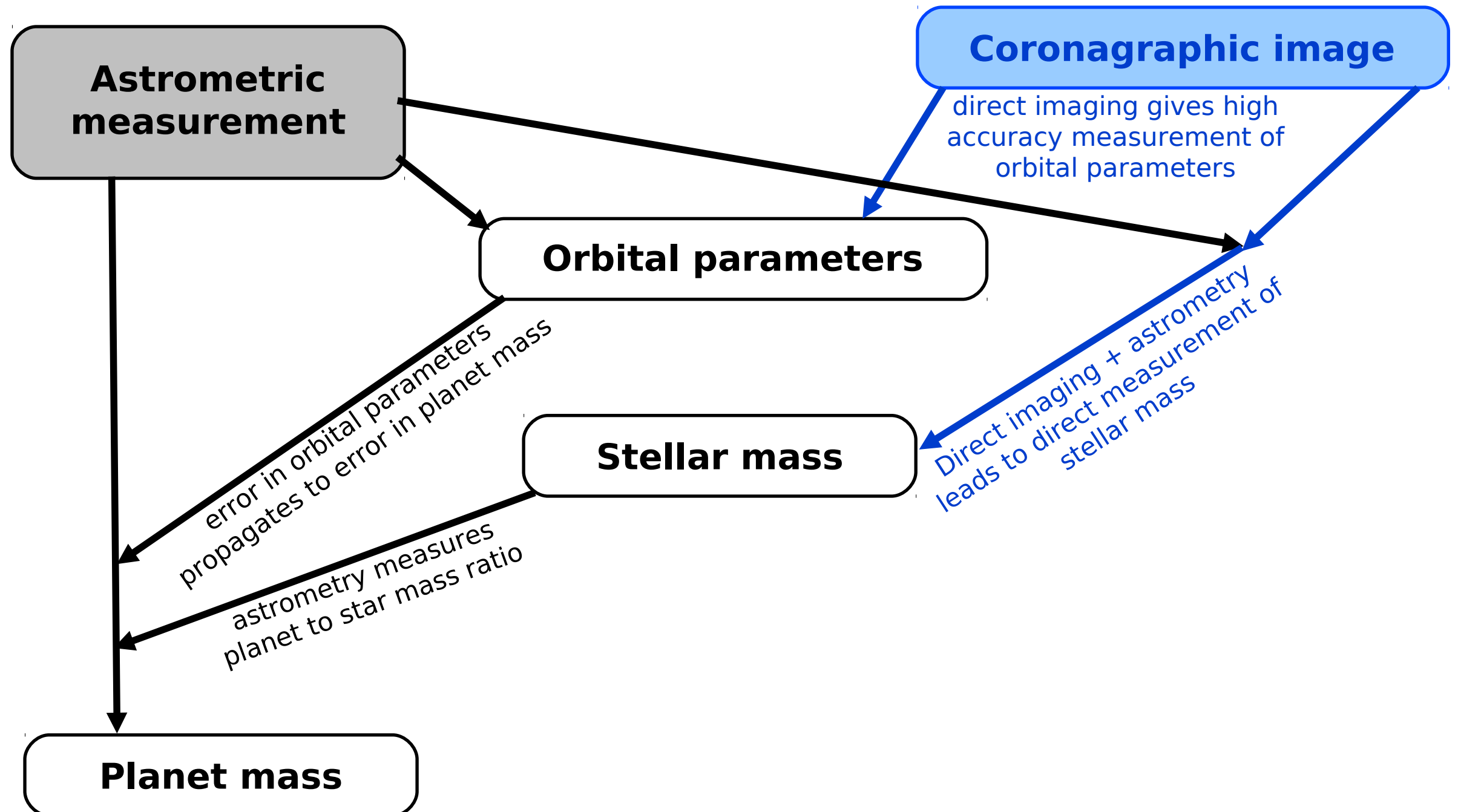
Planetary system characteristics	
Star	Sun analog
Distance	6 pc
Location	Ecliptic pole
Orbit semi-major axis	1.2 AU
Planet mass	1 Earth mass
Orbit excentricity	0.2
Astrometric signal amplitude	0.5 μ as
Orbit apparent semi-major axis	200 mas
Observations	
Number of observations	32 (regularly spaced every 57 days)
Coronagraph: planet position measurement accuracy in coronagraphic image	2.5 mas per axis (= 3.6 mas in 2D): corresponds to diffraction-limited measurement with 100 photon at 550 nm on PECO
Coronagraph: Inner Working Angle	130 mas (coronagraph cannot see planet inside IWA)
Astrometry: accuracy	Variable (to be matched to science requirements)

Combined solution for simultaneous coronagraphy + astrometry

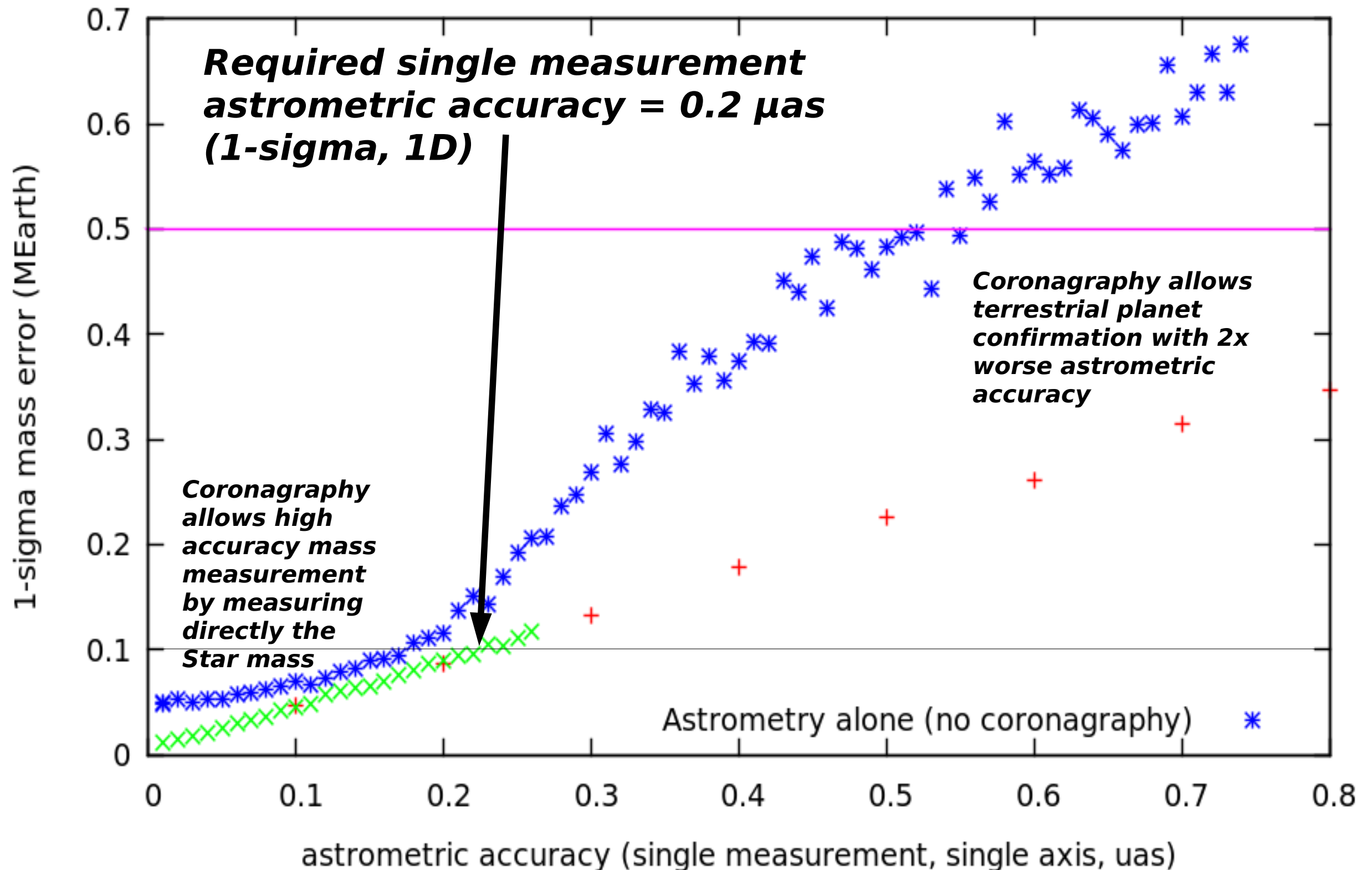


Planet on a 1.2 AU orbit (1.3 yr period), $e=0.2$
orbit orientation on sky: planet outside the
coronagraph IWA for 17 out of the 32
observations.

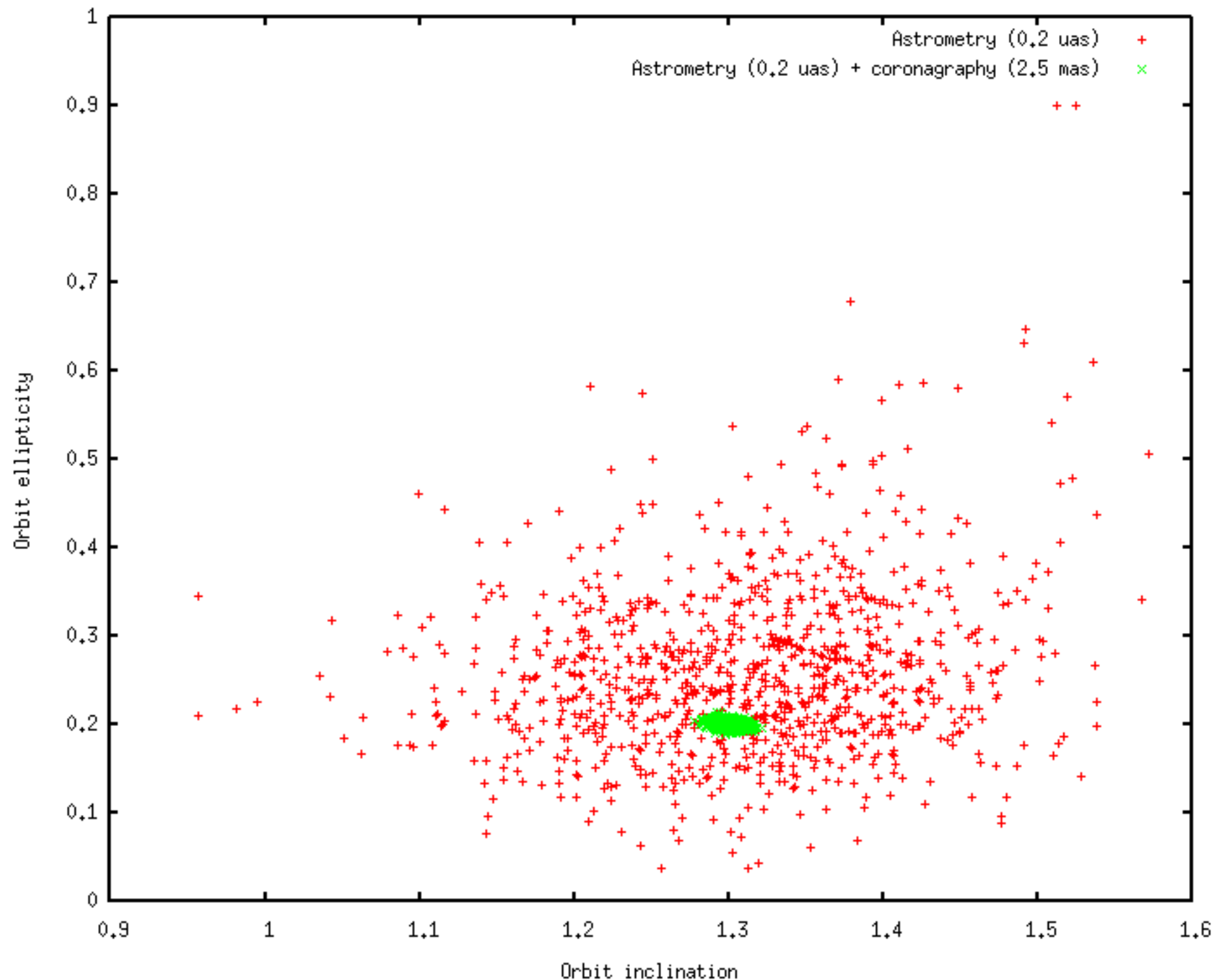
Coronagraphic image measures orbital parameters and stellar mass (with astrometry) -> reduced planet mass error



Combined solution for simultaneous coronagraphy + astrometry



Combined solution for simultaneous coronagraphy + astrometry is very accurate for orbital parameters measurement



Combined solution for simultaneous coronagraphy + astrometry

	Standard deviation	
	Astrometry only	Astrometry + coronagraphy
parallax	0.037 μas	0.035 μas
x proper motion	0.017 $\mu\text{as/yr}$	0.012 $\mu\text{as/yr}$
y proper motion	0.020 $\mu\text{as/yr}$	0.013 $\mu\text{as/yr}$
Planet mass	0.132 ME	0.098 ME
Semi-major axis	0.0228 AU	0.0052 AU
orbital phase	0.653 rad	0.039 rad
orbit inclination	0.0968 rad	0.0065 rad
sma projected PA on sky	0.1110 rad	0.0040 rad
orbit ellipticity	0.098	0.0035
PA of perihelion on orbit plane (w)	0.648 rad	0.0034 rad
stellar mass	0.050 M_{Sun}	0.013 M_{Sun}

~10x better
estimate on
orbital
parameters

Direct stellar
mass
measurement

Exoplanet science with coronagraphy + astrometry + wide field imaging

Provides a complete picture of a planetary system:

CORONAGRAPHY:

- Planets orbits
- Planet atmospheres (spectra, polarization from coronagraph)
- Rotation periods (time photometry from coronagraph)
- Zodiacal cloud: morphology, spectra, polarization (coronagraph)

ASTROMETRY:

- Planet masses

CORONAGRAPHY + CORONAGRAPHY:

- Good census of planets in a system (astrometry + coronagraphy)
- Immunity from confusion issues between multiple planets, zodi clumps
- Immunity from 1yr period blind spot

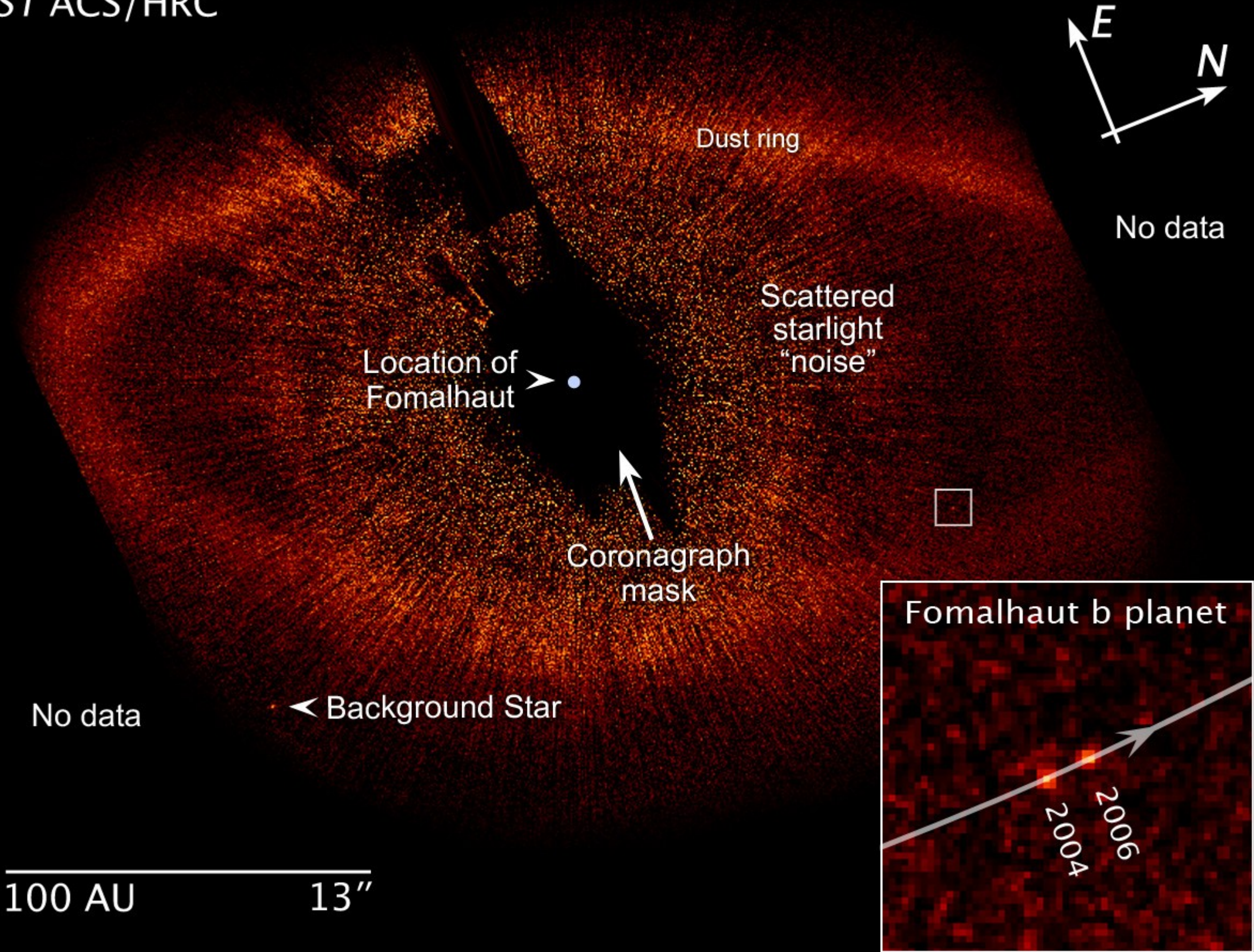
WIDE FIELD IMAGING:

- Very distant planets, possibly ejected
- Debris disks at large separation (Fomalhaut type disks)
- Occultations of field stars by Kuiper belt objects

Also: high precision photometry of field stars

- Microlensing program possible (with pointing to galactic bulge)
stable sharp PSF with good astrometry valuable
- Transit observations

Fomalhaut
HST ACS/HRC



Deep wide field imaging science

Wide field + stable diffraction limited PSF is scientifically valuable for many scientific programs, and will be unique in visible:

- Cosmology: weak lensing, type Ia supernovae
- Galactic astronomy
- Planetary astronomy: search for small & distant objects (asteroids, comets, KBOs)

The dots on PM do not significantly impact sensitivity

Loss in sensitivity is due to 3 effects:

- Light absorbed by the dots → 1% loss in throughput
- Light diffracted out of the PSF core by the dots → 1% loss in flux
- Additional background due to diffraction spikes of central star
 - spikes occupy a tiny fraction of the FOV, and are sufficiently stable to be efficiently removed from images by postprocessing
 - for a $m_V=3.7$ central source, over 95% of the field, additional diffracted light is less than 1% of zodi background
 - mean value for additional diffracted background over the field = 6 ph/pix/day (unfiltered), vs 20000 ph/pix/day for zodi

Astrometric error budget analysis and simulations

Approach & Assumptions

Baseline: 1.4-m telescope, with 0.29 sq deg FOV (0.31 deg radius)

The FOV is chosen to reach performance goal ($0.2 \mu\text{as}$ / measurement) in a sufficiently stable system (Photon noise limited performance for this FOV is $0.044 \mu\text{as}$ single measurement at galactic pole, but actual performance is significantly lower due to distortions and detector limits)

When detailed simulations are required, a smaller FOV system is used ($0.1 \text{ deg radius} = 0.03 \text{ sq deg FOV}$) to ease computations.

Baseline assumes no special requirements on detector or optics, other than a design to support wide field imaging and dots on M1: ASTROMETRY DOES NOT DRIVE TELESCOPE OR INSTRUMENT DESIGN

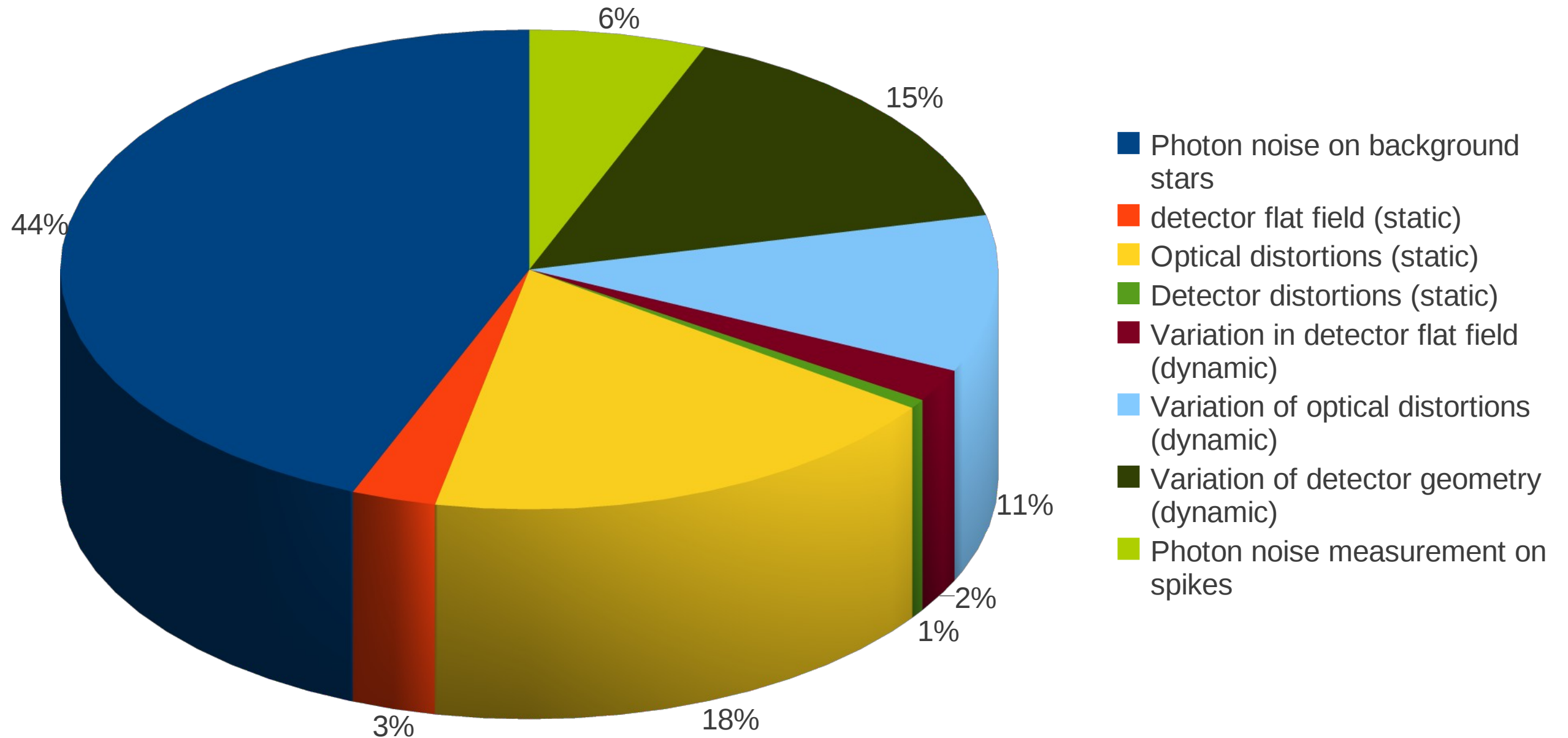
- no special detector requirements (standard errors on flat field, geometry), assumes no calibration beyond what is “standard”
- no component requirement exceeds what has already been demonstrated and manufactured
- assumes no data calibration is done between observations of different stars (pessimistic)
- fraction of primary mirror covered by dots kept small (1%) to avoid loss in sensitivity for general astrophysics and coronagraphy

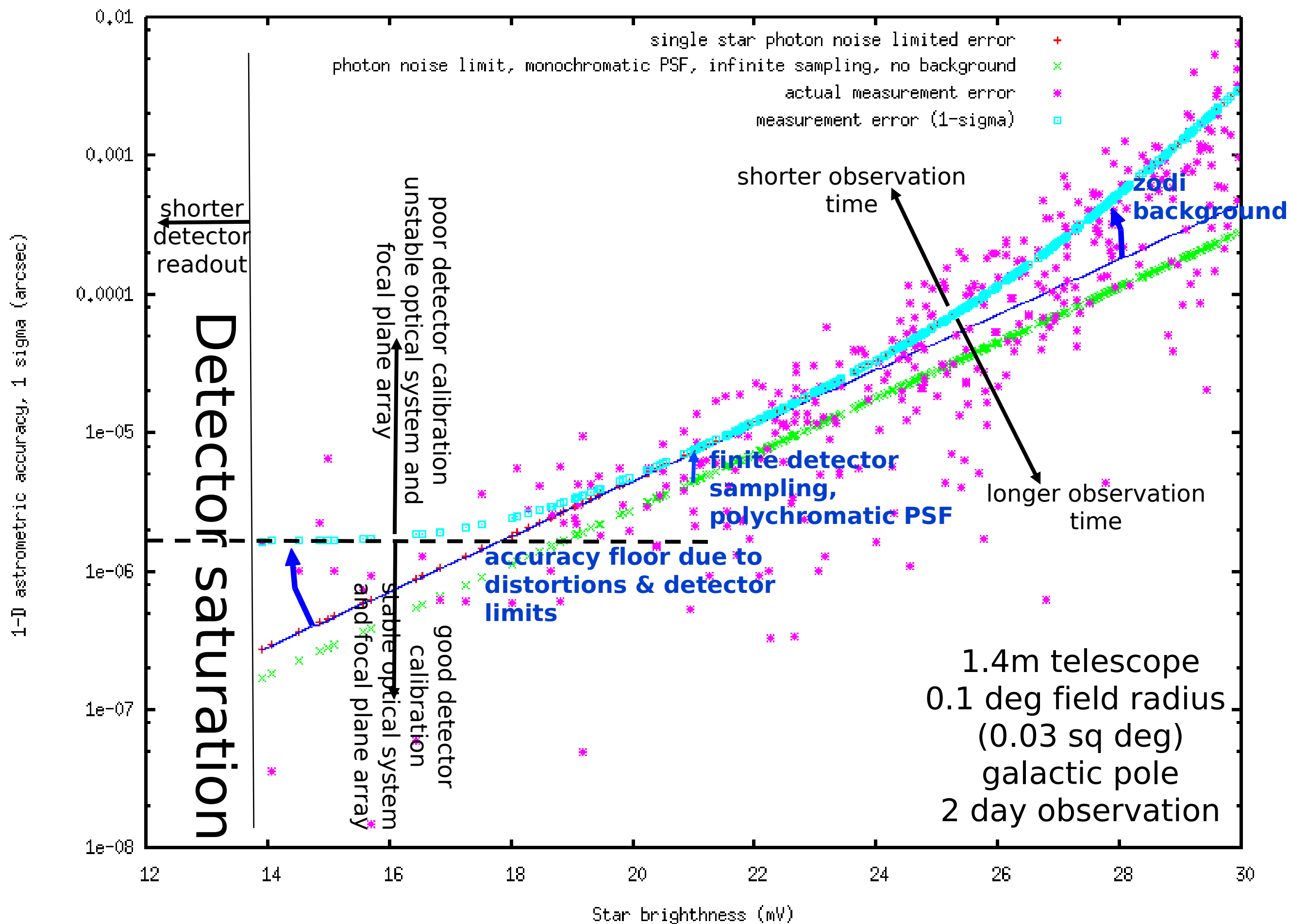
	Baseline design	Value for simulations	Rationale for flight instrument value	Impact on astrometric accuracy
Telescope diameter (D)	1.4 m		PECO sized, cost constrained	Astrometric accuracy goes as D^{-2} , thanks to larger collecting area and smaller PSF size (assuming constant FOV)
Detector pixel size	44 mas		Nyquist at 600 nm	Little impact as long as sampling is close to or finer than Nyquist
Field of view (FOV)	0.29 sq deg (0.31 deg radius)	0.03 sq deg (0.1 deg radius)	low WF error across field, 1.6 Gpix detector	Astrometric accuracy goes as $FOV^{-0.5}$
Single measurement time	48 hr		Typical single observation duration for coronagraph	Astrometric accuracy goes as $t^{-0.5}$
Dot coverage on PM (area)	1%	0.12%	Keeps throughput loss moderate in coronagraph	Larger dot coverage allows observation of fainter sources.
Dot size / pitch (μm)	120 / 932 (black dots)	360 / 2800 (grey dots)	Dot diameter imposed by FOV	More dots = more light in spikes = quicker distortion measurement
Flat field error after calibration, static (high spatial frequency)	1.02% RMS, 6% peak		Conservative estimate for modern detector after calibration	Negligible effect on background PSF measurement (well averaged with roll)
Flat field error, dynamic	0.1% RMS per pixel, uncorrelated spatially and temporally between observations		Undetected cosmic ray impacts on detector	Negligible effect on background PSF measurement, but effect on measurement of spikes locations
Telescope roll	0.33 rad (+/- 10 deg)	1.0 rad (+/- 28 deg)	Manageable PSF elongation at edge of FOV	Larger telescope roll leads to better averaging of detector errors
Uncalibrated change in optics surface between observations for M2 & M3	40 pm		Wavefront measurement repeatability (optical element removed / reinserted) obtained when testing similar sized optics on ground	Larger change in optics surface reduces astrometric accuracy
Static optics surface error (M3 mirror)	1.5 nm		WF error and PSD taken from similar existing optical element	Small impact on performance, as background PSFs are almost fixed between observations
<i>Astrometric accuracy, single measurement, single axis, $m_v=3.7$, galactic pole</i>	<i>0.20 μas</i>	<i>0.63 μas</i>	<i>0.2 μas is required to achieve science goals</i>	

Error budget (baseline system)

	Value	Assumption(s)	Mitigation(s)
Error on background stars position (photon noise, zodi, sampling)	0.128 <i>μas</i>	Galactic pole pointing	Reduce other terms → brighter stars can be used with smaller photon noise
Detector flat field error (static)	0.033 <i>μas</i>	1% RMS, 6% Peak	Better calibration of detector flat field
Optical distortions (static)	0.083 <i>μas</i>	1.5 nm optics for M2 & M3	Better optics
Detector distortions (static)	0.0153 <i>μas</i>	0.2% of pixel size	Project interference fringes on detector
Variation in detector flat field (dynamic)	0.0289 <i>μas</i>	0.1 % RMS	Calibrate flat field regularly
Variation of optical distortions (dynamic)	0.0629 <i>μas</i>	40 pm on surfaces	More stable system More light into spikes Correlate distortions to temperature
Variation of detector geometry (dynamic)	0.0755 <i>μas</i>	~20 mK uncalibrated variations across FPA	More stable temperature control Correlate temperature to distortions Project fringes on detector
Photon noise on spikes	0.0478 <i>μas</i>	Includes zodi photon noise mV = 3.7 star	More light on spikes
TOTAL	0.20 <i>μas</i>	0.2 <i>μas</i> Obtained with 0.29 sq deg FOV	

Error budget: overview (baseline system)





Performance as function of telescope size and FOV (baseline system)

1 % area coverage on PM

$m_v = 3.7$ target

Galactic pole observation

2 day per observation

Larger telescope diameter :

- more light in spikes (D^2), finer spikes ($1/D$) \rightarrow spike calibration accuracy goes as D^{-2}

- more light in background stars (D^2), and smaller PSF ($1/D$) \rightarrow position measurement goes as D^{-2}

Astrometric accuracy goes as D^{-2} FOV $^{-0.5}$

Number of pixels goes as D^{-2} FOV

At fixed number of pixels, larger D is better (FOV can be reduced as D^{-4})

	FOV = 0.03 sq deg	FOV = 0.1 sq deg	FOV = 0.25 sq deg	FOV = 0.5 sq deg	FOV = 1.0 sq deg
D = 1.4 m	0.62 μ as	0.34 μ as	0.22 μ as	0.15 μ as	0.11 μ as
D = 2.0 m	0.30 μ as	0.17 μ as	0.11 μ as	0.07 μ as	0.053 μ as
D = 3.0 m	0.14 μ as	0.074 μ as	0.047 μ as	0.033 μ as	0.023 μ as
D = 4.0 m	0.076 μ as	0.042 μ as	0.026 μ as	0.019 μ as	0.013 μ as

Possible Enhancements (requires changes to telescope design)

Main sources of error:

(1) **optical distortions** (static and dynamic)

Why ? → because of high spatial frequencies in distortions which are not sampled by the spikes (they fall between the spikes)

(2) **variations in detector geometry**

Apodizing the edges of M1 (mitigates issue #1)

→ beam walk effect on M2 and M3 becomes unable to produce distortions that change rapidly with sky position

→ astrometric calibration by spikes becomes much better

Issues:

Small loss in throughput (few % ?)

manufacturing of apodized edge on M1

many issues to check (chromaticity, compatibility with coatings, etc..)

Projecting interference fringes on the detector (mitigates issue #2)

→ allows measurement of detector geometry any time

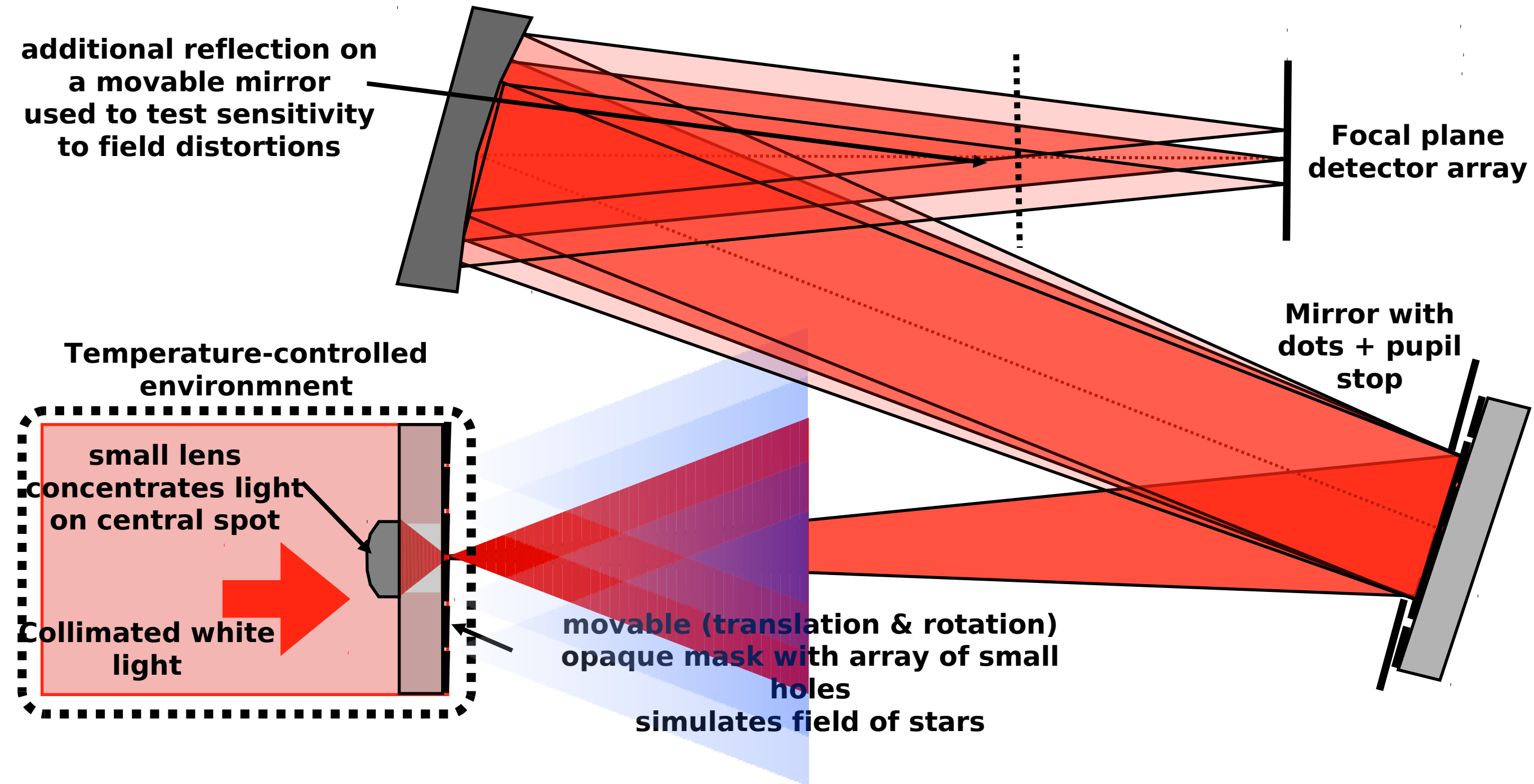
Issues:

Takes time away from observation

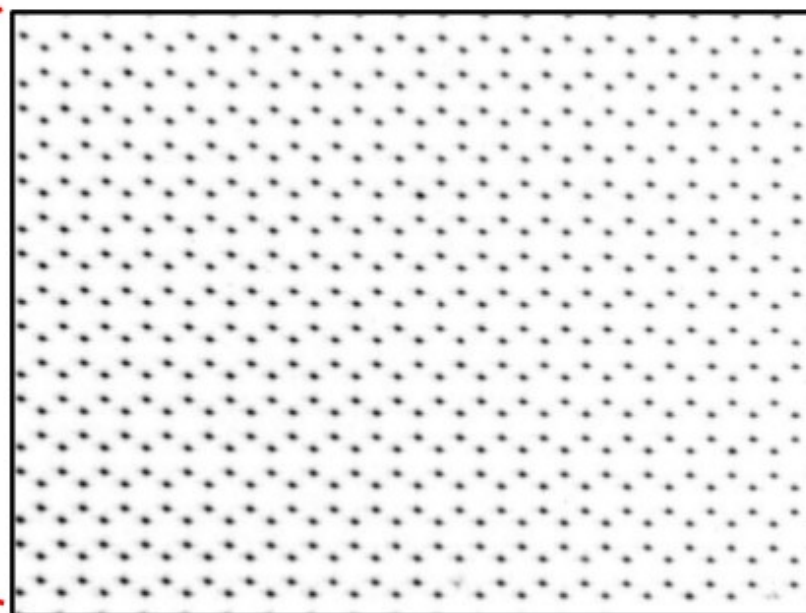
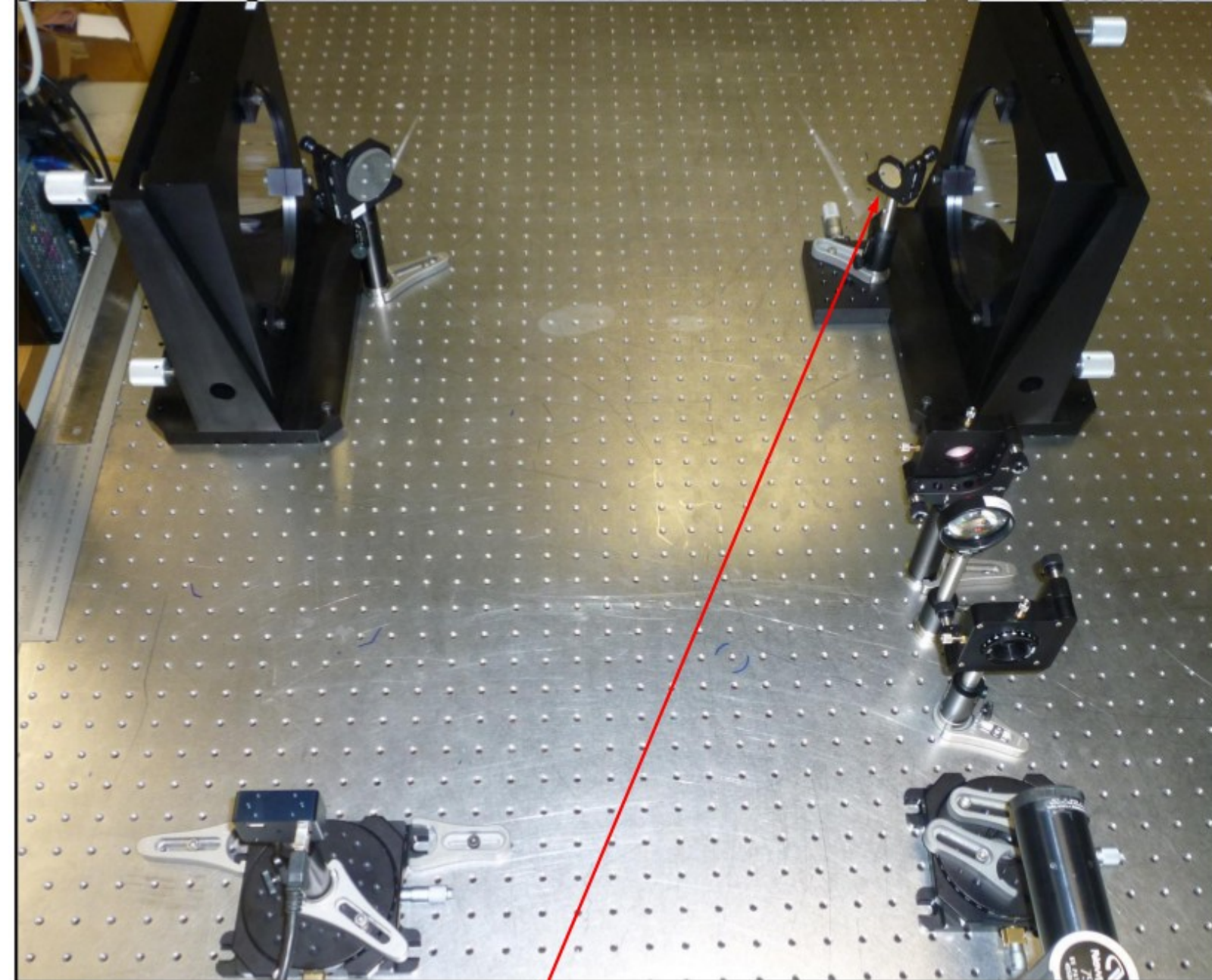
Complexity (add laser, fibers)

Warning: as instrumental errors become smaller, risk and impact of possible companions on field stars increase

lab demo at UofA (Bendek & Ammons)

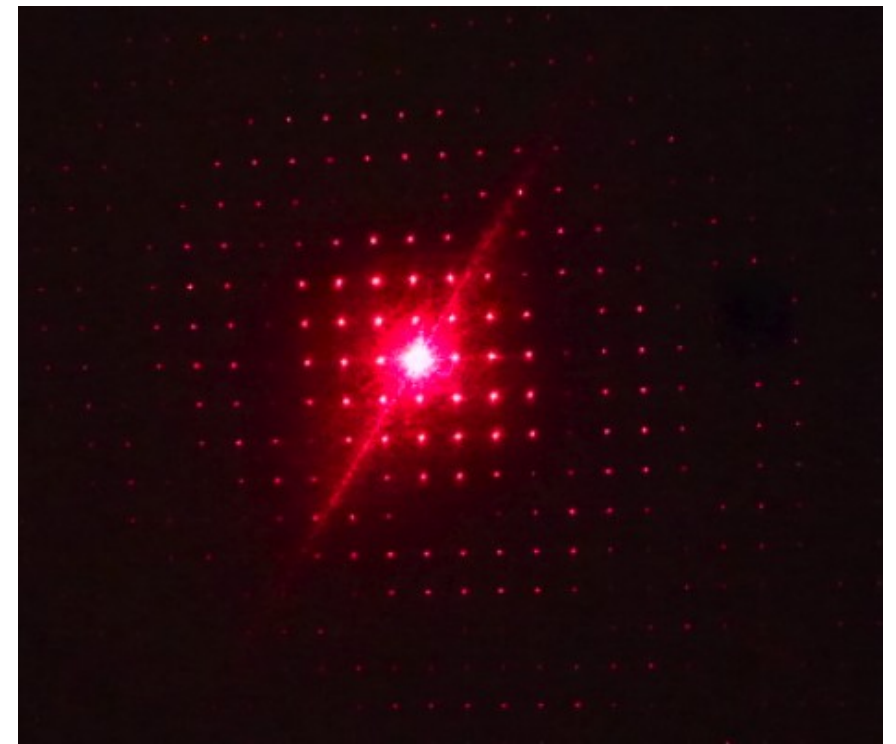
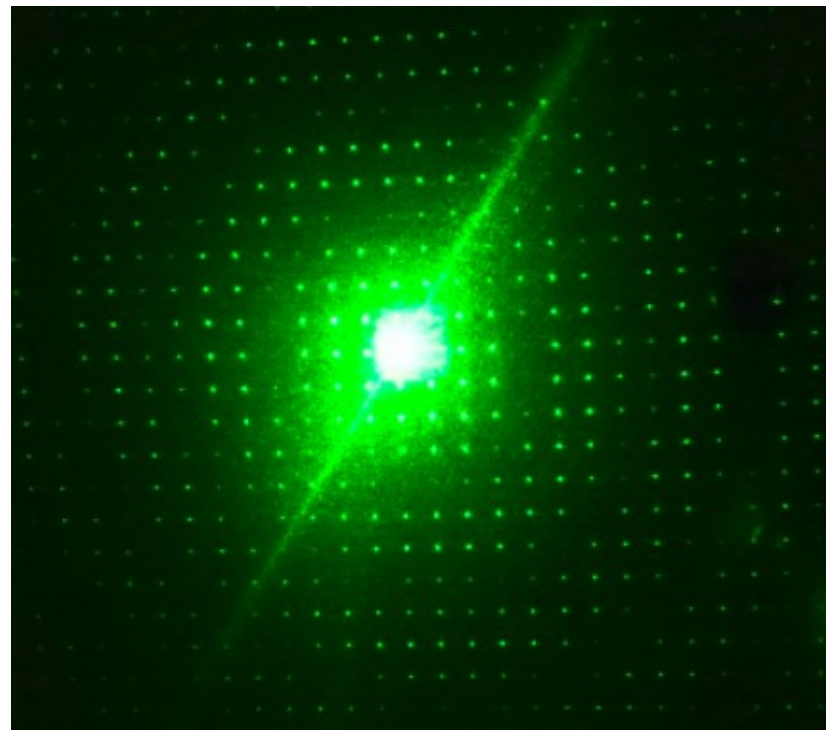
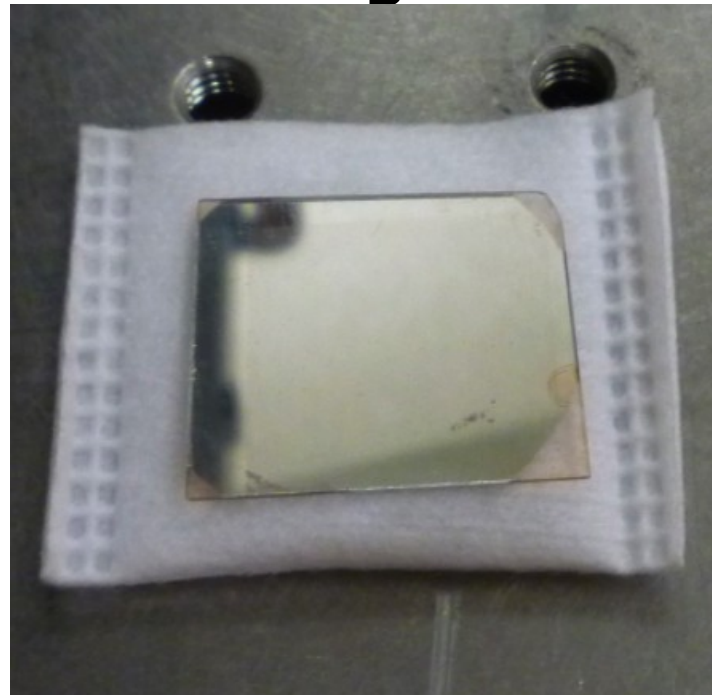


**lab demo at
UofA
(Bendek &
Ammons)**



Preliminary work on mask manufacturing and lab demo at UofA (Bendek & Ammons)

Laser beam reflected on first mask prototype shows main beam (center) + fainter diffraction spots. Spot spacing increases with wavelength.



Mask prototype for lab experiment: 5um holes, 25um apart

NOTE:
For 1.4 m telescope, 0.3 sq deg FOV:
Dot diameter = 120 um
Dot spacing = 932 um





Mag: 101.3 X

Mode: VSI

Surface Data

Date: 11/24/2010

Time: 13:24:50

Surface Statistics:

Ra: 16.03 nm

Rq: 36.93 nm

Rz: 358.76 nm

Rt: 375.54 nm

Set-up Parameters:

Size: 640 X 480

Sampling: 97.76 nm

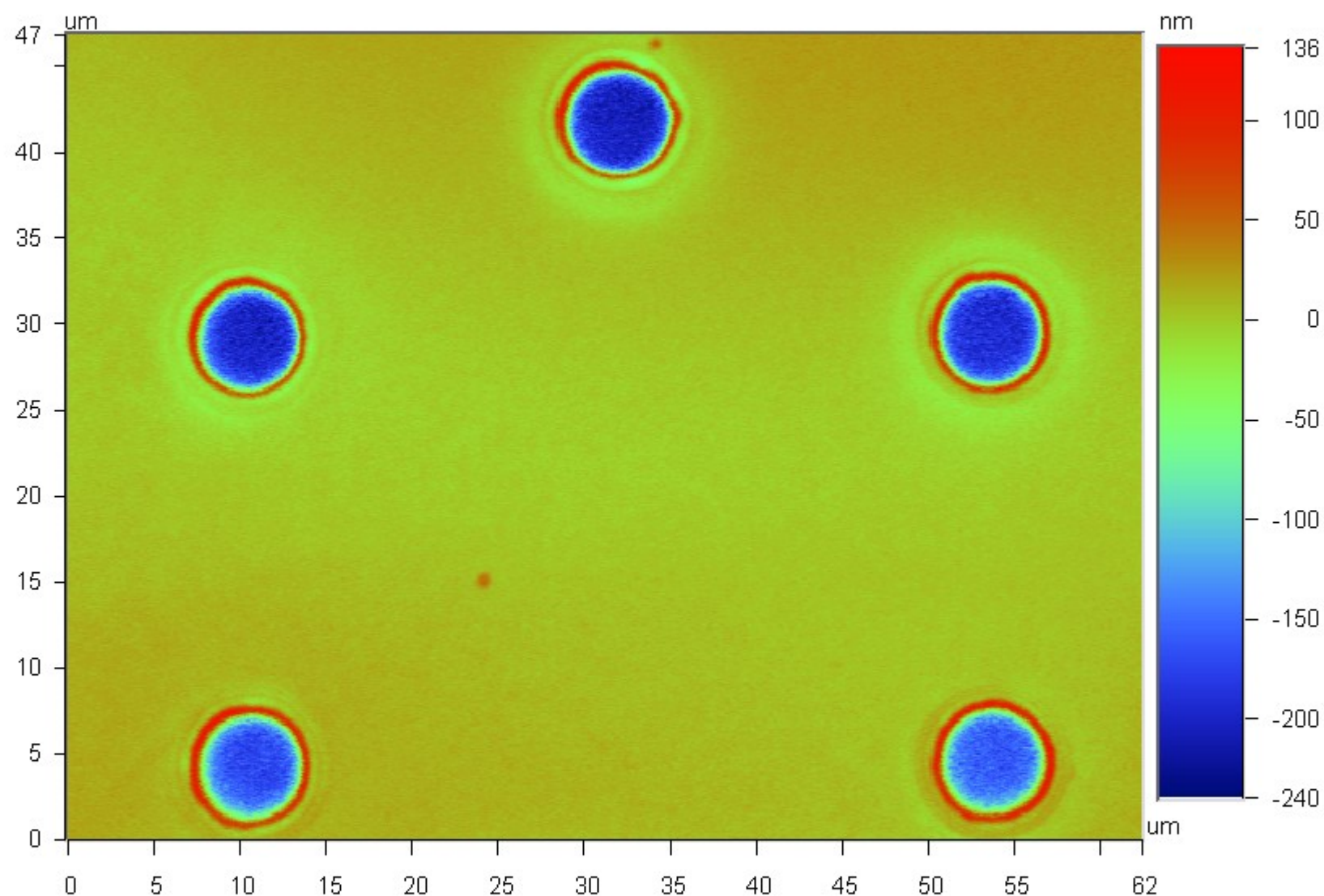
Processed Options:

Terms Removed:

Tilt

Filtering:

None



Title:

Note:

Conclusions

*Coronagraphy, astrometry and wide field imaging can be combined for Simultaneous observation without compromising performance.
Robust concept, relatively insensitive to common astrometric instrumental errors.
→ rich science for both exoplanet science and general astrophysics
→ could be key to gain support and funding for large (>1m) space mission for spectroscopy of habitable exoplanets*

Future work ...

- Lab testbed at UofA: demonstrate performance and algorithms, validate error budget
- Test with coronagraph at NASA Ames and NASA JPL
- We are investigating ground-based system and doing science with it
(Funding from University of Arizona and NASA)

More info ...

Website (includes detailed error budget, algorithms, C source code):

<http://www.naoj.org/staff/guyon/>

→ research → coronagraphic astrometry

Transit spectroscopy
Transit photometry

astrometry

?

***“General”
astrophysics***

coronagraphy



Backup slides

Combined solution derived from simultaneous coronagraphy and astrometry measurements

Known variables:

- **Star location** on the sky (effect of parallax is known except for star distance, aberration of light perfectly known)
- **observing epochs**
- **Stellar mass** (assumed to be known at the 5% accuracy level)
- **measurement noise levels** for astrometry ($\sim \mu\text{as}$), coronagraphy planet position (few mas) and star mass ($\sim 5\%$)

Measurements

Astrometry:

star position
(nb of variables =
 $2 \times \text{\#observations}$)

Coronagraphy:

planet position
(nb of variables =
 $2 \times \text{\#observations}$)

Solution

Maximum likelihood solution for
11 free parameters to be solved for:

- star parallax (1 variables)
- proper motion (2 variables)
- star mass (1 variable)
- planet mass (1 variable)
- orbital parameters (6 variables)

Combined solution from simultaneous coronagraphy and astrometry: method adopted to derive measurement accuracy

Known variables:

- Star location on the sky (effect of parallax is known except for star distance, aberration of light perfectly known)
- observing epochs
- measurement noises on astrometry ($\sim \mu\text{as}$), coronagraphy planet position (few mas) and star mass ($\sim 5\%$)

System defined by 11 free parameters to be solved for:

- star parallax (1 variables)
- proper motion (2 variables)
- star mass (1 variable)
- planet mass (1 variable)
- orbital parameters (6 variables)

Repeat $N \gg 1$ times

Measurements:

Astrometry: star position (2x #observations)

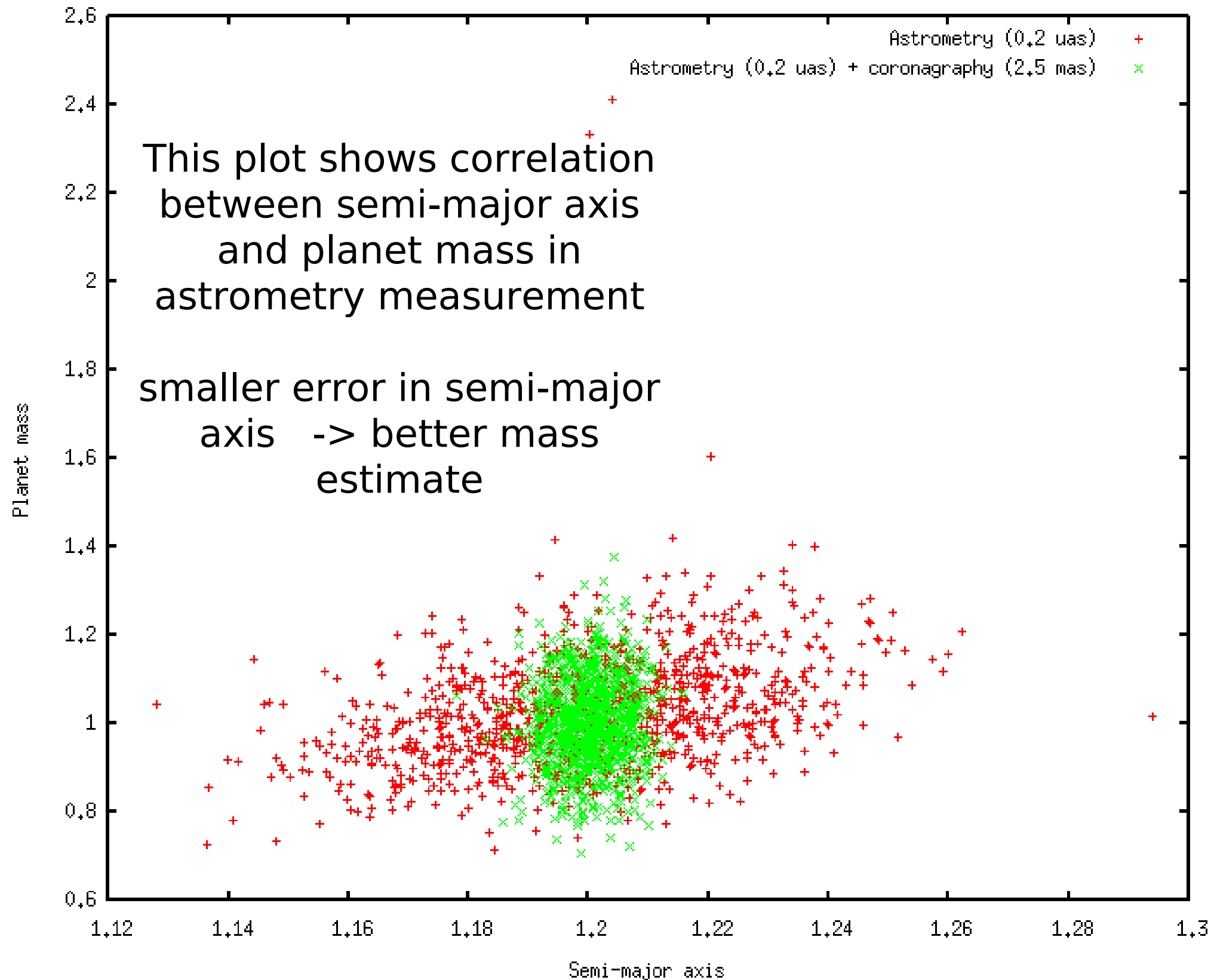
Coronagraphy: planet position (2x #observations)

Stellar mass: derived from stellar luminosity (1)

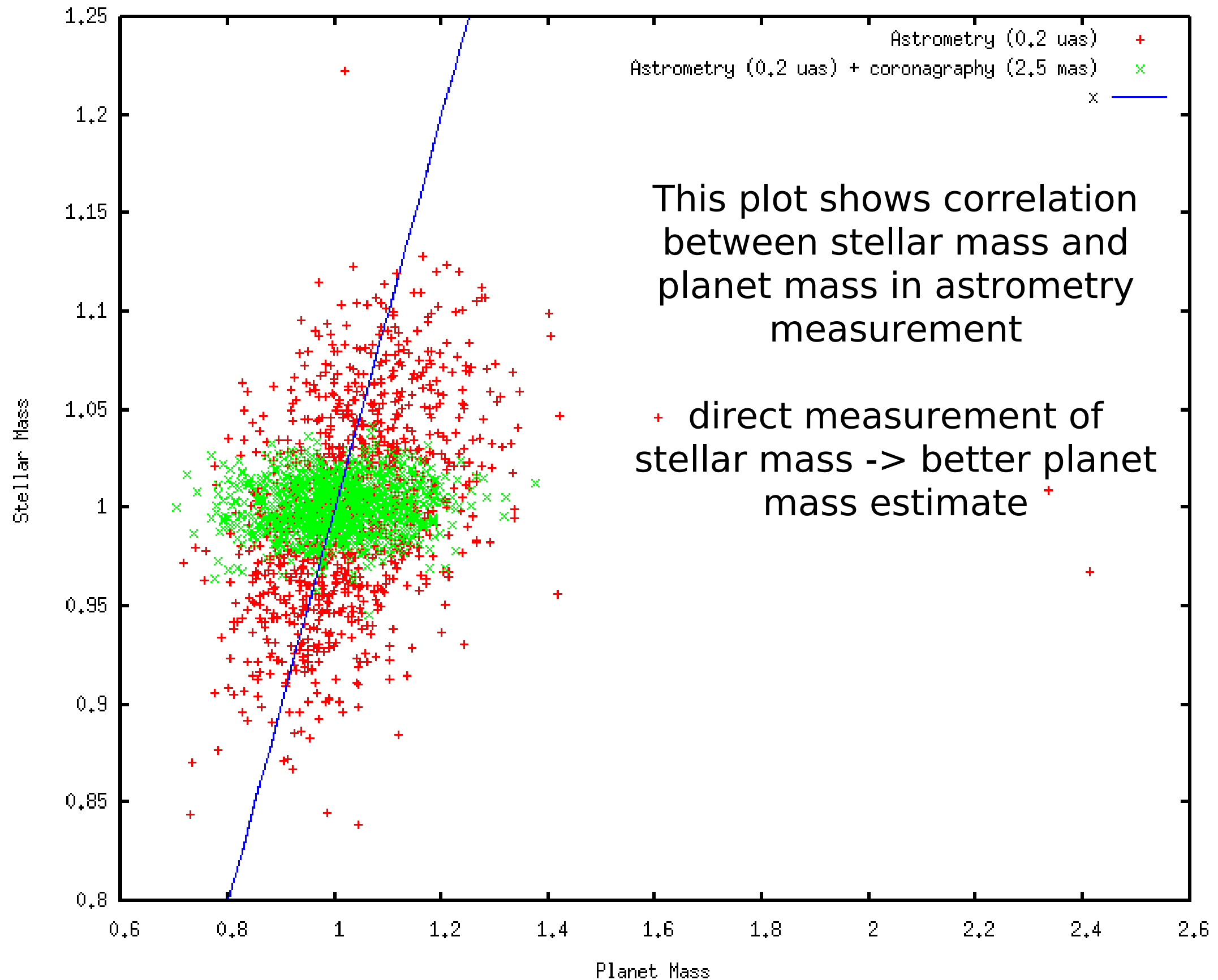
Maximum likelihood solution for 11 parameters

Estimate error on each parameter separately (projection off all solutions on a single axis)
Study covariance between parameters

Better estimate of orbital parameters -> better planet mass estimate



Better estimate of stellar mass -> better planet mass estimate



Benefits of simultaneous coronagraphy + astrometry

Coronagraph images provide an accurate measurement of the orbital parameters (more precise than astrometry), but no mass measurement.

For a 1 M_{Earth} planet on a 200mas radius orbit around a Sun-like star, a 5mas position measurement accuracy in the coronagraphic image ($\sim 1/10 \lambda/D$ in the blue channel of PECO) = $1/40$ orbit radius is equivalent to 0.015 uas astrometric precision.

Note: Position measurement in the coronagraphic image is unlikely to be better than $\sim 5\text{mas}$ (even with $\gg 100$ photon) due to unknown residual speckle field and exozodi structures.

Solving for planet orbit and mass using the combined astrometry + coronagraphy measurements is scientifically very powerful:

- **Reduces confusion with multiple planets.** Outer massive planets (curve in the astrometric measurement) will be seen by the coronagraph.
- Astrometry will **separate planets from exozodi clumps.**
- Astrometric knowledge allows to **extract fainter planets from the images, especially close to IWA**, where the coronagraph detections are marginal.
- Mitigates the **1yr period problem** for astrometry (see next slide).

Simultaneous coronagraphic imaging + astrometry mitigates the 1-yr period problem

Problem:

Astrometric signal of a planet in a yr period orbit is absorbed in the parallax term. With astrometry only, the mass estimate error grows as the planet period becomes closer to 1yr.

The width of this “blind spot” is reduced with a longer mission life.

Example:

1 Earth mass planet at 1.01 AU from a Sun mass star (period = 1.015 yr) at ecliptic pole. Star distance is 6pc. Assuming circular orbits (for both the Earth and the target planet). Planet orbit phase = Earth orbit phase + 1 radian, orbit is face-on.

32 observations over 5 yr, regularly spaced

Astrometry only (0.3 uas error / per measurement):

Mass estimate (unit = Earth) = 3.25485 ± 4.17483 -> Planet is not detected

Astrometry (0.3 uas error / measurement) + imaging (5 mas / measurement):

Mass estimate (unit = Earth) = 1.01314 ± 0.161752

Observation scheme

Telescope pointings assumed to be driven by the coronagraph requirements

Coronagraph observes high priority targets frequently. For PECO (1.4-m diameter telescope), there are 20 high priority targets (= targets around which a super-Earth could be imaged).

Assuming 2-day single pointing, 5 yr total mission, and 70% of observing time devoted to high priority targets, each high priority targets is observed 32 times (2 day per observation).

The large number of revisits is required to mitigate confusion between planets and exozodi structures, multiple planets. It also allows planet brightness and spectra variations to be monitored.

Note: In reality, more time would likely be allocated to the ~7 targets around which PECO can observe an Earth, and less time for the other ~13 targets.

When/if PECO detects an Earth candidate, the corresponding target would likely be observed more intensely.

For this study, it is assumed that the target is observed 32 times during a 5 yr mission. Observations last 2 days and are regularly spaced every 57 days.

Star field

Used “Besancon model” of the galaxy, with default 0.7 mag / kpc extinction.

<http://model.obs-besancon.fr/>

Star count computed for galactic pole on 1sq deg field. Then, sources are randomly distributed in the 1sq deg field.

In 1 sq deg field:

0 star brighter than $m_V = 10$

9 stars brighter than $m_V = 11$

23 stars brighter than $m_V = 12$

149 stars brighter than $m_V = 15$

1181 stars brighter than $m_V = 20$

5248 stars brighter than $m_V = 25$

Galactic pole is conservative assumption, but for most pointings, star count is within 40% of galactic pole star count.

	Galactic pole	50% percentile (30 deg galactic latitude)
$m_V < 10$	0	0
$m_V < 12$	23	22
$m_V < 15$	149	205
$m_V < 20$	1181	1570
$m_V < 25$	5248	6861

Using galaxies for astrometry ?

At $m_V \sim 20$, galaxies outnumber stars at high galactic latitude. Using background galaxies for astrometry should be possible (See for example “The absolute motion of the peculiar cluster NGC 6791” by Bedin et al. 2006 using HST)

Figure on the right shows galaxy counts next to galactic pole (Weir et al. 1995)
J filter ~ 400 to 500 nm
F filter ~ 650 nm

Sylos Labini et al., 2009

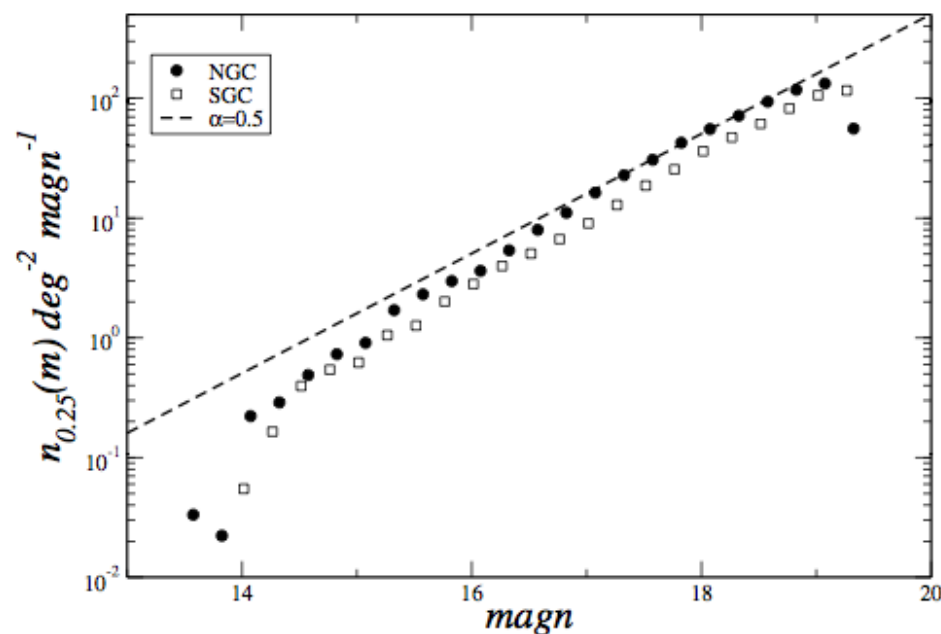


Fig. 19. Differential counts of galaxies, in bins of $\Delta m = 0.25$, as a function of apparent magnitude in the SGC and NGC. A reference line corresponding to $N(m) \sim 10^{\alpha m}$ with $\alpha = 0.5$ is reported.

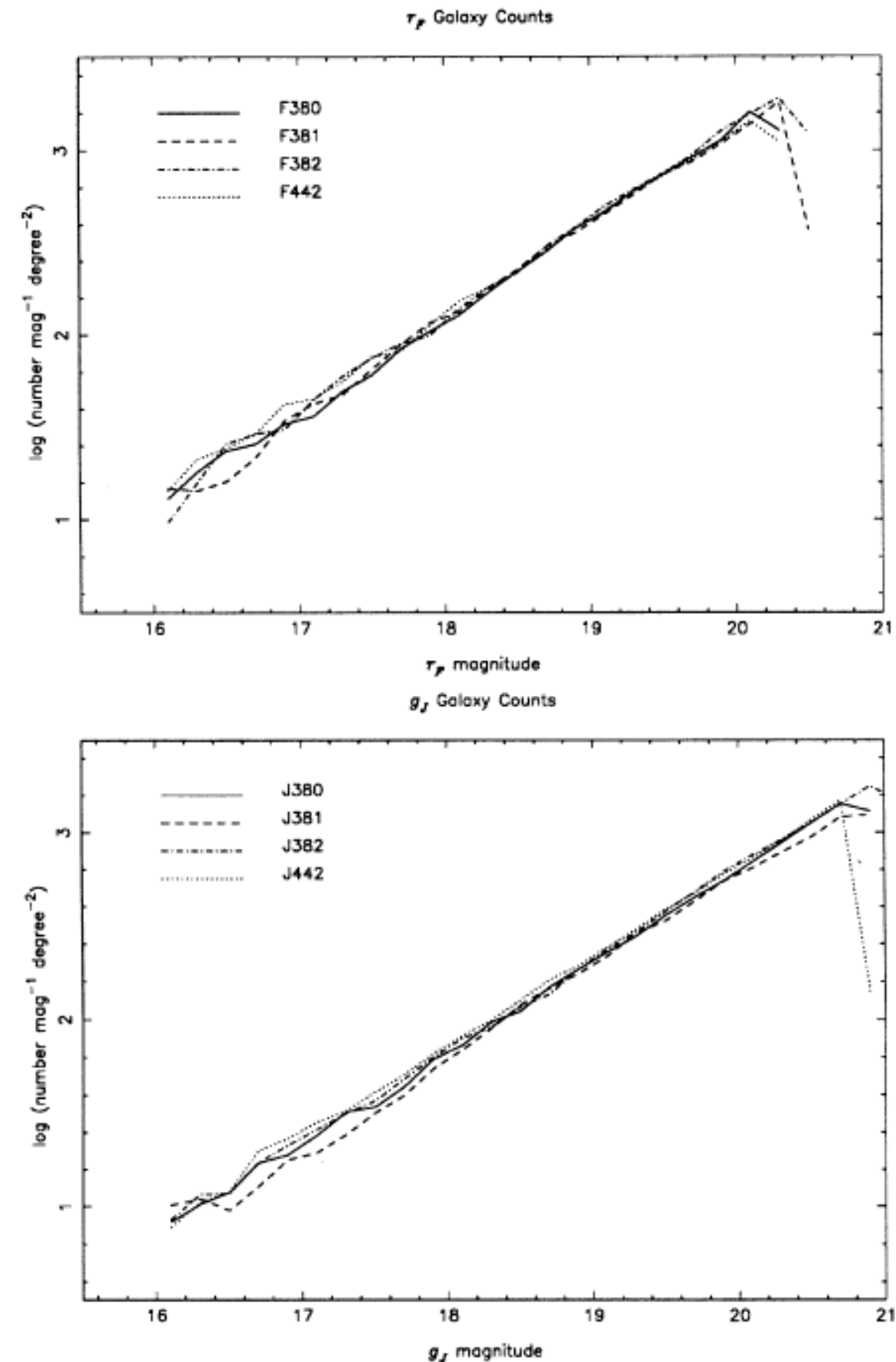


FIG. 7. r - and g -band galaxy counts in our four fields. The sharp falloffs at the faint end are due to truncation of the catalog, by construction, beyond the reliable classification limit, rather than the intrinsic plate detection limit.

Astrometric error in the photon noise limit

For each star, pixel coordinate errors due to photon noise (star + zodi) and sampling are computed.

Estimation uses a 2D polychromatic finely sampled PSF which is moved by a small amount and then binned to the pixel scale. The flux change for each pixel is compared to the noise, and all values are combined with SNR^2 weighting.

Simulation on the right shows the single axis astrometric error for a 2 day observation, 0.03 sq deg at galactic pole, Polychromatic PSF, Nyquist sampling detector at 0.6 μm , 80% optical throughput, 90% detector peak QE (0.36 μm effective bandwidth)

$m_V = 22.5 / \text{sqarcsec zodi}$

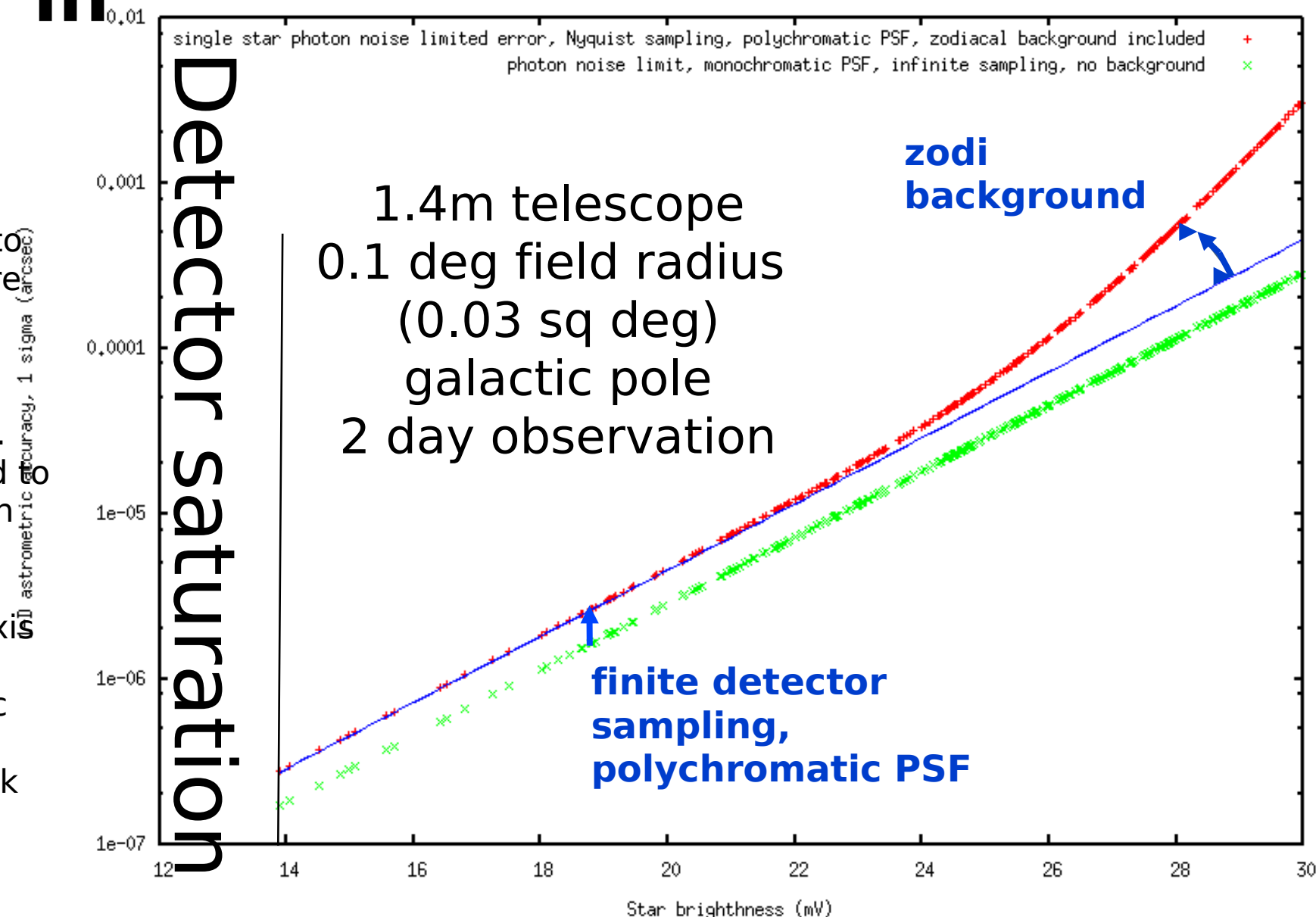
Combined astrometric accuracy = 0.1265 μas
For a 0.25 sq deg (0.5 x 0.5 deg): 0.044 μas

A small number of bright stars (m_V) contribute to most of the measurement accuracy:

If only stars fainter than $m_V = 17$ are included, accuracy = 0.46 μas

If only stars brighter than $m_V = 17$ are included, accuracy = 0.1315 μas

Note: At high galactic latitude, extragalactic sources may be used to increase sensitivity ?



Green points show theoretical 1D astrometric error:
 $\sigma = 0.318 (\lambda/D) / \sqrt{N_{\text{photon}}}$

Red points show 1D astrometric error when zodi, PSF polychromaticity and pixel sampling are taken into account. The difference between the 2 curves is explained by an offset due to detector sampling and PSF polychromaticity (independent of star magnitude) + an increase in measurement error at the faint end due to zodiacal light photon noise.

Simulation description

Simulation assumes:

- 1.4m telescope TMA (Woodruff design)
- 1.5nm surface (3nm WF) optics for M2 and M3, PSD provided by Tinsley
- Circular field of view, 0.2 deg diam (0.03 sq deg) → performance then scaled to 0.29 sq deg to reach goal
- Galactic pole observation (worst case scenario)
- central star is $m_v=3.7$ (faintest of the 7 PECO targets for which an Earth can be imaged in <6hr, 14th brightest target in the 20 high priority targets list)
- 90% detector peak QE, 80% optical throughput (0.96^3 for optics reflectivity x 0.92 due to dots on PM)
- Nyquist sampled detector at 0.6 micron = 44 mas pixels
- Telescope roll = 1 rad (larger angle = better averaging, but more difficult to maintain stability)
- Single epoch observation = 2 day

Distortions in the system are computed with 3D raytracing (code written in C, agreement with Code V results from Woodruff has been checked)

Images produced by Fourier transform, and then distorted according to geometrical optics. Image sizes are 16k x 16k.

Simulation description

Approach:

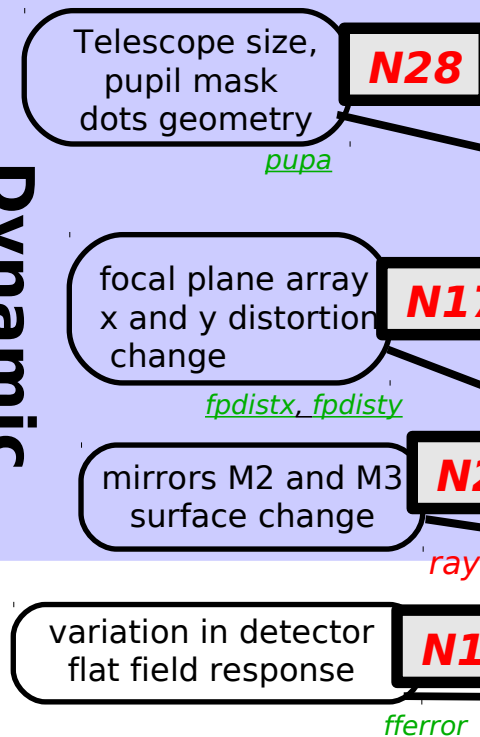
identify important sources of noise and errors

→ develop numerical simulation tool which accurately includes these noises

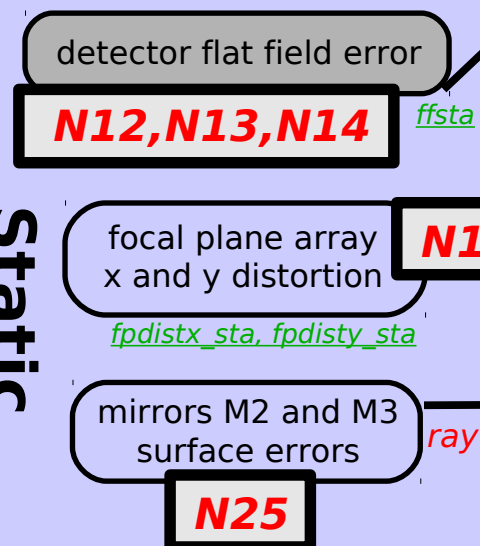
Description		Included in numerical model ?	Notes
Photon noise and related effects (See section 6.1.1)			
N1	Photon noise (field stars)	yes	See Appendix
N2	Pixel sampling (field stars)	yes	See Appendix
N3	PSF polychromaticity (field stars)	yes	See Appendix
N4	Zodiacal light photon noise (field stars)	yes	See Appendix
N5	Central star and zodi photon noise	yes	Affects image of diffraction spikes
Astronomical terms (See section 6.1.2)			
N6	Central star proper motion	yes	fitted/removed in final measurements
N7	Central star parallax motion	yes	fitted/removed in final measurements
N8	Aberration of light	no	Effect is similar to, but much smaller than N6 + N7
N9	Companions around field stars	no	Averaged by large number of field stars
N10	Central star photometric variability	no	Small effect on spikes measurement
N11	Stellar spots and activity	no	Expected to be smaller than $0.1 \mu\text{as}$
Detector (See section 6.1.3)			
N12	Uncalibrated errors in detector flat field	yes	1% RMS. 6% peak
N13	Uncalibrated detector spectral response errors	absorbed in N12	Effect is absorbed in N12 numerical model
N14	Intra-pixel detector sensitivity variations	absorbed in N12	Effect is absorbed in N12 numerical model
N15	Uncalibrated detector geometry error	yes	Assumes unknown ≈ 20 mK temperature inhomogeneity variation
N16	Variations in pixel sensitivities over time	yes	Assumed to be at the 0.1% level (excludes calibration)
N17	Variations in detector geometry over time	yes	Effect is included in N16 numerical model
N18	Detector saturation	approximated	Field stars brighter than $m_V = 14$ are excluded
N19	Readout noise	no	exposure time chosen for photon-noise limited imaging
N20	Uncalibrated detector non-linearity	no	No significant contribution expected in final measurement
N21	Uncalibrated variable errors in readout timing	no	$< 0.01 \mu\text{as}$
Telescope and optics (See section 6.1.4)			
N22	Telescope pointing jitter	no	negligible impact if below diffraction limit
N23	Telescope roll angle errors	no	fitted and removed from final data
N24	Uncalibrated primary mirror surface errors	no	negligible impact if below diffraction limit
N25	Uncalibrated M2 and M3 mirrors surface errors	yes	PSD of manufactured optics used for simulation
N26	Telescope alignment errors	no	known terms fitted, residual $\ll \mu\text{as}$
N27	Plate scale error	no	Less than $1\text{e-}3 \mu\text{as}$
N28	Local random errors in dot positions and size	no	Non-significant if position error $< 10\mu\text{m}$
N29	Non-uniformity in dots coverage	no	Removed from measurement thanks to roll

Input errors and instrument characteristics

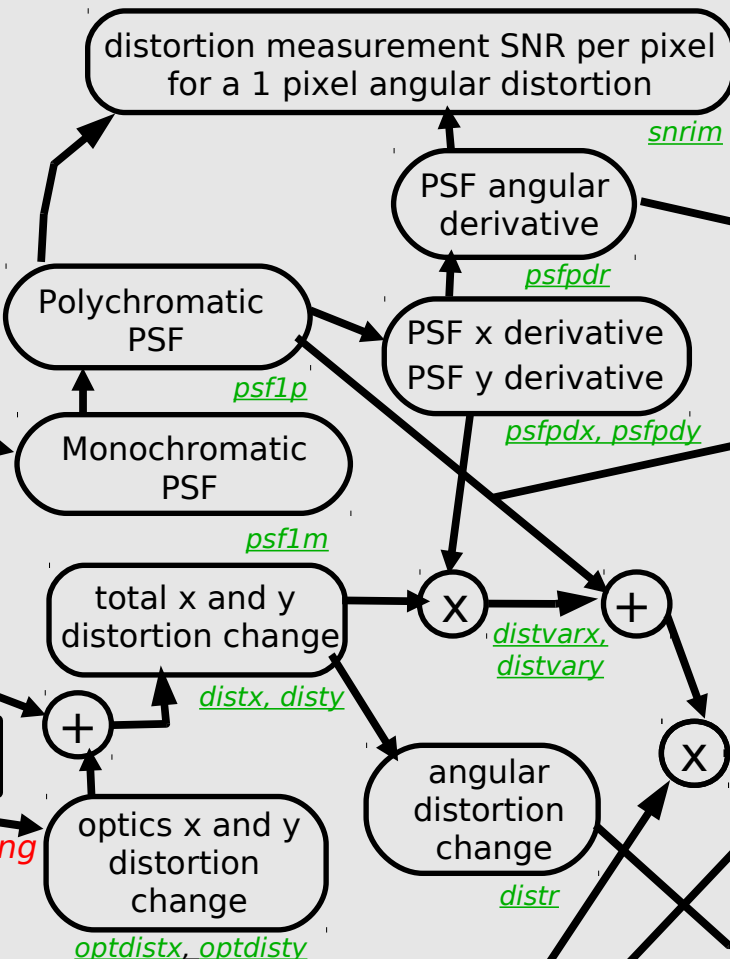
Dynamic distortions



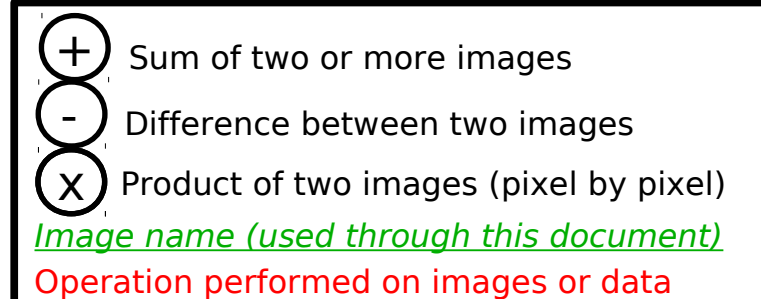
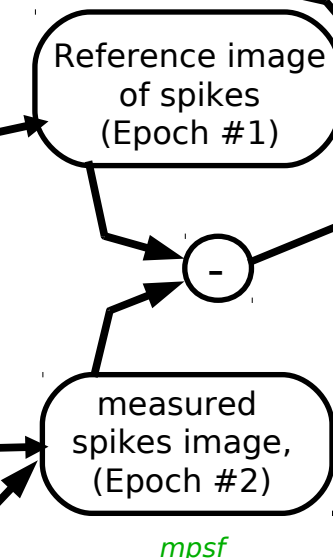
Static distortions



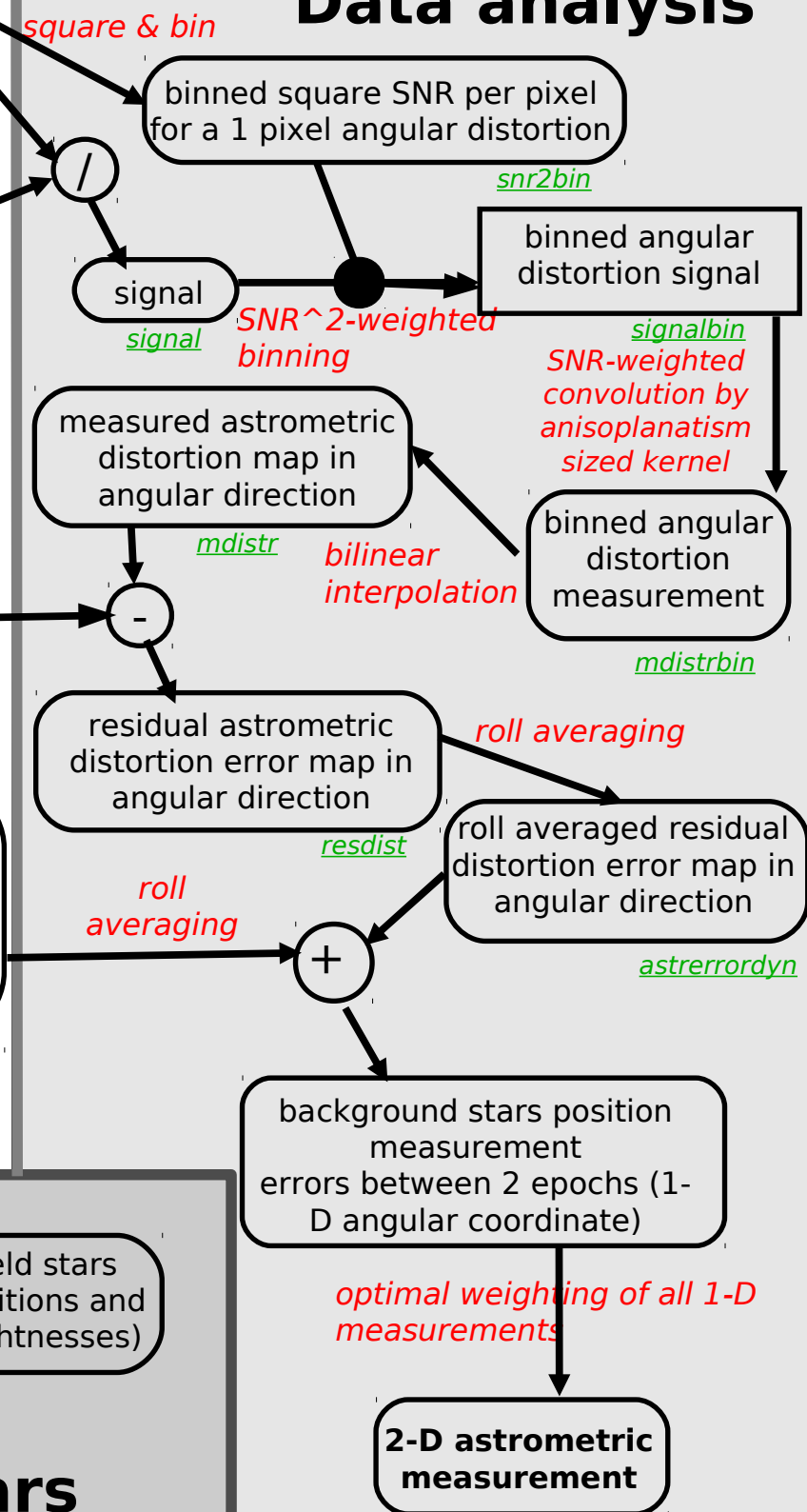
Data simulation



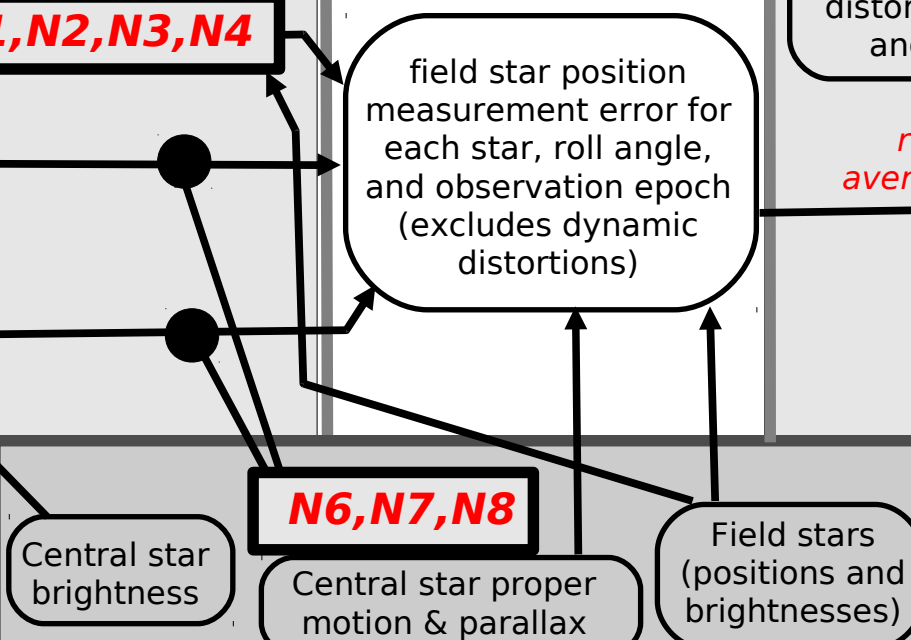
Simulated data



Data analysis



Target and field stars



Simulation details

This series of slides describes in more detail each step of the numerical simulation. A red square is shown in the overall simulation description diagram to indicate which part of the simulation is being described.



Green text label next to boxes show the image or file name used in the source code, to help read the source code.

Input errors and instrument characteristics

Dynamic distortions

Telescope size, pupil mask dots geometry **N28**

focal plane array x and y distortion change **N17**

mirrors M2 and M3 surface change **N25**

variation in detector flat field response **N16**

photon noise due to zodiacal background and central star flux

photon noise error due to zodiacal light and field star flux

detector flat field error **N12,N13,N14**

focal plane array x and y distortion **N15**

mirrors M2 and M3 surface errors **N25**

Static distortions

Data simulation

distortion measurement SNR per pixel for a 1 pixel angular distortion

PSF angular derivative **psfadr**

Polychromatic PSF **psf1p**

Monochromatic PSF **psf1m**

total x and y distortion change **distx, disty**

optics x and y distortion change **optdistx, optdisty**

angular distortion change **distr**

static angular distortion **distr_sta**

total x and y distortion **distx_sta, disty_sta**

optics x and y distortion **optdistx_sta, optdisty_sta**

Central star brightness

Central star proper motion & parallax

Field stars (positions and brightnesses)

Simulated data

Reference image of spikes (Epoch #1)

measured spikes image, (Epoch #2) **mps**

field star position measurement error for each star, roll angle, and observation epoch (excludes dynamic distortions)

Central star brightness

Central star proper motion & parallax

Field stars (positions and brightnesses)

Target and field stars

Data analysis

square & bin

binned square SNR per pixel for a 1 pixel angular distortion **snr2bin**

signal **signal**

measured astrometric distortion map in angular direction **mdistr**

residual astrometric distortion error map in angular direction **resdist**

roll averaged residual distortion error map in angular direction **astrerrordyn**

background stars position measurement errors between 2 epochs (1-D angular coordinate)

2-D astrometric measurement

- $+$ Sum of two or more images
- $-$ Difference between two images
- \times Product of two images (pixel by pixel)
- Image name (used through this document)
- Operation performed on images or data

SNR²-weighted binning

SNR-weighted convolution by anisoplanatism sized kernel

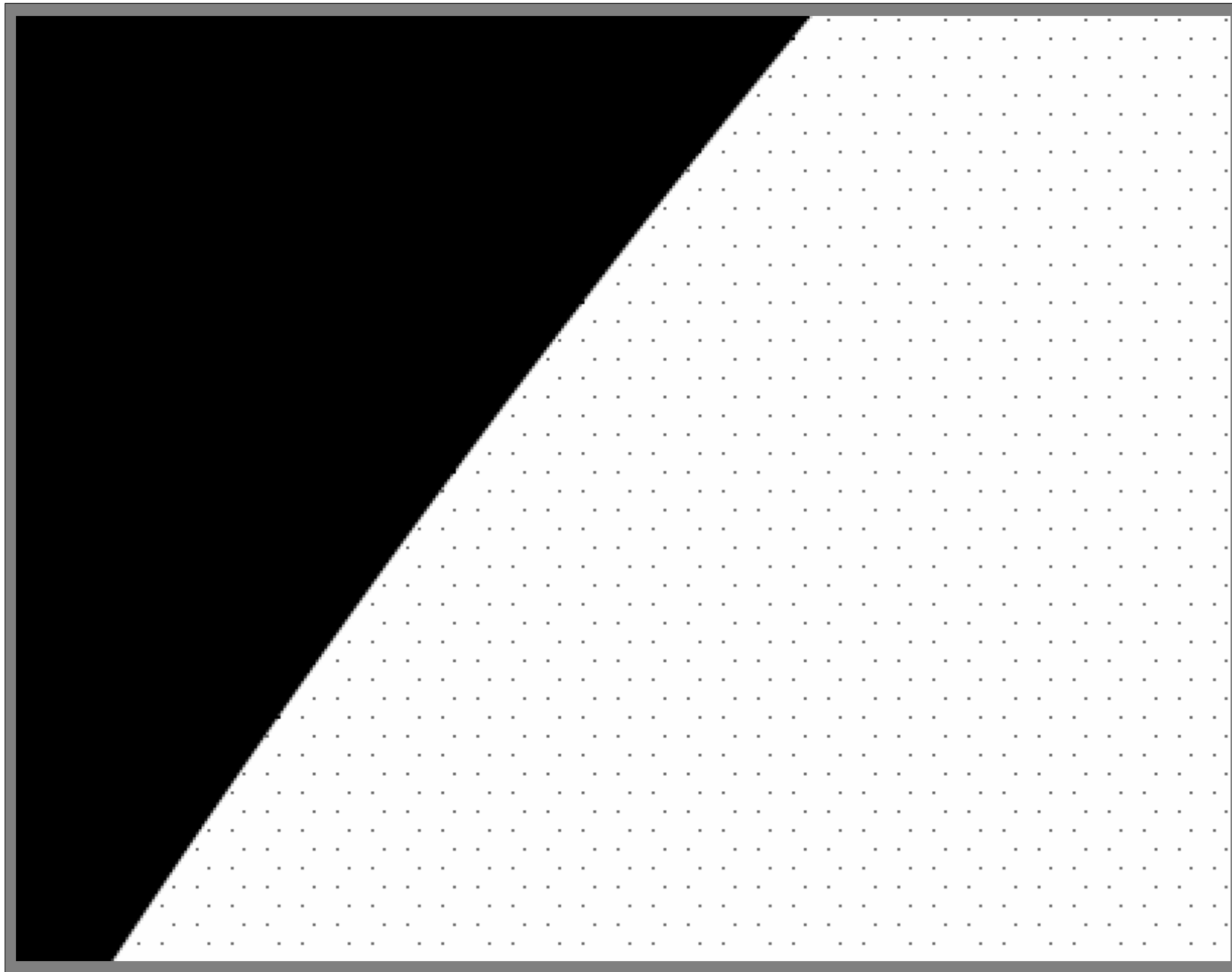
bilinear interpolation

roll averaging

roll averaging

optimal weighting of all 1-D measurements

PM mask



Hexagonal pattern dots. Dots cover 1% of PM surface. Dots are assumed to be perfectly placed, all with same size.

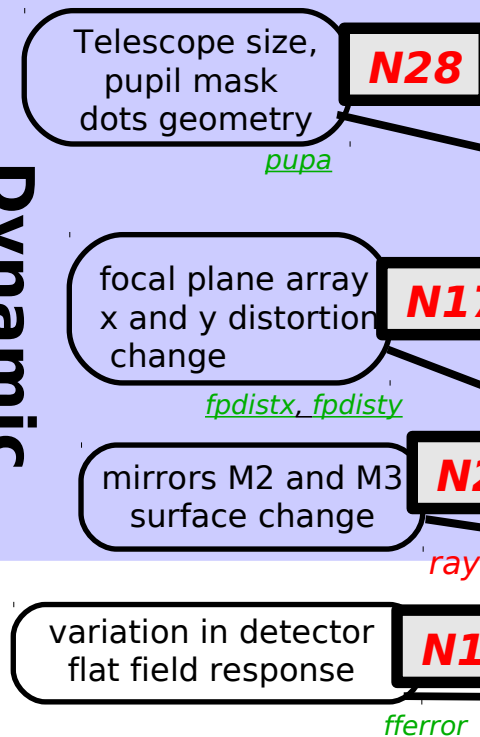
[note: for mission, dot diameter = 72 μm ; spacing = 0.5 mm]

Dots are assumed to be totally black.

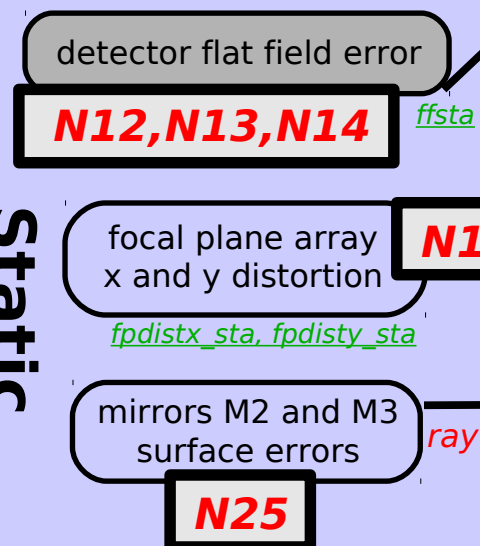
Dots do not affect coronagraph if they are regularly spaced (no low spatial frequency)

Input errors and instrument characteristics

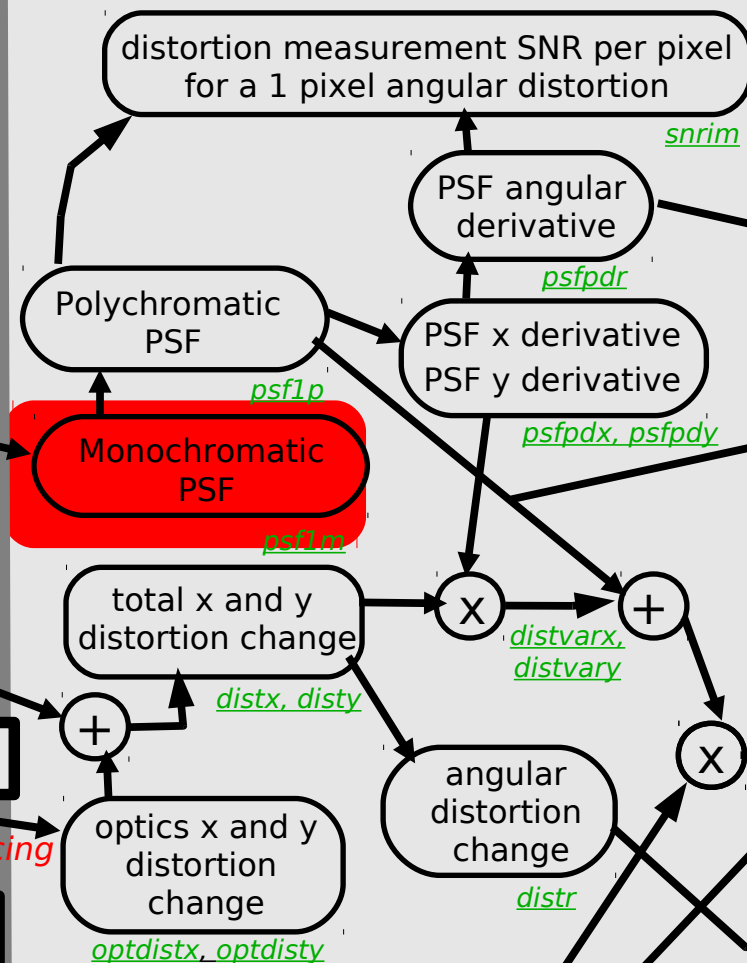
Dynamic distortions



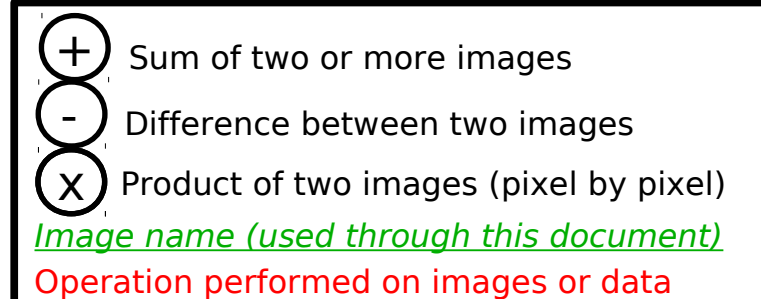
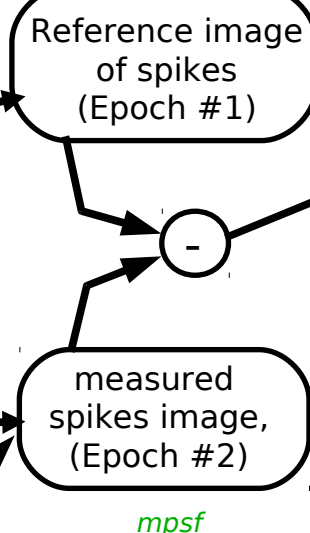
Static distortions



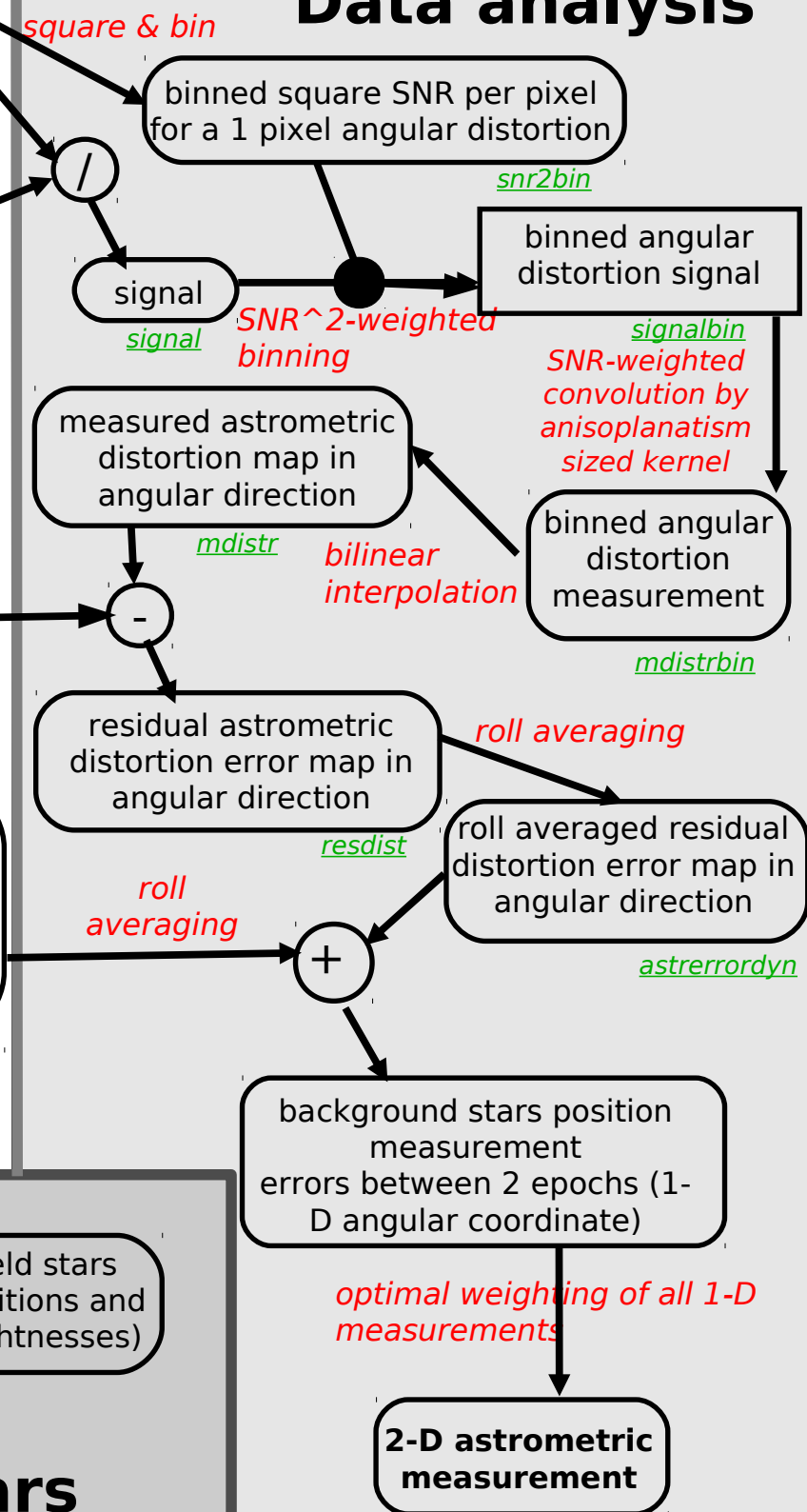
Data simulation



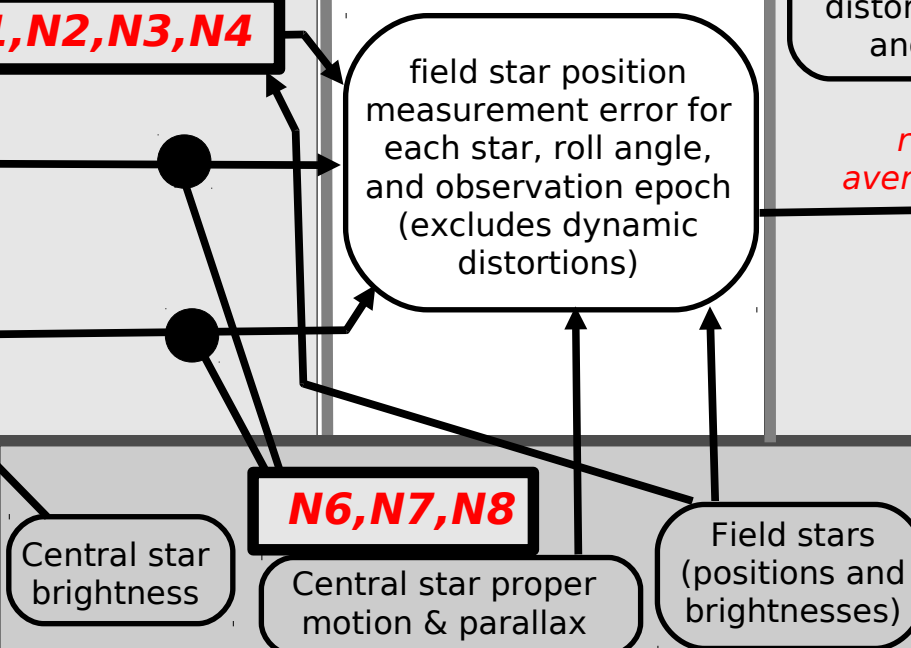
Simulated data



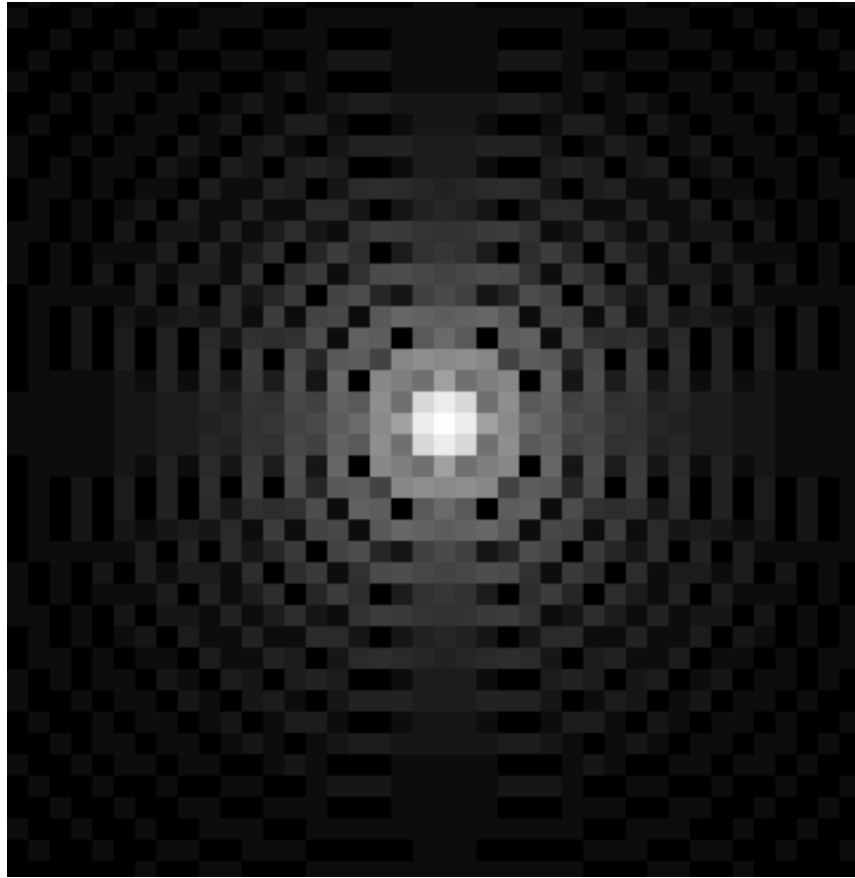
Data analysis



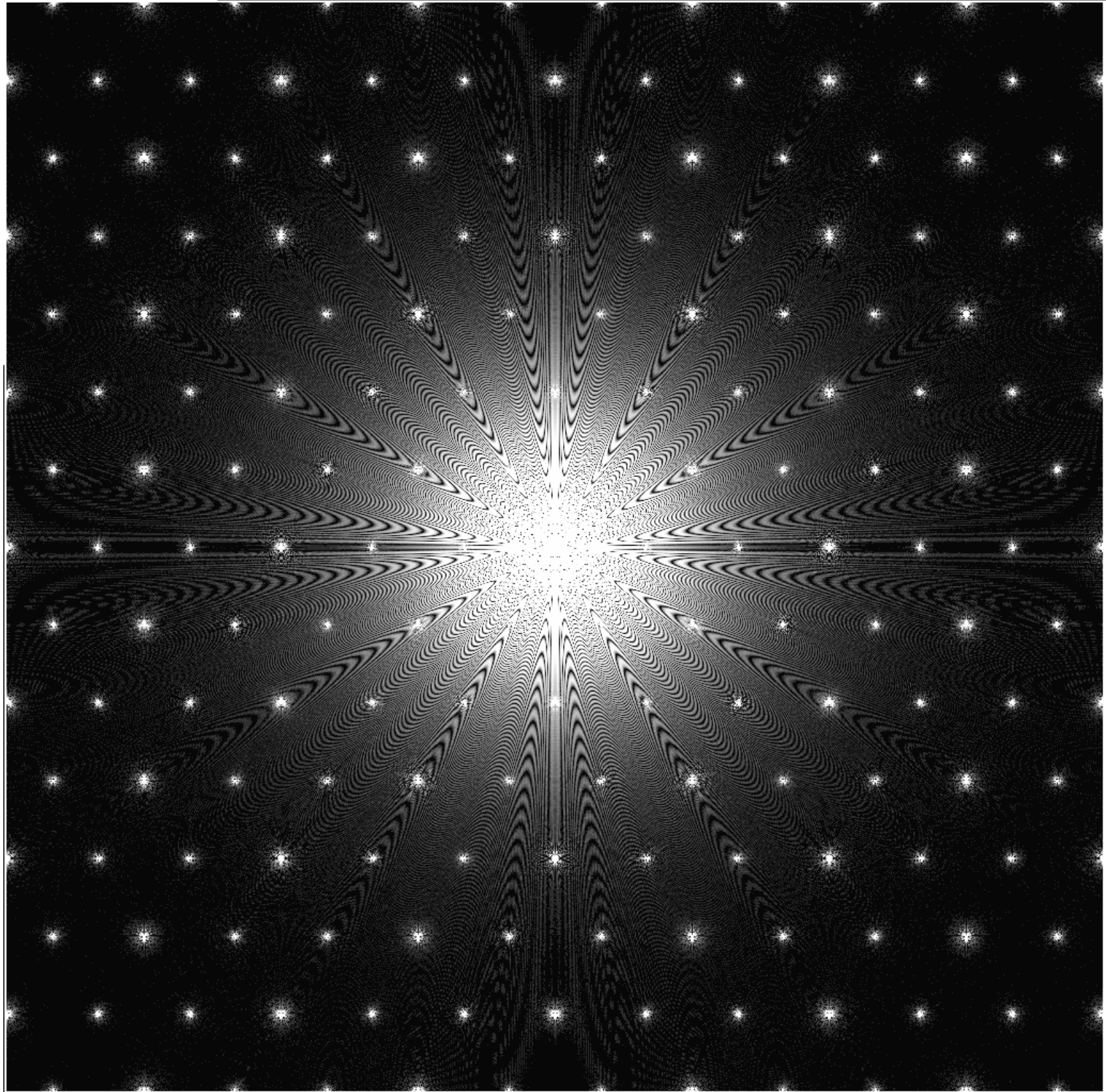
Target and field stars



Monochromatic PSF



Central part of PSF is not
disturbed by dots

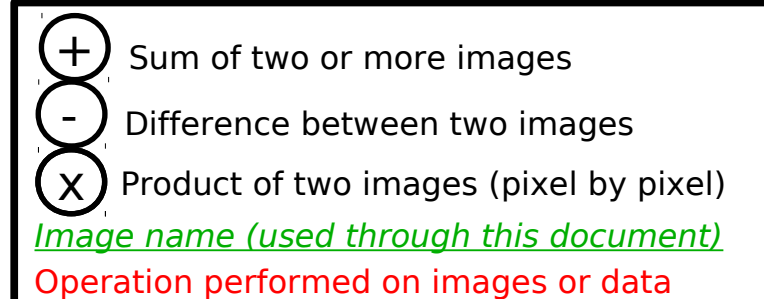


Full field PSF (0.2 deg on a side)
shows 2D grid of diffraction orders

Input errors and instrument characteristics

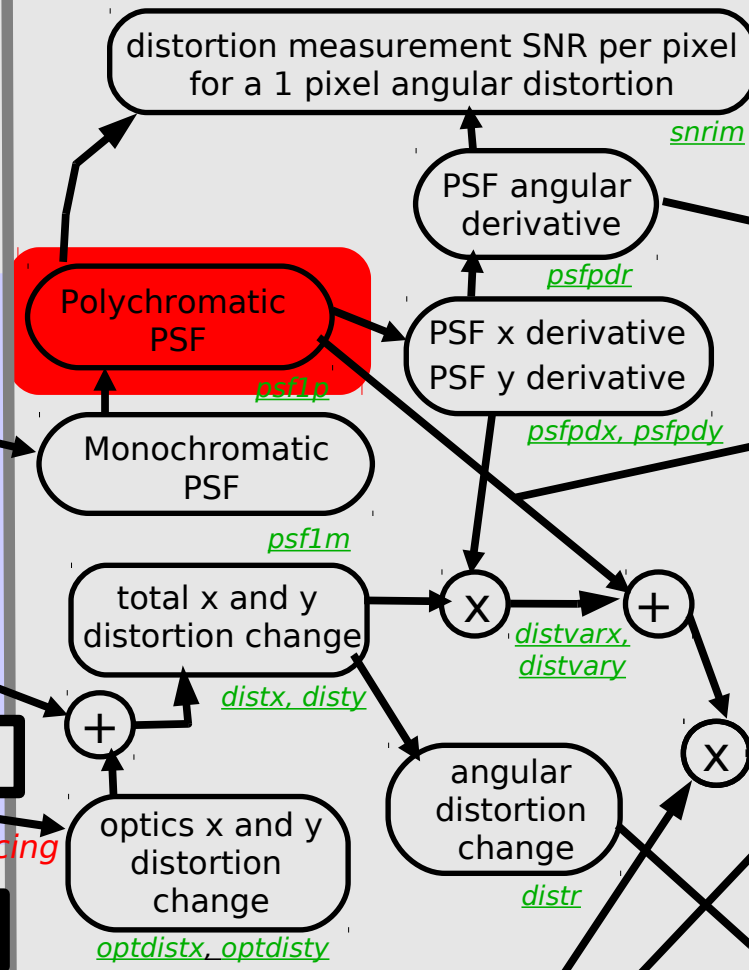
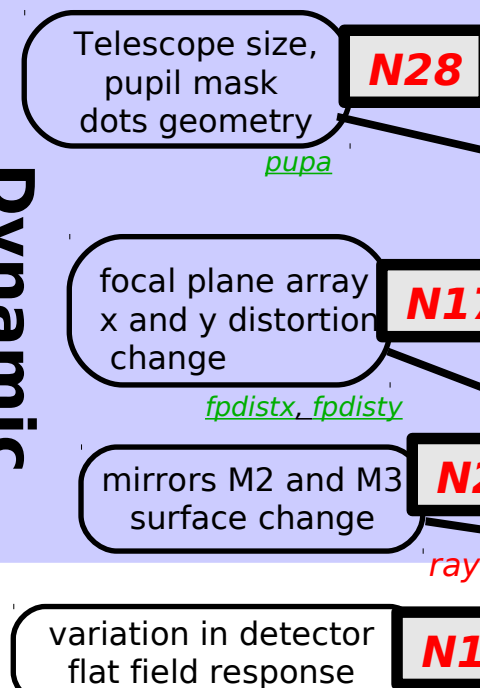
Data simulation

Simulated data



Data analysis

Dynamic distortions



Reference image of spikes (Epoch #1)

measured spikes image, (Epoch #2)

square & bin

binned square SNR per pixel for a 1 pixel angular distortion

signal

binned angular distortion signal

SNR²-weighted binning

measured astrometric distortion map in angular direction

binned angular distortion measurement

residual astrometric distortion error map in angular direction

roll averaging

roll averaged residual distortion error map in angular direction

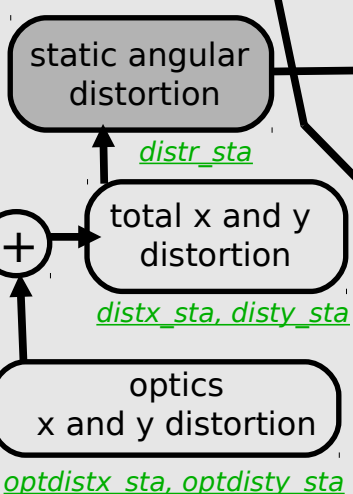
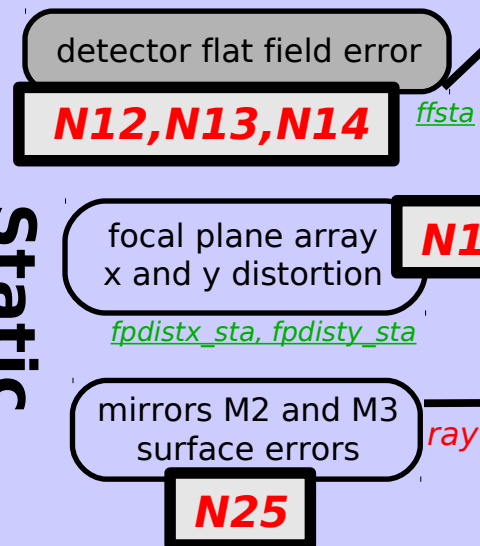
roll averaging

background stars position measurement errors between 2 epochs (1-D angular coordinate)

optimal weighting of all 1-D measurements

2-D astrometric measurement

Static distortions



field star position measurement error for each star, roll angle, and observation epoch (excludes dynamic distortions)

Central star brightness

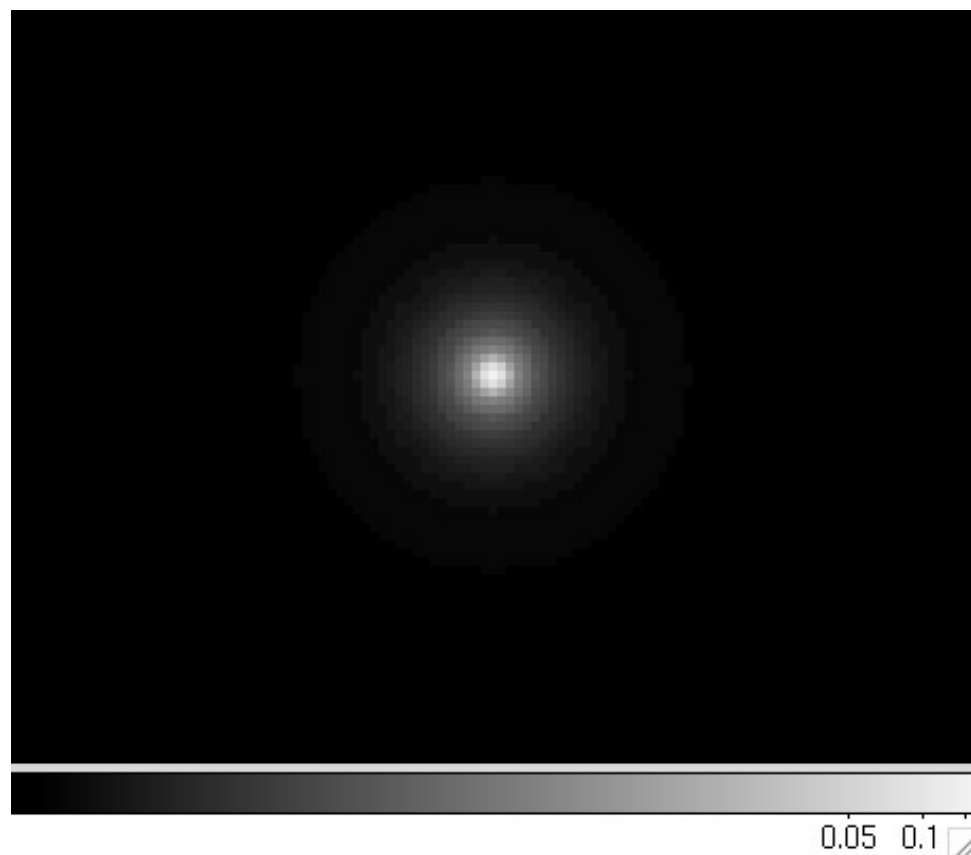
Central star proper motion & parallax

Field stars (positions and brightnesses)

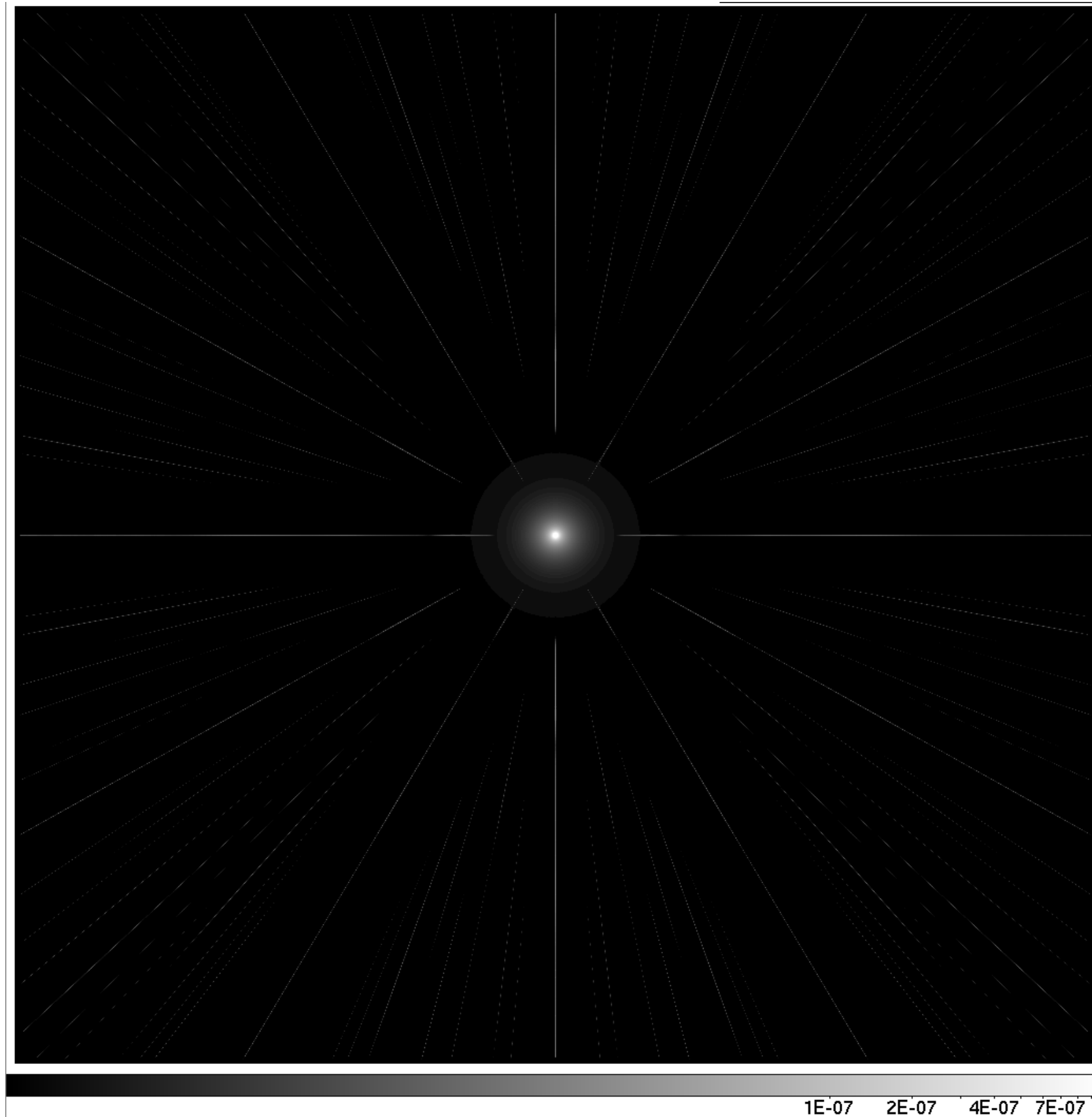
Target and field stars

Polychromatic PSF

Computed as incoherent
sum of 5000
monochromatic PSFs: 50
individual FFTs x 100
radial stretch steps



Central part of PSF



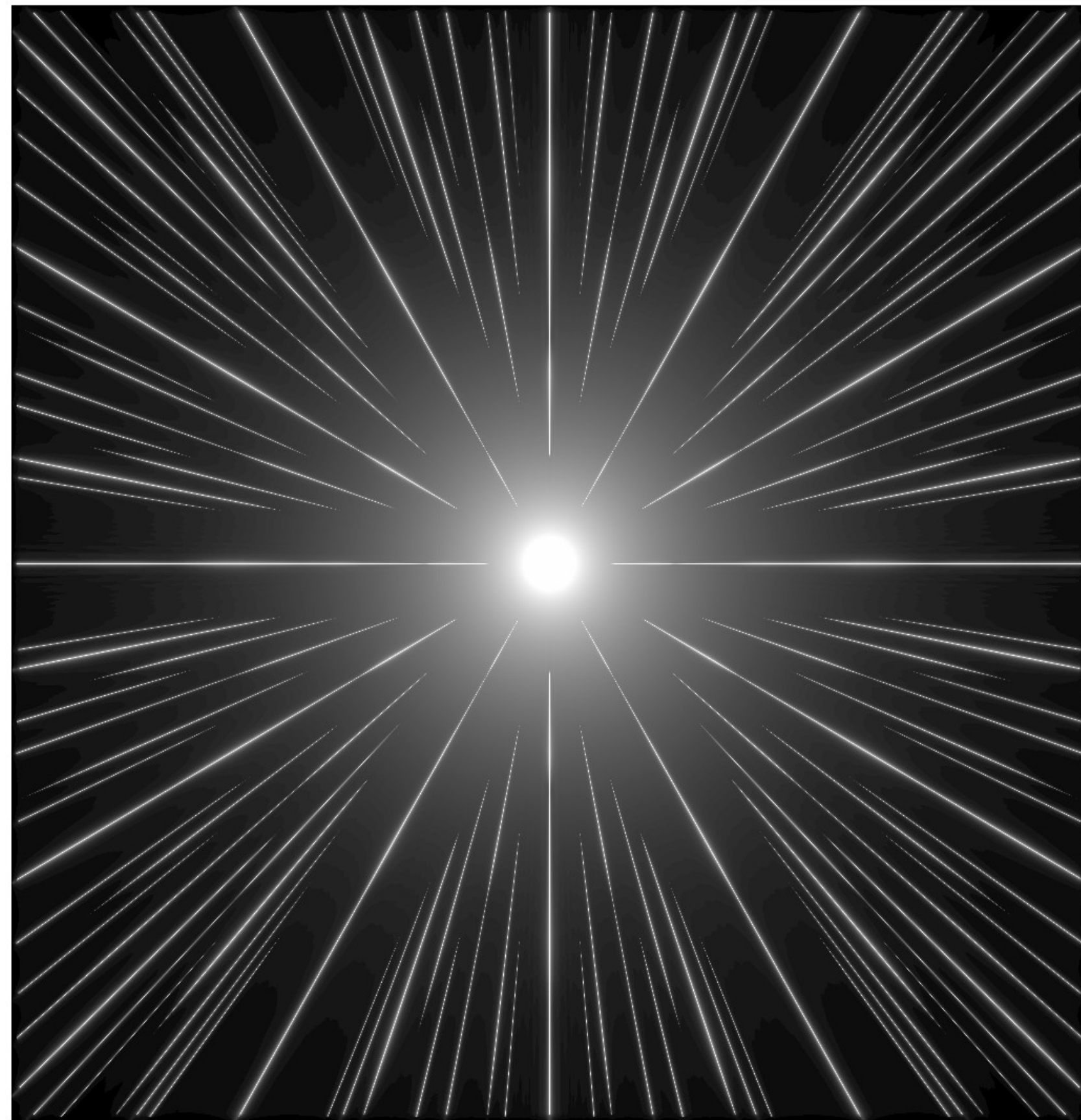
**Full field PSF (0.2 deg on a side)
shows thin narrow spikes**

Polychromatic PSF

Brightest part of spikes is $\sim 10^{-8}$ of central PSF peak
Over most of the field, surface brightness is dominated by zodiacal light, not by spikes.

Scattering by PM surface roughness is much fainter than the spikes, as spikes diffract $\sim 1\%$ of starlight.

Central pixel has 17% of total flux



1E-10 2E-10 4E-10 7E-10

0.2 deg field PSF, log scale

Static distortions

Definition: *Any error static through the mission lifetime.*

Why do purely static errors matter ?

Background PSFs follow different trajectories during the telescope roll for different observation epochs. The trajectories are close (\sim arcsecond level), so what matters is the differential astrometric distortion over a $\sim 1''$ distance.

Main errors:

- Distortions due to optical figure of mirrors M2 and M3
- Focal plane array geometry: position of individual detector chip & variations in pixel size across the detector
- Non-calibrated flat field errors

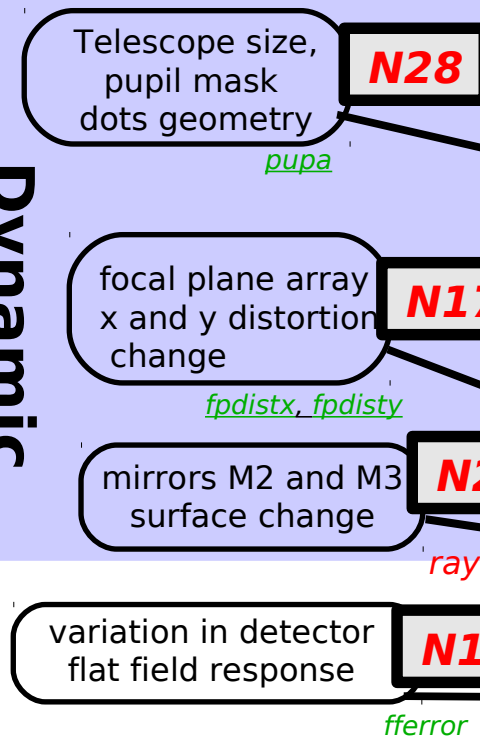
Impact and mitigation:

Static errors are not calibrated by the diffraction spikes:

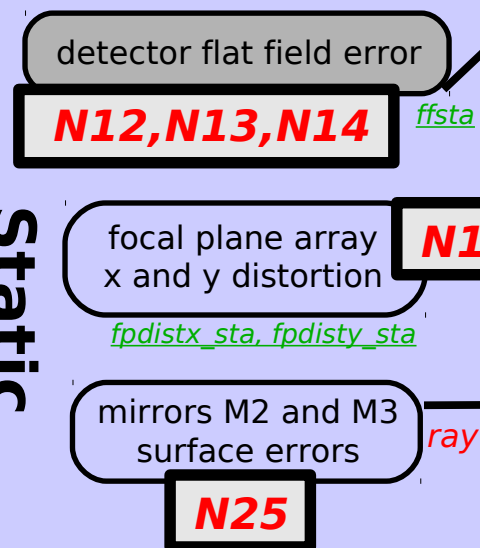
- lack of absolute reference for spikes makes it impossible to calibrate static errors (where should the spikes be in a perfect system ?)
- spikes can only calibrate low order distortions, but relevant static errors are small scale errors

Input errors and instrument characteristics

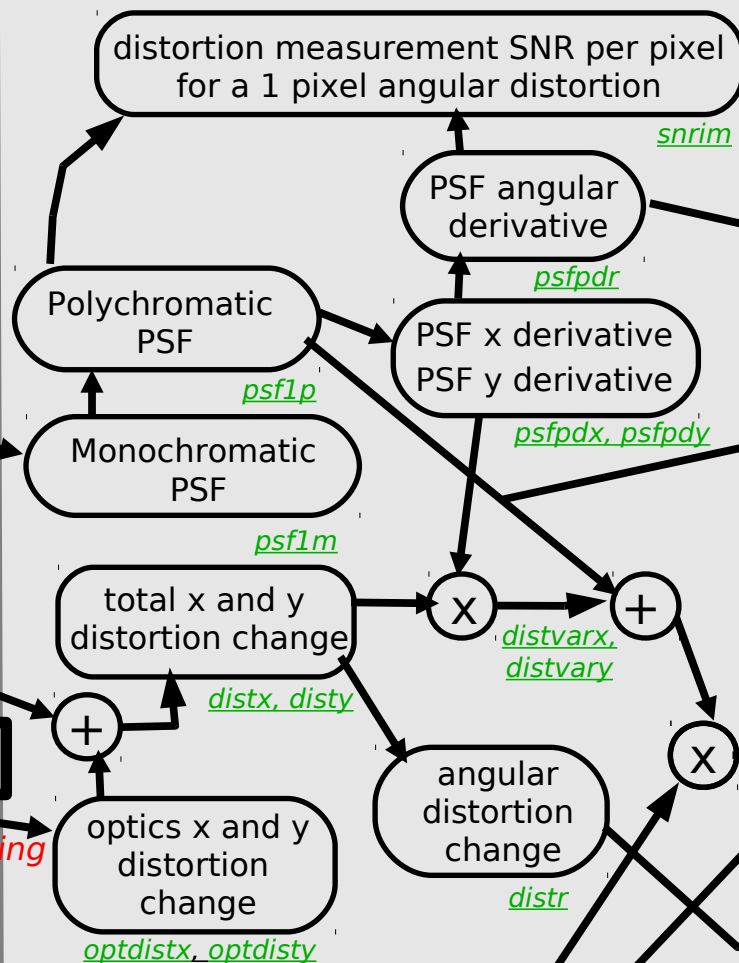
Dynamic distortions



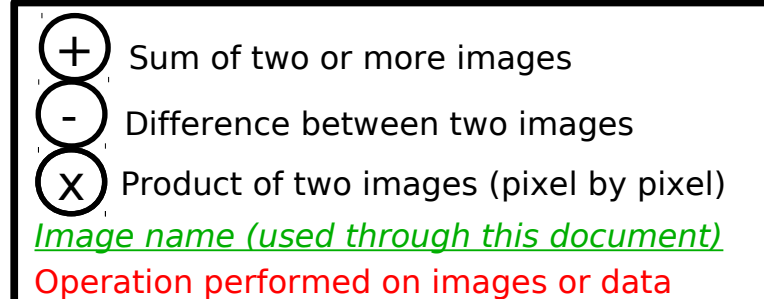
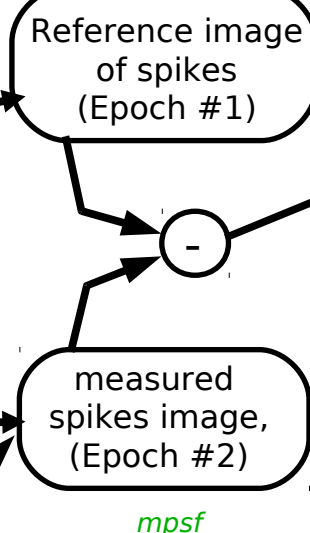
Static distortions



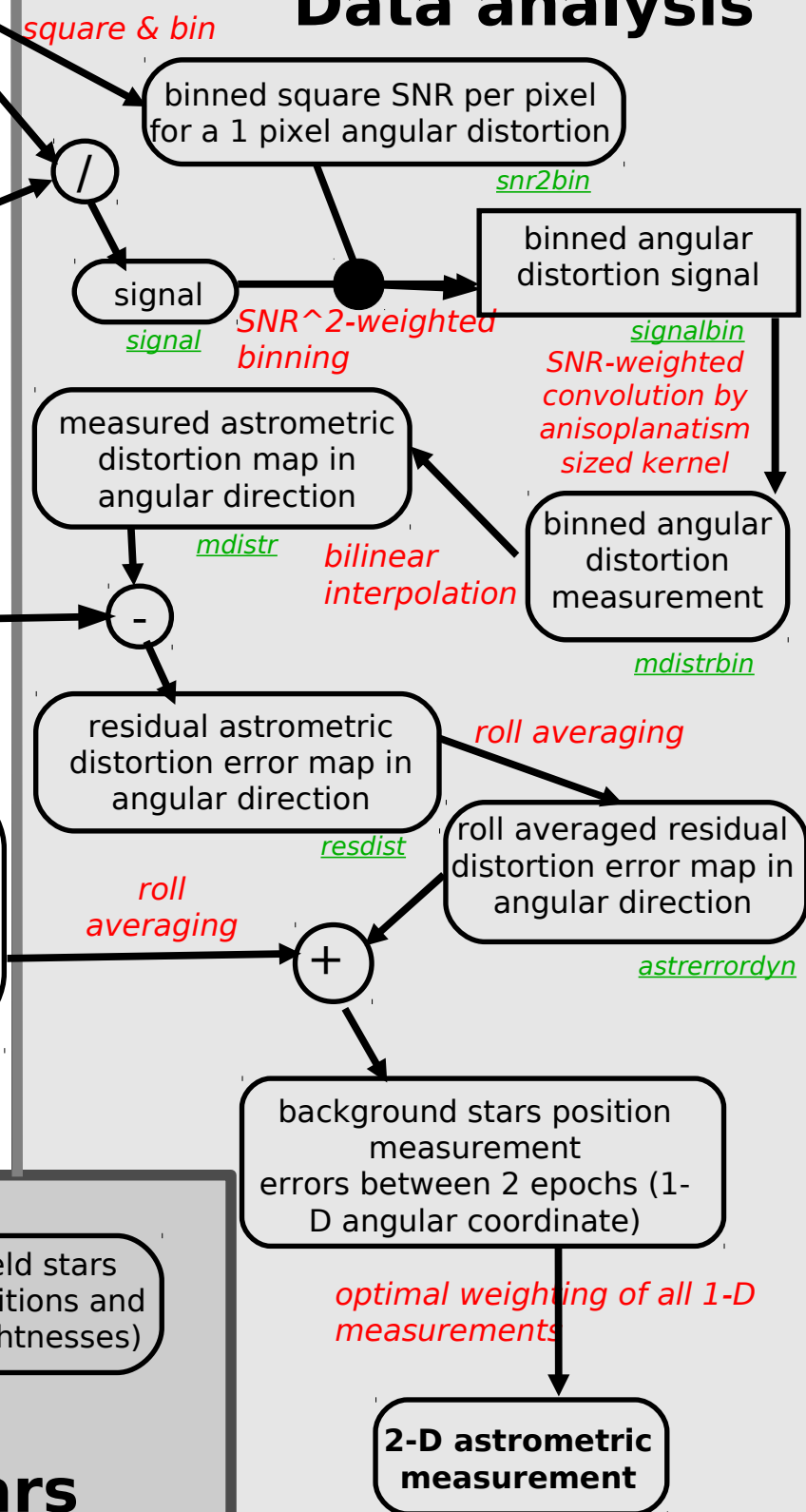
Data simulation



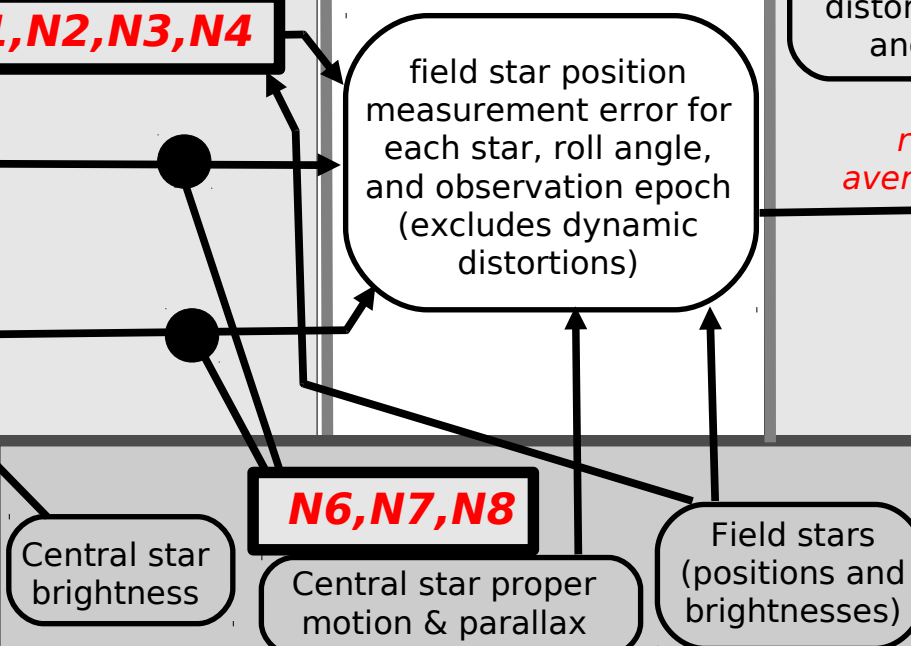
Simulated data



Data analysis



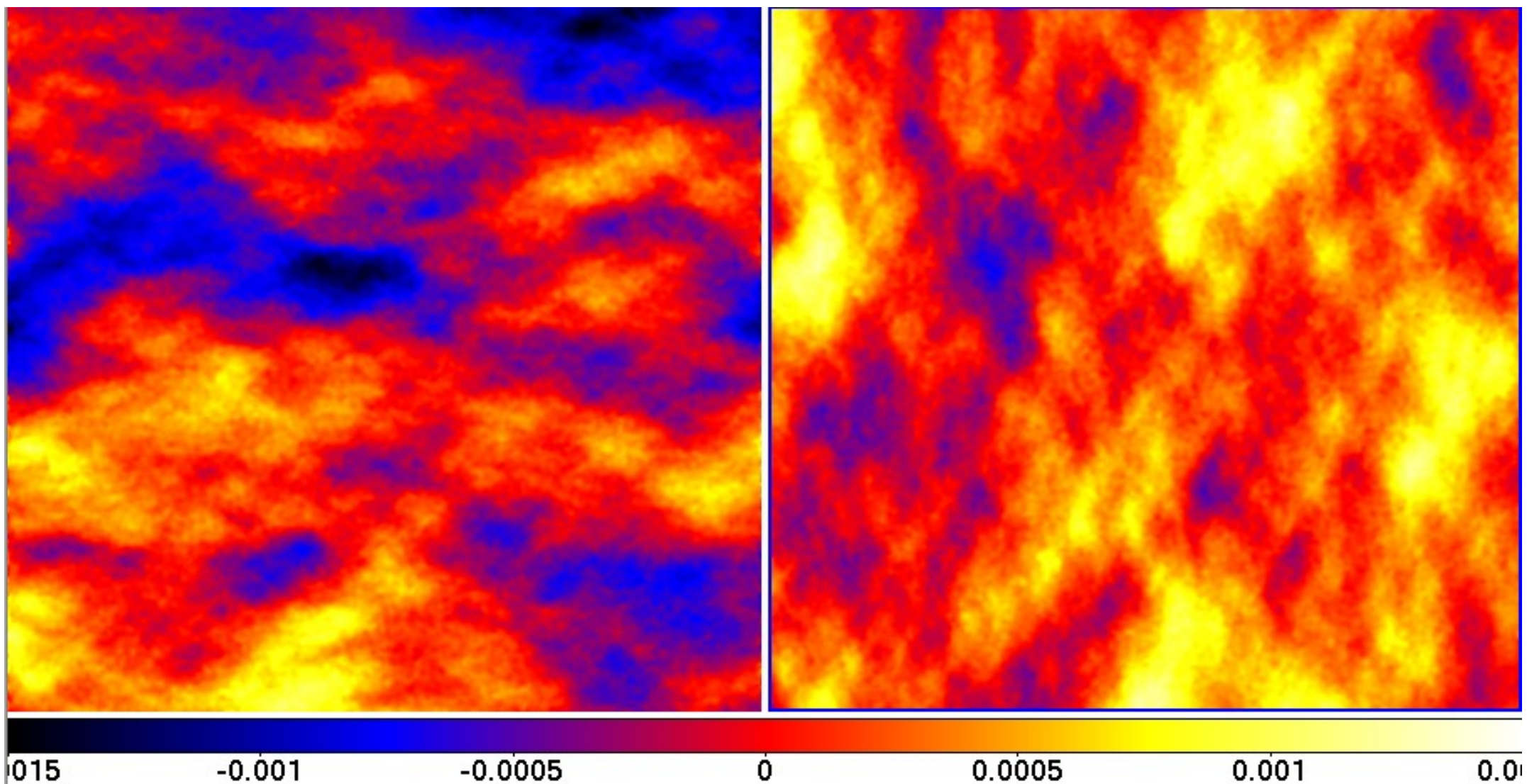
Target and field stars



Static distortion map due to M2 & M3 optical surfaces

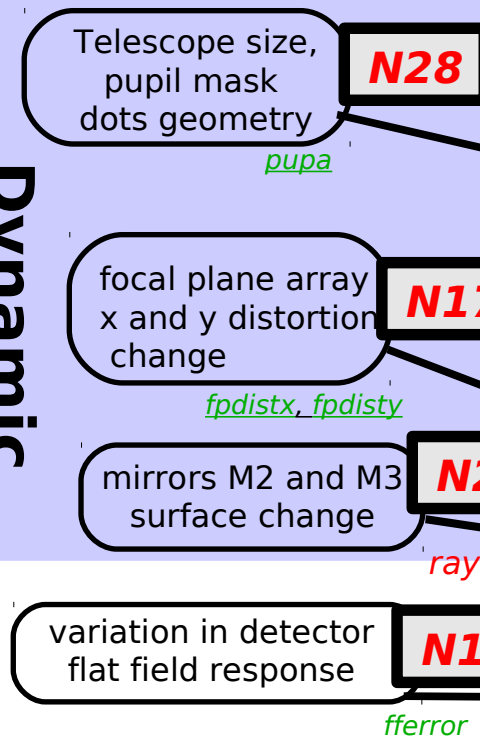
Distortion maps shown below is for 0.46×0.46 deg field. Unit is arcsec; left map is x, right map is y. Distortion map is computed at 220000 positions on the sky with raytracing software written in C (cross-checked with code-V), then interpolation is used to compute the full map. Total number of rays used = $7e11$ (122 day CPU of execution time on 2 GHz CPUs)

Distortion amplitude is ~ 1 mas, dominated by low order modes. The differential distortion over $\sim 1''$ is much smaller.

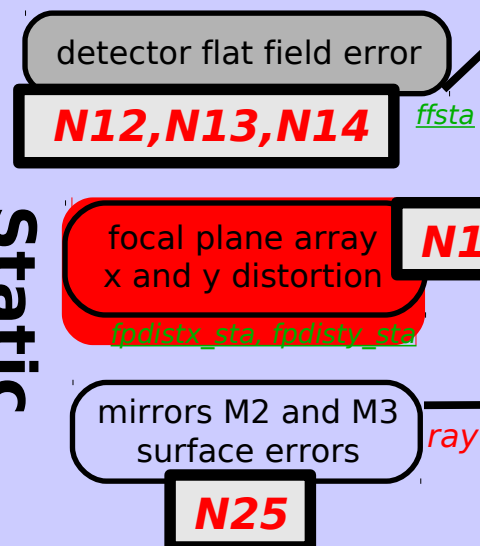


Input errors and instrument characteristics

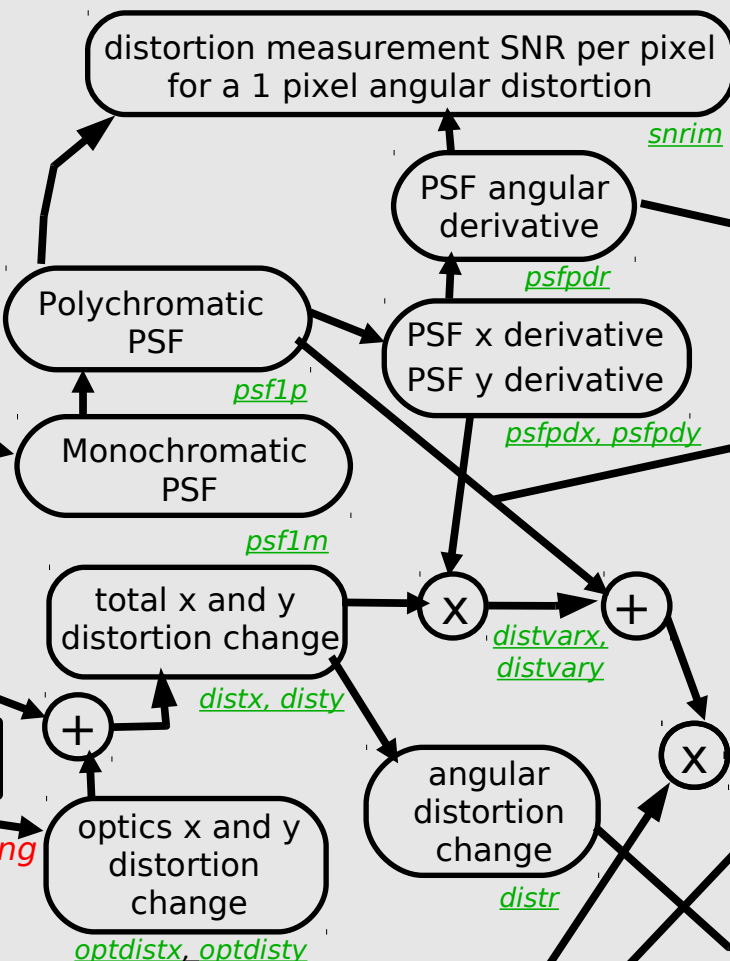
Dynamic distortions



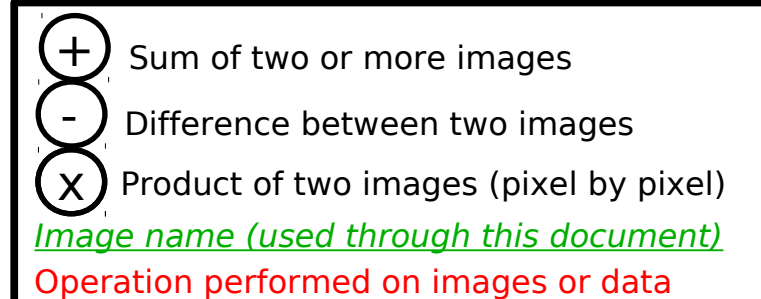
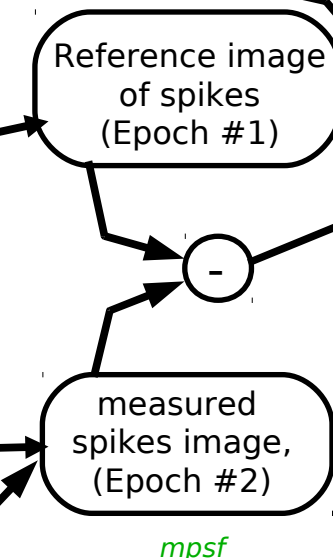
Static distortions



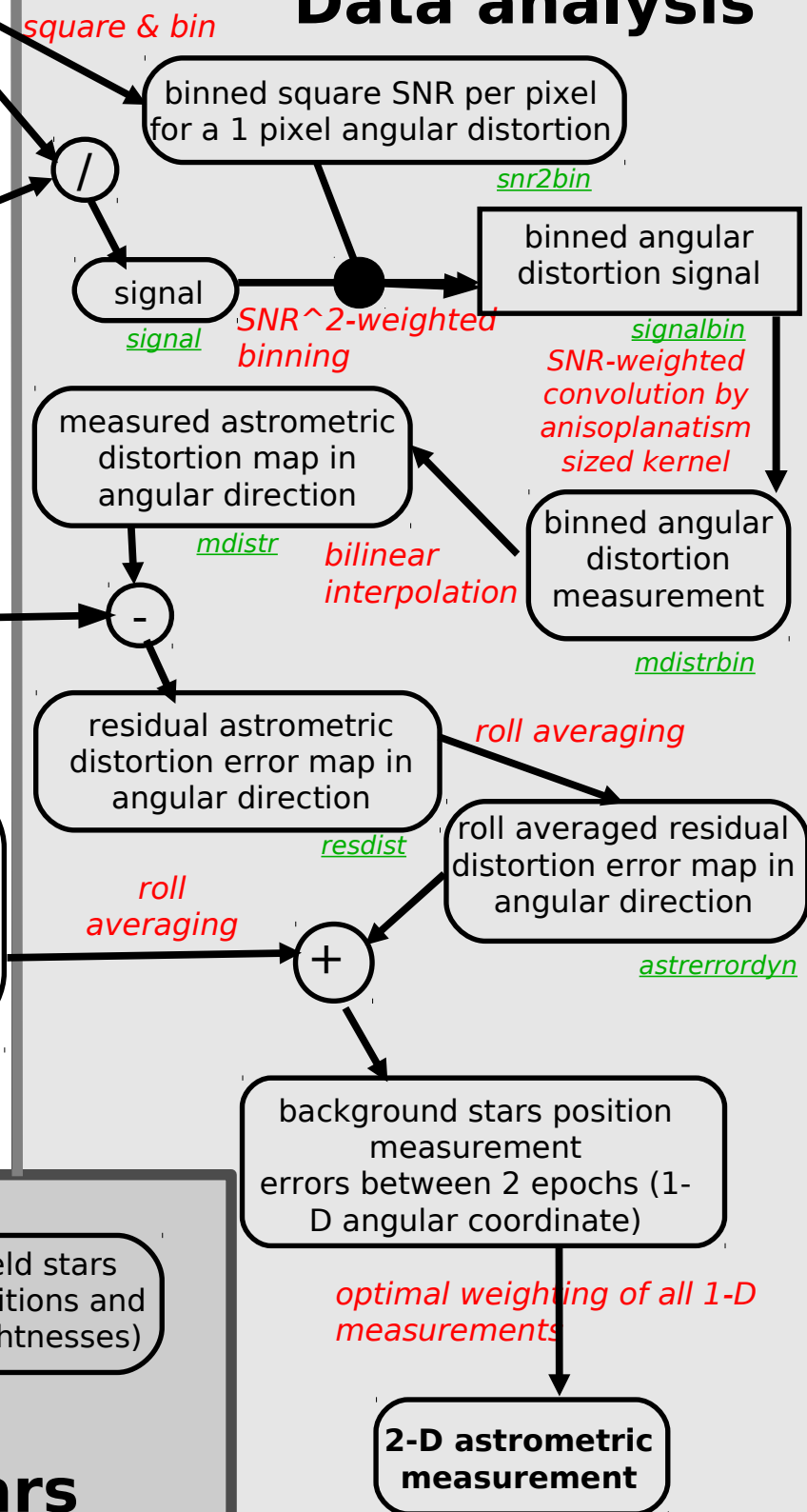
Data simulation



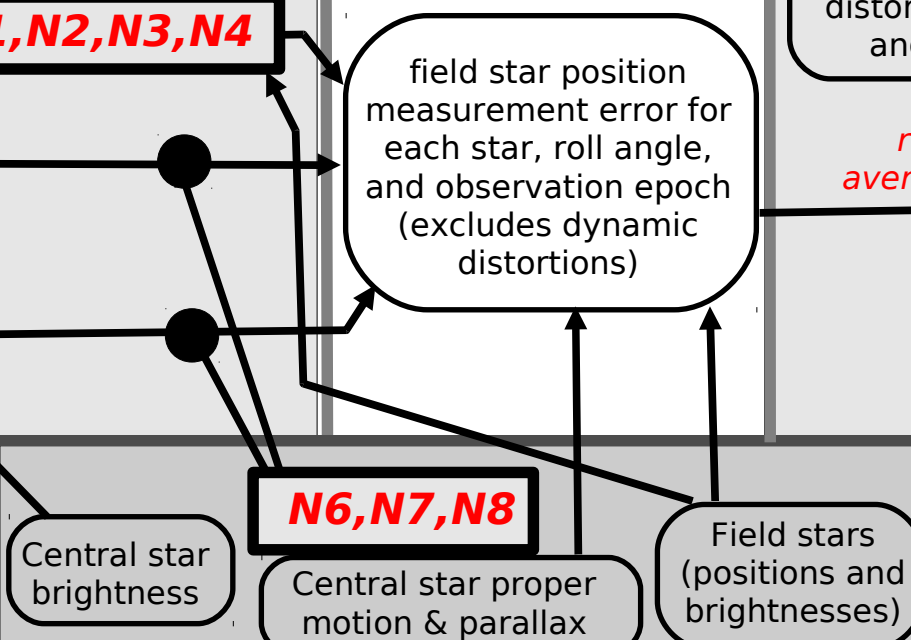
Simulated data



Data analysis



Target and field stars

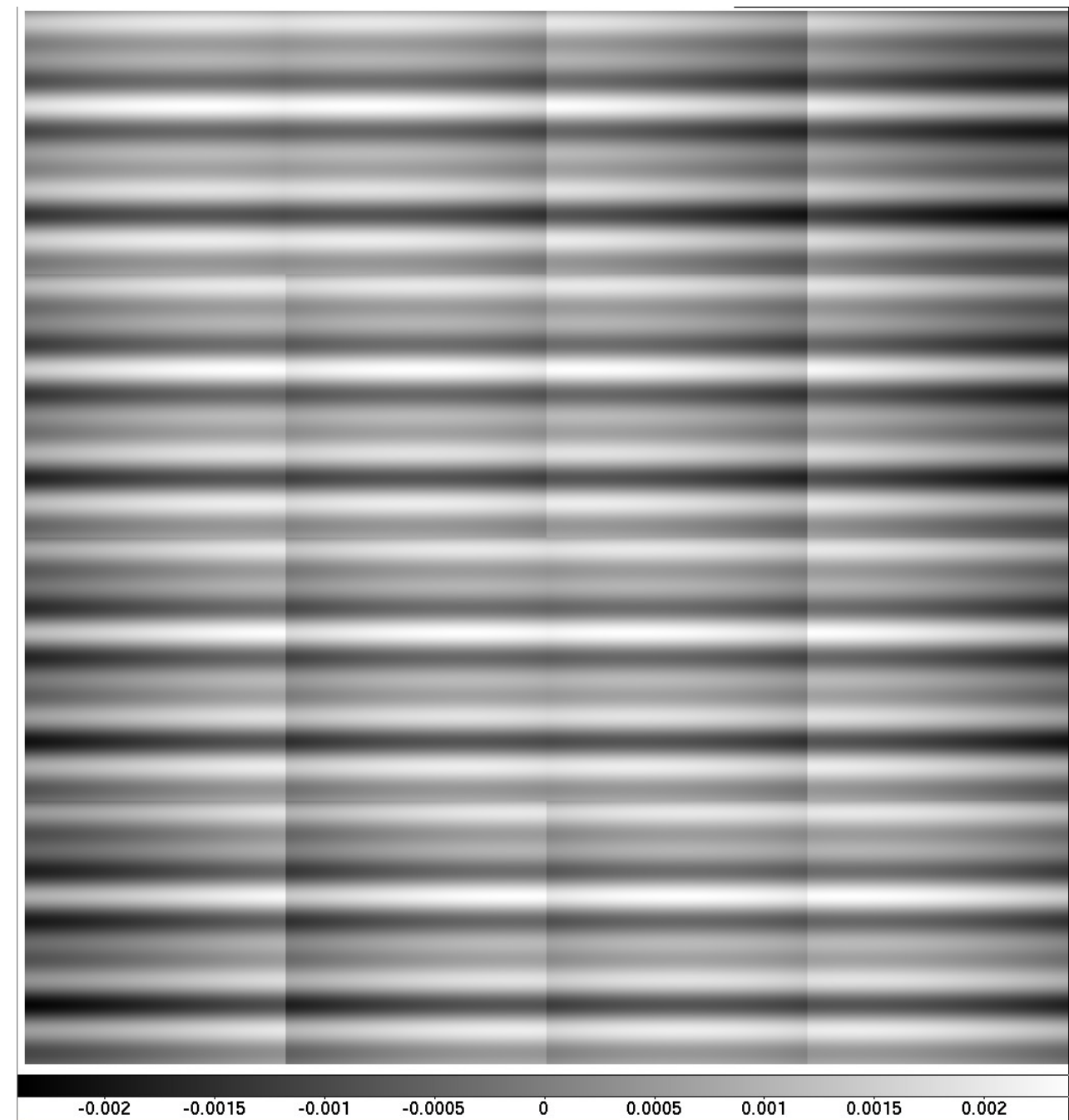
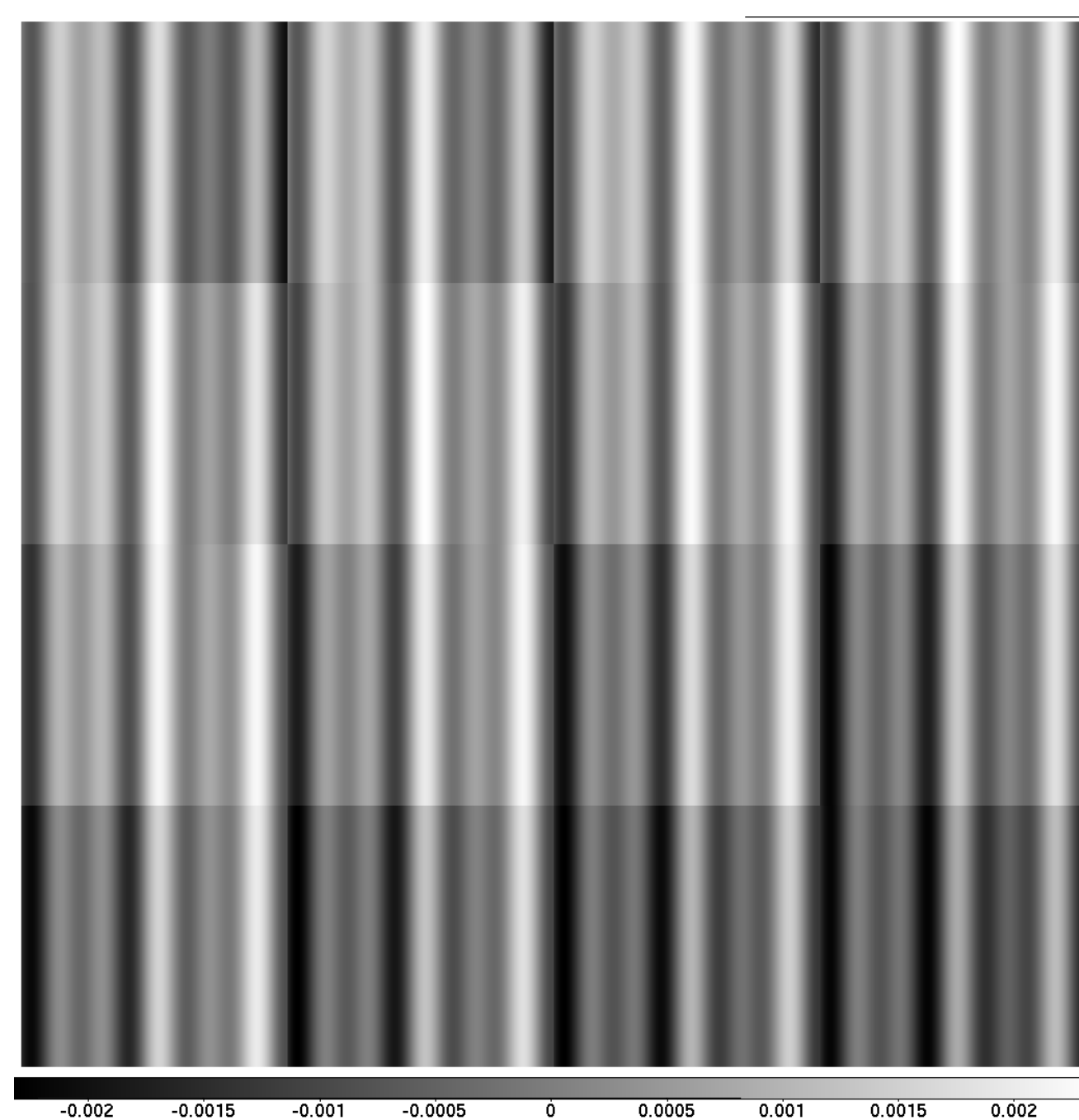


Static distortion map due to uncalibrated focal plane array geometry

Distortion maps shown for 0.2×0.2 deg. Due to pixel size non-uniformity residual after ground/in orbit calibration of detector. Spatial frequencies chosen here put most power in between spikes and at \sim arcsec separation (worst case)

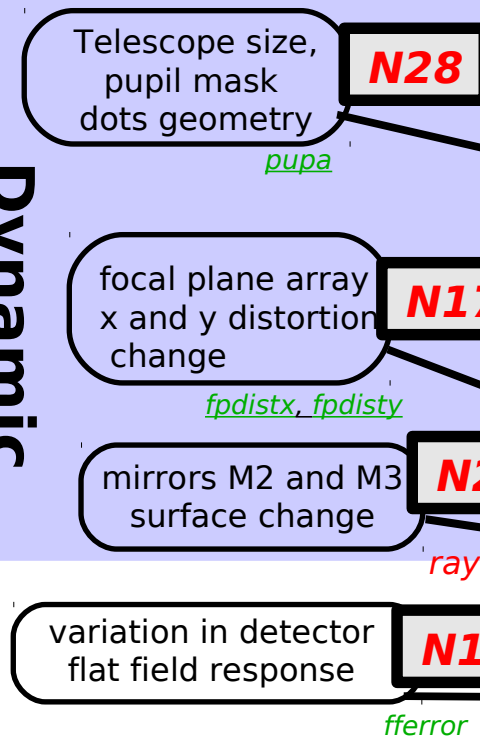
$\sim 2/1000$ pixel amplitude = $90 \mu\text{as}$

left: x, right: y. Unit = pixel (44 mas)

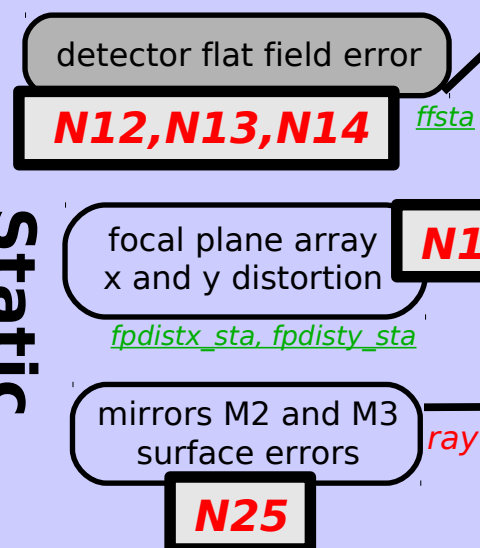


Input errors and instrument characteristics

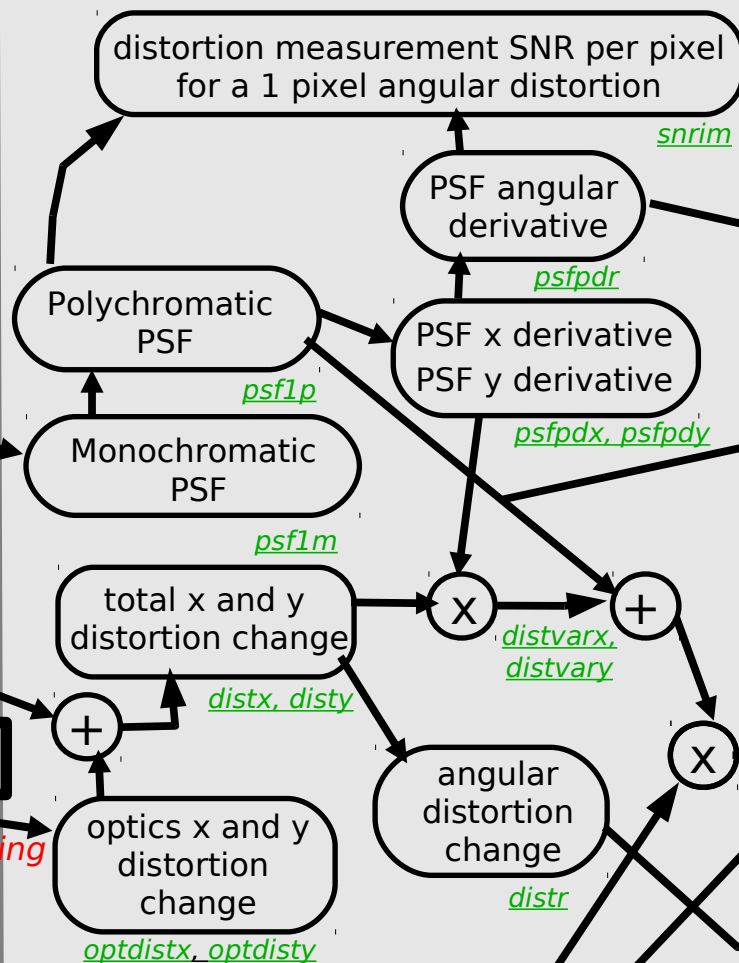
Dynamic distortions



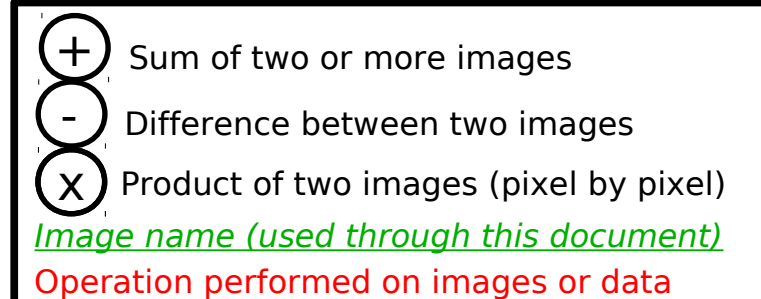
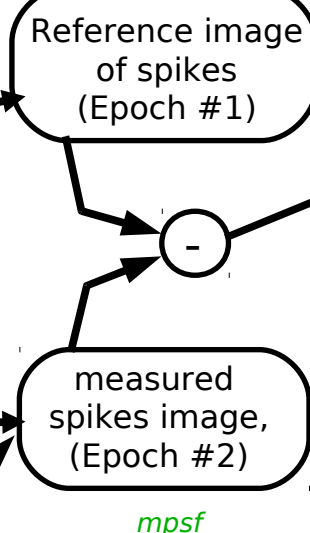
Static distortions



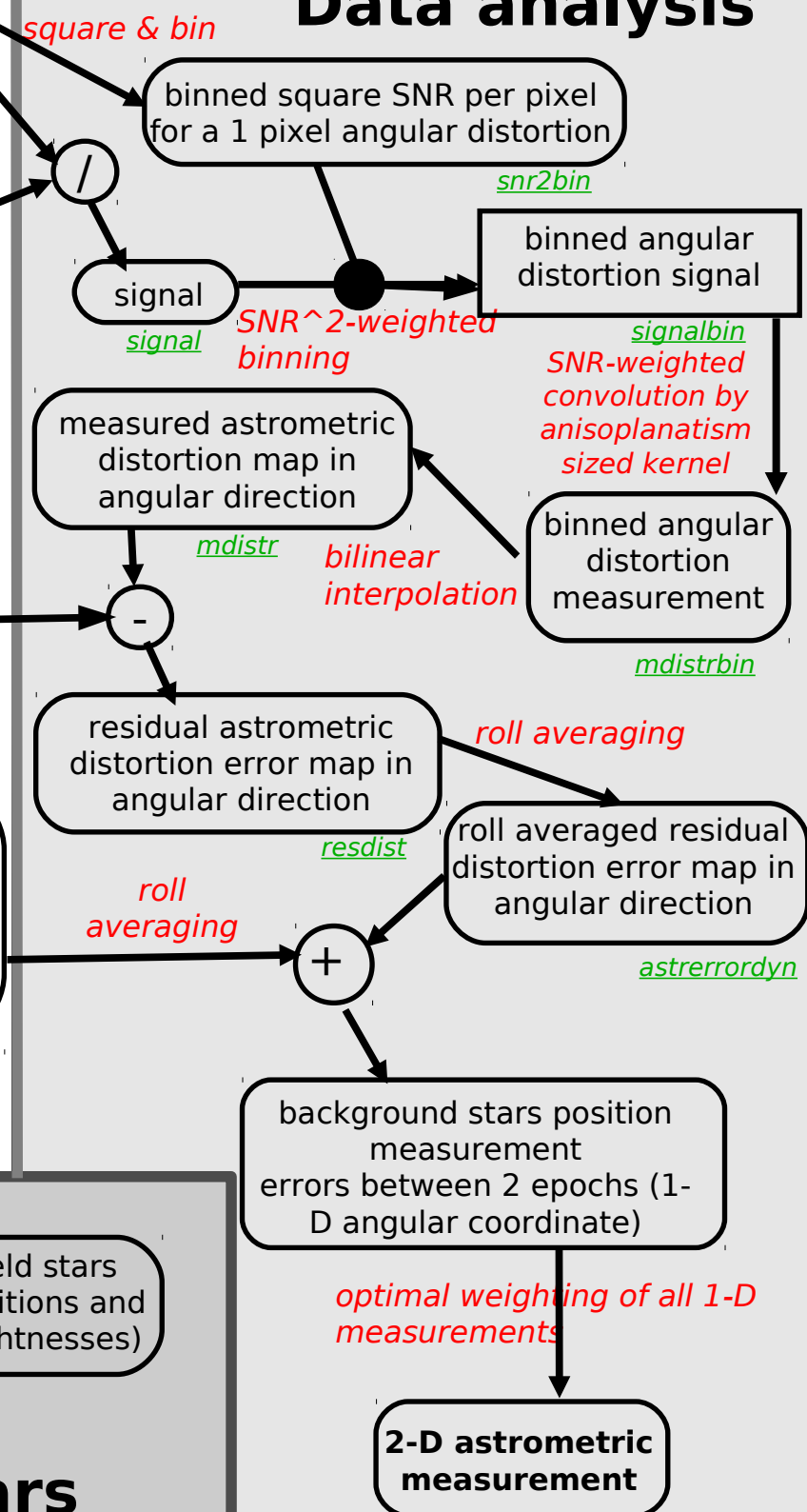
Data simulation



Simulated data



Data analysis



N1,N2,N3,N4

field star position measurement error for each star, roll angle, and observation epoch (excludes dynamic distortions)

N6,N7,N8

Central star brightness

Central star proper motion & parallax

Field stars (positions and brightnesses)

Target and field stars

static angular distortion *distr_sta*

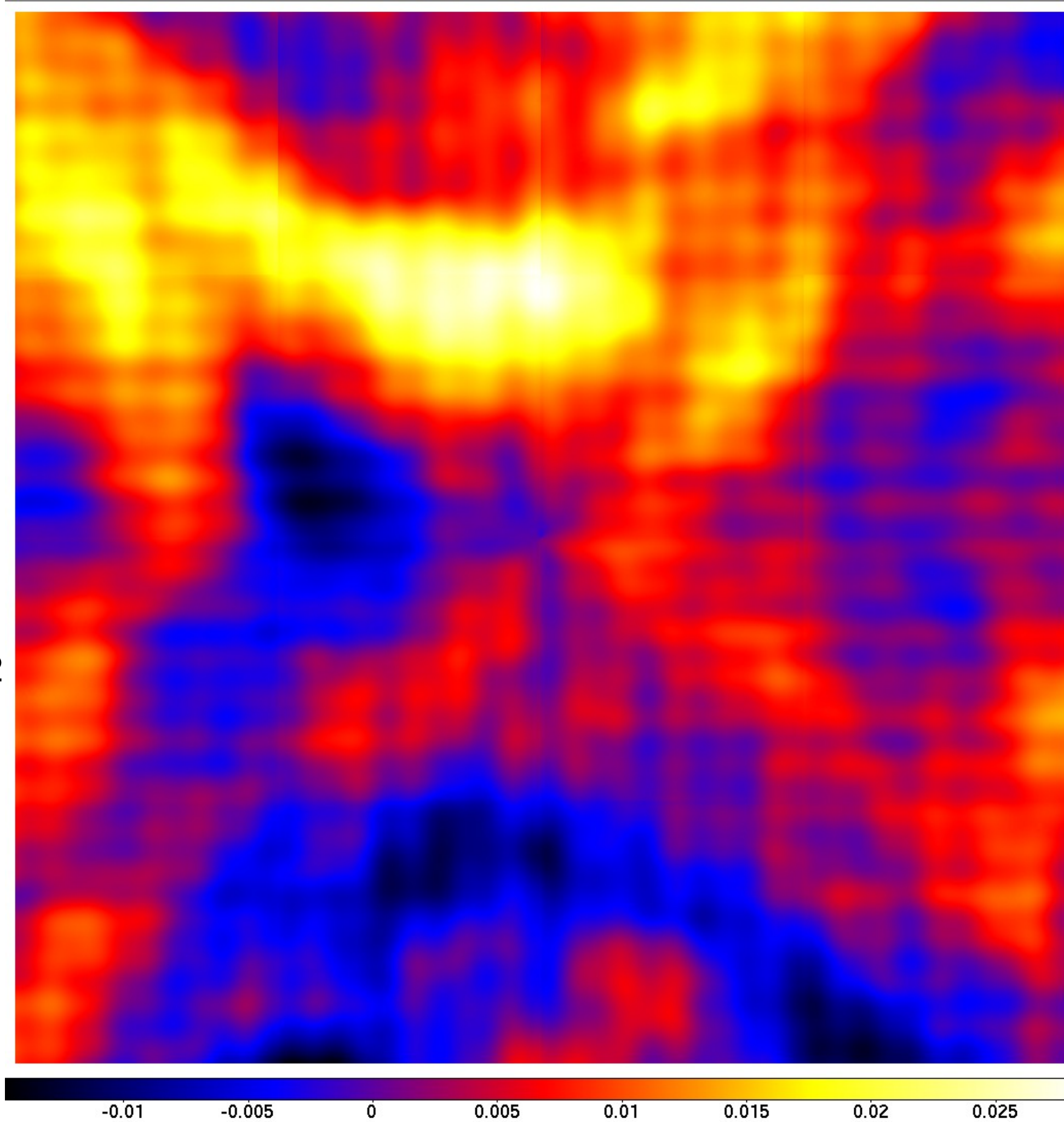
total x and y distortion *distx_sta, disty_sta*

optics x and y distortion *optdistx_sta, optdisty_sta*

Total static distortion map

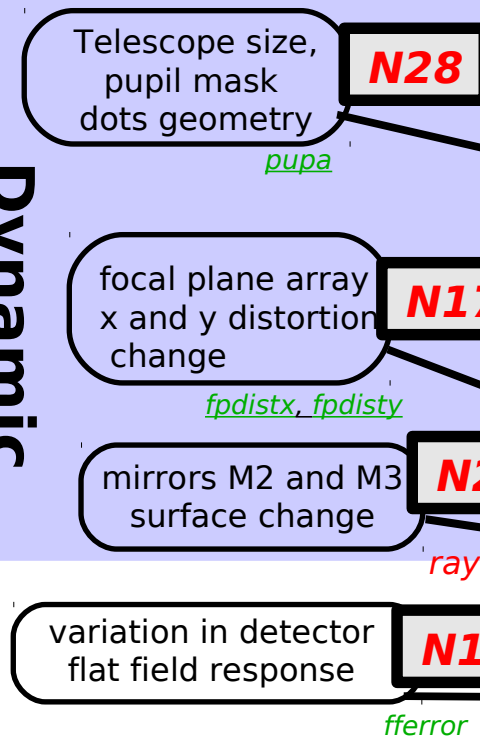
Angular coordinate
distortion
(perp. to spikes)
map shown for 0.2×0.2
deg.
Unit = pixel (44 mas)

distortion is ± 1 mas
approximately

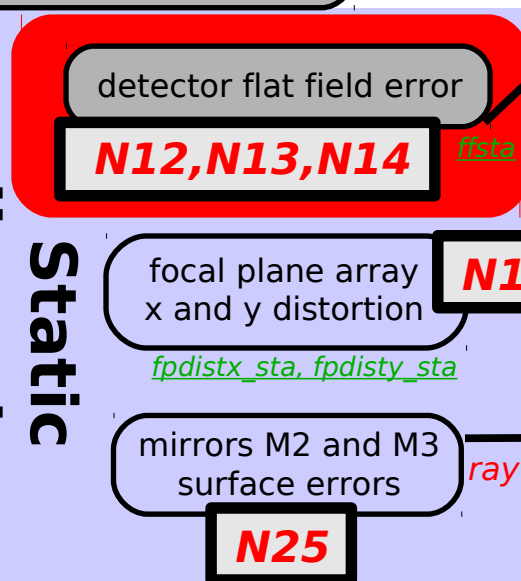


Input errors and instrument characteristics

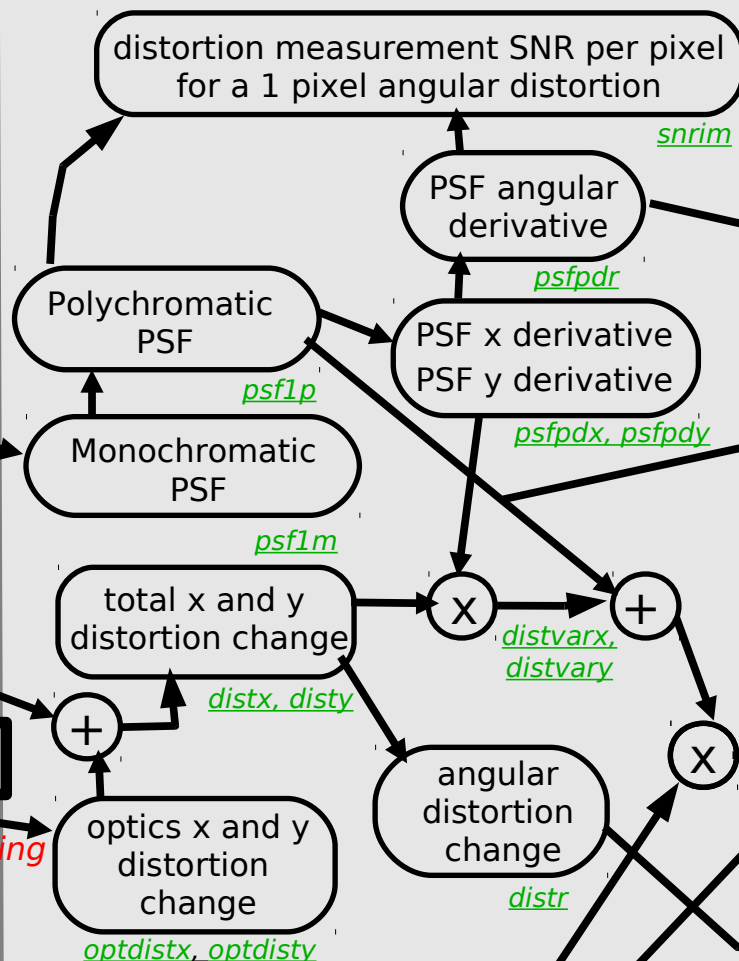
Dynamic distortions



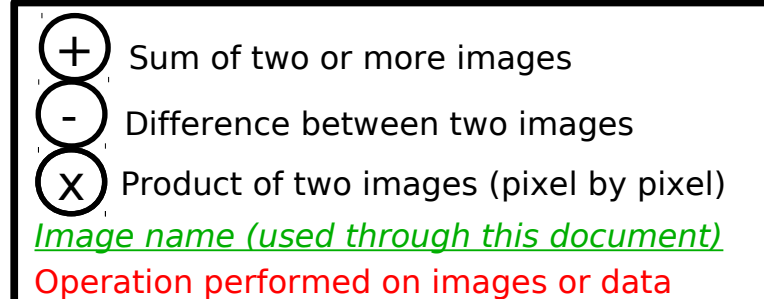
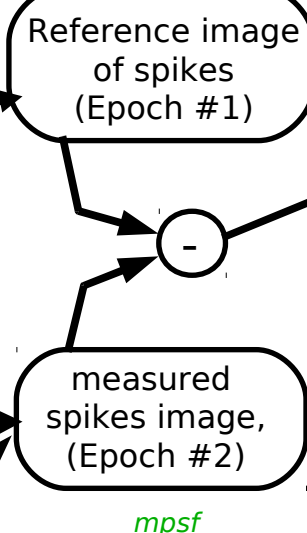
Static distortions



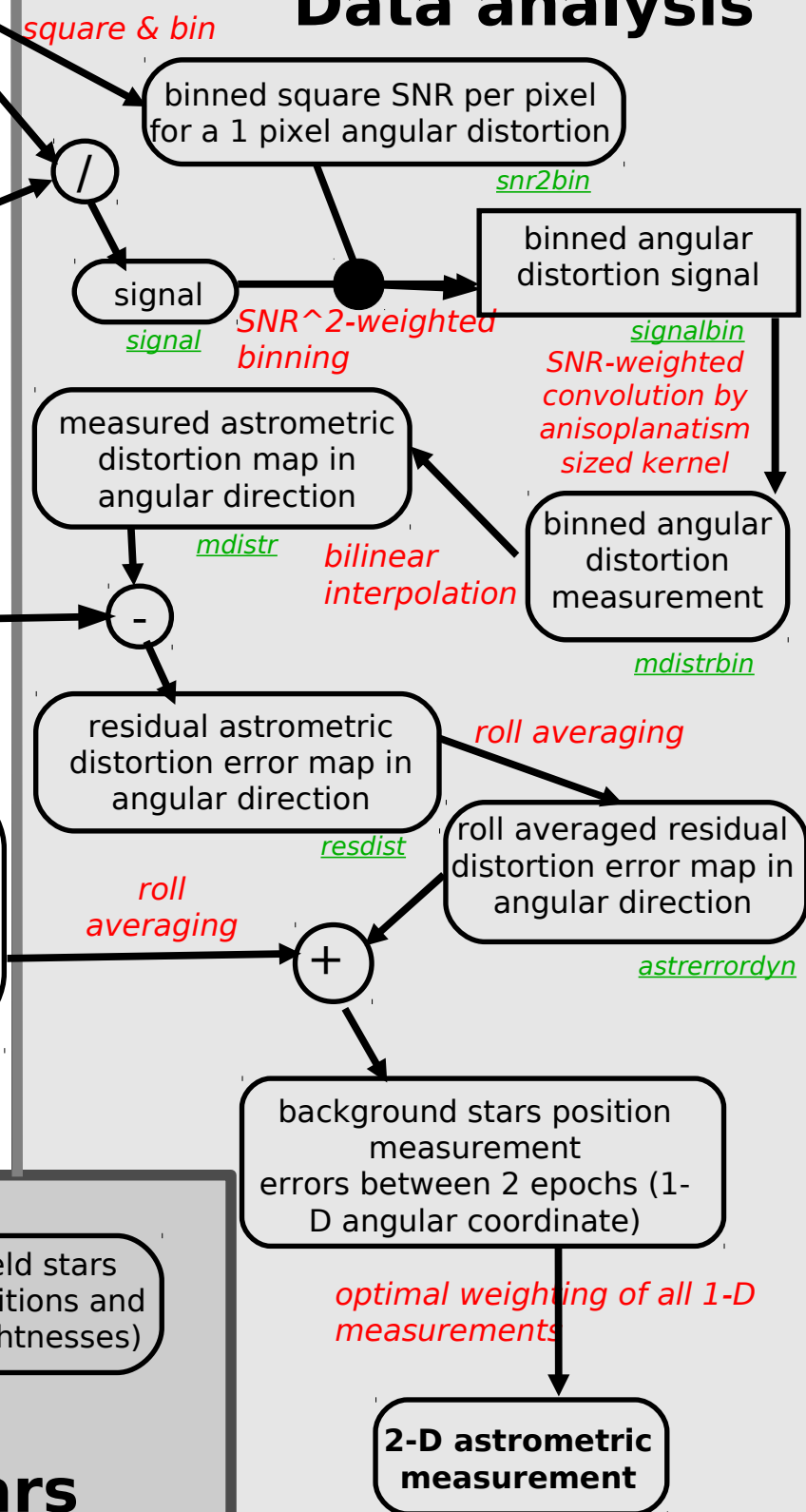
Data simulation



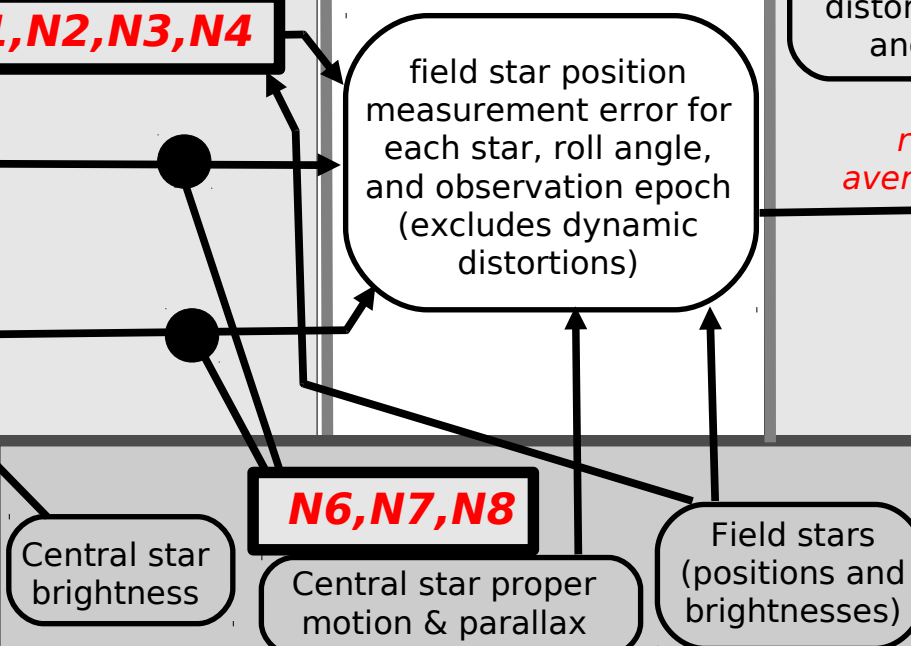
Simulated data



Data analysis



Target and field stars



Static uncalibrated flat field error

1% random error + lines and columns errors

error is +/-6% peak, 1.02% RMS

full frame

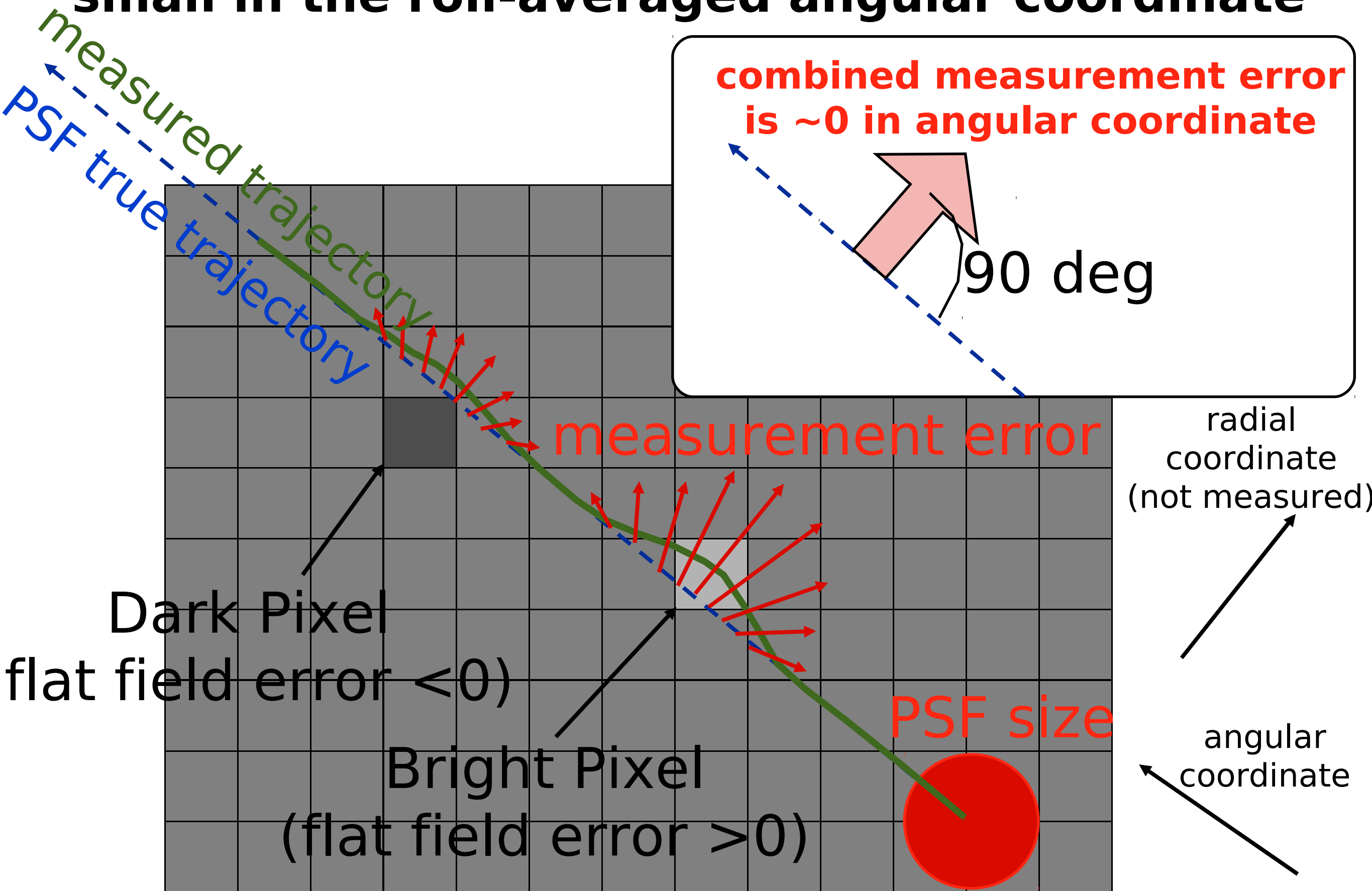
detail



Flat field knowledge requirement

- With 0.2 deg diam, 1 rad roll, measurement is done over ~ 100 stars x 3000 independent positions (separated by more than $1/D$) on the detector = $3e5$ measurements
- $0.2 \text{ uas} = 1/200000 \text{ pixel} \rightarrow$ allowed error (if not correlation) is $< 1/500 \text{ pixel} \sim 1\%$ error on flat field at small scales (pixel to pixel)
- Astrometric error due to pixel-to-pixel flat field errors is strongly anticorrelated along the PSF track on the detector \rightarrow averages closer to $1/N$ than $1/\sqrt{N}$ \rightarrow flat field knowledge errors of a few % should be OK (see next slides)

Detector static errors are expected to be very small in the roll-averaged angular coordinate



measured trajectory
PSF true trajectory

combined measurement error
is ~ 0 in angular coordinate

90 deg

measurement error

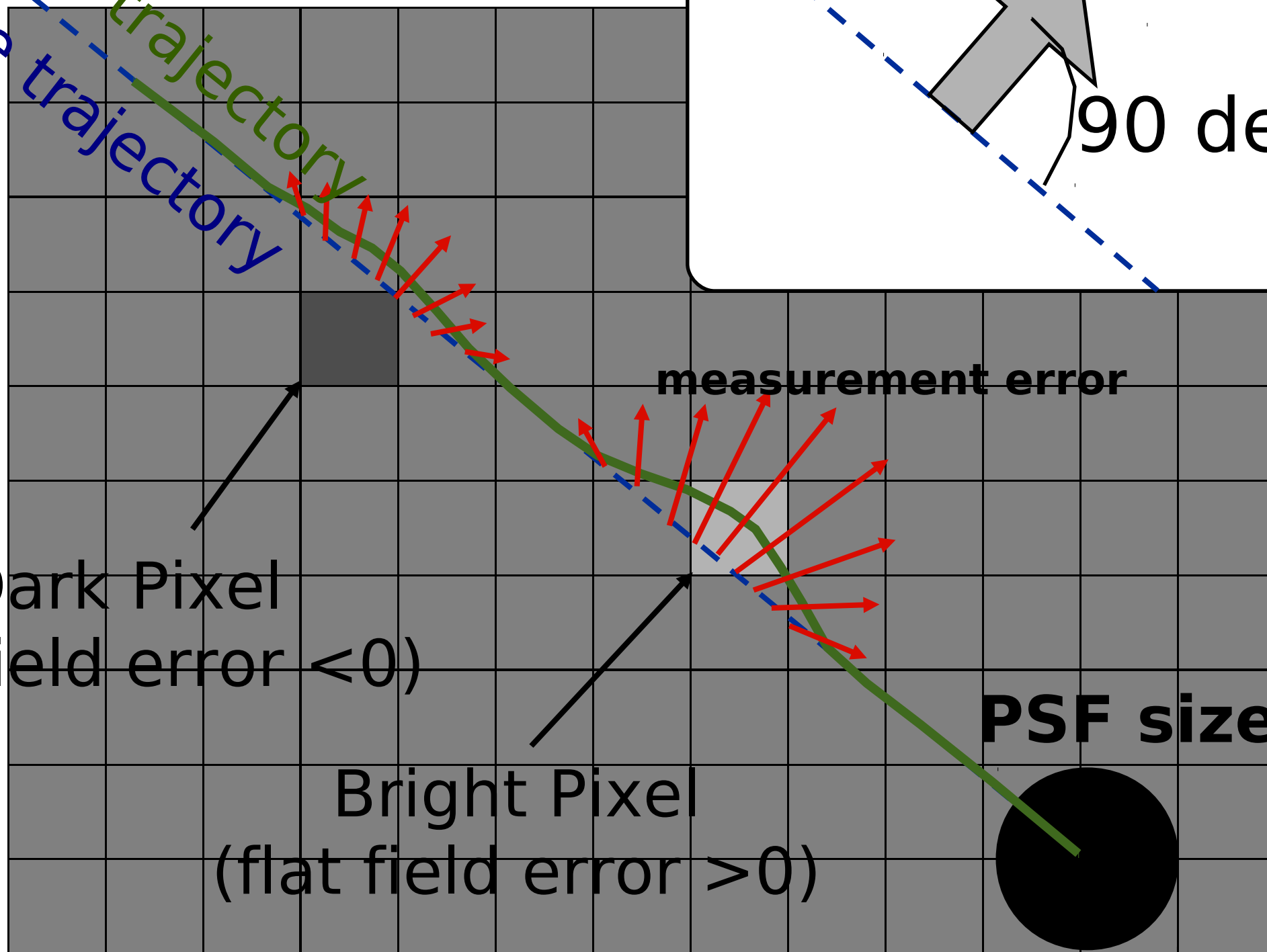
radial
coordinate
(not measured)

Dark Pixel
(flat field error < 0)

Bright Pixel
(flat field error > 0)

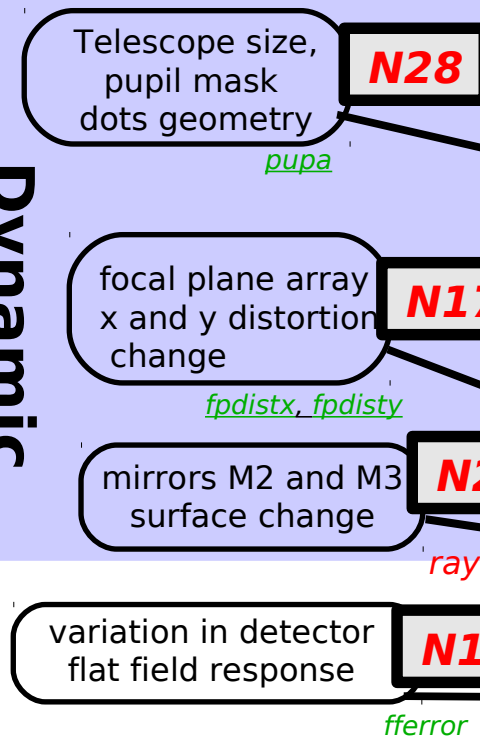
PSF size

angular
coordinate

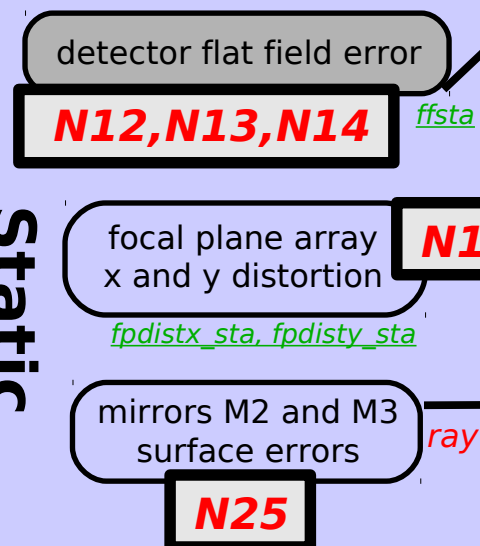


Input errors and instrument characteristics

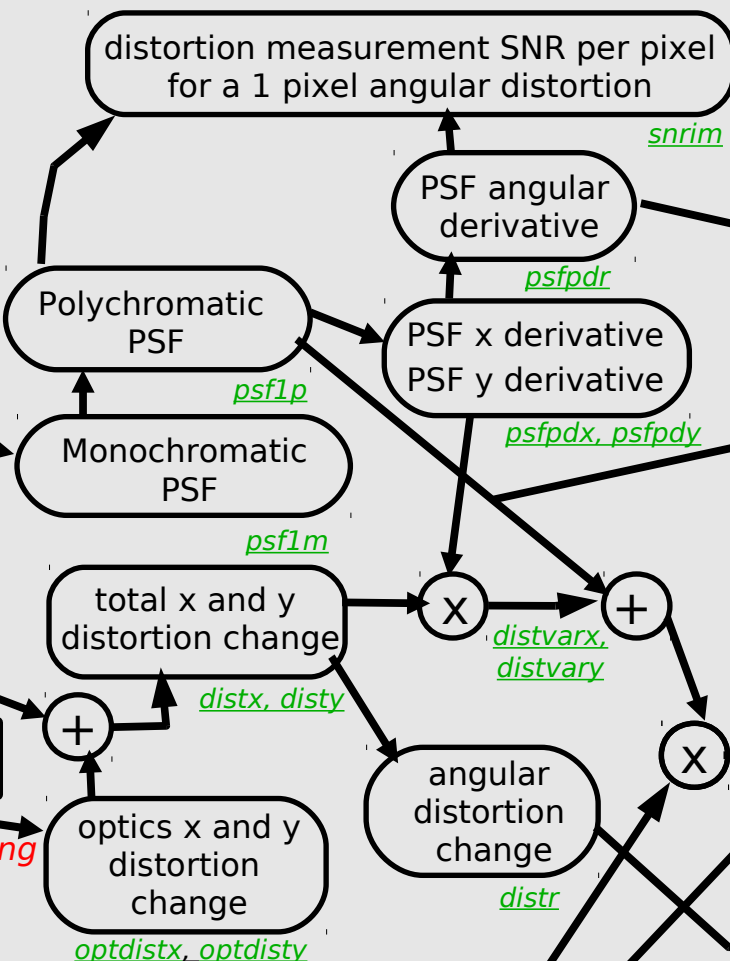
Dynamic distortions



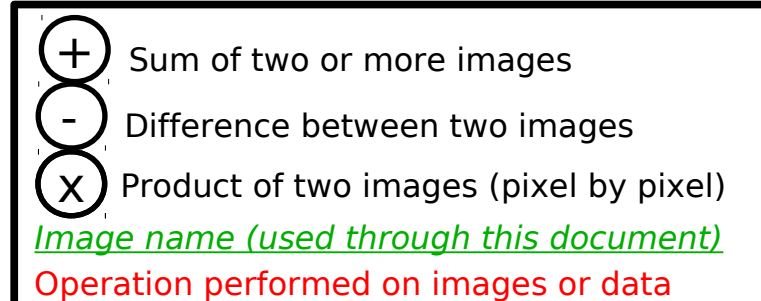
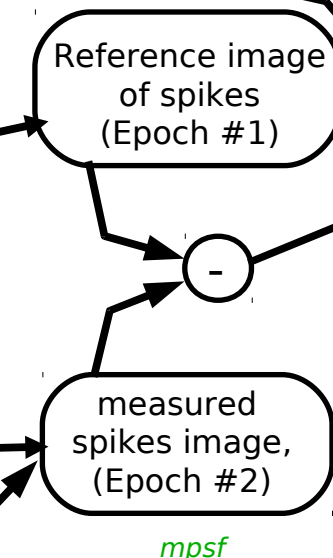
Static distortions



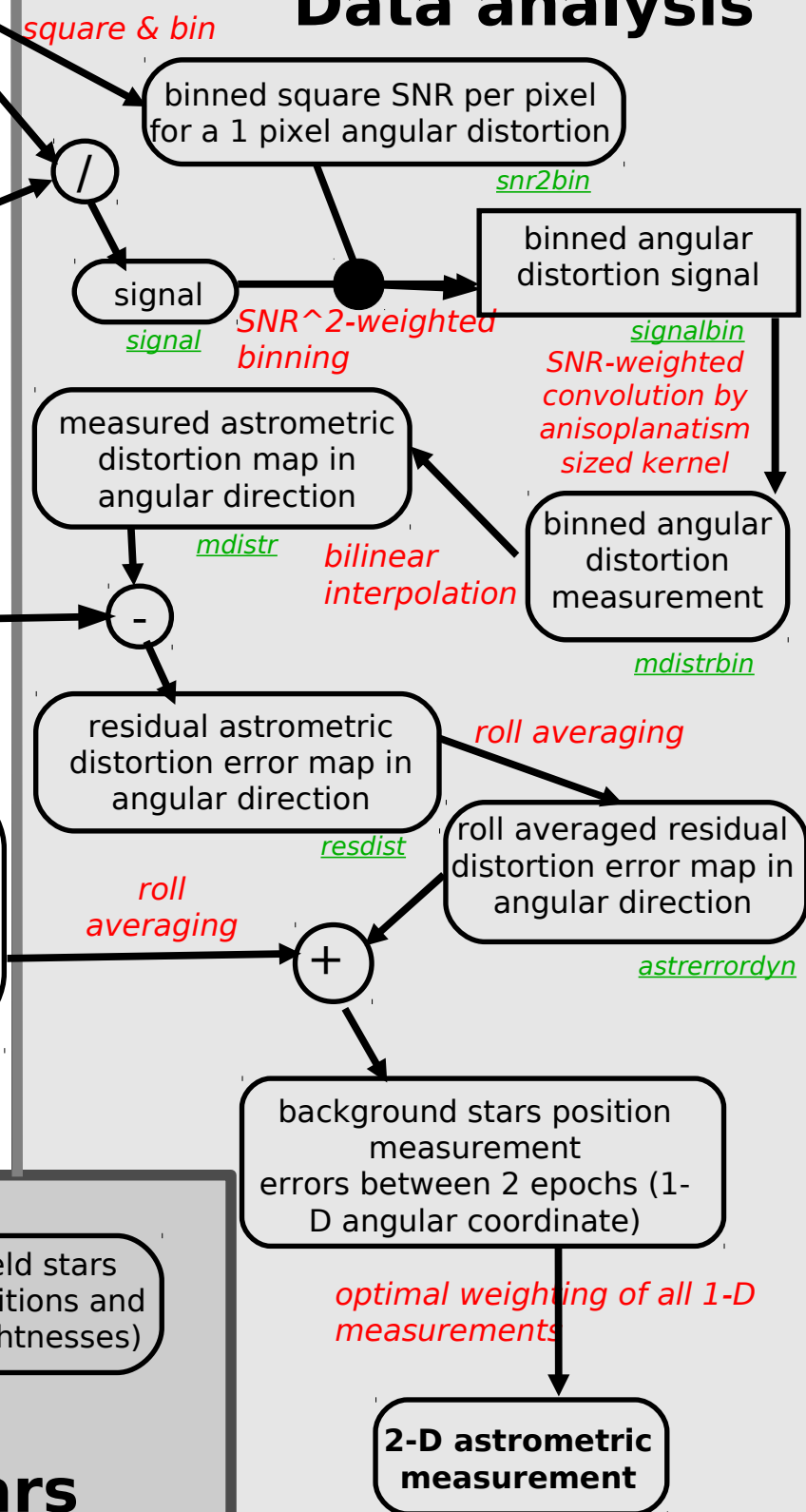
Data simulation



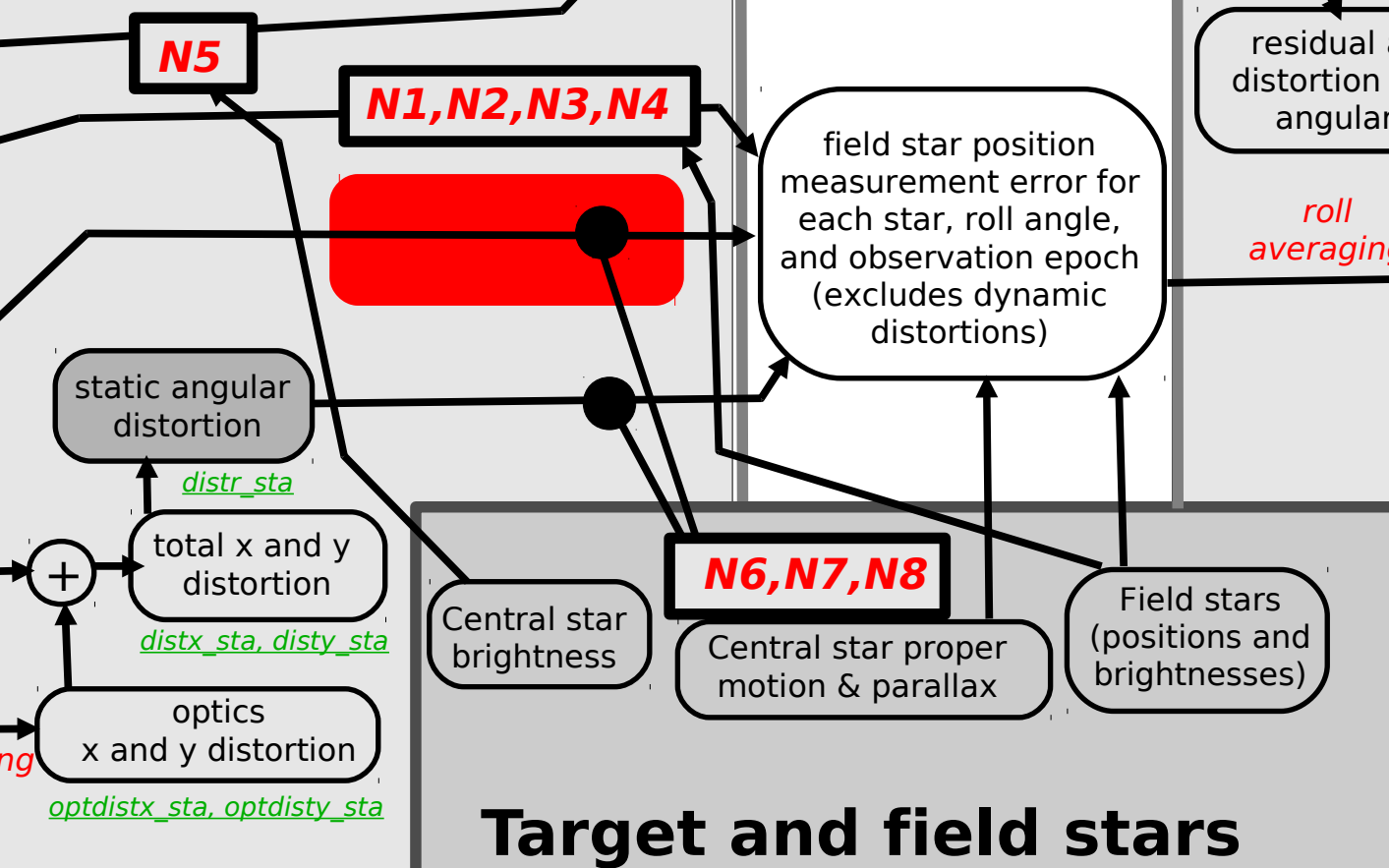
Simulated data



Data analysis



Target and field stars



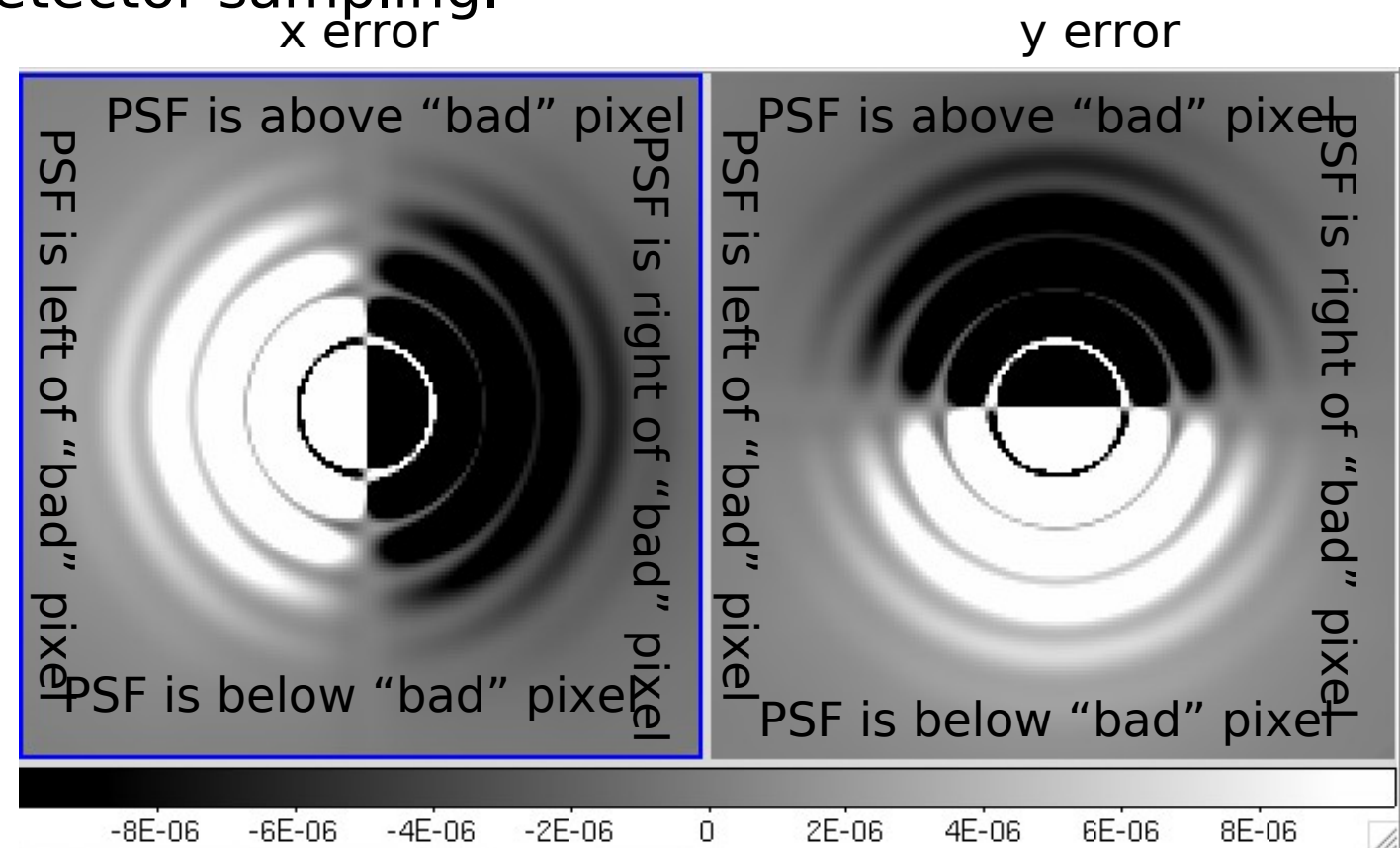
Numerical simulation of astrometric error due to flat field errors

Step 1: pre-compute how a single pixel sensitivity error “pulls” the estimated PSF position (= astrometric error kernel for a single pixel error).

This is done at 0.1 I/D step size, over 10 I/D radius: for each 2-D offset (within 10 I/D radius, with 0.1 I/D step) between the PSF center location and the “bad” pixel, compute the error in PSF position measurement in x and y. Computation uses finely sampled PSFs binned down to the detector sampling.

Maps on the right show how a sensitivity error in a single pixel affects the PSF position measurement.

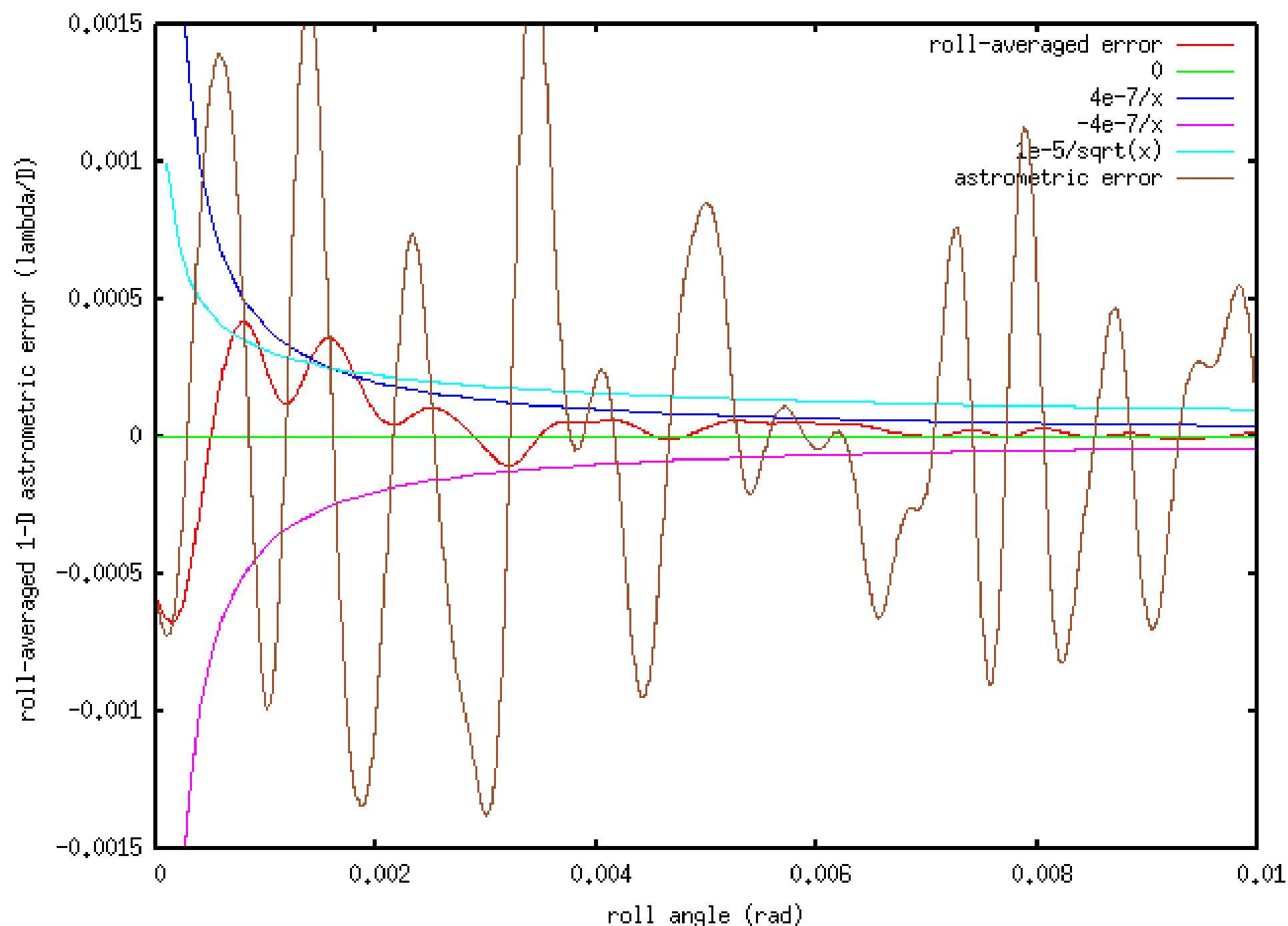
Maps are normalized to the relative pixel sensitivity error. Unit is I/D. Peak value is 0.05: a 1% sensitivity error can move the PSF measured position by $0.0005 \text{ I/D} = 44 \text{ uas}$

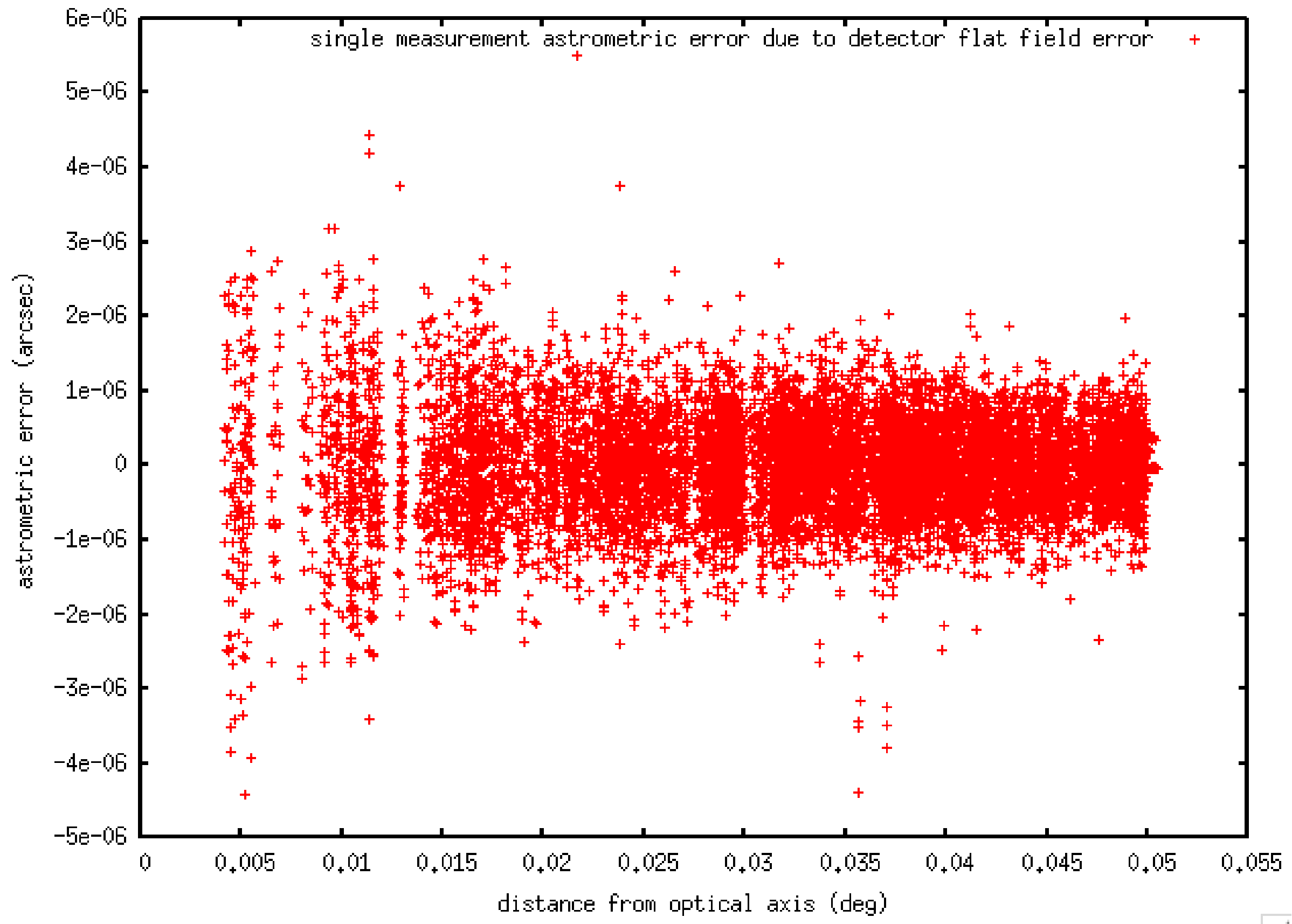


Step 2: For each roll angle and star, compute 2-D PSF position error by summing all errors due to pixels sensitivity errors within a 10 I/D radius of actual PSF position. This computation uses the maps shown above: for each pixel, the fractional offset between the pixel and the PSF is computed, and the corresponding error values (x and y) are derived from bilinear interpolation of the maps computed in step 1.

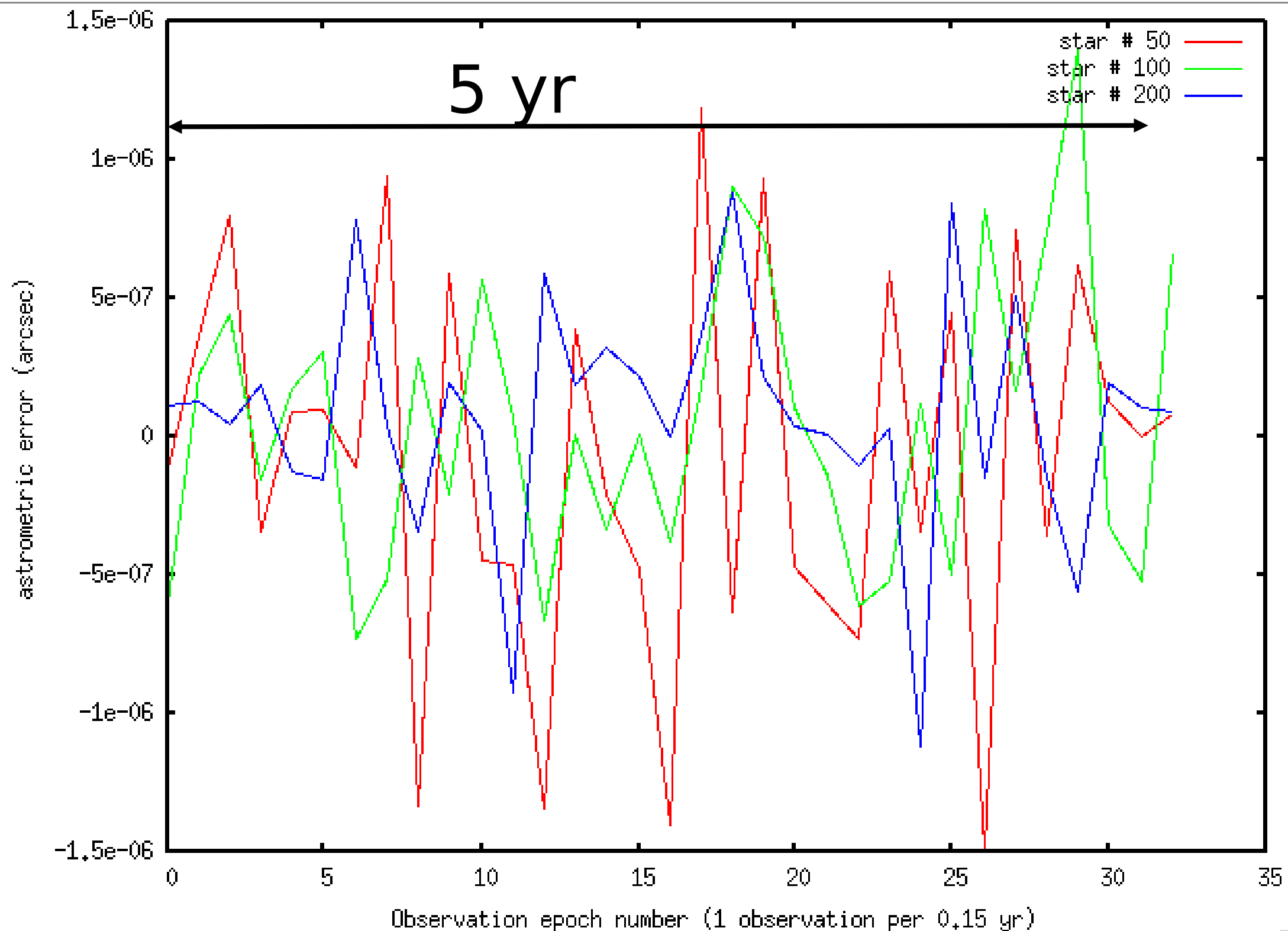
Flat field errors are strongly anticorrelated with roll angle -> they average as $1/N$ instead of $1/\sqrt{N}$

Figure on the left shows 1-D astrometric error for a single star as a function of roll angle. The raw error (brown) is $\sim 10^{-3}$ I/D RMS (~ 0.1 mas). The roll-averaged error (red) goes as $1/\text{roll angle}$.





Astrometric error due to flat field errors is ~ 0.5 uas per star for a 1 rad roll.
Error is stronger for stars closer to the optical axis (less roll averaging)



Single star astrometric error due to flat field errors shows no obvious time correlation in this example (1 arcsec / yr proper motion). With smaller proper motion and more distant stars (small parallax), correlation is expected over two timescales : time for proper motion to move star by 1 pixel, and 1 year period due to parallax.

Intra-pixel sensitivity errors are captured in this analysis

Unknown variations of sensitivity within a pixel show the same anti-correlation behavior, and are captured in this analysis.

Example: top half of a pixel less sensitive than bottom half

If PSF is below the pixel, PSF position error is positive

If PSF is above the pixel, PSF position error is negative

A small error in sensitivity between pixels is similar to a larger error within a pixel.

Intra-pixel sensitivity errors can be simulated by the same analysis as shown here, but with a finer sampling.

Dynamic distortions

Definition: Any change between observations epochs

These changes introduce errors in the measured position of background stars or on the distortion change measured by the spikes image.

Description of main error terms:

- Variation in the optical shape of mirrors M2 and M3 due to thermal and mechanical stresses introduces astrometric distortions that change between the observation epochs
- Rigid body motion of optics (telescope alignment)
- Focal plane array geometry: motion and distortion of individual detector chip due to temperature fluctuation and mechanical stress
- Variations in the flat field response of the detector

Impact and mitigation:

Low order components of dynamic errors are calibrated by the diffraction spikes. To measure how distortions change between observations, the motion of the spikes is measured by comparison of the spike images between the different observation epochs.

Errors in this estimate come from

- photon noise (spikes, zodi)
- changes in the pixel response between the 2 epochs
- interpolation between spikes (no signal between spikes)

Time-variable distortions are not perfectly estimated by the spikes -> astrometric error

Input errors and instrument characteristics

Dynamic distortions

Telescope size, pupil mask dots geometry **N28**
pupa

focal plane array x and y distortion change **N17**
fpdistx, fpdisty

mirrors M2 and M3 surface change **N25**
raytracing

variation in detector flat field response **N16**
fferror

photon noise due to zodiacal background and central star flux

photon noise error due to zodiacal light and field star flux

Static distortions

detector flat field error **N12,N13,N14**
ffsta

focal plane array x and y distortion **N15**
fpdistx_sta, fpdisty_sta

mirrors M2 and M3 surface errors **N25**
raytracing

Data simulation

distortion measurement SNR per pixel for a 1 pixel angular distortion *snrim*

PSF angular derivative *psfpdr*

Polychromatic PSF *psf1p*

Monochromatic PSF *psf1m*

total x and y distortion change *distx, disty*

optics x and y distortion change *optdistx, optdisty*

angular distortion change *distr*

static angular distortion *distr_sta*

total x and y distortion *distx_sta, disty_sta*

optics x and y distortion *optdistx_sta, optdisty_sta*

Simulated data

Reference image of spikes (Epoch #1)

measured spikes image, (Epoch #2) *mps*

field star position measurement error for each star, roll angle, and observation epoch (excludes dynamic distortions)

Central star brightness

Central star proper motion & parallax

Field stars (positions and brightnesses)

Target and field stars

Data analysis

square & bin

binned square SNR per pixel for a 1 pixel angular distortion *snr2bin*

signal *signal*

measured astrometric distortion map in angular direction *mdistr*

residual astrometric distortion error map in angular direction *resdist*

roll averaged residual distortion error map in angular direction *astrerrordyn*

background stars position measurement errors between 2 epochs (1-D angular coordinate)

2-D astrometric measurement

- $+$ Sum of two or more images
- $-$ Difference between two images
- \times Product of two images (pixel by pixel)
- Image name (used through this document)*
- Operation performed on images or data*

SNR²-weighted binning

SNR-weighted convolution by anisoplanatism sized kernel

roll averaging

roll averaging

optimal weighting of all 1-D measurements

Time-variable distortions: M2 and M3

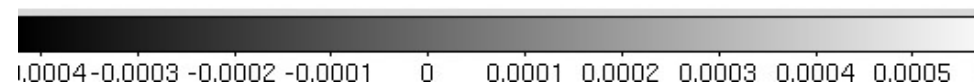
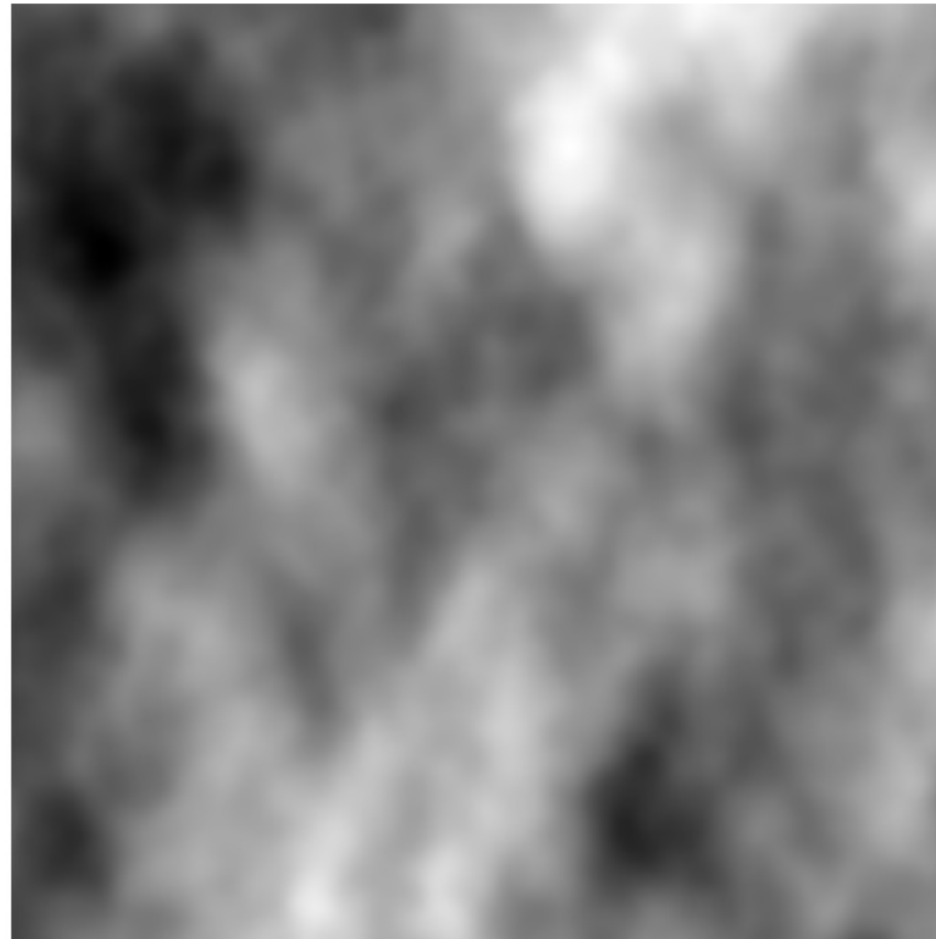
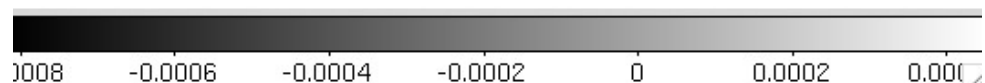
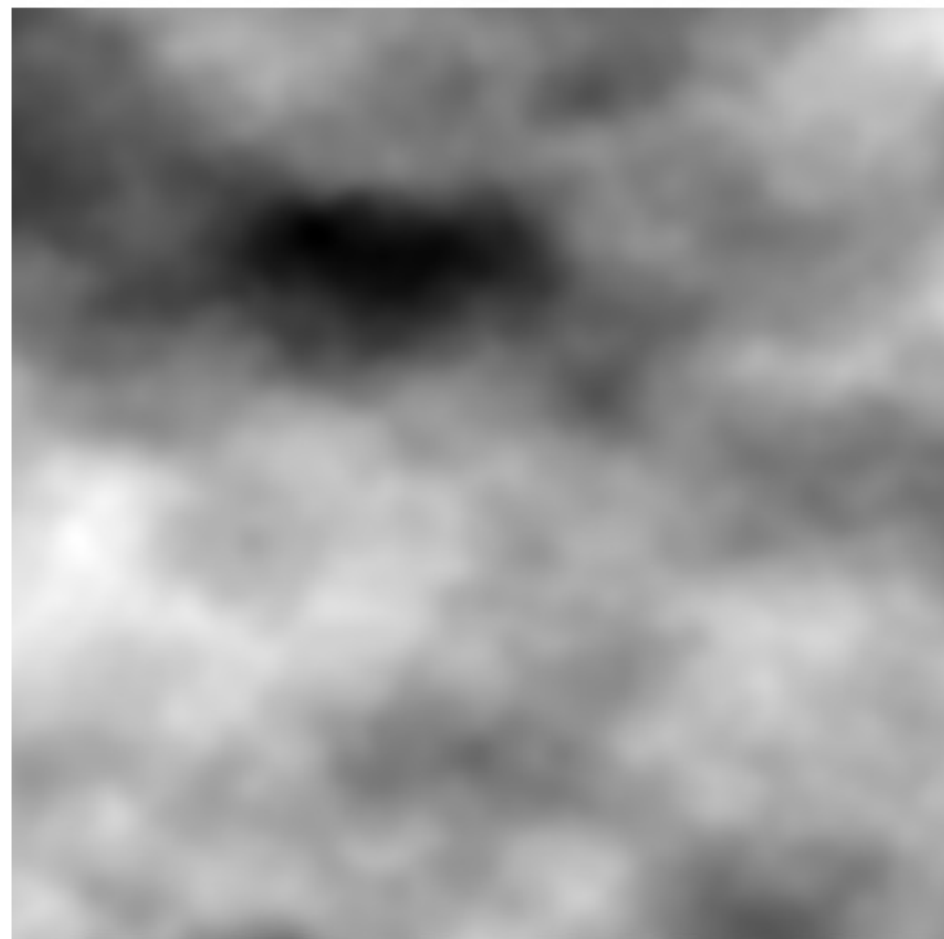
Thermal variations in substrate + mirror mounting:

On 150-350mm apertures, better than 0.1nm RMS wavefront insertion repeatability with 0.25 C temperature stability. (Jay Daniel, L-3 Tinsley, private communication)

Assuming 100mK temperature stability-> 40 pm RMS stability

Material creep :

probably slow process (timescale > single observation) which can be tracked during course of mission by averaging distortions over several consecutive observations. -> not included

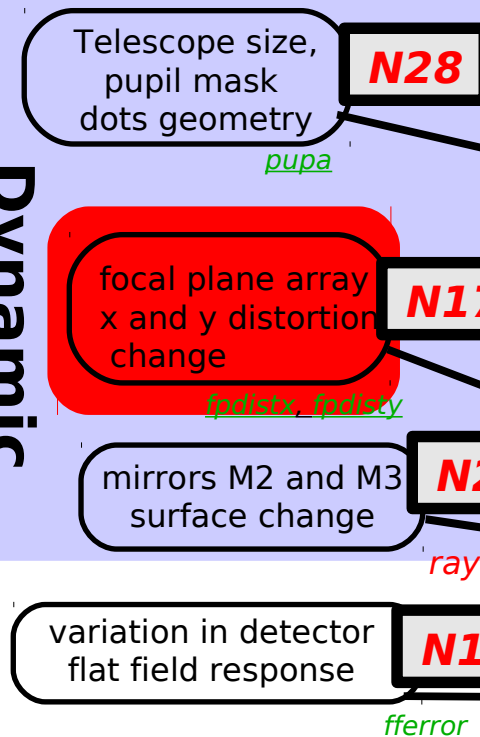


x and y astrometric distortions due to change in the shape of optics is shown on the left.

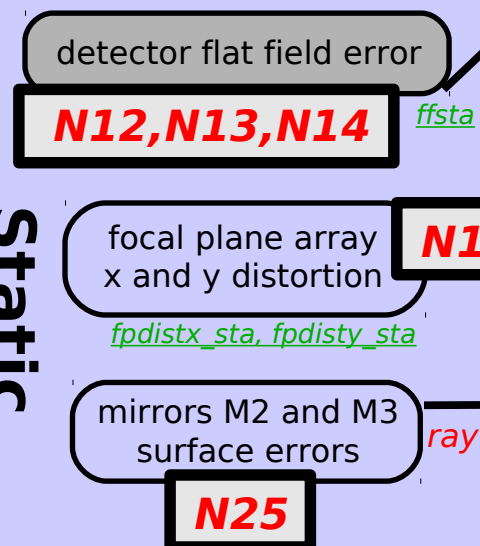
Same as static optical distortions, but scaled by 3%. Unit = pixel (44 mas)

Input errors and instrument characteristics

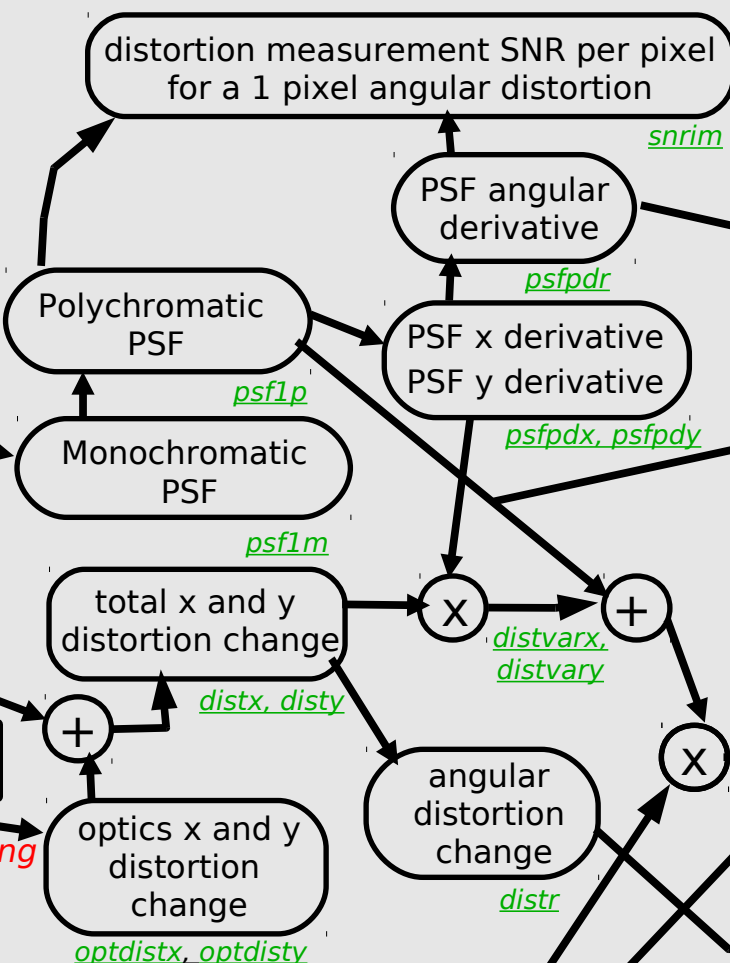
Dynamic distortions



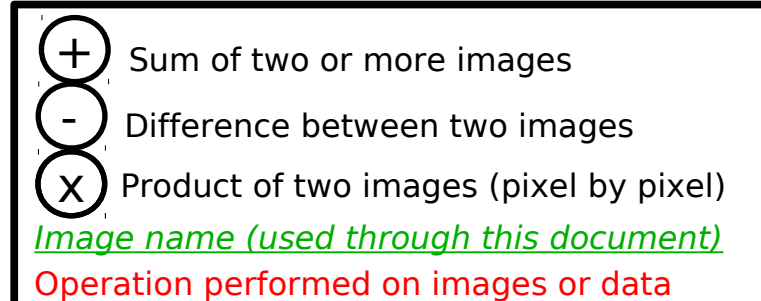
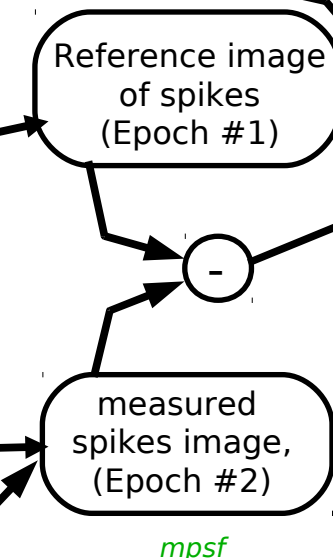
Static distortions



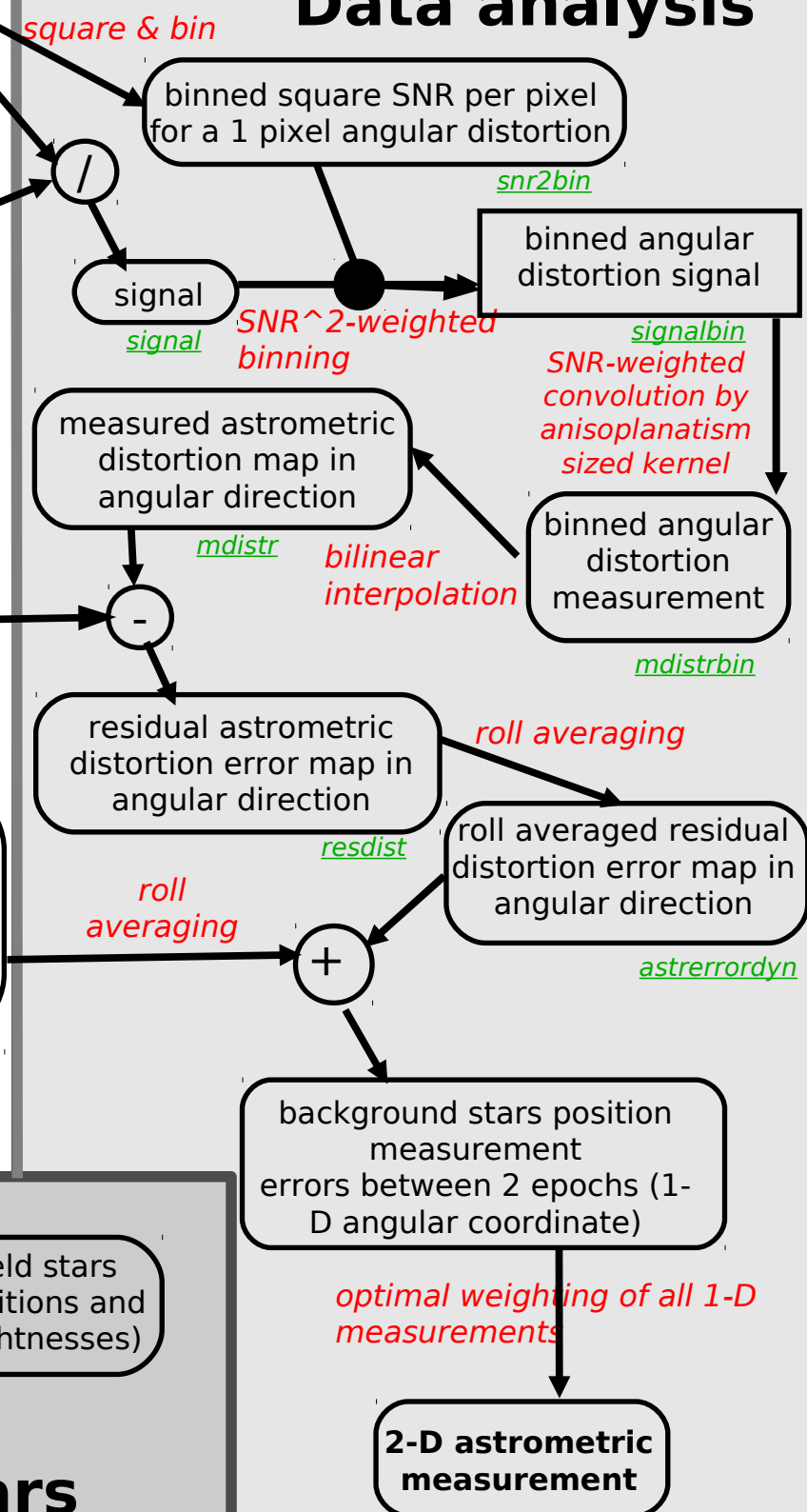
Data simulation



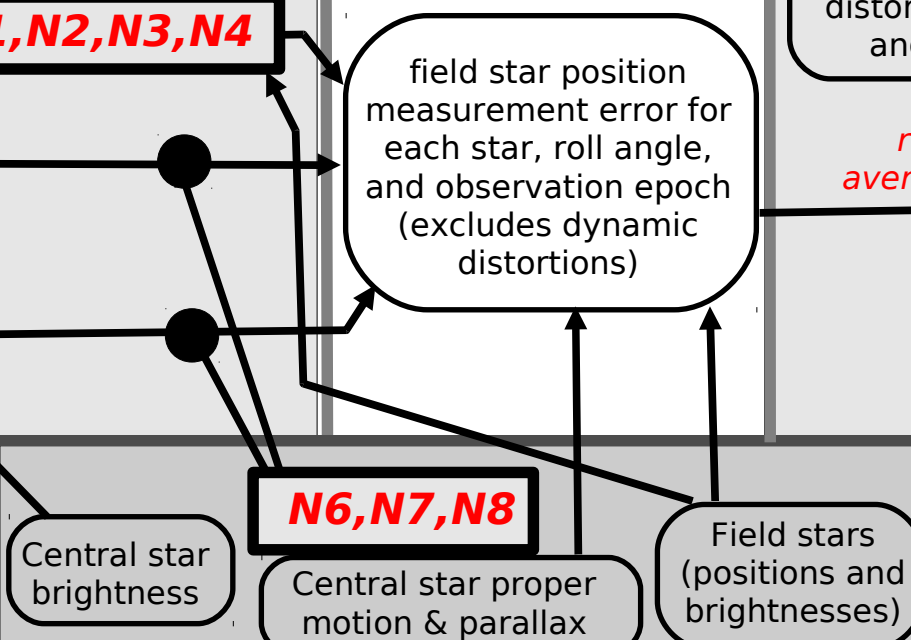
Simulated data



Data analysis



Target and field stars



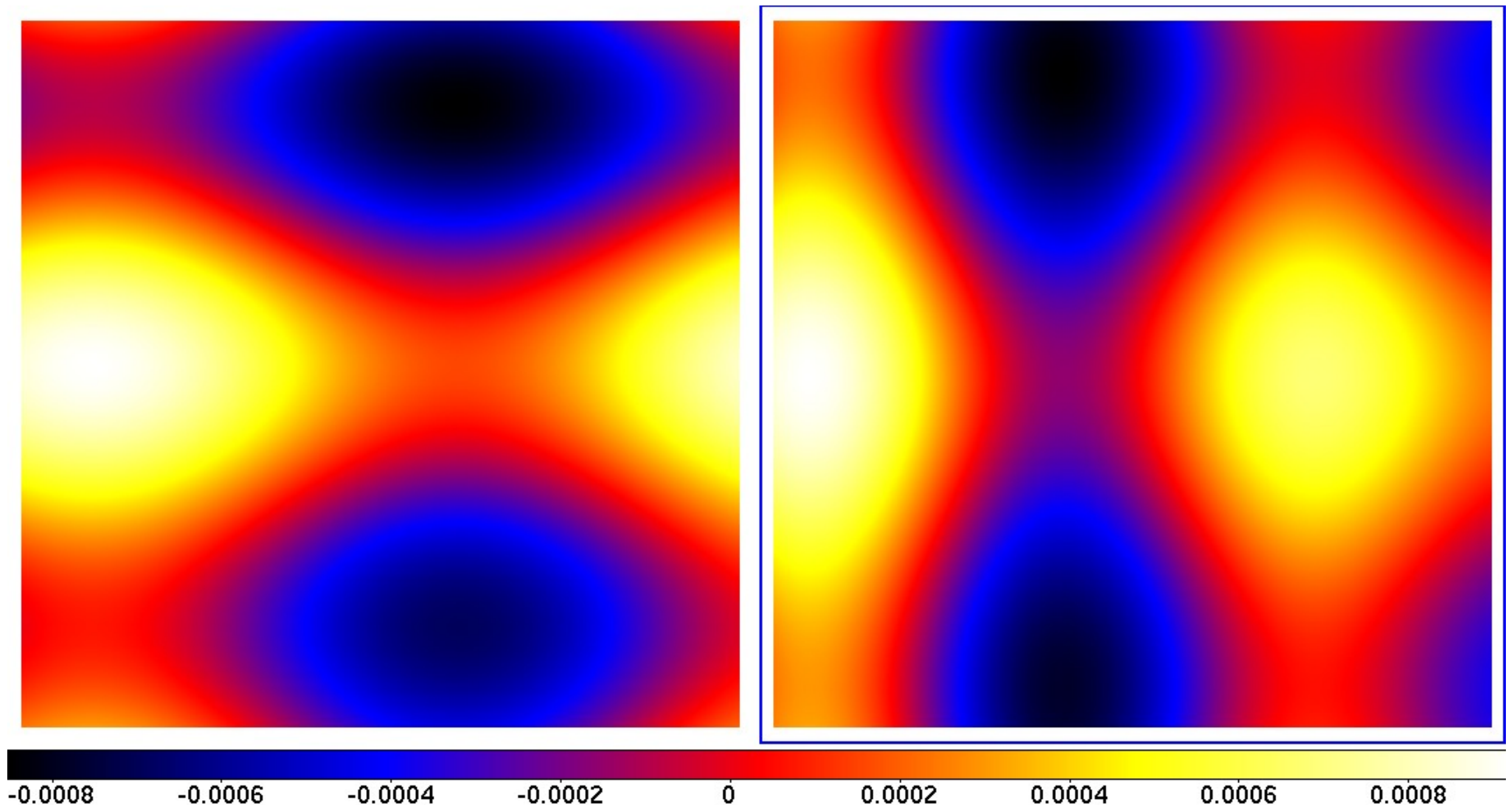
Detector array distortions

A temperature change on a 4k detector changes its linear size by 0.0172 pixel / K, assuming Si (CTE=4.2e-6). This is simulated by a low order term in x distortion with $\pm 1\text{e-}3$ pixel and period \sim single 4k detector size. Translation between detector chips not included here - would need to be fitted as a translation for each chip.

Temperature variations have no effect if homogeneous. We assume here a 20mK non-calibrated variation in the homogeneity of the detector temperature between observations.

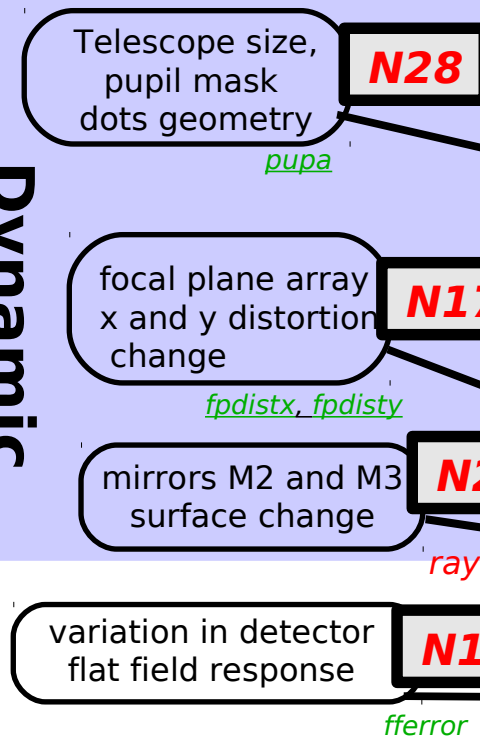
(NOTE: this error could be mitigated by projecting laser fringes on the detector)

Unit = pixel (44 mas)

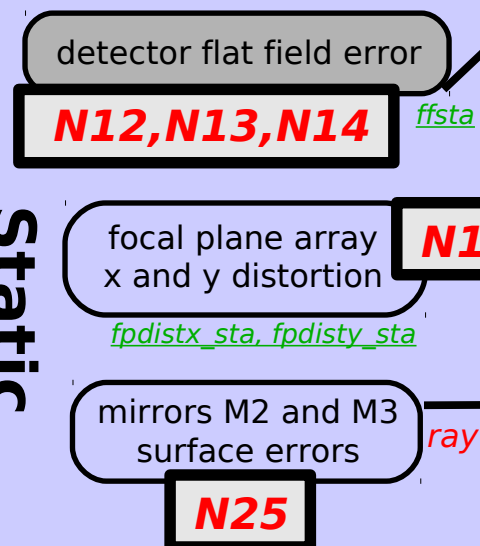


Input errors and instrument characteristics

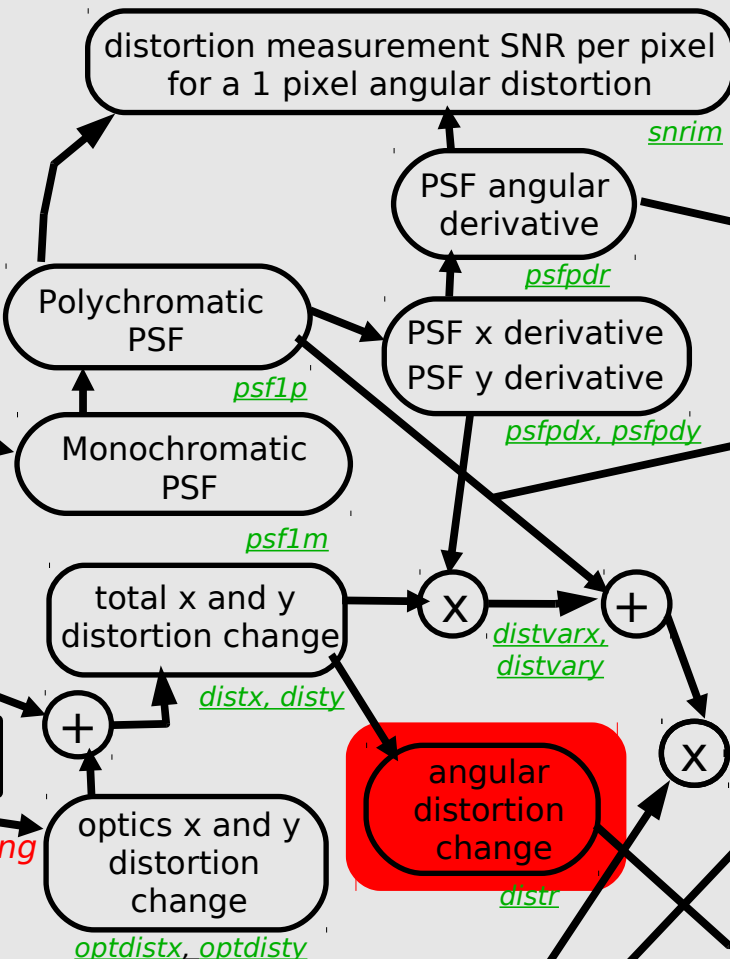
Dynamic distortions



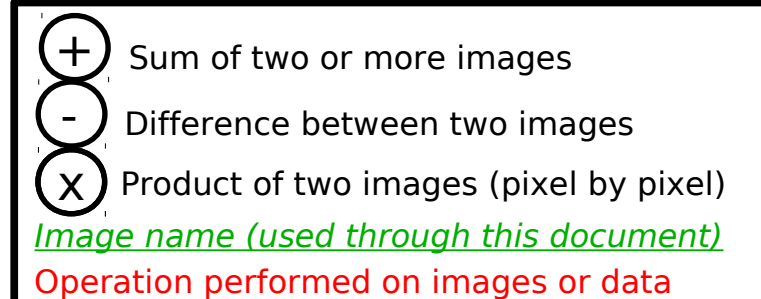
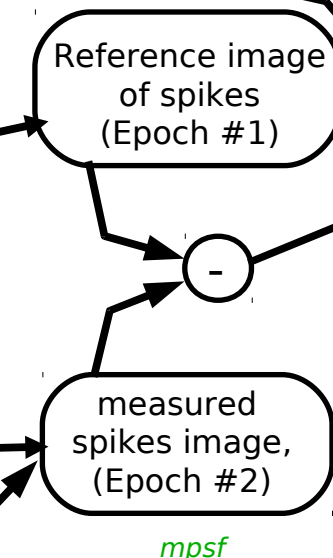
Static distortions



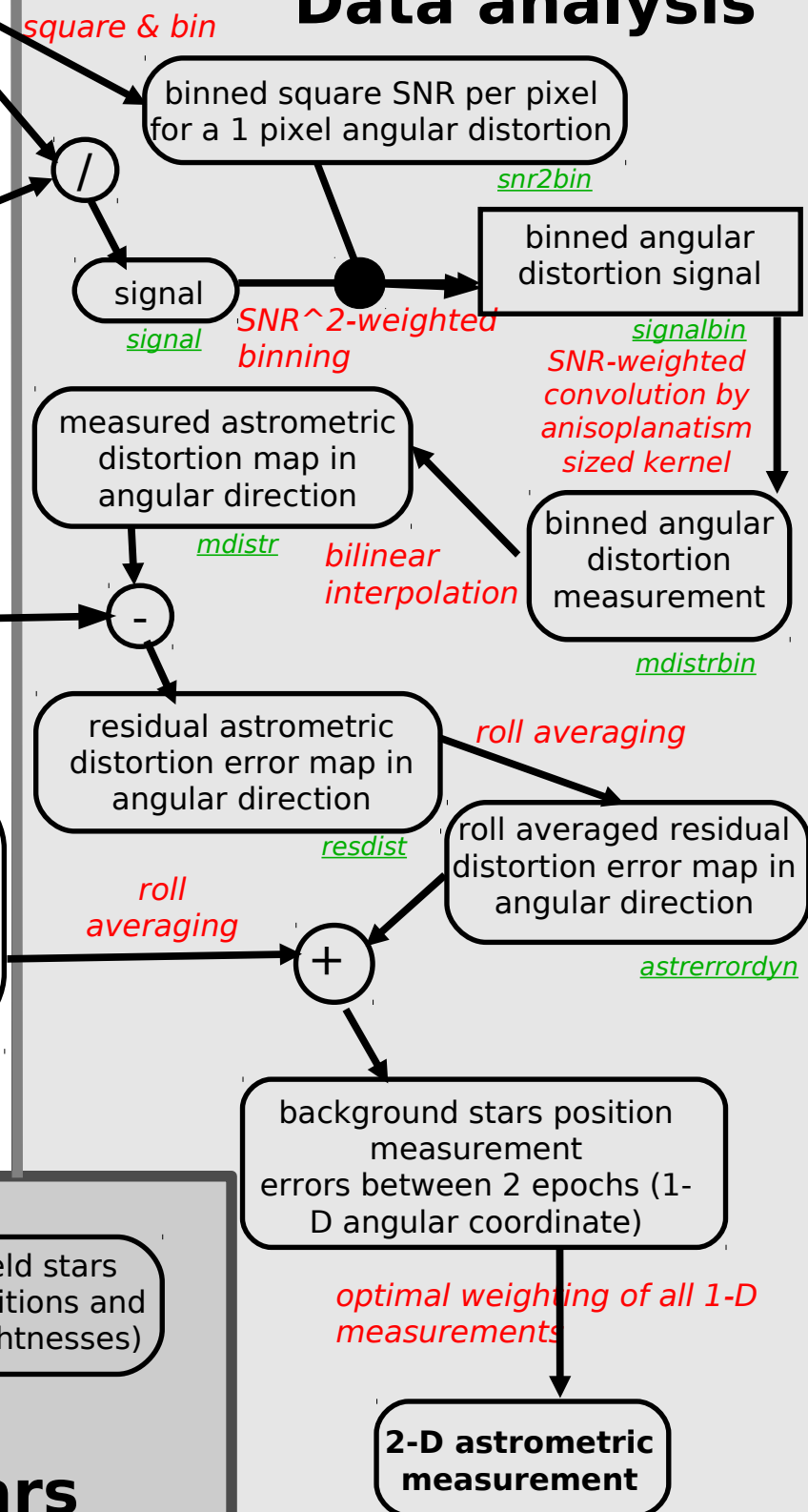
Data simulation



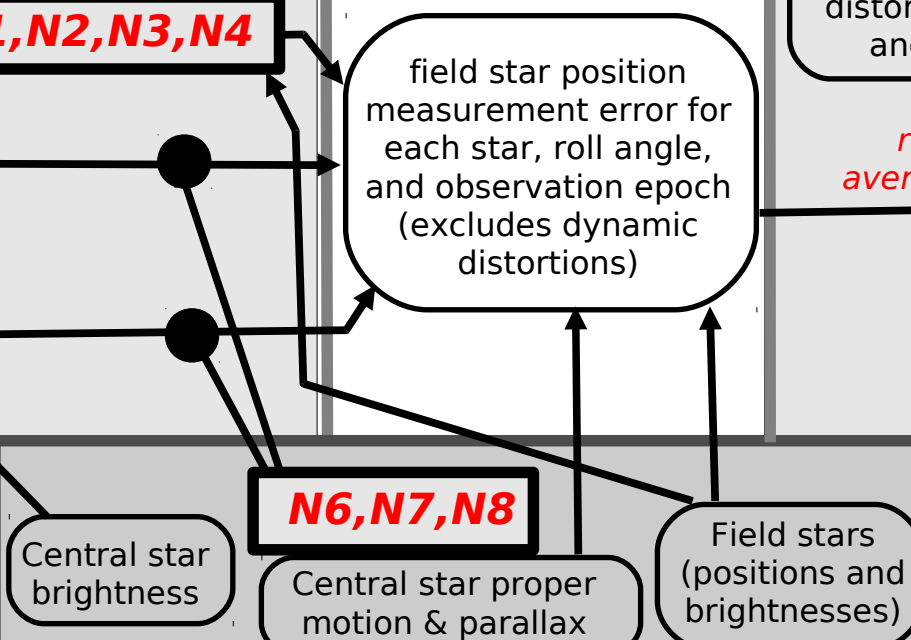
Simulated data



Data analysis

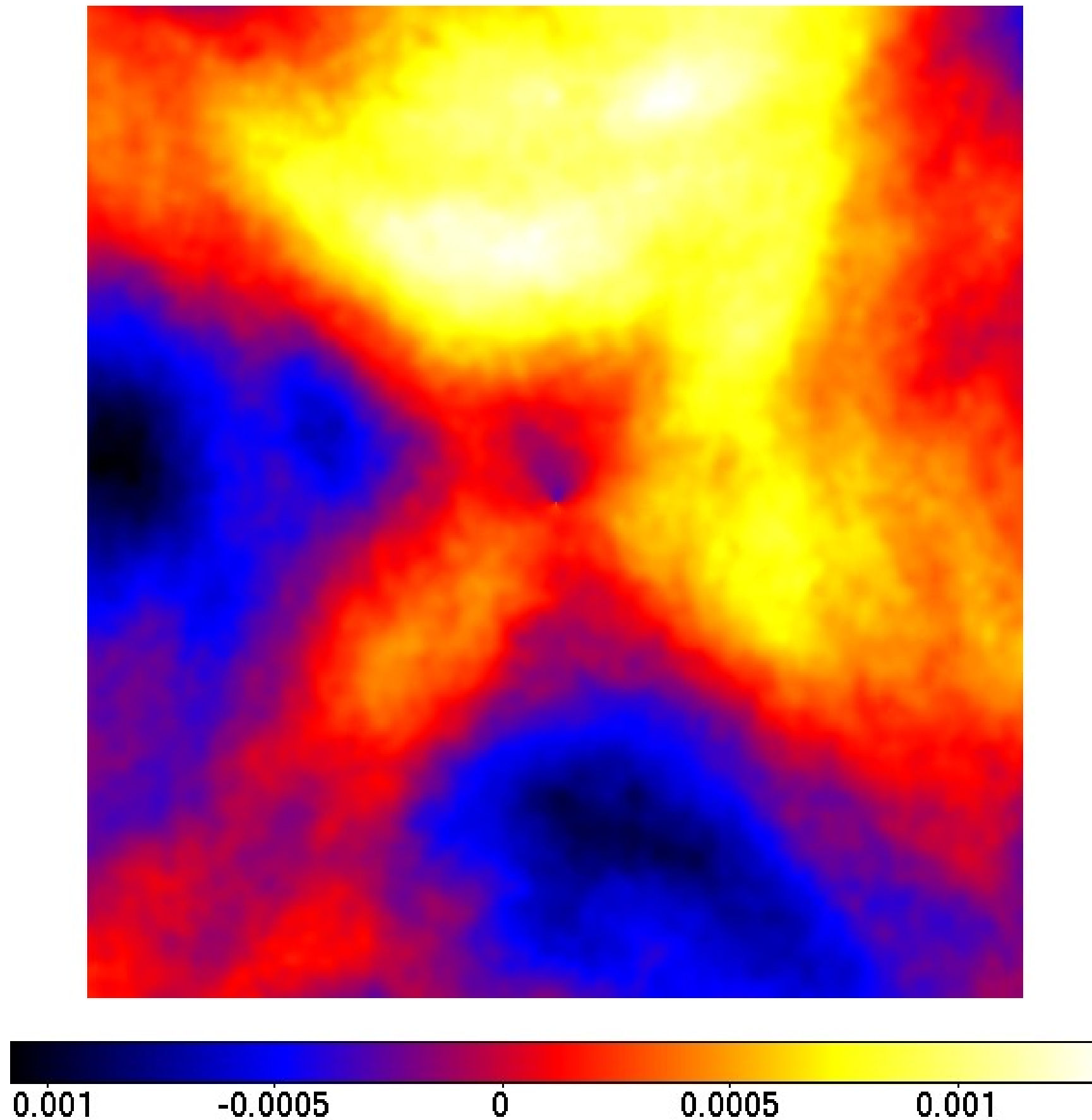


Target and field stars

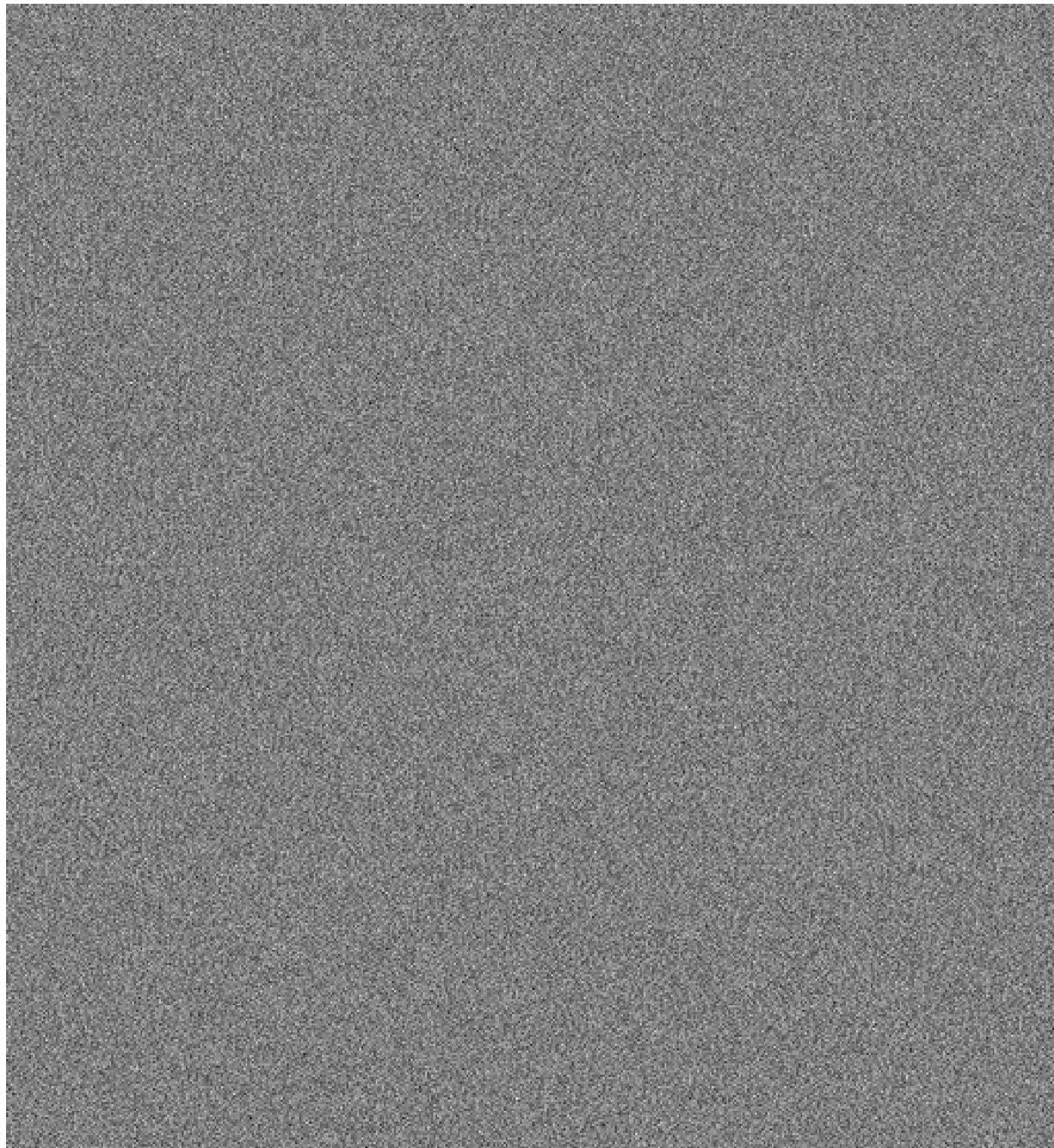


Total angular distortion change

Unit = pixel (44 mas)
Amplitude $\sim 1/1000$ pixel (44 uas)



Flat field change between epochs



Detector response map changes between observation by $1e-3$ (RMS)

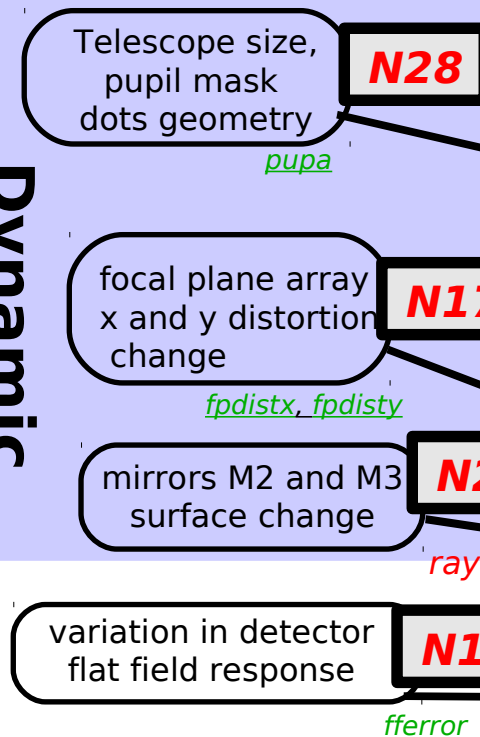
This will produce an error in the measurement of spikes displacements.

Even if the spikes are steady (no distortion), a distortion will be measured.

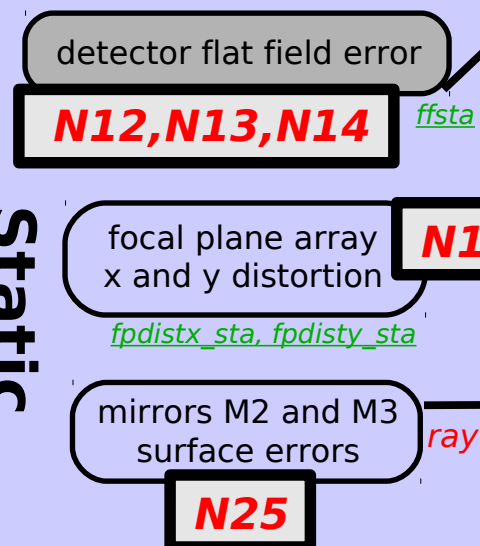
0.995 0.996 0.997 0.998 0.999 1 1.001 1.002 1.003 1.004 1.005

Input errors and instrument characteristics

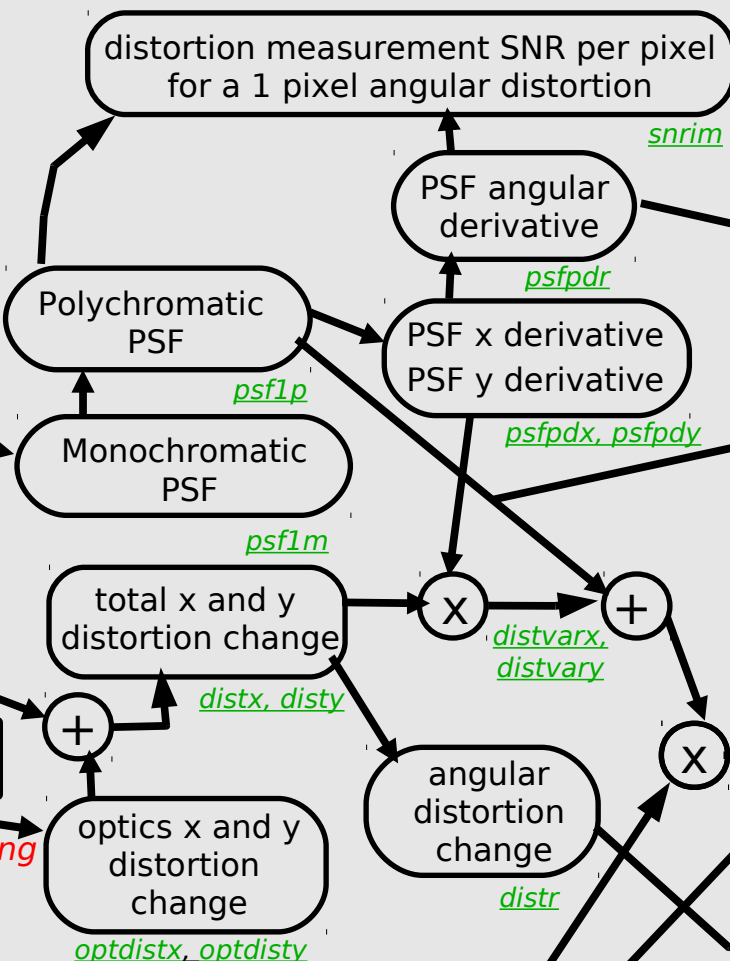
Dynamic distortions



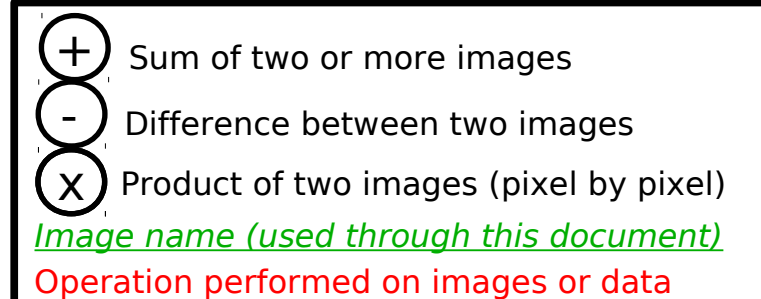
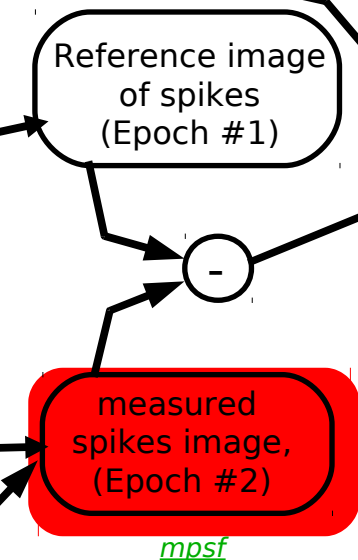
Static distortions



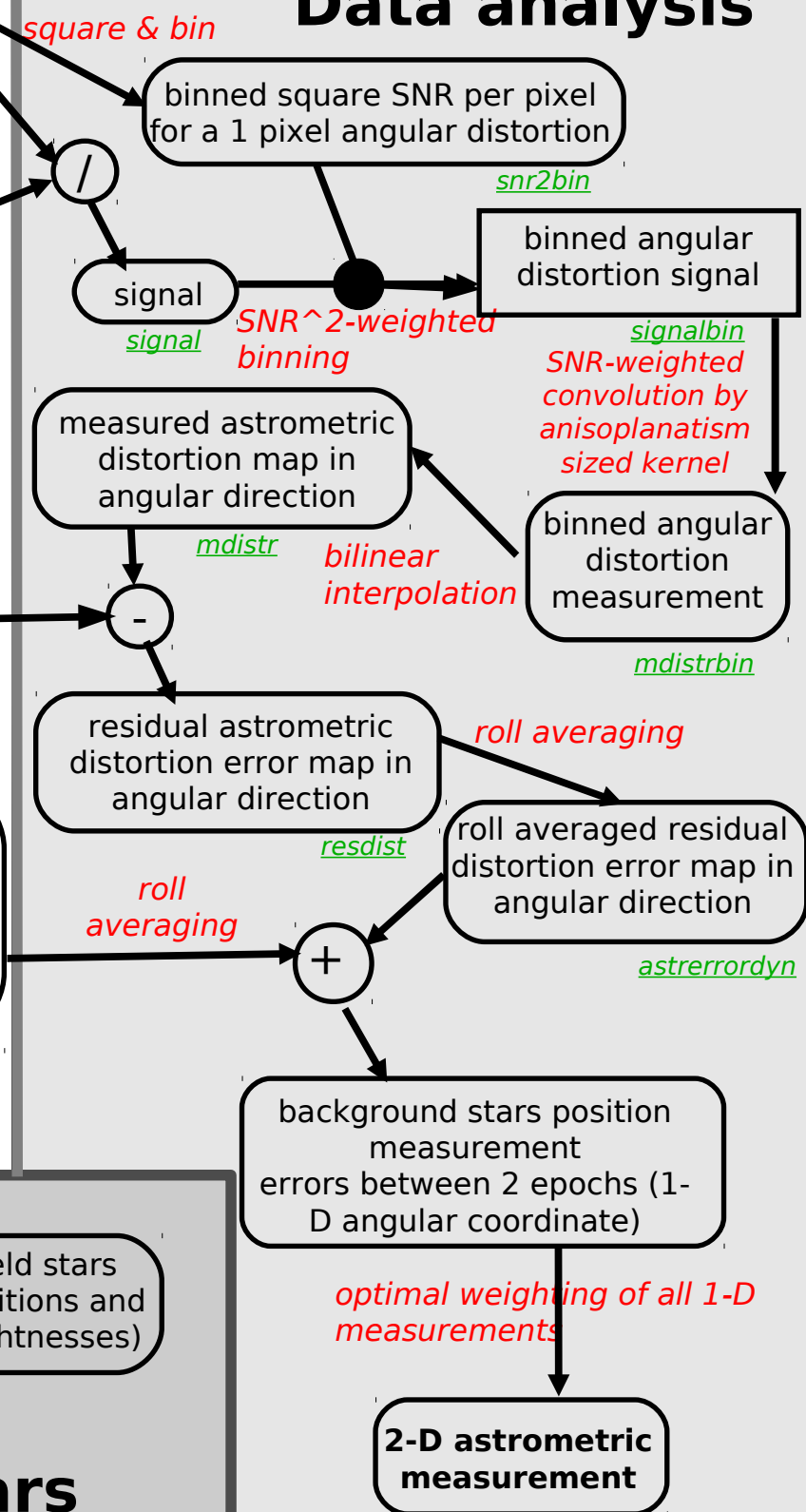
Data simulation



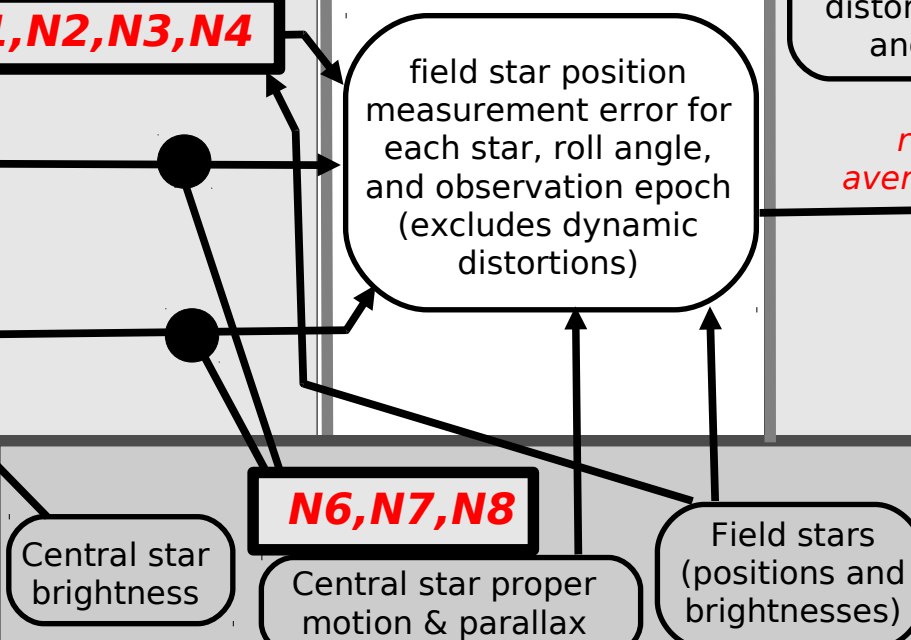
Simulated data



Data analysis



Target and field stars



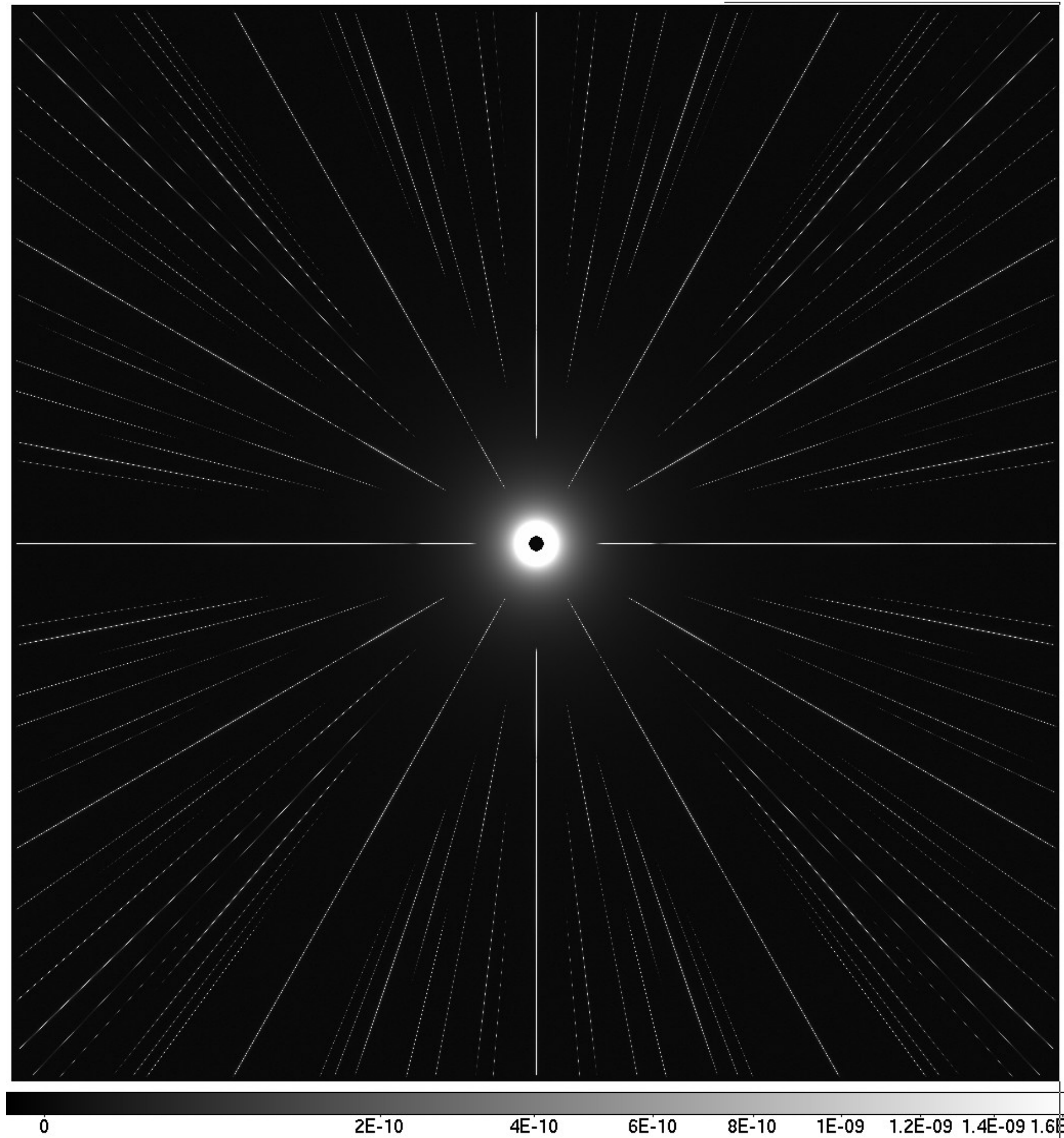
Spikes image, 0.2 deg FOV

Spike image is computed
by:

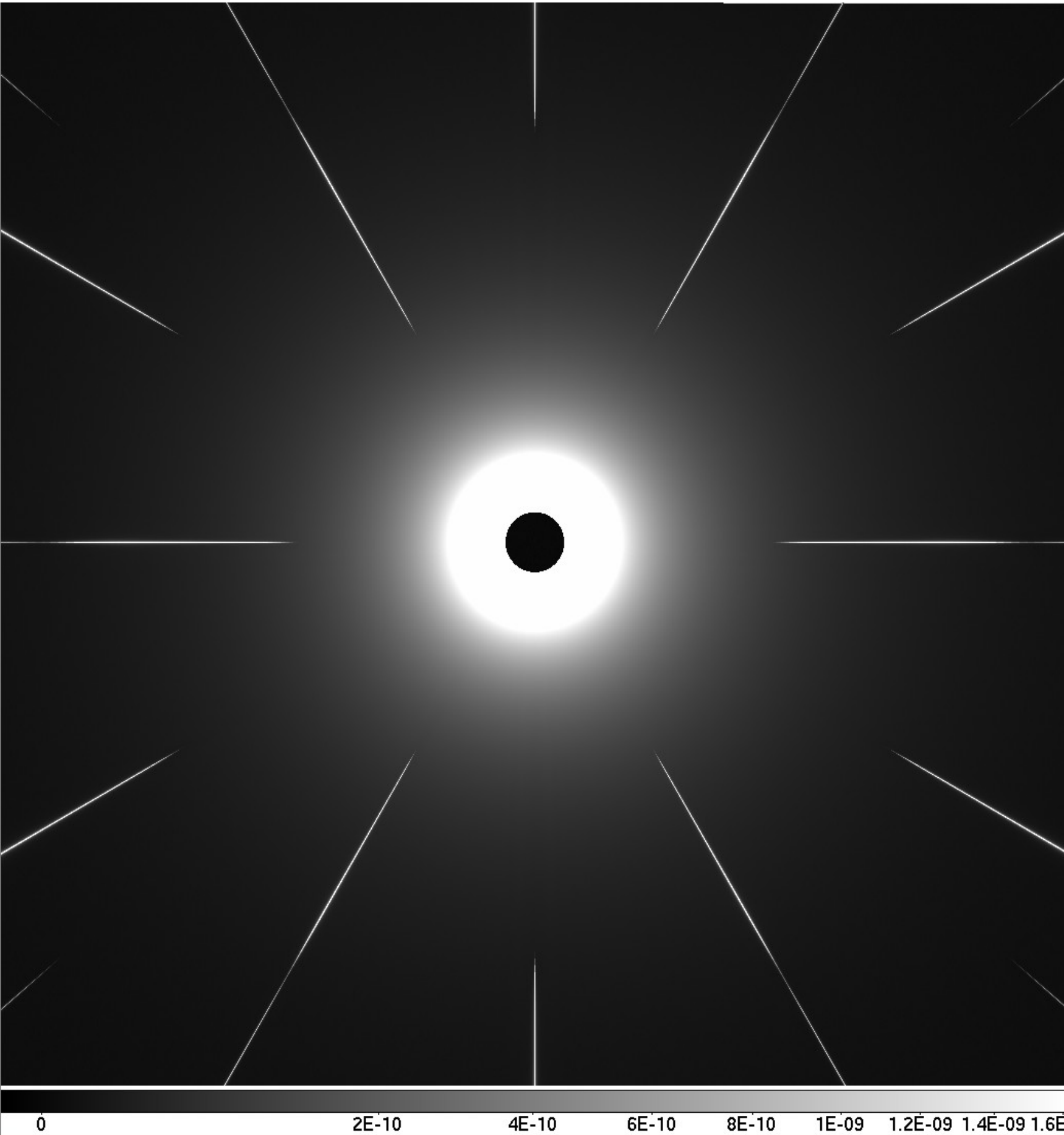
step 1: compute derivative
in x and y for the spikes

step 2: multiply derivative
by x and y distortion maps

step 3: add noise terms
(photon noise, readout
noise, flat field noise)



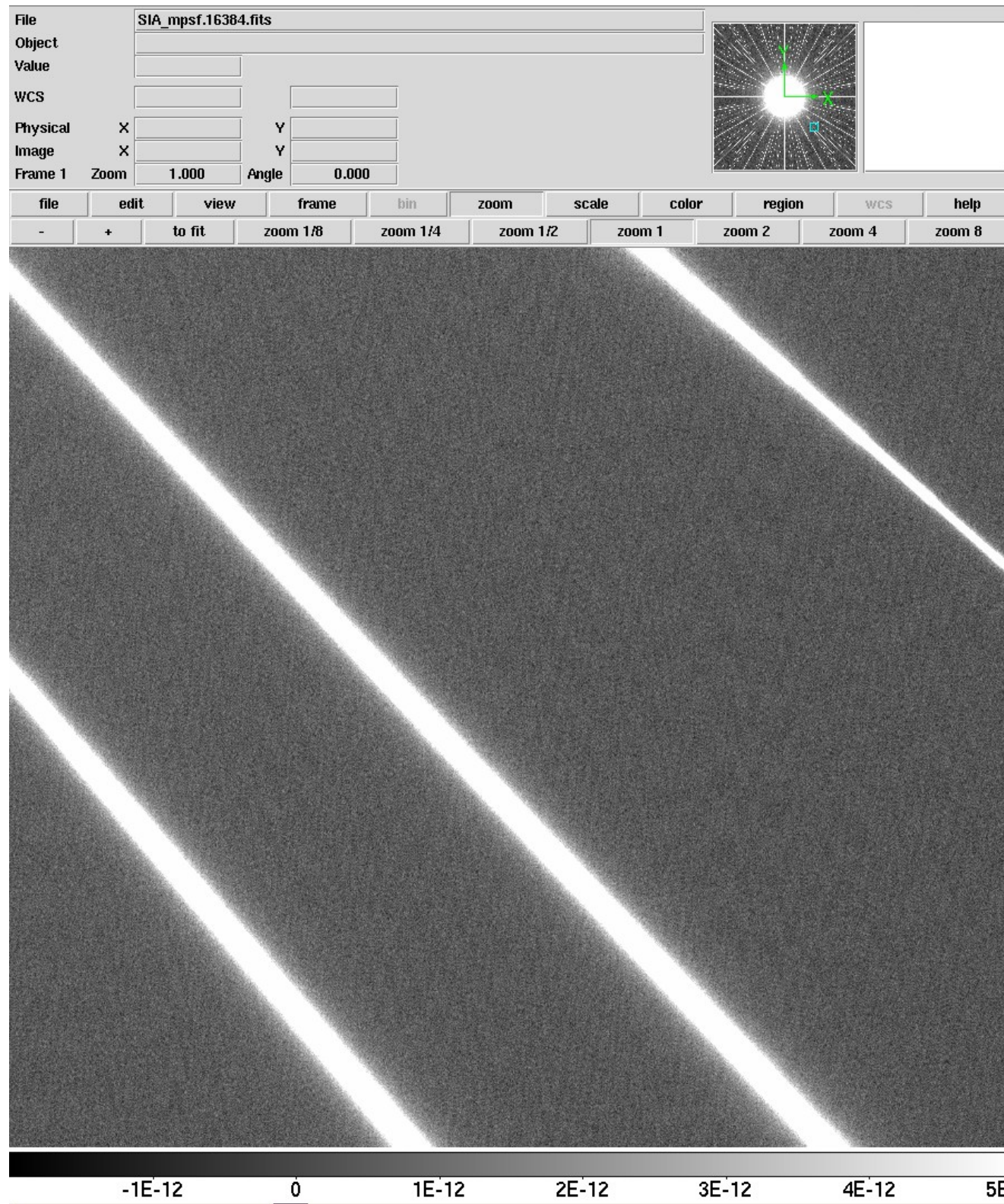
Spikes image (central region, 3'x3')



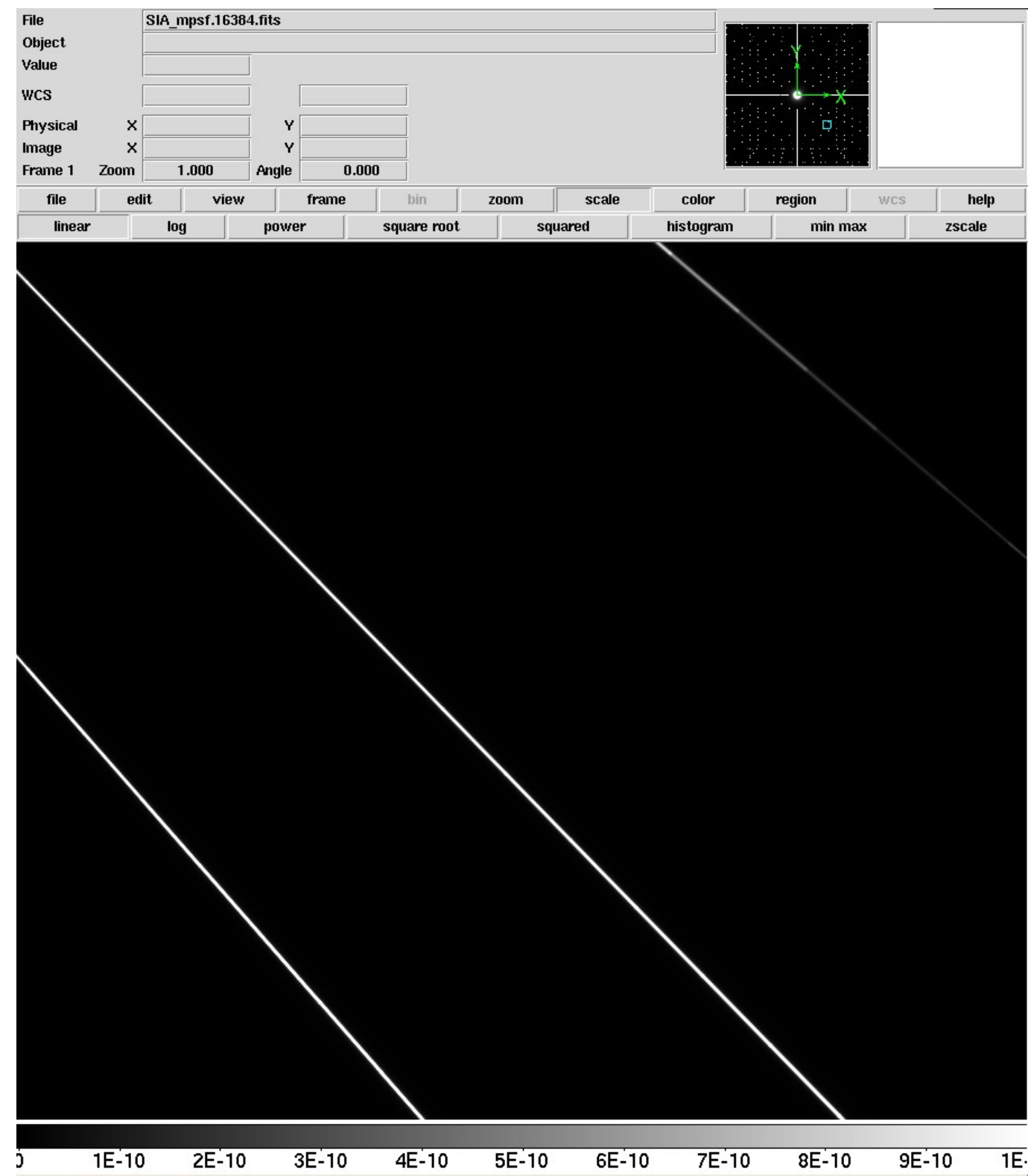
Central part of the field is blocked by the coronagraph pickup mirror.

The spikes do not extend inward to the coronagraphic field.

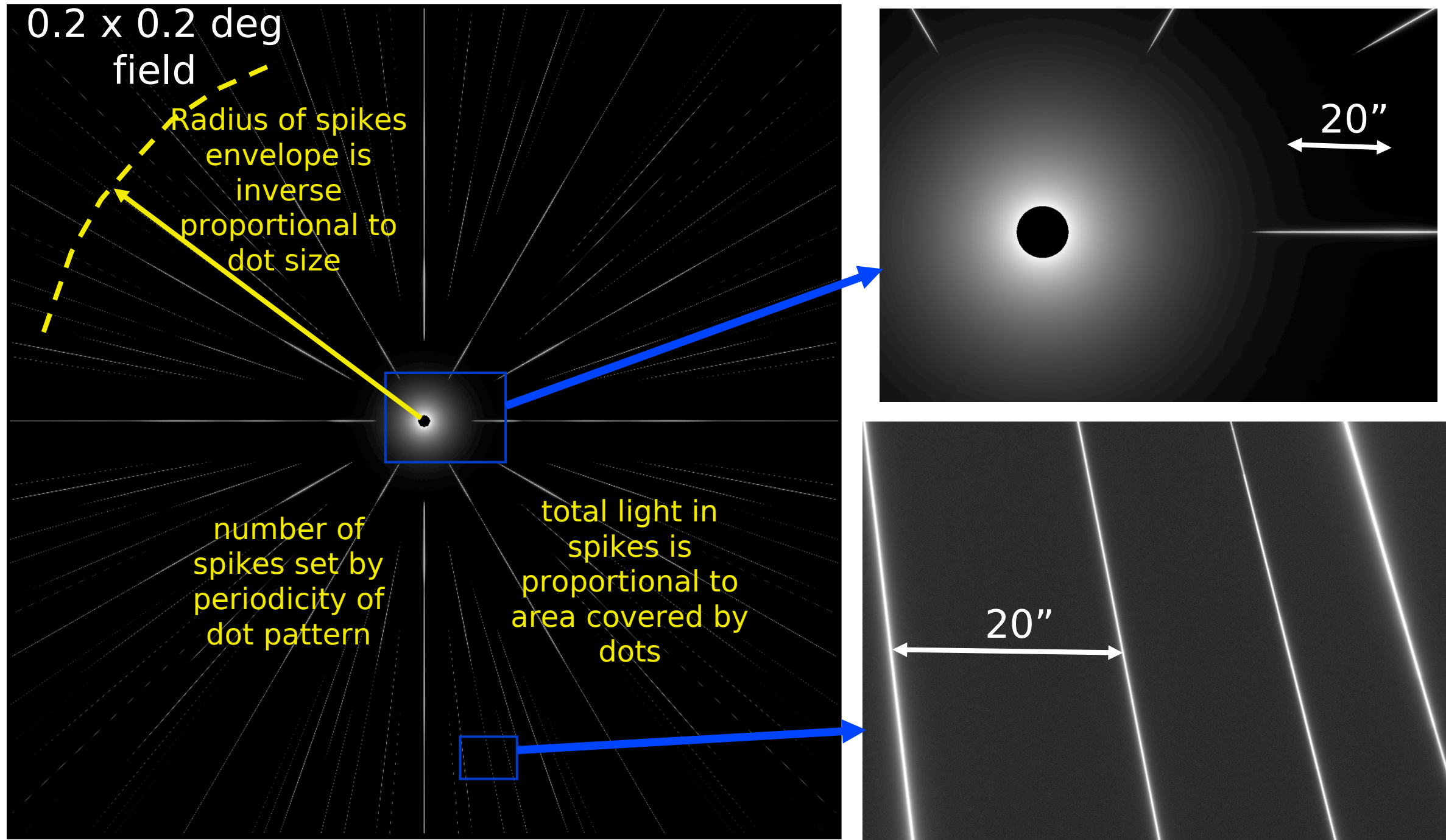
Zodi-subtracted spikes image, no background stars



Photon noise from spikes and zodiacal light are visible in this frame.



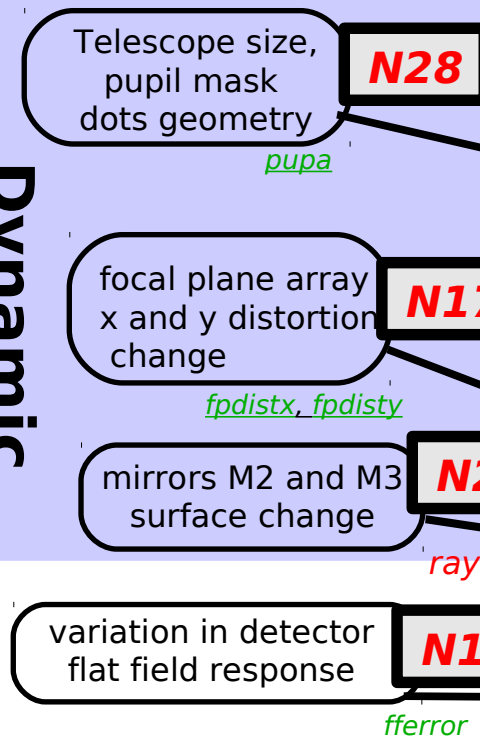
Spikes are I/D wide



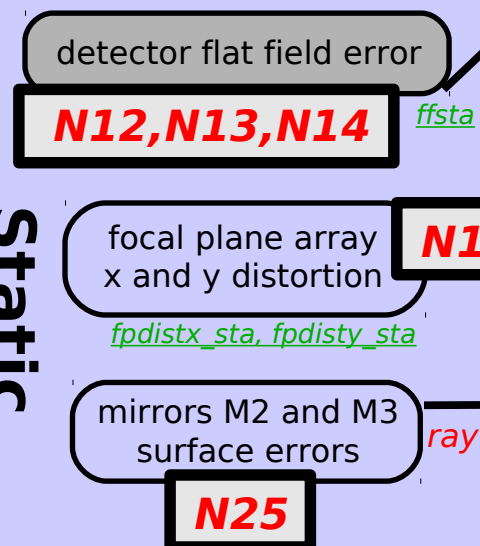
The overall size of the spike envelope, the spikes density (spacing between spikes) and brightness can be chosen by design of the dot pattern.

Input errors and instrument characteristics

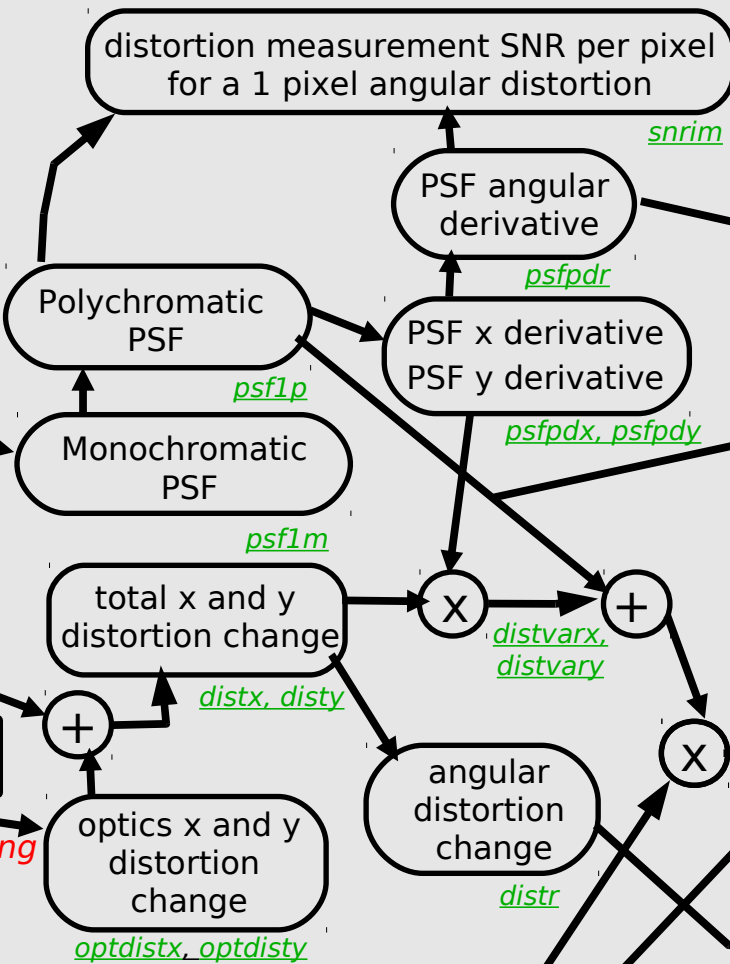
Dynamic distortions



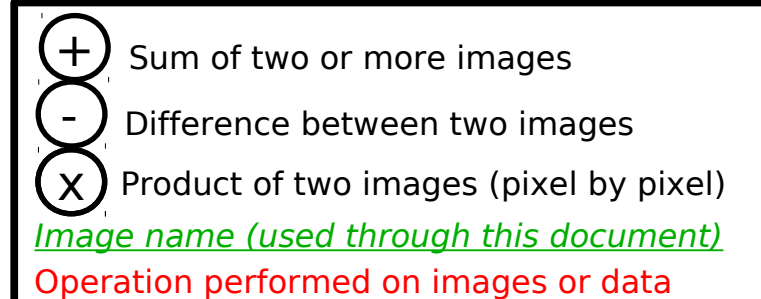
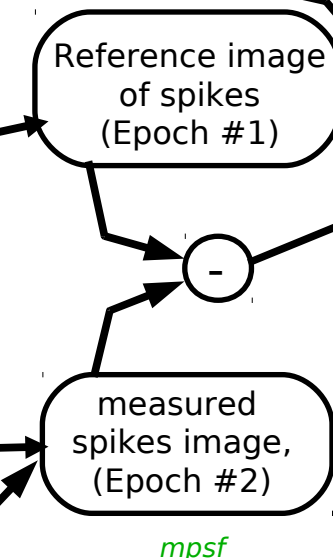
Static distortions



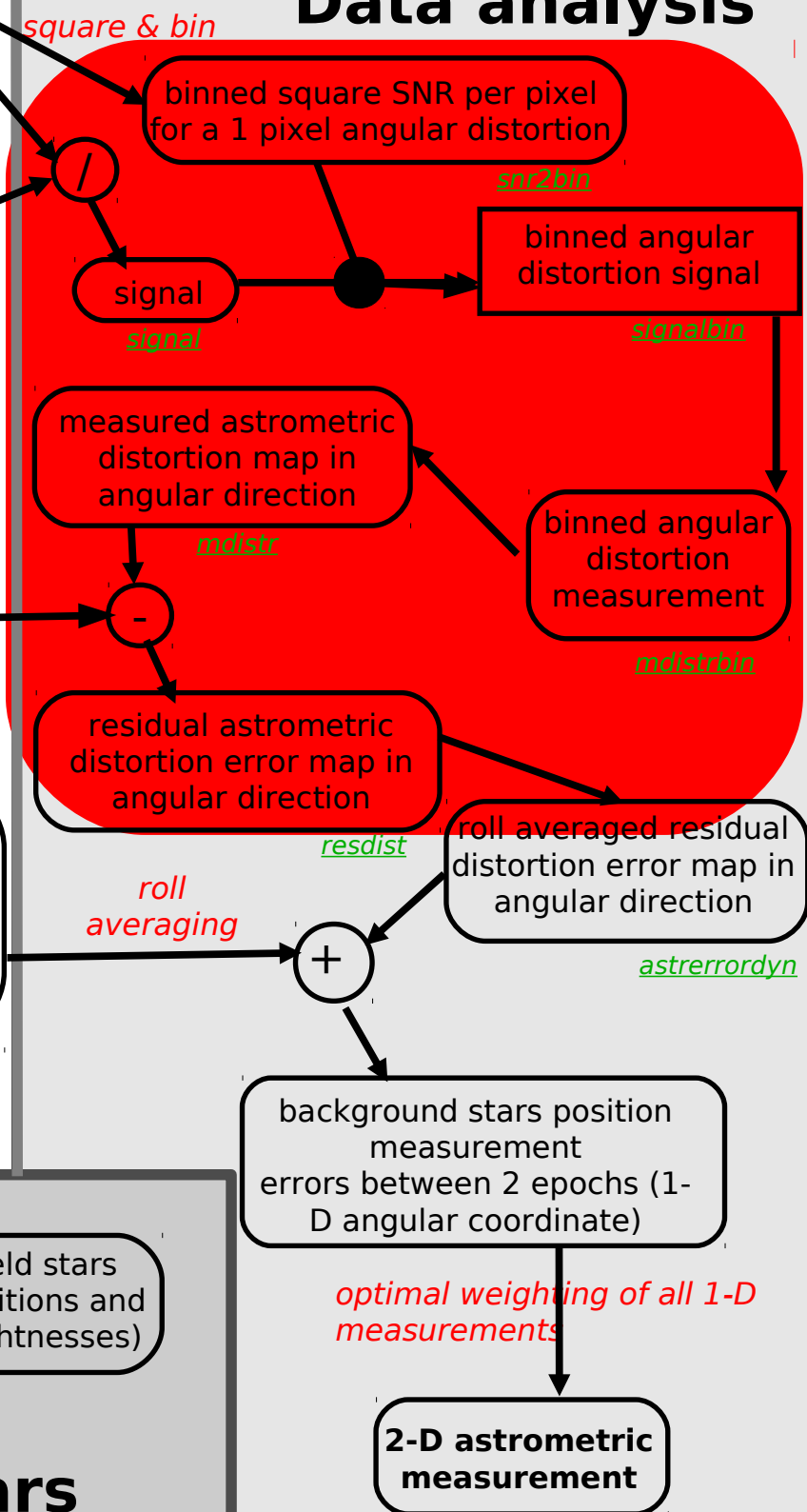
Data simulation



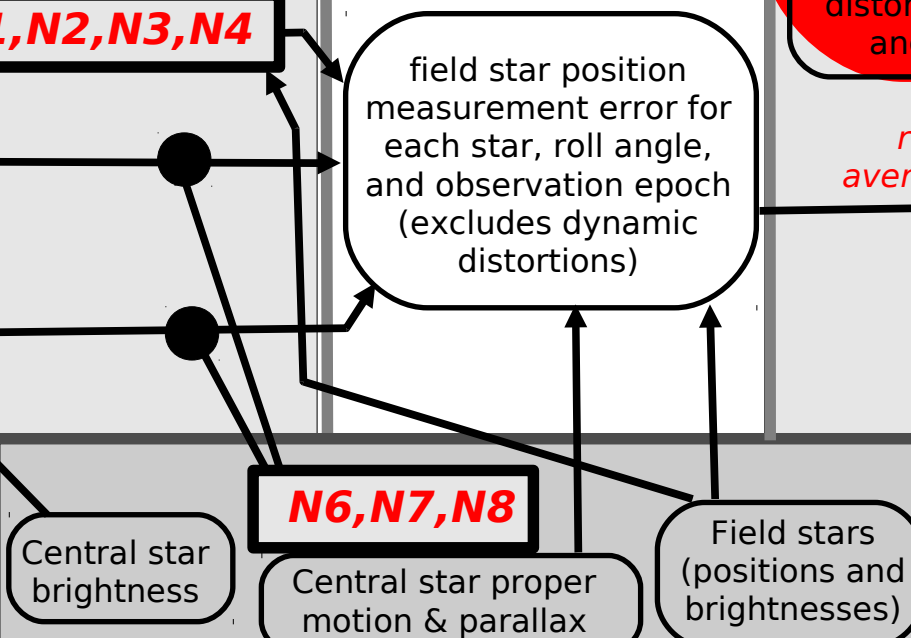
Simulated data



Data analysis



Target and field stars



Distortion measurement

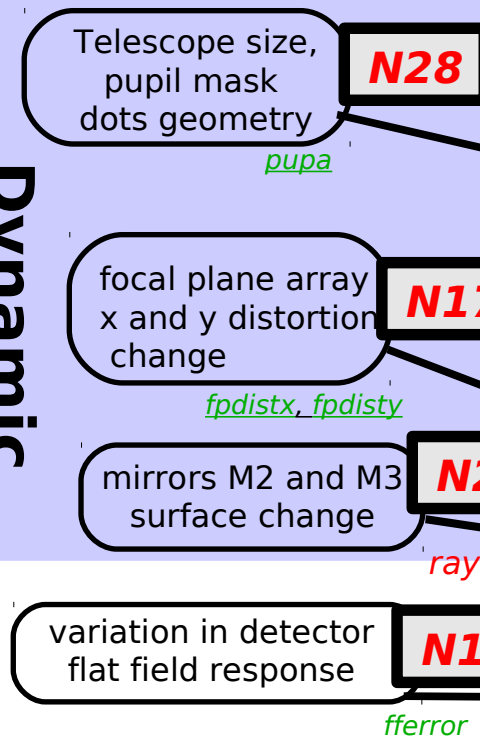
Compute SNR for a 1 pixel angular distortion for each pixel -> SNRmap

Compute signal (unit = pixel of angular distortion) for each pixel = difference between ideal spike image and measured spike image, divided by $d\text{Image}/d\text{Distortion}$ -> Signalmap

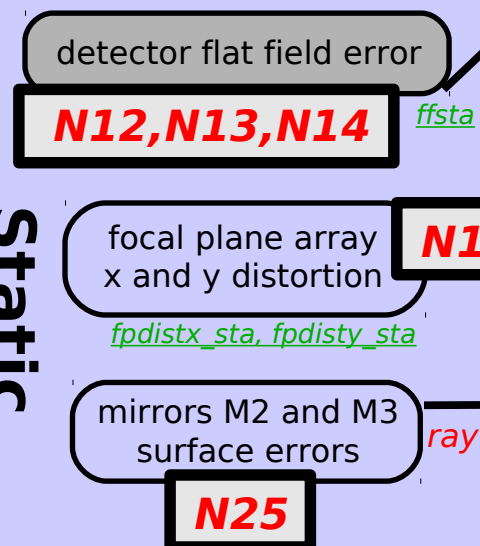
To speed up computation, Signalmap and SNRmap are binned to lower resolution (with optimal weights derived from SNRmap)

Input errors and instrument characteristics

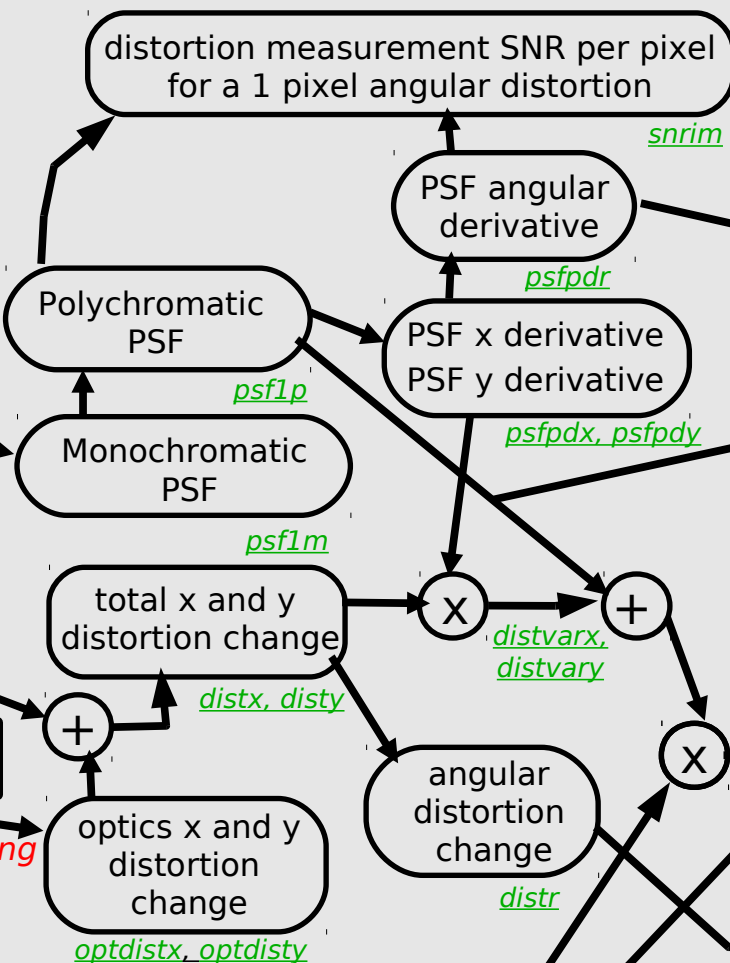
Dynamic distortions



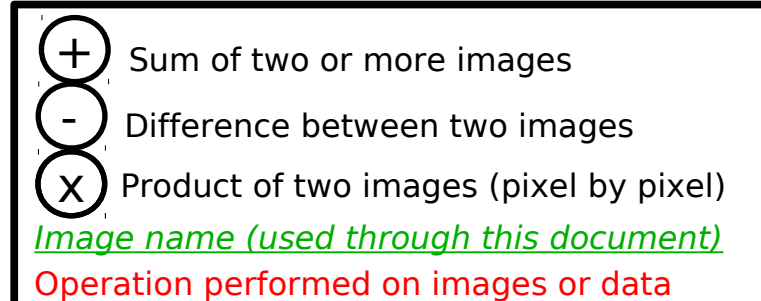
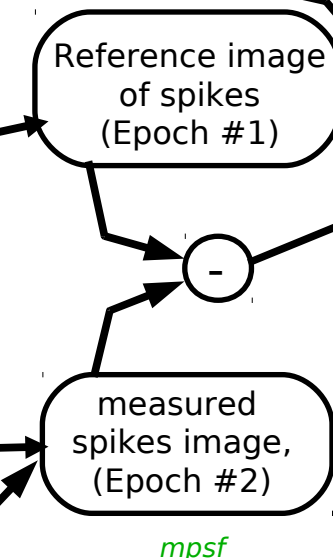
Static distortions



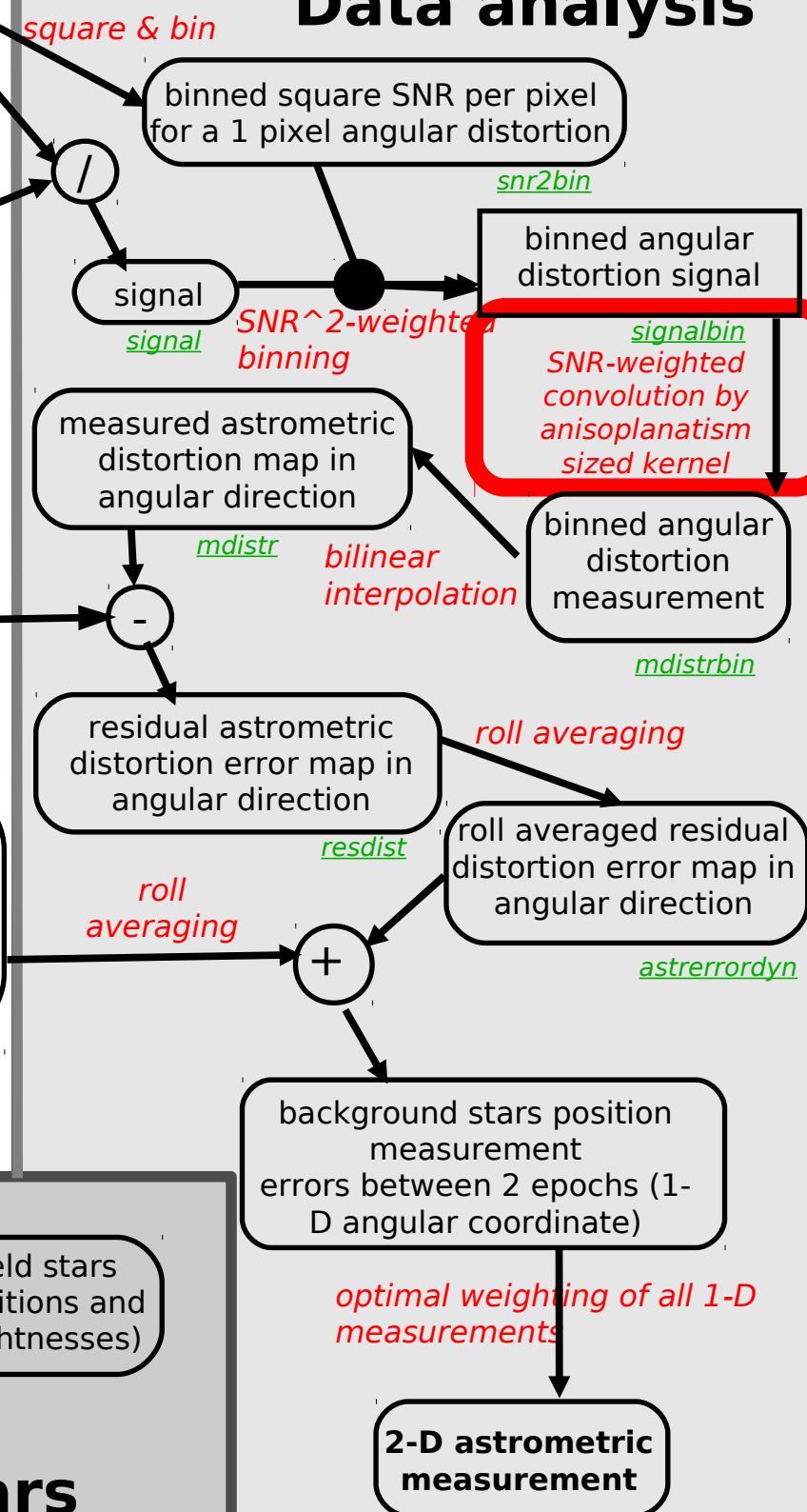
Data simulation



Simulated data



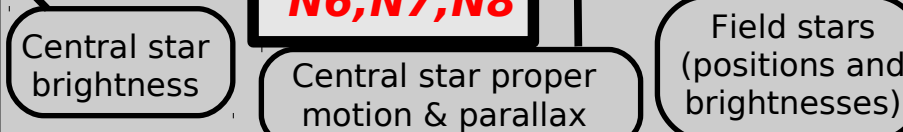
Data analysis



N1,N2,N3,N4

N6,N7,N8

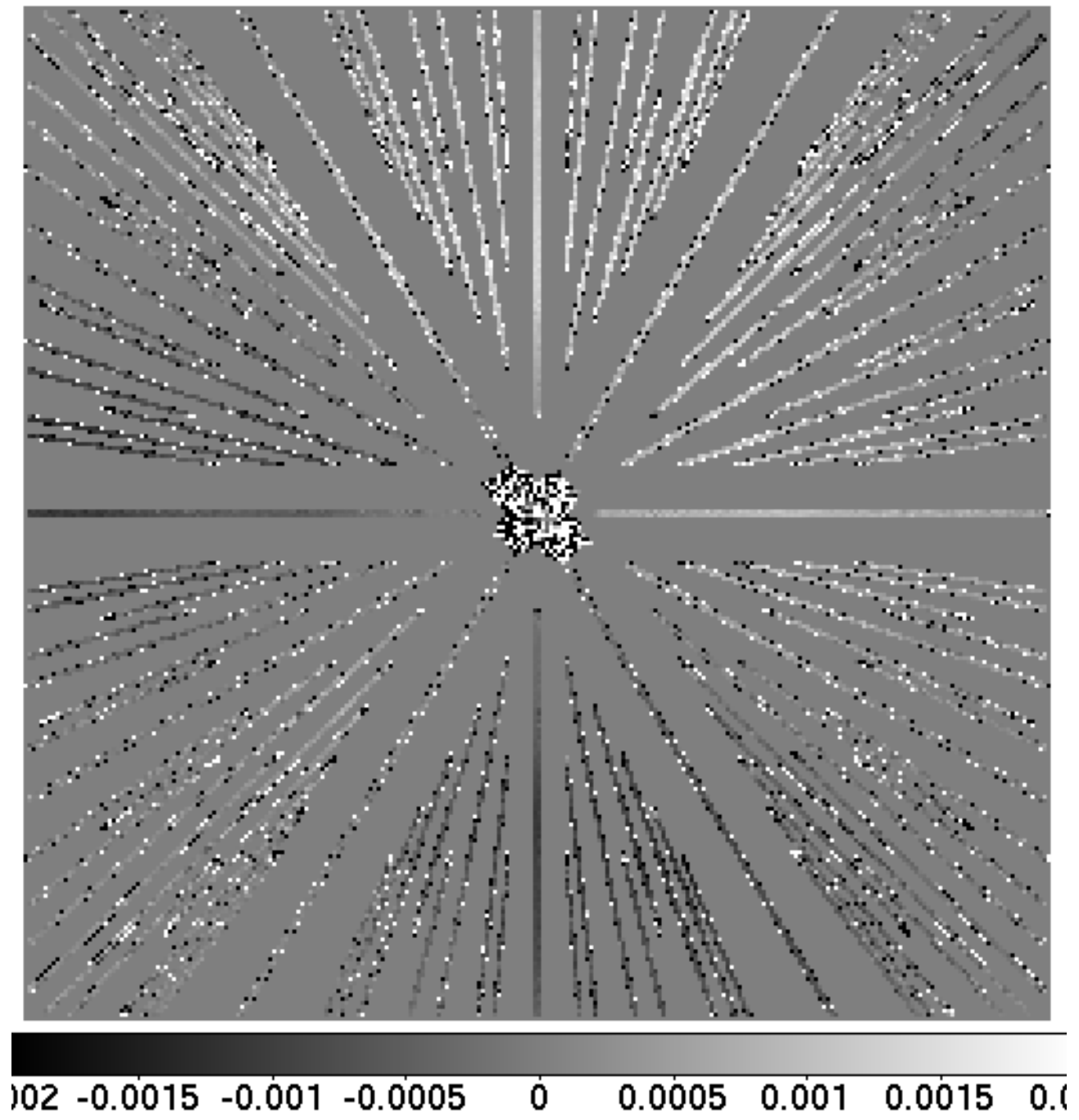
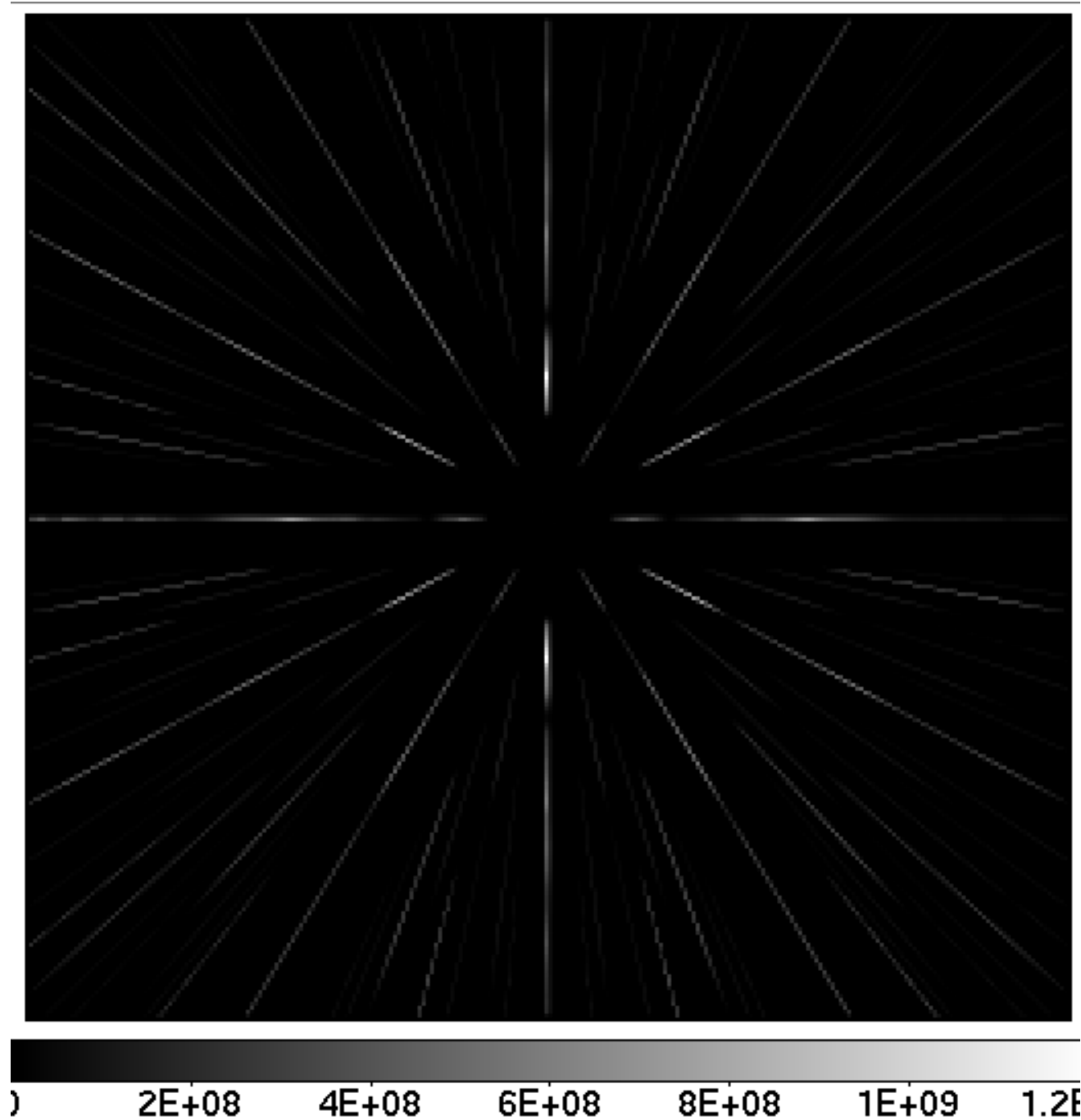
Target and field stars



Distortion measurement

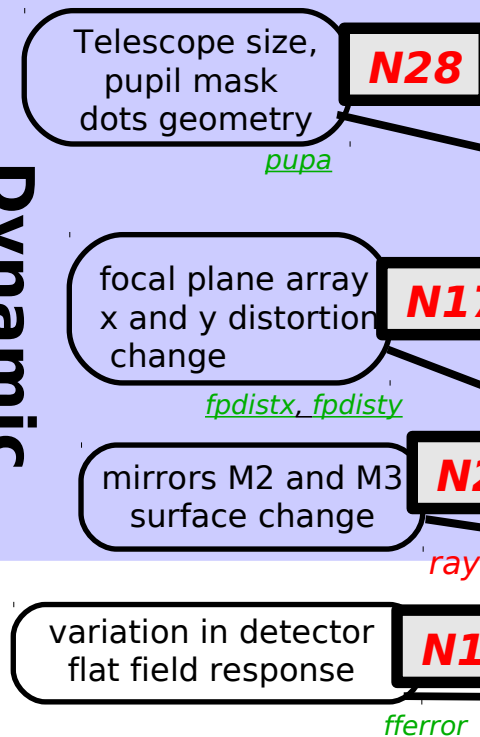
SNR^2

binned Signal (using SNR^2 weighting within each bin)
Value set to zero where SNR is below threshold

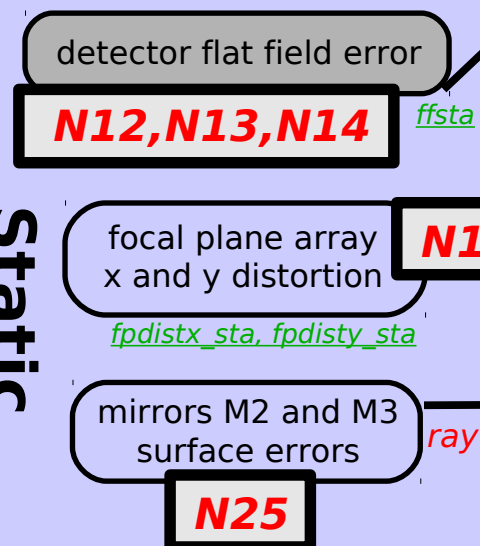


Input errors and instrument characteristics

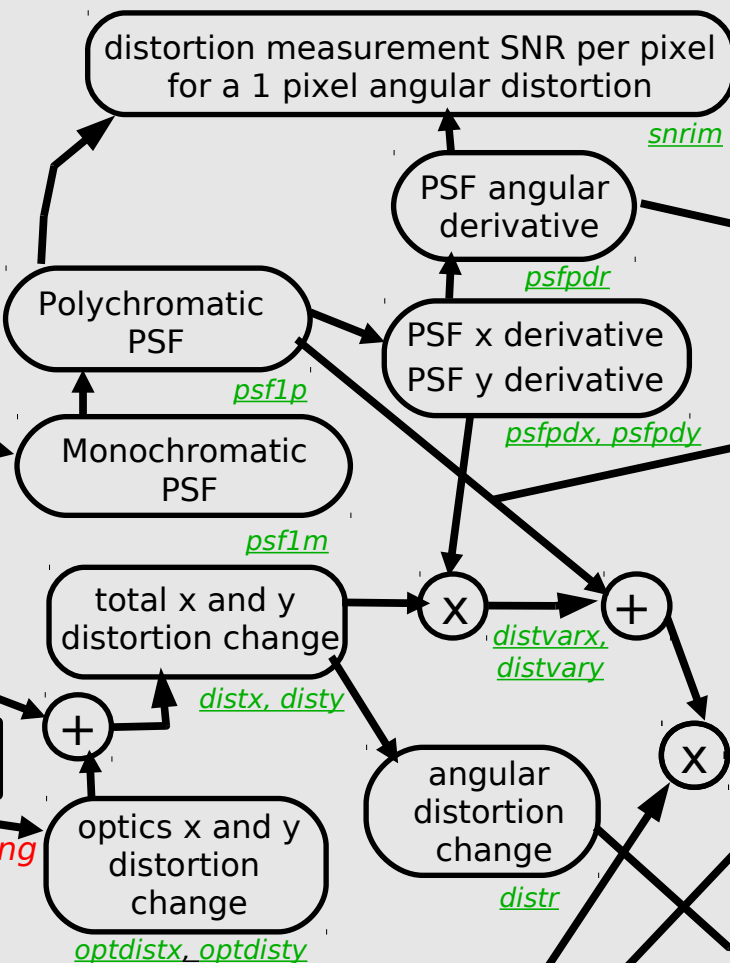
Dynamic distortions



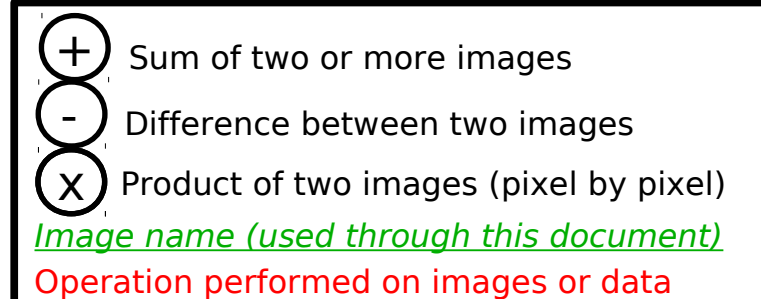
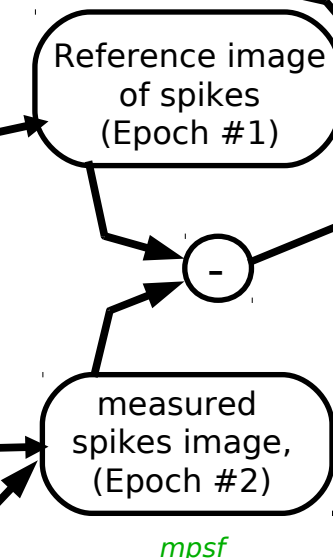
Static distortions



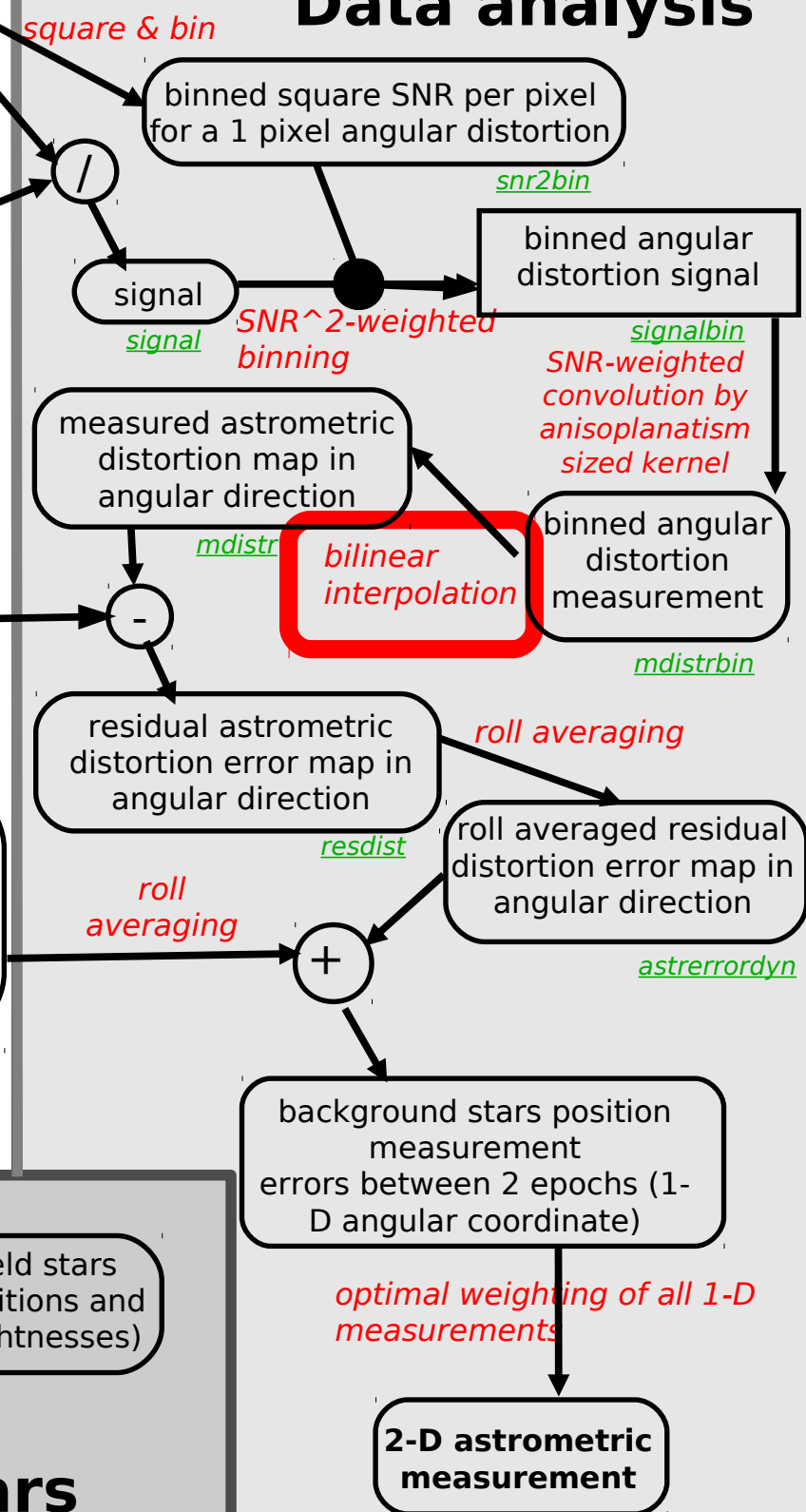
Data simulation



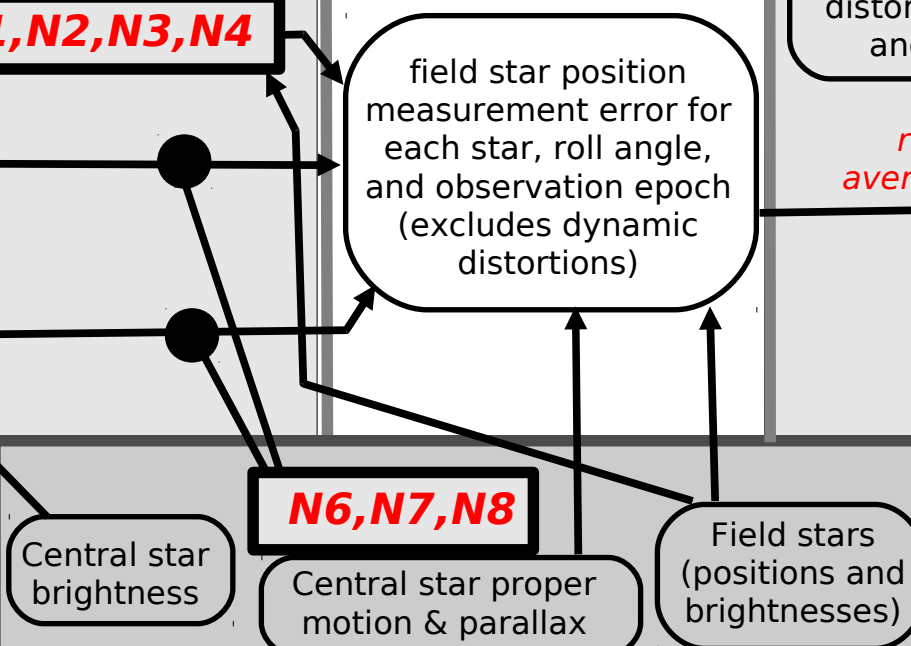
Simulated data



Data analysis



Target and field stars



Distortion interpolation

Convolve signal $\times \text{SNR}^2$ by gaussian kernel, with sigma of the kernel \sim anisoplanatism patch size

Problem: next to a bright spike, the solution will give a flat value with a sharp jump when moving to the next spike.

Estimate for each pixel the effective centroid of the result (different from the pixel location), and the local slope of the distortion \rightarrow using these 2 quantities, correct for the centroid offset error.

Distortion interpolation

```
for(ii=0;ii<sizeb*sizeb;ii++)
    distarray[ii] = 0.0;

for(ii0=0;ii0<sizeb;ii0++)
    for(jj0=0;jj0<sizeb;jj0++)
    {
        v = 0.0;
        vx = 0.0;
        vy = 0.0;
        xt = 0.0;
        yt = 0.0;
        vcnt = 0.0;
        vxcnt = 0.0;
        vycent = 0.0;

        for(kk=0;kk<NBpt;kk++)
        {
            ii = iarray[kk]-ii0;
            jj = jarray[kk]-jj0;
            x = 1.0*ii*SIA_pixscale*binfact; // radian
            y = 1.0*jj*SIA_pixscale*binfact; // radian
            r2 = x*x+y*y;
            r2 /= SIA_corr_aniso_rad*SIA_corr_aniso_rad;
            if(r2<9.0)
            {
                v += varray[kk]*snr2array[kk]*exp(-r2);
                xt += x*snr2array[kk]*exp(-r2);
                yt += y*snr2array[kk]*exp(-r2);
                vcnt += snr2array[kk]*exp(-r2);
            }
        }

        if(vcnt > eps)
        {
            v /= vcnt;
            xt /= vcnt; // effective x
            yt /= vcnt; // effective y
        }

        for(kk=0;kk<NBpt;kk++)
        {
            ii = iarray[kk]-ii0;
            jj = jarray[kk]-jj0;
            x = 1.0*ii*SIA_pixscale*binfact; // radian
            y = 1.0*jj*SIA_pixscale*binfact; // radian
            r2 = x*x+y*y;
            r2 /= SIA_corr_aniso_rad*SIA_corr_aniso_rad;
            if(r2<9.0)
            {
                vx += (varray[kk]-v)*snr2array[kk]*(x-xt)*exp(-r2);
                vy += (varray[kk]-v)*snr2array[kk]*(y-yt)*exp(-r2);
                vxcnt += snr2array[kk]*(x-xt)*(x-xt)*exp(-r2);
                vycent += snr2array[kk]*(y-yt)*(y-yt)*exp(-r2);
            }
        }

        if(vxcnt>eps)
            vx /= vxcnt;
        if(vycent>eps)
            vy /= vycent;

        v -= xt*vx;
        v -= yt*vy;
        distarray[jj0*sizeb+ii0] = v;
    }
}
```

kk is an index to the list of high SNR measurements (5% best pixels)

Convolution by kernel

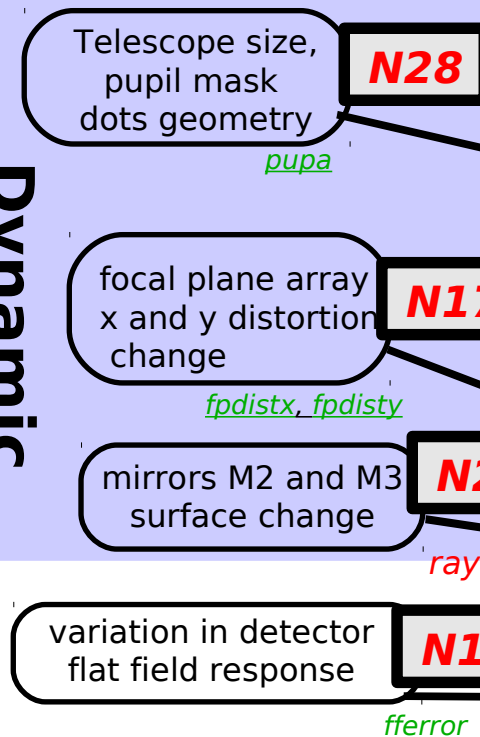
This is the effective centroid to which the computed value corresponds. The centroid gets pulled to bright spikes.

Compute local 2D derivative of the measured distortion

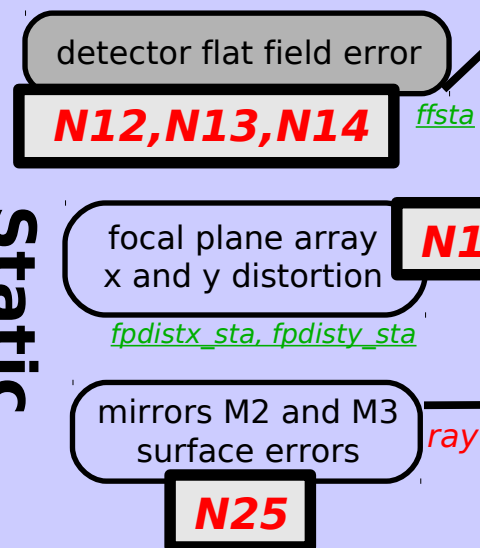
Compensation of error due to centroid offset and local 2D derivative of distortion

Input errors and instrument characteristics

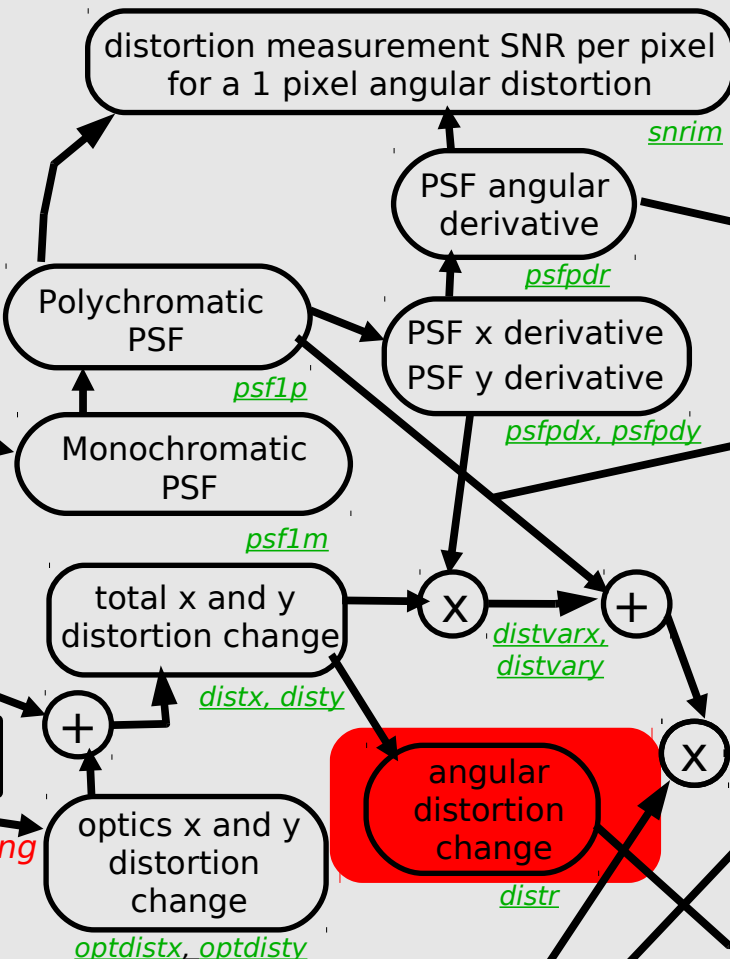
Dynamic distortions



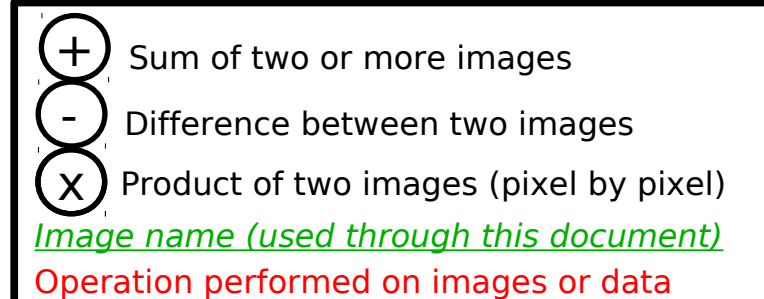
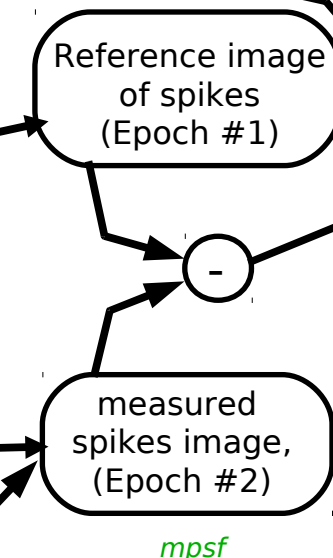
Static distortions



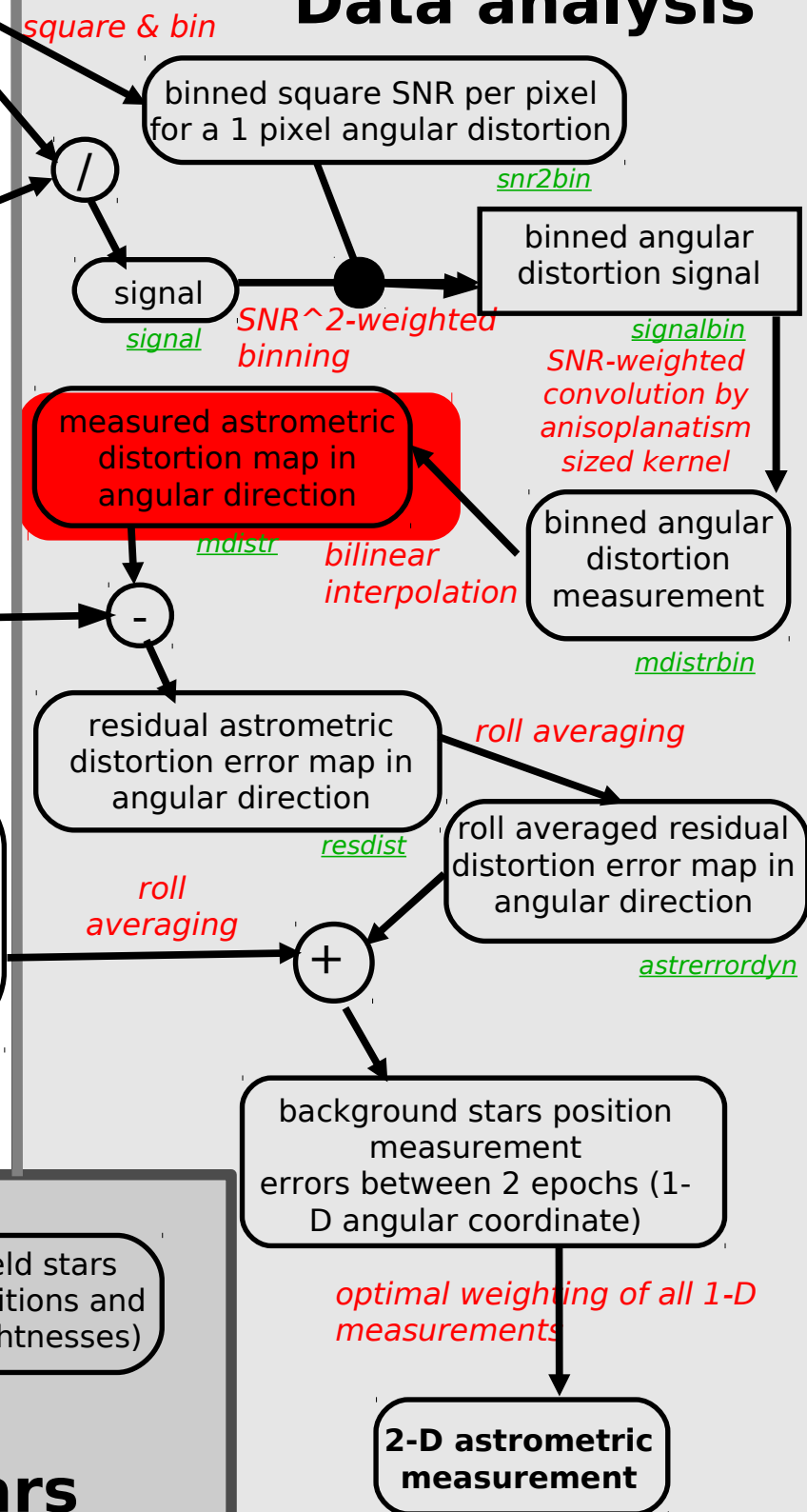
Data simulation



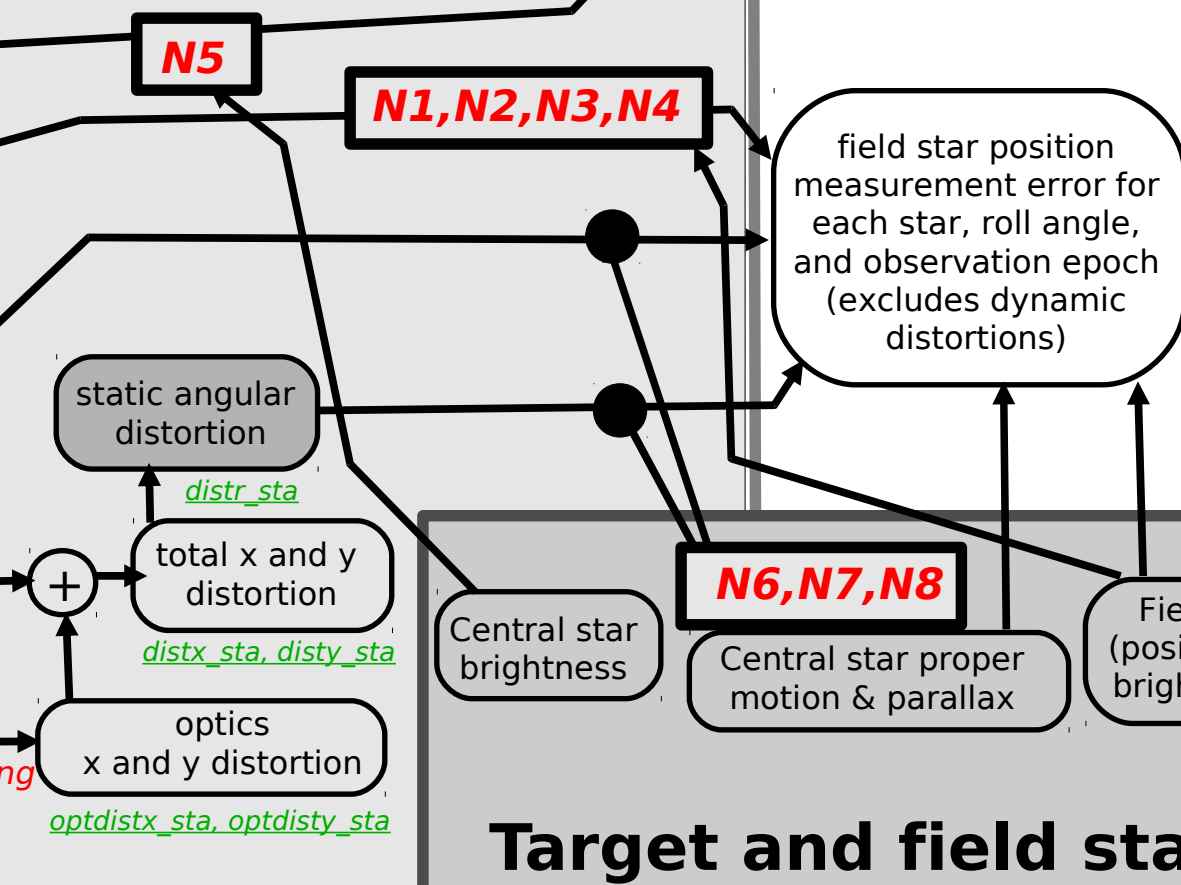
Simulated data



Data analysis



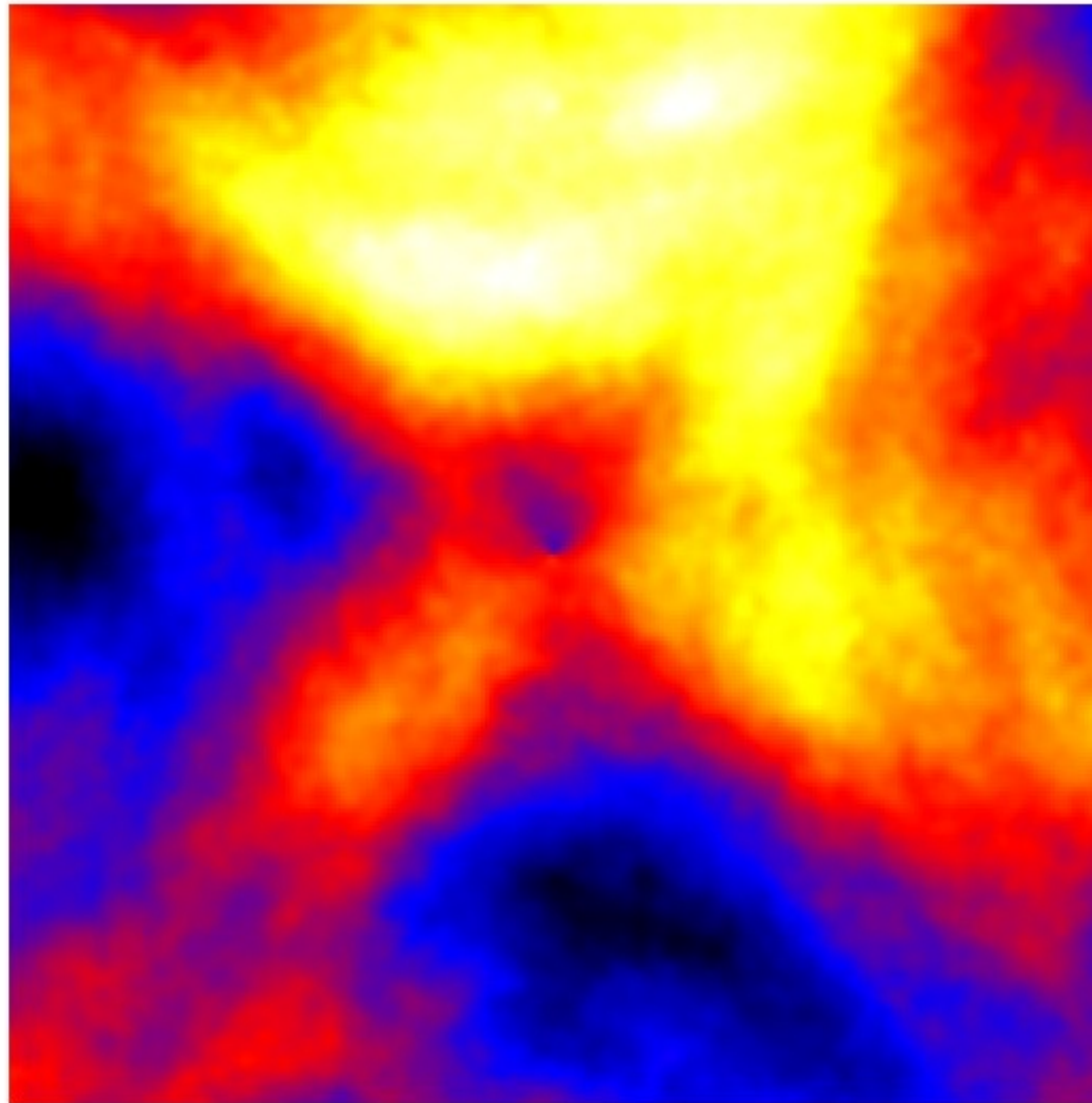
Target and field stars



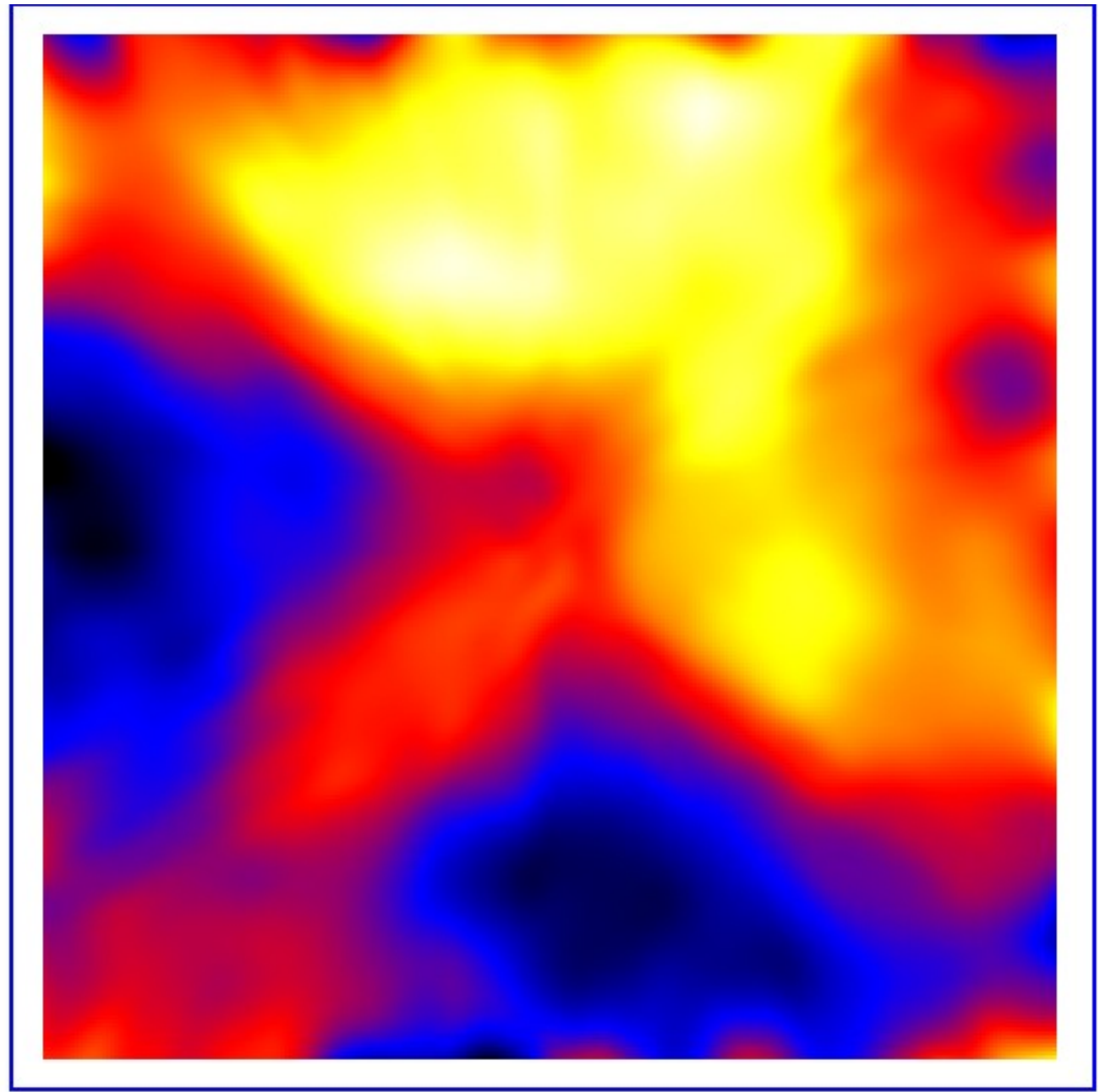
Distortion interpolation

Sigma = 15"

True distortion



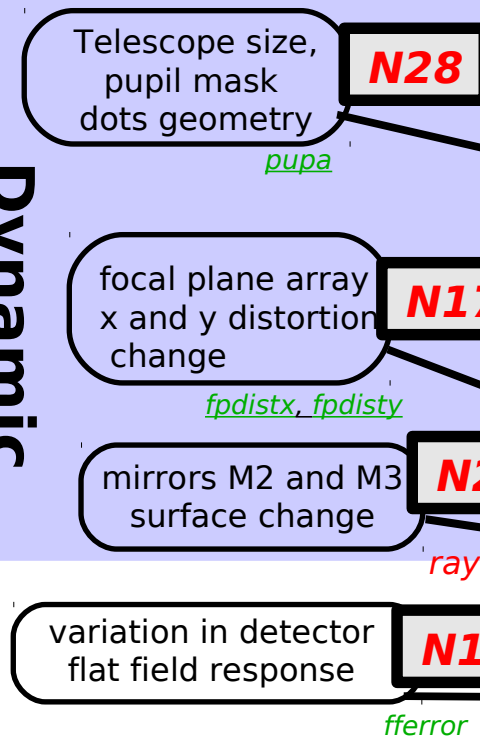
Measured distortion



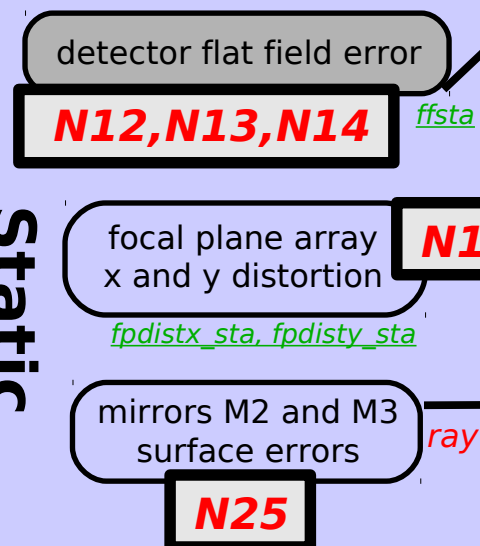
Unit = pixel

Input errors and instrument characteristics

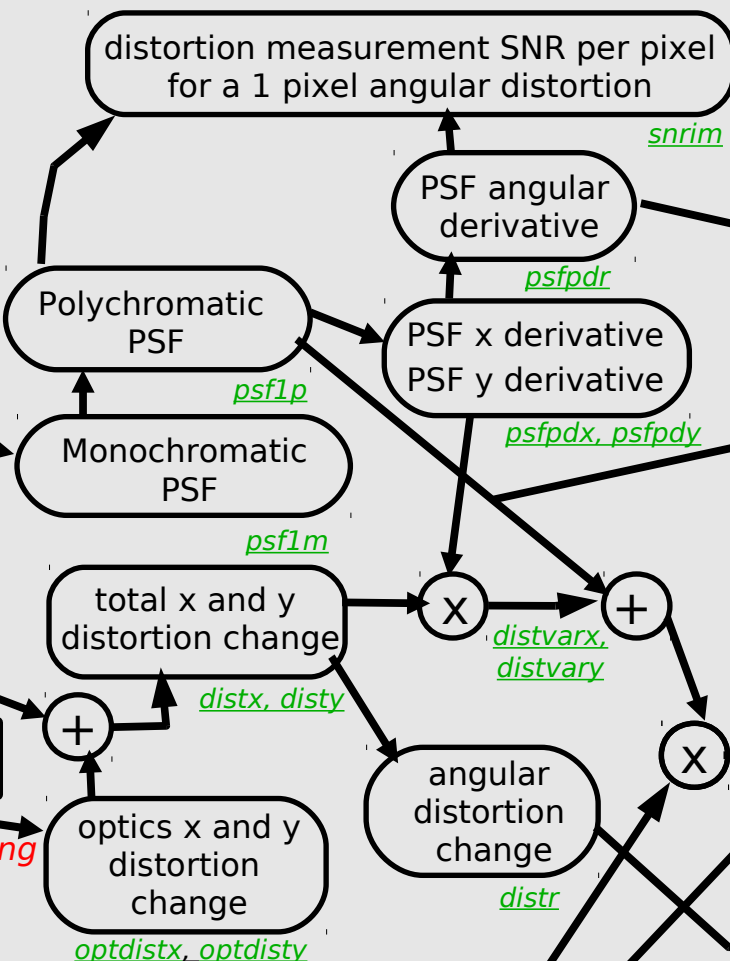
Dynamic distortions



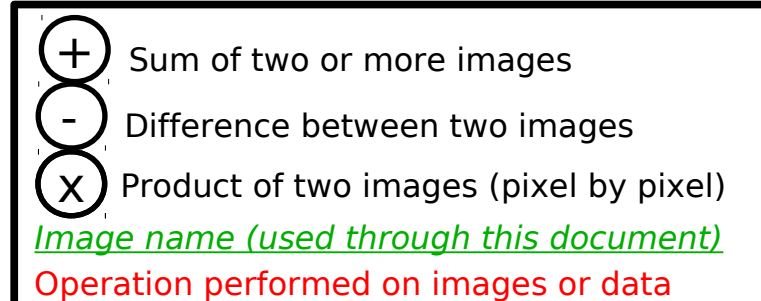
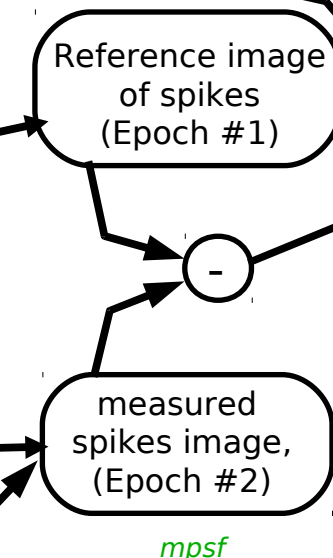
Static distortions



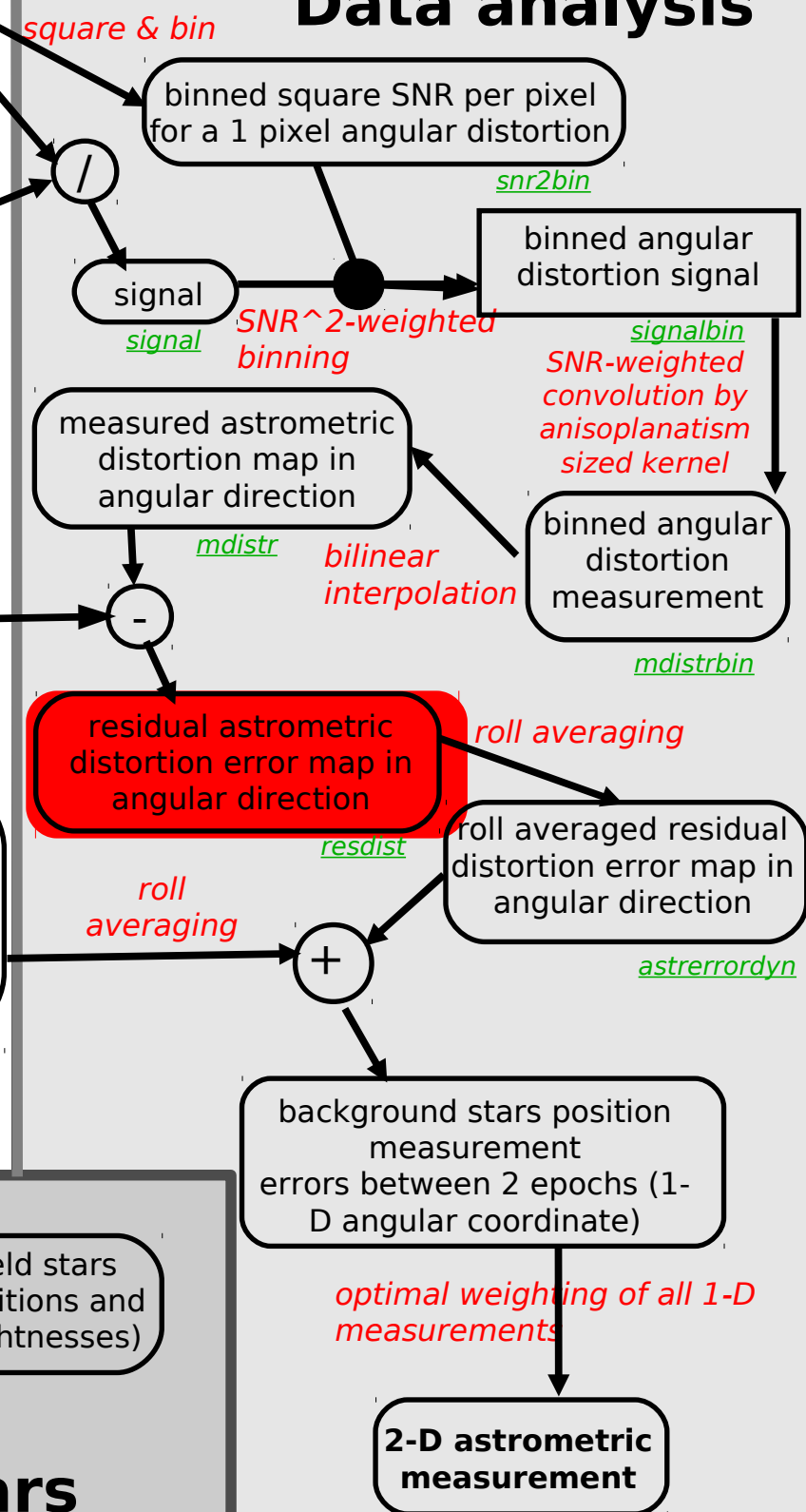
Data simulation



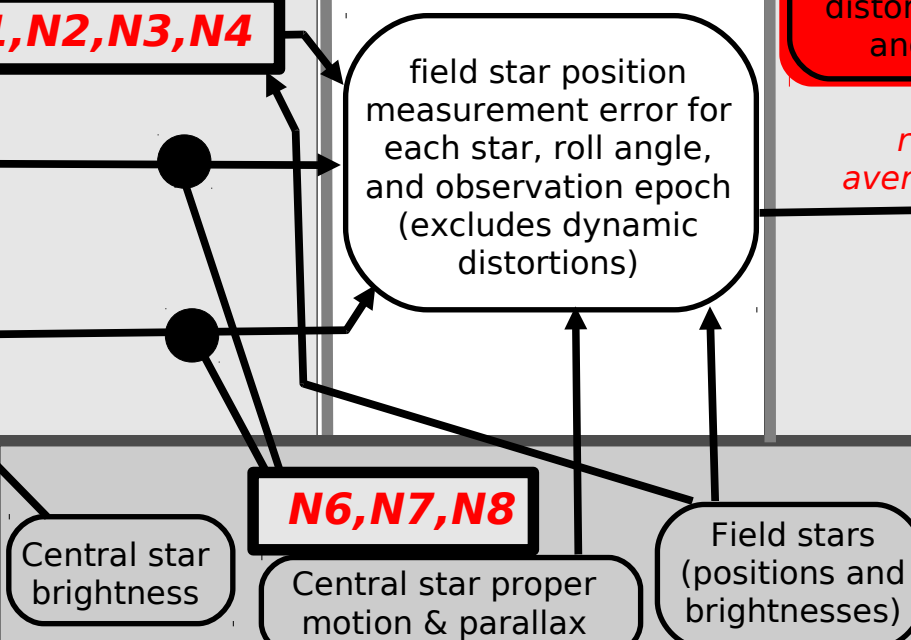
Simulated data



Data analysis



Target and field stars

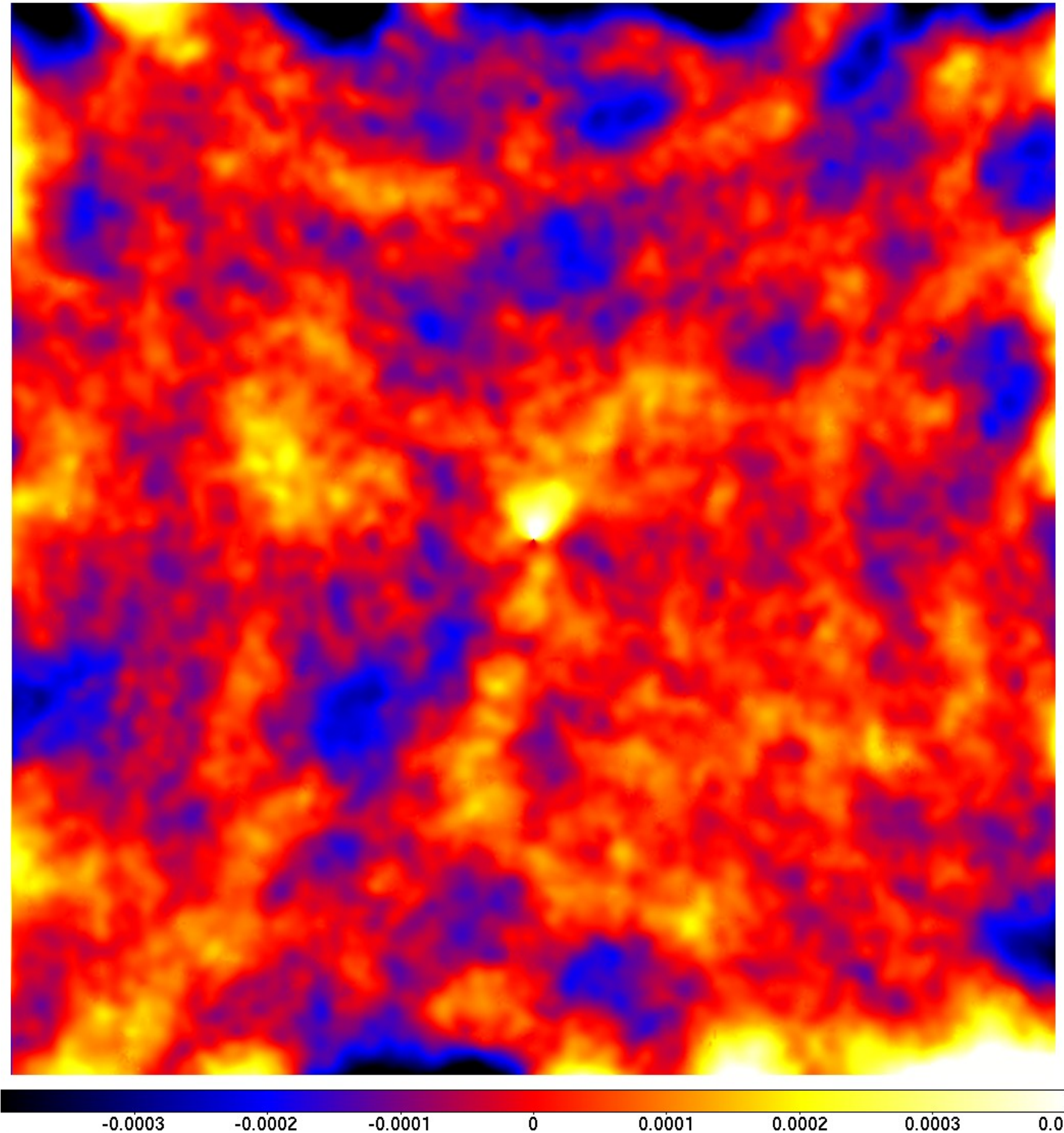


Residual distortion after calibration

Unit = pixel

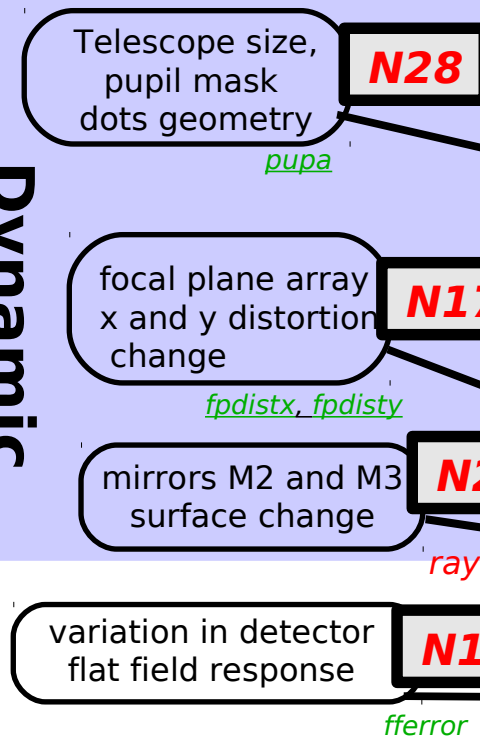
Residual distortion after calibration is $\sim 1e-4$ pix = $4.4 \mu\text{as}$

This is 10x smaller than original distortion, and residual is mostly free of low order \rightarrow will average well with telescope roll.

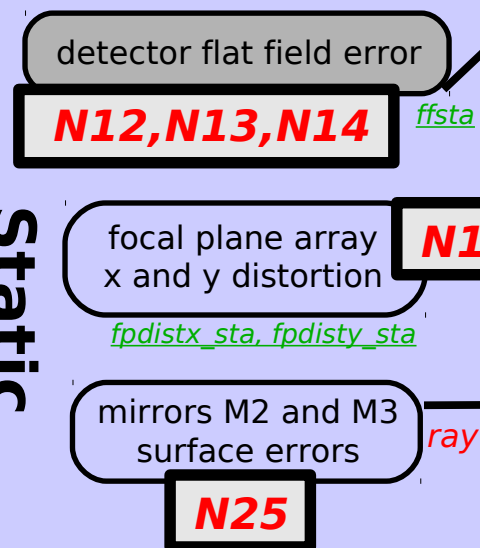


Input errors and instrument characteristics

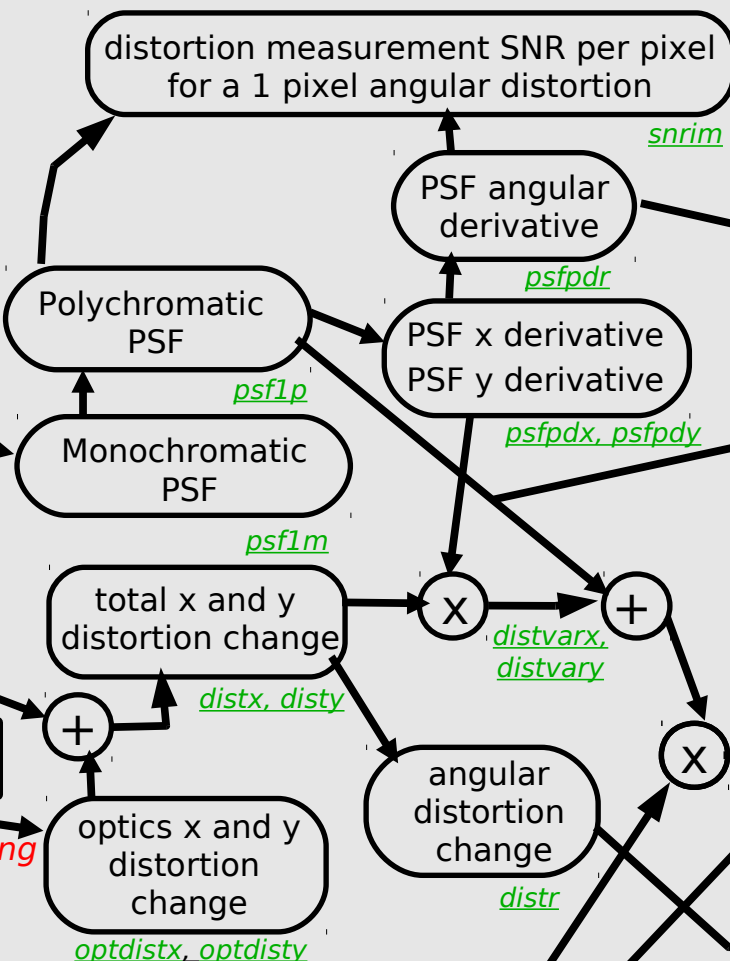
Dynamic distortions



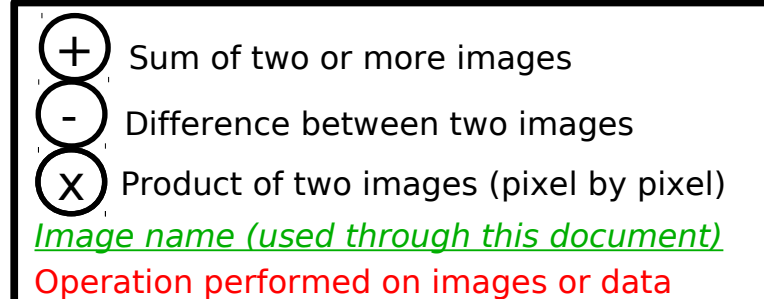
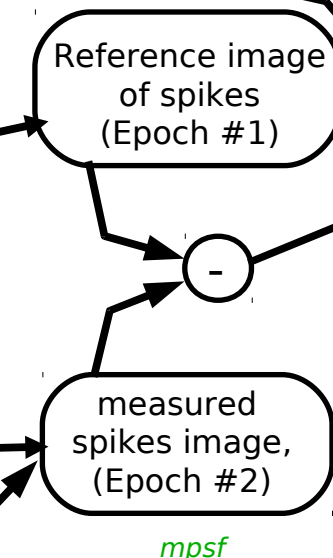
Static distortions



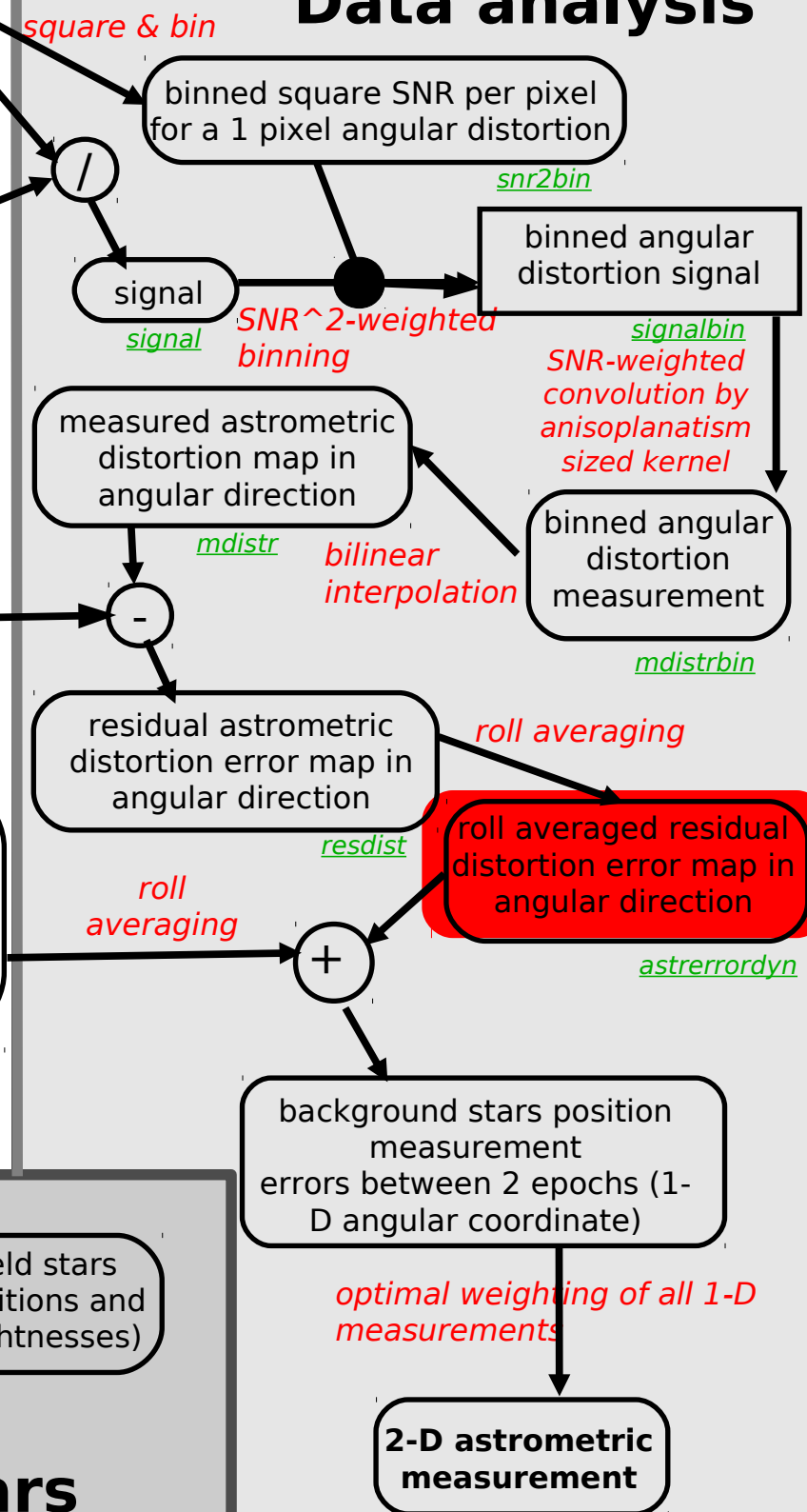
Data simulation



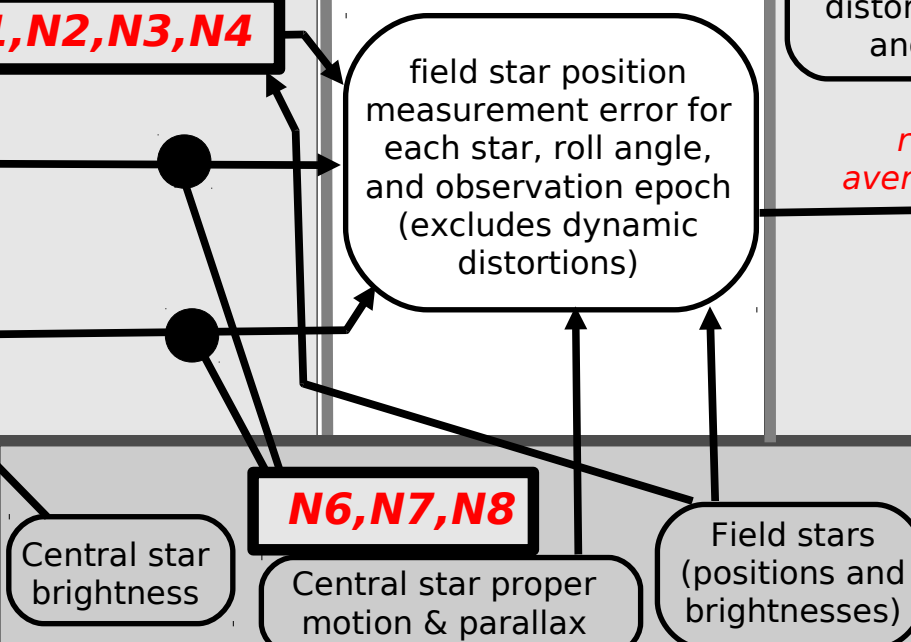
Simulated data



Data analysis



Target and field stars

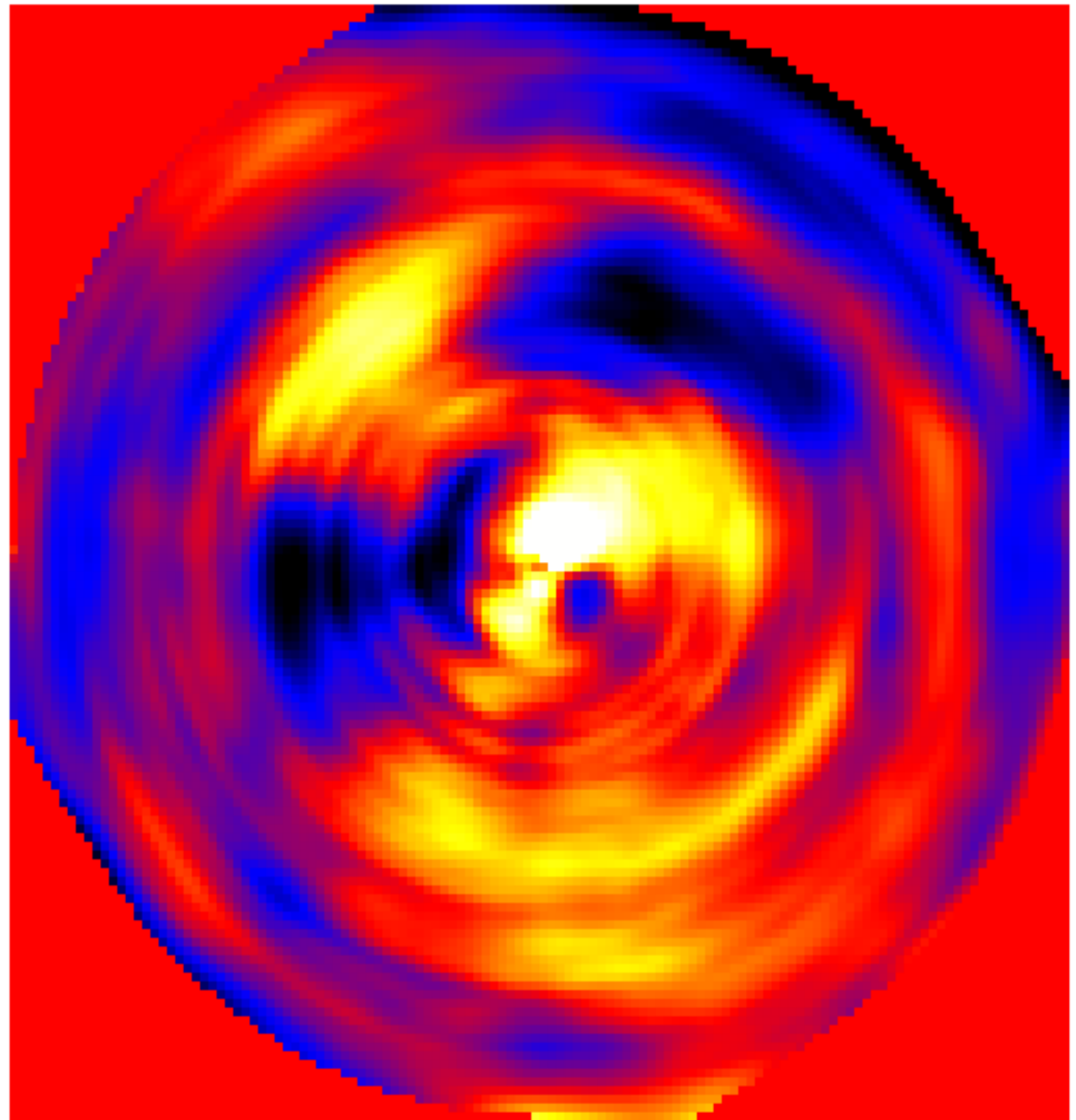


Astrometric error due to distortion changes (after roll)

Unit = arcsec
RMS $\sim \mu\text{as}$

This map is obtained by roll-averaging the distortion map in the previous slide

Error tends to be smaller for stars further out (more averaging thanks to roll)



Final astrometric error

For each star, 1-sigma error is computed as quadratic sum of :

- pixel coordinate error (due to photon noise)
- distortion errors (derived from 2D distortion map)
- flat field error on detector

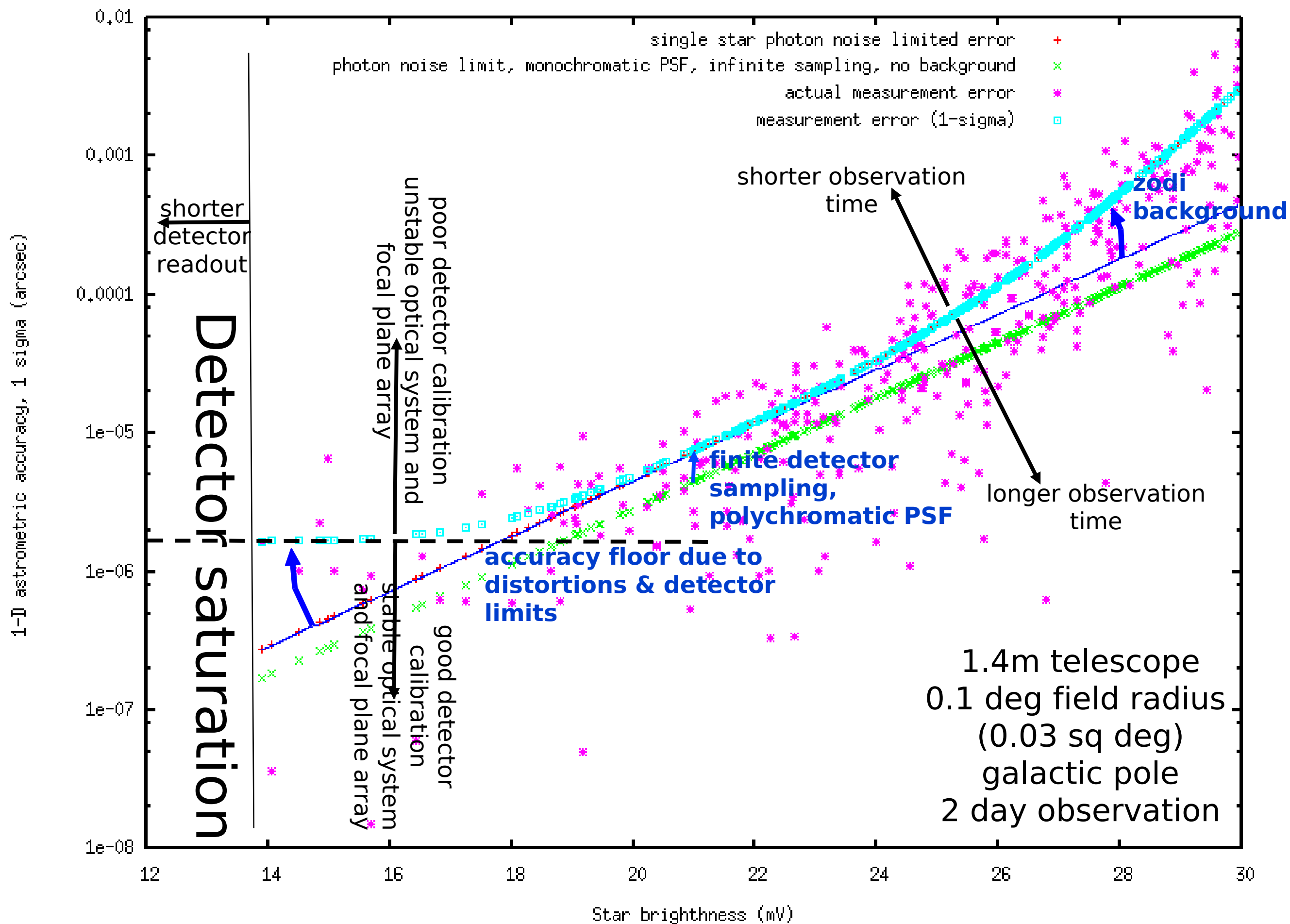
Then, optimally combine all measurement by weighting according to astrometric SNR^2 for each star.

Final astrometric 1 sigma error in this example :

0.63 μas per axis (1-sigma) for 0.03 sq deg (= 0.1 deg radius circular field)

0.2 μas per axis would require 0.29 sq deg (= 0.31 deg radius)

Note: scaling to larger FOV needs to be done more carefully - this is just a rough estimate



Existing mechanical positioning accuracy

Key issue for coronagraphic performance is placement accuracy of dots and their size uniformity.

High precision CMM: $\sim 1 \text{ um}$ over PECO PM seems possible

Example:

- NIST Moore 48 CMM: typical error is $130\text{nm absolute} + 200 \text{ nm per m} = 0.4 \text{ um}$ on PECO PM

http://www.cenam.mx/cmu-mmc/Evento_2007/Presentaciones/John_Stoup-High_accuracy_CMM_measurements_at_NIST.pdf

Work plan

